Developing New Kohn-Sham Density Functionals for Molecules, Atoms, and Solids:
New Methods and Applications

A Dissertation
SUBMITTED TO THE FACULTY OF
UNIVERSITY OF MINNESOTA
BY

Haoyu S. Yu

IN PARTIAL FULFILLMENT OF THE REQUIREMENTS
FOR THE DEGREE OF
DOCTOR OF PHILOSOPHY

Adviser: Donald G. Truhlar

June 2016

Acknowledgments

I sincerely thank my advisor Professor Donald G. Truhlar for his guidance and support throughout my Ph. D. stage. I also want to thank all the Truhlar group members, especially Professor Xiao He, Professor Xuefei Xu, Professor Wenjing Zhang, Professor Roberto Peverati, Professor Xin Zhang, Professor Bo Long, Professor Hannah Leverentz, Dr. Jingjing Zheng, Dr. Alek Marenich, Dr. Rubén Meana Pañeda, Dr. Laura Fernandez, Dr. Wei-Guang Liu, Dr. Sijie Luo, Dr. Ke Yang, Dr. Bo Wang, Dr. Tao Yu, Mr. Kaining Duanmu, Mr. Shaohong Li, Mr. Junwei Bao, Ms. Pragya Verma, and Ms. Xiaoyu Li for discussion and collaboration. Especially thanks to Dr. Prasenjit Seal for helping getting started at the very beginning of my Ph. D stage.

I also want to thank Dr. Benjamin Lynch, and other staff members at Minnesota Supercomputing Institute (MSI) for their kind help. The computing resources from MSI and the Environmental Molecular Sciences Laboratory (EMSL) are greatly appreciated.

Finally, I want to thank my parents, Xiaoming Yu and Lijun Sun and my former roommate Dr. Elliot Twiggs for their love and support.

Dedication

To my parents, friends, and my supervisor Donald G. Truhlar

Abstract

The accuracy of Kohn-Sham density functional theory depends on the exchange-correlation functional. Local functionals depending on only the density (ρ), density gradient ($\nabla\rho$), and possibly kinetic energy density (τ) have been popular because of their low cost and simplicity, but the most successful functionals for chemistry have involved nonlocal Hartree-Fock exchange (HFX). Based on the mathematical form of a nonseparable gradient approximation (NGA), as first employed in the N12 functional, we developed a gradient approximation for molecules (GAM) that is parameterized with a broader data set of molecular data than N12 and with smoothness constraints. By adding the kinetic energy density (τ) to the GAM functional, we developed a new meta-NGA called MN15-L that predicts accurate results for multi-reference systems especially for transition metal ligand binding energies. Adding 44% Hartree-Fock exchange to the MN15-L functional and optimizing the linear parameters of the functional in the presence of Hartree-Fock exchange, we obtained a non-local exchange-correlation functional called MN15 that predicts accurate results for a large variety of properties including single-reference systems, multi-reference systems, and noncovalent interactions.

In this thesis we presents the following studies: (1) Introduction of Density Functional Theory (DFT), (2) Development of Minnesota Database 2015B, (3) The GAM Functional, (IV) The MN15-L Functional, (V) The MN15 Functional, and (VI) Applications of Kohn-Sham Density Functionals.

Table of Contents

Acknowledgements i

Dedication ii

Abstract iii

Table of Contents xi

List of Tables xii

List of Figures xvii

Chapter 1. Introduction 1

1.1 Density Functional Theory 1

1.2 Kohn-Sham Density Functional Theory 3

1.3 First Generation Density Functionals 5

1.3.1 Local Spin Density Approximation 5

1.3.2 Generalized Gradient Approximation 6

1.4 Second Generation Density Functionals 8

1.4.1 Meta Generalized Gradient Approximation 8

1.4.2 Hybrid Density Functionals 9

1.5 Most Recent Density Functionals 11

1.5.1 Range-Separated Functionals 11

1.5.2 Dispersion Corrected Functionals 12

1.6 Summary of Density Functionals 14

1.7 References 15

Chapter 2. Development of Minneosta Database 2015B 19

2.1 Introduction to Database 2.0 20

2.2. Transition Metal Bonding Energies 29

2.2.1 3d Transition-Metal-Containing Molecules……..29

2.2.2 Palladium Complex Bond Energies 30

2.3 Atomic Excitation Energies 32

2.3.1 3d Transition Metal Atomic Excitation Energies 32

2.3.2 4d Transition Metal Atomic Excitation Energies 32

2.3.3 p-block Atomic Excitation Energies 34

2.4 Noncovalent Interactions 35

2.4.1 Noble Gas Dimer Weak Interactions 36

2.4.2 The S66 and S66x8 Databases 36

2.5 Alkyl Bond Dissociation Energies 36

2.6 Main-Group Diatomic Molecules 36

2.7 Other Types of New Databases 36

2.8 Summary 36

2.9 References 36

Chapter 3. The GAM Functional: “Nonseparable Exchange-Correlation Functional for Molecules, Including Homogeneous Catalysis Involving Transition Metals” 44

3.1 Introduction……...……...44

3.2 Computational details 48

3.3 Minnesota Database 2015 49

3.4 Functional for Comparison 51

3.5 Design and Optimization of the GAM Functional..... 52

3.5.1 Functional Form..... 53

3.5.2 Nonseparable Exchange-Correlation Functional Form…….....……54

3.5.3 Additional Correlation Functional Form……..…….....……55

3.5.4 Functional Optimization…….……..…….....……56

3.6 Table of Results…….……..…….....……58

3.6.1 Molecular Energy Database…….……..…….....……..59

3.6.2 Molecular Structure Database…….……..…….....……60

3.6.3 Solid State Database……..…….……..…….....……60

3.6.4 WCCR10……..……..…….……..…….....……60

3.6.5 Separation of O_2 and N_2 on Fe_2(dobdc)……..…….....……..61

3.6.6 Binding Energy of $Pd(PH_3)_2C_2H_4$…..……..…….....…….62

3.6.7 Bond length of Homonuclear Transition Metal Dimer …….....……..62

3.7 Other Results and Discussion…….. …….....……62

3.7.1 Convergence……... …….....……62

3.7.2 Performance of the GAM Functional……... …….....……63

3.7.3 Exchange-correlation Enhancement factor of the GAM Functional.....…….69

3.8 Conclusions…….....…….70

3.9 References..... 71

Chapter 4. The MN15-L Functional: "A New Local Exchange-Correlation Functional for Kohn-Sham Density Functional Theory with Broad Accuracy for Atoms, Molecules, and Solids" 91
4.1 Introduction 91
4.2 Minnesota Database 2015A and Test Data 94
4.3 Compuational Details 94
4.4 Density Functional for Comparison 94
4.5 Design and Parameterization of the MN15-L Functional 97
4.6 Properties of the New Exchange-Correlation Functional 102
4.6.1 Convergence Test 102
4.6.2 Rare Gas Potential Curves 103
4.7 Performance of the MN15-L Functional 104
4.7.1 Atomic and Molecular Energies 105
4.7.2 Molecular Geometries 108
4.7.3 Solid-State Database 108
4.7.4 Additional Test Sets 109
4.7.5 Further Comparison of Results with MN15-L 110
4.8 Conclusions 111
4.9 References 114

Chapter 5. The MN15 Functional: A Kohn-Sham Global-Hybrid Exchange-Correlation Density Functional with Broad Accuracy for Multi-reference and Single-reference Systems and Noncovalent Interactions 133

5.1 Introduction 132

5.2 Databases 136

5.3 Computational Details 137

5.4 Design and Parameterization of the MN15 Functional 138

5.5 Density Functional for Comparison 140

5.6 Performance of the MN15 Functional 141

5.6.1 Performance of Minnesota Database 2015B 143

5.6.2 Performance for S66 and S66x8 Databases 148

5.6.3 Performance for Excitation Energy Database 157

5.6.4 Performance for Transition Metal Barrier Height Database 191

5.6.5 Performance for Transition Metal Coordination Database 191

5.6.6 Performance for Semiconductor Band Gap Database……191

5.6.7 Performance for Transition Metal Bond Length Database 192

5.6.8 Performance for Organic Molecule Geometry Database……....154

5.7 Concluding Remarks……..……...154

5.8 References……..……...156

Chapter 6. Applications of Kohn-Sham Density Functionals 190

6.1 Introduction 193

6.2 What Dominates the Error in the Bond Energy of CaO Predicted by Various Approximation Exchange-Correlation Functionals 195
6.2.1 Computational Details 199
6.2.2 Diagnostics of CaO 201
6.2.3 Results and Discussions 198
6.3 Components of the Bond Energy in Polar Diatomic Molecules, Radicals, and Ions by Group-1 and Group-2 Metal Atoms 200
6.3.1 Decomposition of Bond Energies 201
6.3.2 Results and Discussions 204
6.4 Oxidation State 10 Exists 207
6.4.1 Computational Details 208
6.4.2 Results and Discussions 208
6.5 Water 26-mers Drawn from Bulk Simulations: Benchmark Binding Energies for Unprecedentedly Large Water Clusters and Assessment of the Electrostatically Embedded Three-Body and Pairwise Additive Approximations 212
6.5.1 Computational Methods 213
6.5.2 Results and Discussions 216
6.6 Density Functional Theory of the Water Splitting Reaction on Fe(0): Comparison of Local and Nonlocal Correction Functionals 221
6.6.1 Introduction 222
6.6.2 Computational Methods 227

6.6.3 Results and Discussions…….…….231

6.6.3.1 Utility of Coupled Cluster Calculations to Serve as Reference Data……...…...231

6.6.3.2 Basis Set Effects in CCSD(T) Calculations…….……...……...…….233

6.6.3.3 Barrier Heights and Energies of Reaction by Density Functional Theory for Catalysis at the Bare Metal Atom…….……..235

6.6.3.4 Barrier Heights and Energies of Reaction by Density Functional Theory for Catalysis at the Solid-Vacuum Interface…….…..……..238

6.6.4 Conclusion……..241

6.7 Calcium Metal Adsorption on the Metal-Organic Framework NU-1000: Interface Structure and Energetics……..242

6.7.1 Computational Methods…….…….242

6.7.2 Results and Discussions…….…….244

6.8 Computational Thermochemistry: Automated Generation of Scale Factors for Vibrational Frequencies Calculated by Electronic Structure Model Chemistries……...249

6.8.1 Introduction...…….…….249

6.8.2 The Scale Factor Optimization Process…….…….252

6.8.3 Program Descriptions…….256

6.8.3.1 Freqscale.py…...…….…….256

6.8.3.2 input.py and pbs.py…….258

6.8.4 Discussion…….…….261

6.8.5 Concluding Remarks.…….261

6.9 References……………..…………………………………………………………….263

Bibliography..……………..…………………………………………………………….310

List of Tables

Table 2.1 Database 2.0 41

Table 2.2 Database 2015B 41

Table 3.1 Databases included in Minnesota Database 2015… ……76

Table 3.2 Exchange-correlation functional tested in this paper……79

Table 3.3 Optimized and inherited parameters of the GAM functional……80

Table 3.4 MUE (kcal/mol) for the Molecular Energy Database and its subdatabases: GAM compared to LSDA and other gradient approximations……..81

Table 3.5 MUE (kcal/mol) for the Molecular Energy Database and its subdatabases: GAM compared to meta and hybrid functionals ……..83

Table 3.6 MUE (kcal/mol) for the Molecular Structure Database and its subdatabases..84

Table 3.7 Mean unsigned errors for lattice constants and nearest neighbor distances in Å, band gaps in eV, and cohesive energies in eV/atom…….85

Table 3.8 Mean unsigned errors for the WCCR10 database in kcal/mol …….86

Table 3.9 Binding enthalpies (kcal/mol) of O_2 and N_2 bound to the 88-atom cluster model of Fe-MOF-74 calculated using GAM……..86

Table 3.10 Binding energies (kcal/mol) of C_2H_4 bound to $Pd(PH_3)_2$ calculated using GAM and various basis sets…….87

Table 3.11 Homonuclear transition metal dimers: equilibrium bond lengths (Å) and mean unsigned errors as compared to experiment……..87

Table 3.12 Errors for Bond Dissociation Energy (kcal/mol) of FeC……88

Table 4.1 Databases included in Database 2015A……...117

Table 4.2 Optimized and inherited parameters of the MN15-L functional…….120

Table 4.3 Rankings and Average Ranking of MN15-L Compared to Other Local Functionals……...121

Table 4.4 Rankings and Average Ranking of Local MN15-L Compared to Selected Hybrid Functionals……..122

Table 4.5 MUE (kcal/mol) for the Molecular Energy Databases: MN12-L compared to MN15-L……..124

Table 5.1 Databases included in Database 2015B……..163

Table 5.2 Multi-reference systems and single-reference systems in Database 2015…..166

Table 5.3 Databases for testing only……167

Table 5.4 Optimized parameters of the MN15 functional……...168

Table 5.5 Exchange–correlation functionals tested against Database 2015B……..169

Table 5.6 MUE (kcal/mol) for the AME471 database and its subdatabases: LSDA and other gradient approximations…….171

Table 5.7 MUE (kcal/mol) for the AME471 database and its subdatabases: meta-GGAs, MN12-L, MN15-L, and global-hybrid GGAs…….172

Table 5.8 MUE (kcal/mol) for the AME471 database and its subdatabases: range-separated-hybrid GGAs, global-hybrid meta-GGAs, MN15……..173

Table 5.9 MUE (kcal/mol) of top ten best functionals for charge transfer database (CT7)……..174

Table 5.10 MUE (Å) for the Molecular Structure 10 Database and its Subdatabases….175

Table 5.11 The rankings (out of 83 functionals) of 12 selected functionals for 28 atomic and molecular databases……..177

Table 5.12 The performance (kcal/mol) of 18 selected density functionals for the S60 and S492 databases and subdatabases……178

Table 5.13 The performance (kcal/mol) of 18 selected density functionals for the S66 and S66x8 databases and subdatabases……..179

Table 5.14 The mean unsigned errors (MUE, in eV) of 60 selected methods for the vertical excitation energies of 30 valence, 39 Rydberg, and all 69 transitions…….180

Table 5.15 The mean unsigned errors (MUE in kcal/mol) of transition metal reaction barrier heights……182

Table 5.16 Mean unsigned errors (kcal/mol) for the WCCR10 database…….183

Table 5.17 Mean unsigned errors for the SBG31 database in eV……..184

Table 5.18 Homonuclear transition metal dimers: equilibrium bond lengths (Å) and mean unsigned errors as compared to experiment……..185

Table 5.19 Mean unsigned errors for the SE47 database in Å……..186

Table 6.1 Bond Dissociation Energy, Charge on Ca in CaO and Excitation Energy of Ca^{+}(s). Sorted in Order of Increasing Magnitude of excitation energy…….273

Table 6.2 Comparison of Chemical Properties of CaO Calculated by six Functionals.275

Table 6.3 Average Mean Unsigned Errors (AUE) over 25 Energetic Data (8IP, 3EA, 6IE, and 8BDE) from Eight SR Molecules, 20 Energetic Data (3IP, 2EA, 3EE, 5IE and 7BDE)

from Seven MR Molecules, and 43 Energetic Data (8IP, 4EA, 3EE, 13IE, 15BDE) from All 15 Molecules, Arranged by Type of Functional and Sorted in Order of Increasing Magnitude of the Overall Error (kcal/mol) for Each Type…….276

Table 6.4 Mean Unsigned Errors and Mean Signed Errors of 54 Methods Over 13 Geometric Data from 12 Main-group Molecules Sorted in the order of Increasing Magnitude of MUE(Å)……278

Table 6.5 Mean Unsigned Errors and Mean Signed Errors of Dipole Moment of All 15 Molecules Sorted in Order of Increasing Magnitude of the Error (Debye)…….280

Table 6.6 Reaction energies, enthalpies, and free energies for reactions 1-13 in kcal/mol……282

Table 6.7 Hirshfeld Charges and CM5 Charges of T_d structures of IrO_4^+ and PtO_4^{2+}….283

Table 6.8 Hirshfeld, CM5, and density dipole moments (in Debye) of the polar structures of PtO_4^{2+} and IrO_4^+……...283

Table 6.9 Mean Errors (kcal per mole of water molecules) for Electrostatically Embedded Many-Body Approximations……...284

Table 6.10 Relative computer times[a] for a calculation on $(H_2O)_{26}$…….285

Table 6.11 Mean Errors (kcal per mole of water molecules) for Many-Body and Electrostatically Embedded Many-Body Approximations…….286

Table 6.12 The mechanism of the water splitting reaction on Fe(0)……..287

Table 6.13 Density Functional tested in the current work……..288

Table 6.14 Relative energies (in units of kcal/mol) of various species at CCSD(T)-3*s*3*p*-DKH level of theory for Fe(0)–H_2O system based on the B97-1/cc-pVTZ geometries..290

Table 6.15 The calculated errors (kcal/mol) of CCSD(T)-3s3p-DKH/CBS calculations for the bond dissociation energies of FeH and FeCl as compared to experimental data…291

Table 6.16 Classical (zero-point-energy exclusive) energies of reaction ΔE_{rxn} for reactions R1-R5 and the overall reaction R_O; forward and reverse classical barrier heights for reactions R2 and R4[a]. Mean unsigned deviations (MUDs) are computed with respect to CCSD(T)-3*s*3*p*-DK/CBS results. (Units: kcal/mol)……..292

Table 6.17 The hybrid functionals tested in the current work and their percentage of nonlocal Hartree-Fock exchange (%*X*)……..297

Table 6.18 Heats of reaction for Ca reacting with NU-1000……298

Table 6.19 The ZPE15 database: experimental ZPEs for the 15 molecules used in this work……299

List of Figures

Figure 1.1. Difference between three kinds of range separation functionals..... 18

Figure 3.1 Ar-Ar Potential Curve, the bonding energies are calculated with GAM/aug-cc-pVQZ and GAM/aug-cc-pV6Z level of theory. The Reference is from the Tang-Toennies model…….88

Figure 3.2 Enhancement Factor of 14 GGAs, N12, and GAM…….90

Figure 4.1 Minnesota Database 2015A……126

Figure 4.2 Ar-Ar potential curve calculated by M06-L, MGGA_MS2, and MN15-L with grids (250,590) compared to with the experimental value……..127

Figure 4.3 Enhancement factor of MN15-L verse reduced density gradient plot at α=1.0……127

Figure 4.4 Mean unsigned errors (MUEs) for transition metal bond energies (TMBE33) and reaction barrier heights databases (BH76)……128

Figure 4.5 Mean unsigned errors for four databases, including main-group bond energies (MGBE137), excitation energy (EE18), isomerization energy (IsoE14), and hydrocarbon thermochemistry (HCTC20)……128

Figure 4.6 Mean unsigned errors for the noncovalent interaction database (NC51), the atomic and molecular energy database (AME422), and the atomic and molecular energy database without absolute energies (AME405xAE)……129

Figure 4.7 Mean unsigned errors for molecular structure databases (MS10) and its subdatabases (DG6L and DGH4)……129

Figure 4.8 Mean unsigned errors for solid-state databases including lattice constants (LC17), semiconductor band gaps (SBG31), and solid-state cohesive energies (SSCE8)……130

Figure 4.9 Mean unsigned error of 10 ligand dissociation energies of large transition metal complexes (WCCR10)…….130

Figure 4.10 Mean unsigned error of seven transition metal dimer bond lengths (TMDBL7)…….131

Figure 5.1 The percentage of all atomic and molecular databases (AME471), the number after a name means the number of data in this database, for example, SR-MGM-BE9 mean 9 pieces of bonding energy data in this database. The explanation of the these names are shown in Table 5.1…….187

Figure 5.2 The structure of $Pd(PH_3)_2C_6H_8$ in subdatabase PdBE2…….188

Figure 5.3 Reaction barrier heights of Rhenium catalyzed reaction……...189

Figure 6.1 Enthalpy profile of reaction (3): $PtO_4^{2+} \rightarrow PtO_2^{+} + O_2^{+}$. The spin states for T_d, TS1, C_{2v}, TS2, C_s, and TS are all singlet. The spin states for O_2^{+} and PtO_2^{+} are doublet……..300

Figure 6.2 HOMO of IrO_4^{+} (left) and PtO_4^{2+} (right)……301

Figure 6.3 Schematic energy profile of the five-step water splitting reaction at atomic Fe(0)…….302

Figure 6.4 Illustration of the Fe+H2O → H-Fe-O-H reaction on (100) iron surface…..303

Figure 6.5 Relative energies for equilibrium structures C1, C2, and C3 (see Fig. 2) and

transition structures B1 and B2 as calculated by five density functional methods at geometries optimized by PBE. All energies are in kcal/mol……..304

Figure 6.6 Predicted structures (optimized in the cluster calculation) of the initial Zr_6 oxide node with attached benzoates (to model linkers), the intermediate product $Zr_6C_{56}O_{32}H_{54}Ca$ formed during the reaction of Ca with a node-bound water-hydroxyl complex, which releases two H atoms, and the final product $Zr_6C_{56}O_{30}H_{54}Ca$ after losing two oxygen atoms. The lost H and O are expected to remain transiently bound to the solid in some way but quickly associate with another Ca to make solid $Ca(OH)_2$ nanoparticles (bound in some way to the MOF), as described in Reaction 1……305

Figure 6.7 (A) The slab model of (001) surface of NU-1000 optimized in the periodic calculation with lattice constants constrained at bulk values. (B) 50% of surface benzoic acid reacting with Ca. (C) 100% of surface benzoic acid reacting with Ca……306

Figure 6.8 The most stable proton topology on the face of the Zr_6 node of NU-1000 and the proposed products of Ca reacting with protons. The figure only show one of four faces with $–OH_x$ of Zr_6 node……307

Figure 6.9 The product of Ca reacting with different number of protons on Zr_6 node optimized in the periodic calculation (as listed in Table 6.18)……308

Figure 6.10 Two Ca deposited on pyrene optimized in the periodic calculation (as listed in Table 6.18): (A) inside the triangular pore; (B) outside the triangular pore……309

Chapter 1. Introduction

1.1 Density Functional Theory

Density functional theory (DFT) is a method in which the electron density rather than the many-electron wave function is used for calculations of the electronic structure of many-electron systems.[1] DFT has become very popular among computational chemists and physicists due to its simplicity and low computational cost.

The Schrödinger equation is the key equation of quantum mechanics. This second order, partial differential equation determines the spatial shape and the temporal evolvement of a wave function in a given potential and for given boundary conditions. The goal of most quantum chemical approaches that are used for electronic structure problems is the approximate solution of the time-independent, non-relativistic Schrödinger equation for the electrons in the field of fixed nuclei:

$$H\psi(\vec{r}_1,\vec{r}_2,...,\sigma_1,\sigma_2,...) = E\psi(\vec{r}_1,\vec{r}_2,...,\sigma_1,\sigma_2,...) \qquad (1.1)$$

In equation (1.1), H is the Hamiltonian operator, E is the total energy of a specific system, $\vec{r}_1,\vec{r}_2,...$ denotes the coordinates of the electrons, and $\sigma_1,\sigma_2,...$ denotes their spin coordinates. The Schrödinger equation is an eigenvalue equation with the eigenfunctions $\psi_n(\vec{r}_1,\vec{r}_2,...,\sigma_1,\sigma_2,...)$ and the eigenvalues E_n. The eigenvalues of the Schrödinger equation E_n are discrete for bound states of the electrons, but form a continuum for unbound states of the electrons; this thesis is concerned with bound states. The lowest eigenvalue is the ground-state energy, and other higher eigenvalues are excited-state

energies. The knowledge of $\psi_n(\vec{r})$ and E_n implies the knowledge of all relevant physical parameters of the system. However, solving the Schrödinger equation is a nontrivial task. For example the Schrödinger equation for benzene involves the coordinates of 42 electrons, meaning 126 spatial degrees of freedom and 42 electron spin coordinates. Because of the Pauli Principle, ψ_{benzene} is an antisymmetric function in the electron coordinates, and it has126 spatial degrees of freedom and 42 spin coordinates; therefore it is essentially impossible to solve completely accurately. Nevertheless, quantum chemistry seeks to make predictions with chemical accuracy.

Shortly after the Schrödinger equation was proposed, Thomas and Fermi independently developed a model for describing the approximate electron density $\rho(\vec{r})$ and the ground-state energy E of a large atom or molecule with a large number of electrons.[2,3,4] Since the theory is formulated in terms of electron density, it is viewed as a precursor of DFT. In this theory one writes the ground-state energy of an atom as

$$\begin{aligned} E &= T + U_{\text{eN}} + U_{\text{ee}} \\ &= C_{\text{F}} \int \rho(\vec{r})^{5/3} dr + \int \rho(\vec{r}) V_{\text{N}}(\vec{r}) dr + \frac{1}{2} e^2 \int \frac{\rho(\vec{r})\rho(\vec{r}')}{|\vec{r} - \vec{r}'|} dr dr', \end{aligned} \tag{1.2}$$

In equation (1.2), the total energy of an *N*-electron system E equals to the sum of three terms T, U_{eN}, and U_{ee}. The first term is the kinetic energy of electrons, C_{F} is a constant, and $\rho(\vec{r})$ is the electron density at a given point $\vec{r}$ in three-dimensional space.. The second term is the potential energy of electrons due to the nucleus, where $V_{\text{N}}(\vec{r})$ is the nuclear attractive potential of an electron at position $\vec{r}$. The third term is the potential

energy due to electron repulsion. Even though this model inspired people to pay attention to the electron density approach, it failed to predict the existence of stable molecules.[5]

Density functional theory as we know it today was born in 1964 when a landmark paper by Hohenberg and Kohn appeared in the Physics Review.[6] They proved that within the Born-Oppenheimer approximation, any atomic, molecular, or condensed-matter system of electrons is completely determined by the electron density $\rho(\vec{r})$. Here we will briefly introduce the first and second Hohenberg-Kohn theorem:

The first Hohenberg-Kohn theorem:

For any system of interacting particles in an external potential $V_{\text{ext}}(\vec{r})$, the density is uniquely determined (in other words, the external potential is a unique functional of the density).

The second Hohenberg-Kohn theorem:

A universal functional $F[\vec{\rho}]$ for the energy E can be defined in terms of density $\rho(\vec{r})$. The $F[\vec{\rho}]$ delivers the lowest energy if and only if the input density is the true ground state density $\rho_0(\vec{r})$, where (…) denotes the arguments of a function and […] denotes a functional dependence.

1.2 Kohn-Sham Density Functional Theory

The most successful way to implement DFT is the method proposed by Kohn and Sham in 1965.[7] This method is so widely used that when most researchers call DFT today they really mean Kohn-Sham DFT (KS-DFT). In KS-DFT the density of the system

under consideration is represented by a single Slater determinant (Eq. 1.3) of a fictitious non-interacting system.

$$\Phi_{\mathrm{SD}} = \frac{1}{\sqrt{N!}} \det\{\chi_1(\overrightarrow{x_1})\chi_2(\overrightarrow{x_2})...\chi_N(\overrightarrow{x_N})\} \tag{1.3}$$

The Slater determinant Φ_{SD} is an approximation to the true *N*-electron wave function. χ_i is the *i*th spin-orbital, and $\overrightarrow{x_1}$ denotes $\vec{r}_1, \sigma_1$. The total energy of the system can be written as

$$E[\rho] = E_{\mathrm{Ne}}[\rho] + T[\rho] + J[\rho] + E_{\mathrm{xc}}[\rho] \tag{1.4}$$

where E_{Ne}, T, and J are the nuclei-electron attraction, kinetic energy, and electron-electron repulsion respectively. E_{xc} is called the exchange-correlation energy, which accounts for all the remaining parts of the energy. By taking the variational minimum of the total energy with respect to the electron density ρ, we can derive the Kohn-Sham equation (Eq. 1.5):

$$\hat{f}^{\mathrm{KS}}\chi_i = \varepsilon_i\chi_i \tag{1.5}$$

where $\hat{f}^{\mathrm{KS}}$ is called the Fock operator, which can be written as (Eq. 1.6):

$$\hat{f}_i^{\mathrm{KS}}(r_1) = -\sum_A^M \frac{Z_A}{r_{iA}} - \frac{1}{2}\nabla_i^2 + \int \frac{\rho(r_2)}{r_{12}} dr_2 + V_{xc}(r_1) \tag{1.6}$$

where the four terms in equation 1.6 are the counterparts of the ones in equation 1.4. The exchange-correlation potential is defined as the derivative of the exchange-correlation energy with respective the electron density (Eq. 1.7):

$$V_{xc} = \frac{\delta E_{xc}}{\delta \rho} \tag{1.7}$$

We can solve the equation 1.4 and 1.6 by the self-consistent field (SCF) method, where we input an initial guess for the electron density term and update all the other terms iteratively until convergence is achieved. Then we can obtain the total energy by integrating (Eq. 1.4)

The Kohn-Sham equations are in principle exact. If we know the exact form of E_{xc} and V_{xc}, we can obtain the exact energy; there is approximation in the Kohn-Sham equations. The approximation only enters when we want to decide the explicit form of E_{xc} and V_{xc}. Modern density functional developments mainly focus on getting good functional forms of exchange-correlation energy, and from these one can obtain the exchange-correlation potential. In the following subsections we will review various density functionals developed since 1965.

1.3 First Generation Density Functional

1.3.1 Local Spin Density Approximation (LSDA)

In 1965 Kohn and Sham introduced the local density approximation (LDA) for the exchange-correlation energy. In this approximation, one assumes that at each point in space the exchange-correlation energy per particle is given by its value for a homogeneous electron gas (also known as uniform electron gas or UEG) $e_{\mathrm{xc}}[\rho(\vec{r})]$. The UEG is defined as a large number *N* of electrons in a cube volume *V*, through which there

is uniform spread of positive charge sufficient to make the system neutral. The UEG is then defined as the limit $N \to \infty,\ V \to \infty$, with the density $\rho = N/V$ remaining finite. The local spin density approximations (LSDA) are a class approximations to the exchange-correlation energies that only depend on spin densities ρ_α and ρ_β.[8,9,10]

$$E_{\mathrm{xc}}^{\mathrm{LSDA}}[\rho_\alpha, \rho_\beta] = \int d\vec{r}\rho(\vec{r})\varepsilon_{\mathrm{xc}}(\rho_\alpha, \rho_\beta) \tag{1.8}$$

In equation (1.8), $\varepsilon_{\mathrm{xc}}(\rho_\alpha, \rho_\beta)$ stands for the exchange-correlation energy of the uniform electron gas[10] per electron at a given point in space. The LSDA is very simple and has been widely applied in solid-state physics, with good results for ground-state geometries and vibrational frequencies.[11] However, the density of a molecule is not uniform, and sometimes it has rapid changes. Therefore, LSDA molecular energies have systemic errors, including overestimating the bonding energies and large absolute errors for atomization energies.

1.3.2 Generalized Gradient Approximation (GGA)

In the 1980s, the GGA was developed to approximation the exchange-correlation energy; a GGA depends not only on the density but also on the gradient of the density. (See Eq. 1.9)

$$E_{\mathrm{xc}}^{\mathrm{GGA}}[\rho(\vec{r})] = \int d\vec{r} f[\rho(\vec{r}), \nabla\rho(\vec{r})] \tag{1.9}$$

This approximation is based on the gradient expansion of the exchange hole, and originally it was based on real- space cutoffs chosen to guarantee that the hole is negative everywhere and represents a deficit of one electron.[12] In comparison with the LSDA,

GGAs tend to improve energies and atomization energies.[13] The revolution in popularizing KS-DFT was initiated by the exchange GGA proposed by Becke[14] in 1988 (denoted as B88 or often just as B) and by the correlation functionals of Perdew (P86), [15] Perdew and Wang[16] (PW91), and Lee, Yang, and Parr[17] (LYP). The LYP correlation functional contains parameters fit to the helium atom, and it provides an exact cancellation of the self-interaction error in one-electron systems. When exchange is separated from correlation, the correct scaling of exchange under a uniform expansion of all coordinates is achieved only[18] if the exchange energy density is separable, that is, if it is a sum over spins σ of a function of ρ_α times a function of s_σ^2 where s_σ is the dimensionless gradient proportional to $\left|\rho_\sigma\right| / \rho_\sigma^{4/3}$; standard GGAs for exchange all satisfy this. The B88 exchange functional has the correct asymptotic behavior at long range for the exchange energy density, and it incorporates a parameter optimized by fitting to the Hartree-Fock exchange energies of six noble gas atoms (from He to Rn). Popular functional forms for GGA exchange functionals are rational function expansions in the reduced gradient[19,20] and polynomials of such functions.[21]

More recently we proposed parameterizing functionals with the same ingredients (spin densities and their reduces gradients) but without using a separable form for exchange and without separately parameterizing exchange and correlation since only their sum is important; we called such a functional a nonseparable gradient approximation (NGA). [22] Such a functional is more flexible, and the two functionals

parameterized this way, called N12[22] and GAM,[23] have better average performance than GGAs, which will be discussed in detail in chapter 3.

1.4 Second Generation Density Functionals

1.4.1 Meta Generalized Gradient Approximation

The most popular other local ingredient is the kinetic energy density (See Eq. 1.10)

$$\tau = \sum_{i}^{N} \frac{1}{2} |\nabla \phi_i(r)|^2 \tag{1.10}$$

Adding this to a GGA or an NGA results in what is called a meta-GGA[24,25,26,27,28] or meta-NGA.[29] There are several advantages of employing kinetic energy density. First it can distinguish between regions of space where the density is due to a single orbital from regions where it is due to multiple orbitals.[30,31] This can allow the exchange-correlation functional to recognize regions containing only a single electron where self-interaction error can be especially significant. Second, using kinetic energy density allows one to distinguish regions of decaying density from bonding regions. This can allow the exchange-correlation functional to distinguish between atoms on the surface of a molecule or solid, where the density decays in some directions, from atoms in an interior, where it is surrounded by bonding regions.[32] Some of the widely used meta-GGAs are VSXC,[33] which reproduces exact exchange energies in molecules very well; τ-HCTH,[34] which improves the performance over HCTH[35] for atomization energies, electron

affinities, ionization potentials, dissociation energies of transition metal complex, and hydrogen bonds; and M06-L,[36] which predicts good results for transition metal systems. More recently we developed two meta-NGAs, MN12-L[29] and MN15-L,[37] which have the same ingredients as meta-GGAs, but without using a separable form for exchange and without separately parameterizing exchange and correlation. We are going to discuss these two functionals in detail in chapter 4.

1.4.2 Hybrid Density Functionals

Motived by reexamination of the adiabatic connection formula for the exchange-correlation energy, [38,39,40,41] Becke investigated a new density functional, which mixed exact exchange (Hartree-Fock exchange) energy and the LDA exchange-correlation energy together. [42] (See Eq. 1.11)

$$E_{\mathrm{xc}} = 0.5E_{\mathrm{x}}^{\mathrm{exact}} + 0.5E_{\mathrm{xc}}^{\mathrm{LSDA}}[\rho] \tag{1.11}$$

This exchange-correlation functional is also called the Becke half-and-half approach. In later work, the percentage of Hartree-Fock exchange (X) is usually empirically optimized to improve performance, with optimum values in the range of 5–60, and one uses a GGA rather than the LSDA. Functionals that incorporate a certain percentage of Hartree-Fock exchange is called hybrid functionals. In 1993, Becke reported a three-parameter functional, called B3PW91,[43] which was fitted against main-group atomization energy data and has 20% Hartree-Fock exchange ($X = 20$). By replacing the PW91 GGA correlation functional with the LYP GGA correlation functional, Stephens et al.[44]

obtained the B3LYP functional, which has been widely used in computational chemistry for the past twenty years.

One of the advantages of including Hartree-Fock is that it removes or lessons the self-interaction error, which is the error due to the electron feeling the field generated by itself. This has many chemical consequences. For example, self-interaction tends to make Kohn-Sham orbitals too delocalized, and Hartree-Fock exchange ameliorates or corrects that tendency. Self-interaction error also leads to a large error the electric field felt by an electron far from the nuclei; Hartree-Fock exchange corrects this. However, there are disadvantages of including Hartree-Fock exchange. One of them is that it introduces static correlation error, which is error one makes when one calculate the exchange energy by Hartree Fock theory.

Various hybrid functionals have been developed after B3LYP functional. By adding 25% HF exchange to the PBE approximation, Perdew, Ernzerhof, and Burke reported a functional called PBE0, [45] which gives better results for reaction barrier heights, metal bond energies, and hydrocarbon chemistry than B3LYP. In 1998, Handy et. al. proposed a new hybrid functional named B97-1,[46] which is a re-parameterization of B97 functional[47] in the presence of HF exchange. The B97-1 predicts very good results for transition metal bond energies. More recently we develop a hybrid meta-NGA called MN15,[48] which has 44% HF exchange that gives good results for a variety of chemical properties. We are going discuss this functional in chapter 5.

1.5 Other Recent Density Functionals

1.5.1 Range-Separated Functionals

As we saw in section 1.4.2, some functionals treat the percentage X of HF exchange as a constant. When X is treated as a constant, the functional is called a global hybrid functional. When X is treated as nonconstant, the functional is called range-separated hybrid functionals. In a range-separated functional, X depends on the interelectronic separation (See Eq. 12).

$$r_{12} = |r_1 - r_2| \tag{1.12}$$

Where r_1 and r_2 are the coordinates of two electrons. This is most simply done by dividing the interelectronic interaction terms into a short-range (SR) part and a long-range (LR) part, for example[49] (Eq. 13)

$$\frac{1}{r_{12}} = \frac{\mathrm{erf}\left(\omega r_{12}\right)}{r_{12}} + \frac{\left[1 - \mathrm{erf}\left(\omega r_{12}\right)\right]}{r_{12}} \tag{1.12}$$

Range separation has been applied in a variety of ways. The initial usage was to include more Hartree-Fock exchange at long range than at short range, sometimes increasing from $X = 0$ to $X = 100$, sometimes from finite X to $X = 100$. Functionals in which X increases with $\mathbf{r}_{12}$ are called long-range corrected or LC functionals.[49,50,51,52,53,54,55,56,57] Functionals in which X decrease to zero at long range are called screened-exchange or SX functionals.[58,59] The motivation for LC functionals is improving accuracy of electronically excited states with charge transfer character without introducing too much

static correlation error in ground states. The motivation for SX functionals is twofold. One is that electron correlation screens electron exchange at large distances because of dielectric shielding (as in a solid).[60,61] One can think of this as arising from a cancellation of exchange and correlation effects at large interelectronic separation. [62] The other is that it reduces the cost of calculations in plane wave codes.

In order to benefit from both LC and SX approaches, it has been suggested to use three ranges, with X increasing from short range to middle range and then decreasing from middle range to long range.[63]

Another way to use range separation has nothing to do with Hartree-Fock exchange. Rather was used to employ one parameterization of a meta-GGA at short range and another parameterization at long range.[64] This accounts for exchange and correlation effects associated with the short-range (SR) and the long-range (LR) portions of the Coulomb interactions depending differently on the independent variables. All these three kinds of range separation are shown in Figure 1.1.[65]

1.5.2 Dispersion-Corrected Functionals

Dispersion interactions were originally modeled by London, and his formulas apply only at long range where the subsystems have no charge cloud penetration.[66] In the strict meaning of the term, "dispersion force" applies only in such regions. As subsystems begin to overlap there is no unique way to partition the interaction energy into dispersion and the reminder, although there are reasonable ways to do so in an approximate sense.[67] However, when doing this, the dispersion component of the interaction energy no longer

satisfies the inverse power laws of long-range dispersion; rather it is damped by overlap. This overlap also leads to Pauli repulsion, and when the inter-subsystem distance is reduced to the van der Waals distance, since that represents equilibrium geometry, the repulsive force exactly cancels the attractive force (and therefore is not negligible). Functionals with local correlation, such as MN15[48] and the other functionals cannot treat inverse power dependence of long-range dispersion, but in principle they can treat attractive noncovalent interactions at the van der Waals geometry.

Grimme and coworkers developed the methods of dispersion correction as an add-pm to standard Kohn-Sham density functional, called D3[68] of – for a later version – D3(BJ), [69] which provides better nonbonded distances. The PW6B95-D3 functional[70,73] is one of the best functionals for the GMTKN30[71,72] database for general main group thermochemistry, kinetics, and noncovalent interactions developed by Stefan Grimme.[73]

In 2012, Nørskov and coworkers reported density functionals for surface science, which they called BEEF-vdw[74] (which stands for Bayesian error estimation functional with van der Waals correction). By including the molecular formation energies, reaction energies, reaction barrier heights, noncovalent interactions, and solid-state properties into a training set, the BEFF-vdw functional is designed to be useful for complex problems in materials science.

In 2014, Head-Gordon and coworkers developed a range-separated hybrid functional called ωB97X-V,[75] which is fitted by choosing the most transferable parameters from the B97-type power series and a nonlocal van der Waals density

functional VV10 functional.[76] The ωB97X-V is trained on a large number of thermochemistry and noncovalent data, as a result the functional shows promising results on weak interaction and thermochemistry properties. Since the ωB97X-V does not containing any multi-reference systems in the training set, it is not suggested to use such a functional for systems having multi-reference character. The previously developed functional ωB97X-D also gives good results for thermochemistry and noncovalent interactions, but failed to predict multi-reference systems – especially systems containing transition metals. By using the same design strategy, a meta gradient approximation paired with VV10 nonlocal functional called B97M-V is developed by Head-Gordon and coworkers in 2015.[77] The B97M-V predicts accurate results for noncovalent interactions, but the performance of thermochemistry, especially reaction barrier heights (4.82 kcal/mol for BH76 database[78]) are not as good as ωB97X-V (1.96 kcal/mol for BH76). By including the part of the noncovalent correlation functional VV10, both B97M-V and ωB97X-V perform very well against the S66x8 database and the error reduced by a factor of three comparing to ωB97X-D, which already predicts good noncovalent interactions.

1.6 Summary of Denisty Funcitonals

In the above five sections we discussed various density functionals including, the local spin density approximation (LSDA), gradient approximation (GGA and NGA), meta gradient approximation (meta-GGA and meta-NGA), hybrid functionals (hybrid GGA, hybrid meta-GGA, and hybrid meta-NGA), range-separated functionals (LC and SX), and dispersion corrected functionals (D3 and D3BJ). Progress in developing more

accurate density functionals has involved adding ingredients, designing flexible forms that can best represent the important physics of the electron distribution, and parameterizing against larger and better chosen databases.

One design principle in building the Minnesota functionals is the use of large variety of database and a flexible mathematical functional form capable of fitting, for example, transition metal bond energies and reaction barrier heights, multi-reference systems, thermochemistry, and noncovalent interactions. In the following sections we will focus on the development of Minnesota functionals and their applications.

1.7 References

[1] R. G. Parr and W. Yang, in Density Functional Theory of atoms and molecules, (Oxford University Press, Inc, 1989); R. M. Dreizler and E. K. U. Gross, in Density Functional Theory, (New York, Plenum Press, 1995).

[2] L. H. Thomas, *Math. Proc. Cambridge Philos. Soc.*, 1927, **23**, 542.

[3] E. Fermi, *Rend. Accad. Naz. Lincei*, 1927, **6**, 602.

[4] P. A. M. Dirac, *Math. Proc. Cambridge Philos. Soc.*, 1930, **26**, 376.

[5] E. Teller, *Rev. Mod. Phys.* 1962, **34**, 627.

[6] P. Hohenberg, W. Kohn, *Phys. Rev.* 1964, **136**, B864.

[7] W. Kohn and L. J. Sham, *Phys. Rev.* 1965, **140**, A1133.

[8] J. P. Perdew and A. Zunger, *Phys. Rev. B* 1981, **23**, 5048.

[9] S. H. Vosko, L. Wilk and M. Nusair, *Can. J. Phys.* 1980, **58**, 1200.

[10] J. P. Perdew and Y. Wang, *Phys. Rev. B* 1992, **45**, 13244.

[11] S. Lundqvist and N. H. March, in Theory of the Inhomogeneous Electron Gas, (Plenum, New York, 1983)

[12] J. Perdew and W. Yue, *Phys. Rev. B* 1986, **33**, 8800.

[13] J. Perdew, J. Chevary, S. Vosko, K. Jackson, M. Pederson, D. Singh and G. Fiolhais, *Phys. Rev. B* 1992, **46**, 6671.

[14] A. D. Becke, *Phys. Rev. A* 1988, **33**, 3098.

[15] J. P. Perdew, *Phys. Rev. B* 1986, **33**, 8822.

[16] J. P. Perdew, in *Electronic Structure of Solids '91*, edited by P. Ziesche and H. Eschrig (Akademie Verlag, Berlin, 1991), pp. 11–20.
[17] C. Lee, W. Yang, and R. G. Parr, *Phys. Rev. B* 1988, **37**, 785.
[18] M. Levy and J. P. Perdew, *Int. J. Quantum Chem.* 1994, **49**, 539.
[19] A. D. Becke, *J. Chem. Phys.* 1986, **84**, 4524.
[20] J. P. Perdew, K. Burke, and M. Ernzerhof, *Phys. Rev. Lett.* 1996, **77**, 3865.
[21] A. D. Becke, *J. Chem. Phys.* 1997, **107**, 8554.
[22] R. Peverati and D. G. Truhlar, *J. Chem. Theory Comput.* 2012, **8**, 2310.
[23] H. S. Yu, W. Zhang, P. Verma, X. He, and D. G. Truhlar, *Phys. Chem. Chem. Phys.* 2015, **17**, 12146.
[24] J. P. Perdew, *Phys. Rev. Lett.* 1985, **55**, 1665.
[25] S. K. Ghosh and R. G. Parr, *Phys. Rev. A* 1986, **34**, 785.
[26] A. D. Becke and M. R. Roussel, *Phys. Rev. A* 1989, **39**, 3761.
[27] T. V. Voorhis, G. E. Scuseria, *J. Chem. Phys.* 1998, **109**, 400.
[28] A. D. Becke, *J. Chem. Phys.* 1998, **109**, 2092.
[29] R. Peverati and D. G. Truhlar, *Phys. Chem. Chem. Phys.* 2012, **14**, 13171.
[30] A. D. Becke, *J. Chem. Phys.* 1996, **104**, 1040.
[31] Y. Zhao and D. G. Truhlar, *J. Phys. Chem. A* 2005, **109**, 5656.
[32] L. Ferrighi, B. Hammer, and G. K. H. Madsen, *J. Am. Chem. Soc.* 2009, **131**, 10605.
[33] T. V. Voorhis, G. E. Scuseria, *J. Chem. Phys.* **109**, 1998, 400.
[34] A. D. Boese, N. C. Handy, *J. Chem. Phys.* 2002, **116**, 9559.
[35] A. D. Boese and N. C. Handy, *J. Chem. Phys.* 2000, **114**, 5497.
[36] Y. Zhao and D. G. Truhlar, *J. Chem. Phys.* 2006, **125**, 194101.
[37] H. S. Yu, X. He, and D. G. Truhlar, *J. Chem. Theory Comput.* 2016, **12**, 1280.
[38] J. Harris and R. O. Jones, *J. Phys. F* 1974, **4**, 1170.
[39] O. Gunnarsson and B. I. Lundqvist, *Phys. Rev. B* 1976, **13**, 4274.
[40] D. C. Langreth and J. P. Perdew, *Phys. Rev. B* 1977, **15**, 2884.
[41] J. Harris, *Phys. Rev. A* 1984, **29**, 1648.
[42] A. D. Becke, *J. Chem. Phys.* 1993, **98**, 1372.
[43] A. D. Becke, *J. Chem. Phys.* 1993, **98**, 5648.
[44] P. J. Stephens, F. J. Devlin, C. F. Chabalowski, and M. J. Frisch, *J. Phys. Chem.* 1994, **98**, 11623.
[45] C. Adamo and V. Barone, *J. Chem. Phys.* 1999, **110**, 6158.

[46] F. A. Hamprecht, A. J. Cohen, D. J. Tozer and N. C. Handy, *J. Chem. Phys.* **109**, 1998, 6264-6271.
[47] A. D. Becke, *J. Chem, Phys.* 1997, **107**, 8554.
[48] H. S. Yu, X. He, S. Li, and D. G. Truhlar, *Chem. Sci.* 2016, DOI: 10.1039/c6sc00705h
[49] J.-D. Chai and M. Head-Gordon, *J. Chem. Phys.* 2008, **128**, 084106.
[50] J. Toulouse, F. Colonna, and A. Savin, *Phys. Rev. A* 2004, **70**, 062505.
[51] T. Yanai, D. Tew, and N. C. Handy, *Chem. Phys. Lett.* 2004, **393**, 51.
[52] I. C. Gerber and J. C. Ángyán, *Chem. Phys. Lett.* 2005, **415**, 100.
[53] O. A. Vydrov and G. E. Scuseria, *J. Chem. Phys.* 2006, **125**, 234109.
[54] J.-W. Song, S. Tokura, T. Sato, M. A. Watson, and K. Hirao, *J. Chem. Phys.* 2007, **127**, 154109.
[55] J. D. Chai and M. Head-Gordon, *Phys. Chem. Chem. Phys.* **10**, 6615 (2008) .
[56] R. Peverati and D. G. Truhlar, *J. Phys. Chem. Lett.* 2011, **2**, 2810.
[57] C. W. Tsai, Y. C. Su, G. D. Li, and J. D. Chai, *Phys. Chem. Chem. Phys.* 2013, **15**, 8352.
[58] R. Peverati and D. G. Truhlar, *Phys. Chem. Chem. Phys.* 2012, **14**, 16187.
[59] J. Heyd, G. E. Scuseria, and M. Ernzerhof, *J. Chem. Phys.* 2003, **118**, 8207.
[60] N. W. Ashcroft and N. D Mermin, *Solid State Physics* (Saunders College, Philadelphia, 1976), pp. 337-344
[61] Y. Guo, J. Robertson, and S. J. Clark, *J. Phys.: Condens. Matter* 2015, **27**,025501.
[62] B. G. Janesko, T. M. Henderson, and G. E. Scuseria, *Phys. Chem. Chem. Phys.* 2009, **11**, 4443.
[63] T. M. Henderson, A. F. Izmaylov, G. E. Scuseria, and A. Savin, *J. Chem. Theory Comp.* 2008, **4**, 1254.
[64] R. Peverati and D. G. Truhlar, *J. Phys. Chem. Lett.* 2012, **3**, 117.
[65] R. Peverati and D. G. Truhlar, *Phil. Trans. R. Soc. A* 2014, **372**, 20120476.
[66] F. London, *Trans. Faraday Soc.* 1937, **33**, 8b-26.
[67] K. Szalewicz, *Wiley Interdiscip. Rev.: Comput. Mol. Sci.*, 2012, **2**, 254.
[68] S. Grimme, J. Antony, S. Ehrlich, and H. Krieg, *J. Chem. Phys.* 2010, **132**, 154104.
[69] S. Grimme, S. Ehrlich, and L. Goerigk, *J. Comput. Chem.* 2011, **32**, 1456.
[70] Y. Zhao and D. G. Truhlar, *J. Phys. Chem. A* 2005, **109**, 5656.
[71] L. Goerigk and S. Grimme, *J. Chem. Theory Comput.* 2010, **6**, 107.
[72] L. Goerigk and S. Grimme, *J. Chem. Theory Comput.* 2011, **7**, 291.
[73] L. Goerigk and S. Grimme, *Phys. Chem. Chem. Phys.* 2011, **13**, 6670.
[74] J. Wellendorff, K. T. Lundgaard, A. Møgelhøj, V. Petzold, D. D. Landis, J. K. Nørskov, T. Bligaard, and K. W. Jacobsen, *Phys. Rev, B* 2012, **85**, 235149.
[75] N. Mardirossian and M. Head-Gordon, *Phys. Chem. Chem. Phys.* 2014, **16**, 9904.

[76] O. Vydrov and T. V. Voorhis, *J. Chem. Phys.* 2010, **133**, 244103.
[77] N. Mardiossian and M. Head-Gordon, *J. Chem. Phys.* 2015, **142**, 074111.
[78] Y. Zhao, B. J. Lynch, and D. G. Truhlar, *J. Phys. Chem. A* 2004, **108**, 2715.

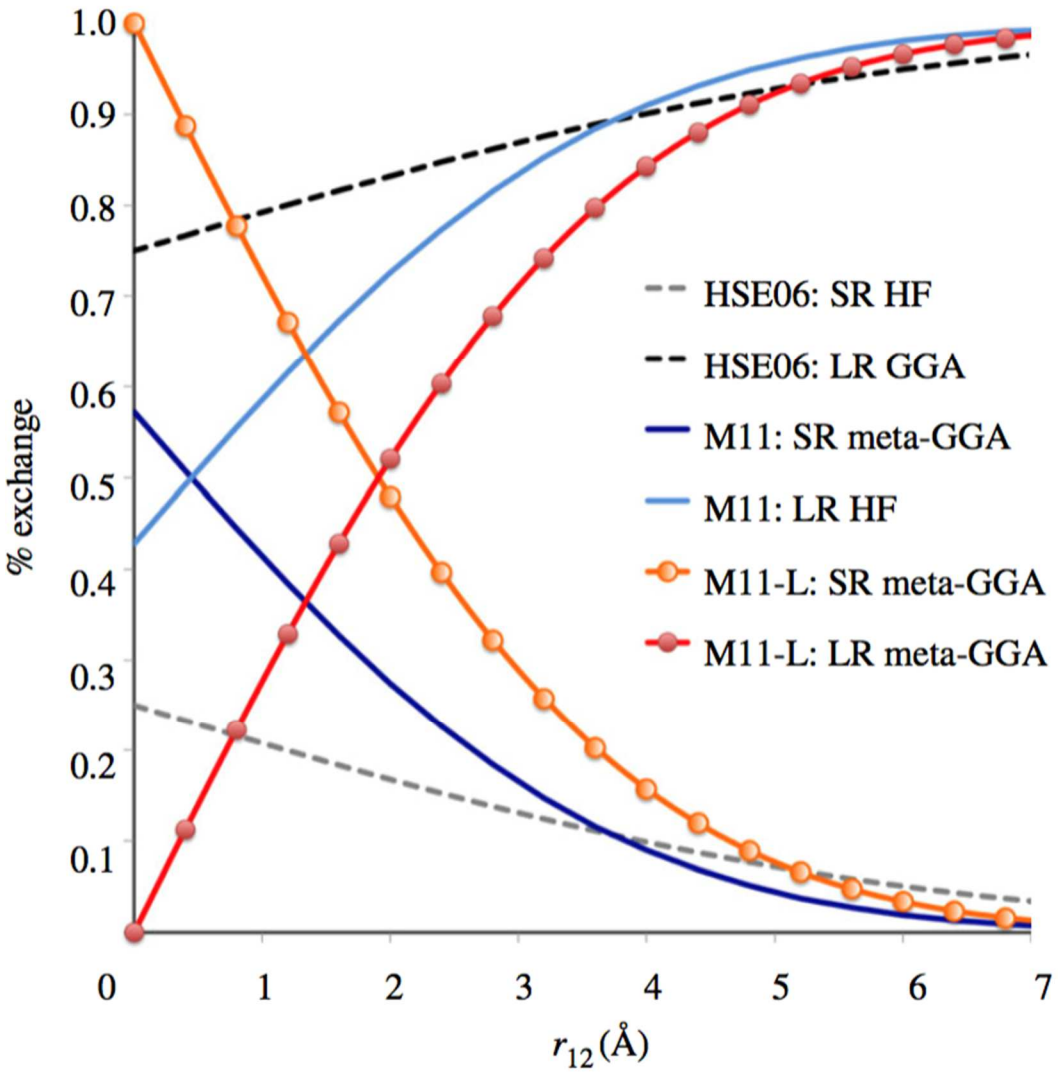

Figure 1.1 Difference between three kinds of range separation: screened exchange (HSE06, dashed shades of black), long-range corrected exchange (M11, solid shades of blue), and dual-range exchange (M11-L, solid with dots, shades of red) functionals.

Chapter 2. Development of Minnesota Database 2015B

Adapted with permission from:

H. S. Yu, X. He, S. Li, and D. G. Truhlar, Chem. Sci. 2016, DOI: 10.1039/c6sc00705h

R. Peverati and D. G. Truhlar, Phil. Trans. R. Soc. A 2014, 372, 20120476.

W. Zhang, D. G. Truhlar, and M. Tang, J. Chem. Theory Comput. 2013, 9, 3965.

S. Luo, B. Averkiev, K. R. Yang, X. Xu, and D. G. Truhlar, J. Chem. Theory Comput. 2014, 10, 102.

K. Yang, R. Peverati, D. G. Truhlar, and R. Valero, J. Chem. Phys. 2011, 135, 044118.

2.1 Introduction to Database 2.0

Many databases have been collected and used throughout the years by our group for the application and development of DFT. Here I am going to explain one of the largest databases developed by our group in 2012, which is called Database 2.0.[1] The Database 2.0 contains four comprehensive databases, representing energetic and structural properties for chemistry and physics, which are CE345 (chemistry energetic database with 345 data), PE39 (physics energetic database with 39 data), CS20 (chemistry structural database with 20 data), and PS47 (physics structural database with 47 data). Each of these four categories has its own subset, which are show in Table 2.1. Each database is dubbed with an acronym representing the particular property considered (e.g. MGAEs for main-group atomization energies), followed by the number of data in the subset (e.g. 109 data), and eventually—if there has been more than one version—by the last two digits of the year of latest version of the database (e.g. 11 for

2011); if the is not specified, it means that the database is at its first generation and no revision of its data has ever been made. These rules not only applies to Database 2.0 but also Minnesota Database 2015B.

All energetic data in the Database 2.0 are Born-Oppenheimer potential energy difference without zero-point energy or thermal vibrational, rotational or translational contributions. The chemistry energetic database, CE345, has 15 non-overlapping subsets of different properties; Calculations are performed at fixed geometries so that all methods are compared at the same set of predetermined geometries, which are presented in Table 2.1. The systems, basis sets, geometries, and references of each of these 15 subsets are explained below:

— *Main-group atomization energies* (*MGAE109/11*). The MGAE is composed of 109 atomization energies. It was introduced as an expansion of Database/3[2] and Database/4[3] and was first used for DFT development in the test set of the M05 functional.[4] The database was most recently updated in 2011[5] by using more accurate reference data from W4,[6] W4.2,[6] W4.3[6], and W4.4[7] calculations. Geometries for all molecules are obtained at the QCISD/MG3 level of theory,[8] and we used the MG3S basis set for single-point energies.[9]

— *Single-reference metal bond energies* (*SRMBE13*). This database and the next one for multi- reference bond energies were recently formulated[10] and expanded[11], based on previous work on systems containing metals.[12,13] The first four data in this database are the bond dissociation energies for diatomic molecules containing

metals that have positive MP2 binding energies, in particular: Ag_2, CuAg, Cu_2 and Zr_2. The next eight data are extracted from a previous database by choosing those that have B1 diagnostics[13] smaller than 10 kcal mol^{-1} , in order to include only data with single-reference character: AgH, CoH, $Cr(CH_3)^+$, $Cu(H_2O)^+$, FeH, LiCl, LiO and $V(CO)^+$. The final datum was added recently[11] by adding the bond energy for AlCl[14]. We used the def2-TZVP basis set[15,16] for the SRMBE13 database. Bond energies for all molecules in this database are equilibrium ones (D_e), obtained from the experimental bond energy in the ground vibrational state (D_0).

— *Multi-reference bond energies* (*MRBE10*). This database contains 10 systems with high multi-reference character. Five data come from a previous database of multi-reference metal bond energies (MRMBE5[10]): Cr_2, V_2, $Ni(CH_2)^+$, $Fe(CO)_5$ and VS. Bond energies for these molecules are bond energy at equilibrium (D_e), obtained from the experimental bond energy in the ground vibrational state (D_0), as for the previous database. The remaining five data are taken from Karton *et al*.[14] and do not involve metals. All these data have high multi-reference character according to the %[(T)] diagnostic[6] (they all also have B1 diagnostics[13] greater than 10 kcalmol^{-1}), and the detailed dissociation reactions are: $B_2 \rightarrow 2B$, $O_3 \rightarrow O_2 + O$, $C_2 \rightarrow 2C$, $S_4 \rightarrow 2S_2$ and $Cl_2O \rightarrow Cl_2 + O$. Geometries for these five

reactions are obtained at the QCISD/MG3 level of theory[8]. For the MRBE10 database, we used the def2-TZVP basis set.[15,16]

— *Isomerization of large organic molecules* (*IsoL6/11*). This database was introduced in order to include larger molecules in the training and performance evaluation of density functionals, and it is based on a larger database from Grimme, called IsoL22[17]. However, as some of the reference data in the original IsoL22 are questionable, we[18] recalculated the reference energy for six of the smallest molecules in Grimme's database by using the accurate CCSD(T)-F12a/aug-cc-pVDZ method[19,20,21,22,23], and collected the results in the IsoL6/11 set. Geometries for this set are taken from the original work of Grimme and co-workers[17] and are optimized at the B97-D/TZVP level[24,25]. For this database, we used the MG3SXP basis set[26].

— *Ionization potentials* (*IP21*). The ionization potential (IP) database[27] contains data from six main-group atoms (C, S, O, P, Si and Cl), seven transition metal atoms (Cr, Cu, Mo, Pd, Rh, Ru and Zn) and eight molecules (SH, Cl_2, OH, O_2, PH, PH_2, S_2 and FeC). Calculations on molecules involve separately optimized geometries for neutral molecules and cations. The equilibrium bond length of FeC is obtained[28] from the experimental bond length[29] in the ground vibrational state, while geometries for all other molecules are obtained at the QCISD/MG3[8] level of theory. We used the MG3S basis set[9] for the main-group atoms and all molecules

except FeC, for which we used the SDD + 2fg[30] basis for Fe and the def2-QZVPP basis[16] for C; we used the cc-pVTZ-DK basis set[31] for the transition metal atoms. The scalar relativistic effects are included in the calculations of the seven transition metal atomic IPs by using the Douglas–Kroll–Hess (DKH) second-order scalar relativistic Hamiltonian[32,33,34], while they are included in the calculations of FeC with the SDD relativistic effective core potential[30].

— *Electronic affinities* (*EA13/03*). The electronic affinities (EA) database [35,4,70,9] contains six main-group atoms (C, S, O, P, Si and Cl) and seven molecules (SH, Cl_2, OH, O_2, PH, PH_2 and S_2). Reference data and geometries are obtained at the QCISD/MG3 level of theory[8]. Calculations on molecules involve separately optimized geometries from neutral molecules and anions. For this database, we used the MG3S basis set[9].

— *Proton affinities* (*PA8/06*). The proton affinities (PA) database[36] contains the proton affinities of the following small molecules: NH_3, H_2O, C_2H_2, SiH_4, PH_3, H_2S, HCl and H_2. As for the previous two sets, calculations involve separately optimized geometries from neutral and charged (in this case protonated) molecules. Geometries are obtained at the MP2/6-31G(2df,p) level of theory. For this database, we used the MG3S basis set[9].

— *Alkyl bond dissociation energies* (*ABDE12*). This database is a merger of ABDE4/05 and □ABDEL8. ABDE4/05 contains four bond dissociation energies

of small R–X organic molecules, with R = methyl and isopropyl, and X = CH_3 and OCH_3. D_0 values were taken from a paper by Izgorodina *et al*.[37], and we used the B3LYP/6-31G(d) zero-point vibrational energies scaled with a scale factor of 0.9806 to obtain our best estimate of the D_e values in the database. For this database, we used the MG3S basis set[9]. ABDEL8 is from a 2011 paper[10].

— *Hydrocarbon chemistry* (*HC7*/*11*). This database consists of seven cases of hydrocarbon data that are sensitive to medium-range correlation energy. HC7 is the combination of the HC5 database[38] with two isodesmic reactions (involving adamantane and bicycle [2.2.2] octane) that were singled out as difficult cases by Grimme. All geometries are obtained at the MP2/6-311+G(d,p) level of theory. The original reference data for this database were published in the original paper[39], and some inconsistencies in the reference data were corrected[10]. For this database, we used the 6-311+G(2df,2p) basis set[40].

— *Thermochemistry of* π *systems* (π*TC13*). This database containing π systems[4,41] is composed of three isomeric energy differences between allene and propyne as well as higher homologues (which correspond to cumulenes and polyenes—this subset is called π IE3/06), five proton affinities of conjugated polyenes (PA-CP5/06) and five proton affinities of conjugated Schiff bases (PA-SB5/06). Geometries for all the molecules in this database are obtained at the MP2/6-31+G(d,p) level of theory, and we used the MG3S basis set[9].

— *Hydrogen transfer barrier heights* (*HTBH38*/*08*). This database contains 38 transition state barrier heights for 19 hydrogen transfer (HT) reactions, 18 of which involve radicals as reactant and product. Six reference data in the HTBH38 database were revised in 2008[42]. All geometries are obtained at the QCISD/MG3 level of theory[8]. For this database, we used the MG3S basis set[9]. All reactions in HTBH38/08 are isodesmic.

— *Non-hydrogen transfer barrier heights* (*NHTBH38*/*08*). The original version of this database was created in 2004[43] by joining three older databases containing 38 transition state barrier heights for non-hydrogen transfer (NHT) reactions. NHTBH38/08 contains 12 barrier heights for heavy-atom transfer reactions, 16 barrier heights for nucleophilic substitution (NS) reactions, and 10 barrier heights for non-NS unimolecular and association reactions. As for the previous case, geometries are obtained at the QCISD/MG3 level of theory[8]. Eighteen reference data in the NHTBH38 database were revised in 2008[42]. For this database, we used the MG3S basis set[9].

— *Non-covalent complexation energies* (*NCCE31*/*05*). Several databases have been developed in our group for various kinds of non-covalent interactions, and currently we use HB6/04[44], CT7/04[44], DI6/04[44], WI7/05[45] and PPS5/05[45]. The geometries for the benzene dimers in the NCCE31/05 database are taken from Sinnokrot & Sherrill[46], while geometries for all other molecules in this database are optimized at the MC-QCISD/3 level [2,47]. For this database, we used the MG3S

basis set[9].

— *Difficult cases* (*DC9*/*12*). In this database of difficult cases for DFT, we used the data from our previous DC10 database and omitted the datum for the atomization energy of ozone. The omission is to avoid a repetition in the database, as ozone is also present in the MRBE10 set. The /12 suffix was added to the name to avoid confusion with a database by Grimme which is called DC9, but contains different data. All geometries are obtained at the MP2/6-311+G(d,p) level of theory[8], while we used the MG3S basis set[9] for the calculations.

— *Atomic energies* (*AE17*). Total atomic energies of the atoms from H to Cl. Reference data are from[48]. We recently updated the basis set for this database to use a more complete basis set that includes core-polarization functions; in particular, we now use the □cc-pwCV5Z basis set[49] for H, He and atoms from Be to Ne and from Al to Ar, while we used the cc-pCVQZ basis set[50] for Li, Be, Na and Mg atoms.

The solid-state physics energetic set, PE39, has two non-overlapping primary subsets containing, respectively, cohesive energies and band gaps. For this set, the lattice constants of the solids were reoptimized for each method studied. The primary subsets that compose the physics energetic database are as follows.

— *Solid-state cohesive energies* (*SSCE8*). This set includes the cohesive energies of eight solids: C, Si, SiC, Ge, NaCl, NaF, LiCl and LiF. We first used this

database for the evaluation of the SOGGA functional[51]; reference data are taken from 52, and the geometry of each solid is optimized for each method. For this database, we used the m-6-311G* basis set.[53]

— *Semiconductors band gaps* (*SBG31*). This database was recently created for the evaluation of the performance of our M11-L functional.[54] It contains band gaps for four unary semiconductors from group 14 (C, Ge, Si, SiC), six binary semiconductors from groups 2 and 16 (MgS, MgSe, MgTe, BaS, BaSe, BaTe), 14 binary semiconductors from groups 13 and 15 (BP, BAs, AlP, AlAs, AlSb, GaN, β-GaN, GaP, GaAs, GaSb, InN, InP, InAs, InSb), and seven binary semiconductors composed of group 12 and an element from group 16 (ZnO, ZnS, ZnSe, ZnTe, CdS, CdSe, CdTe). Reference data are taken from 53,55,56. In this database, we follow the usual convention of comparing single-particle gaps from calculations (that is, band energy gaps, which are the crystal analogue of orbital energy gaps in molecules) with experimental optical gaps. Band gaps are calculated at the optimized geometry for each method. For this database, we used the m-6-311G* basis set.[53]

The chemistry structural database, CS20, is composed of two non-overlapping primary subsets containing a total of 20 geometrical data. The primary structural databases are as follows.

— *Main-group hydrogenic bond lengths* (*MGHBL9*). The MGHBL9 database of

the structural set contains nine hydrogenic bond lengths[51]. For this database, we used the 6- 311+G(2df,2p) basis set.[40]

— *Main-group non-hydrogenic bond lengths* (*MGNHBL11*). This set contains 11 non- hydrogenic bond lengths and is composed of nine data from the older MGNHBL10 set[51], with the addition of the bond length of MgS[57]. For this database, we used the 6-311+G(2df,2p) basis set.[40]

Finally, the solid-state physics structural database, PS47, is composed of four non-overlapping primary subsets containing a total of 47 structural data from 44 solids, as follows.

— *Main-group lattice constants* (*MLC4*). The main-group solid-state lattice constants set is composed of four main-group metals: Li, Na, K and Al. Reference data were taken from[52]. For this database, we used the m-6-311G* basis set[53].

— *Ionic lattice constants* (*ILC5*). The ionic solid-state lattice constants set is composed of five ionic solids: NaCl, NaF, LiCl, LiF and MgO. Reference data were taken from[52]. For this database, we used the m-6-311G* basis set[53].

— *Transition metals lattice constants* (*TMLC4*). The transition metals solid-state lattice constants set is composed of four transition metals: Cu, Rh, Pd and Ag. Reference data were taken from[52]. For this database, we used the m-6-311G* basis set[53].

— *Semiconductors lattice constants* (*SLC34*). This database[54] is composed of the lattice constants of the same semiconductors as in SBG31; the difference of three data from the number of data in the band gaps database is explained by the fact that three solids with wurtzite structure (GaN, InN, ZnO) require the specification of two lattice constants. Reference data are equilibrium values [53,58,59,60,61] obtained by removing the zero-point anharmonic expansion so that we can directly compare our calculated results with the experimental data.

In order to improve the performance of Minnesota functionals, we enlarge our training database by adding different components including transition metal bond energies, atomic excitation energies, more noncovalent interactions, sulfur molecule atomization energies, more alkyl bond dissociation energies, and diatomic geometries of heavy-atom molecules to the Database 2.0, which will be discussed in the following sections

2.2 Transition Metal Bond Energies

2.2.1 3d Transition-Metal-Containing Molecules

One of the greatest challenges for density functional theory is the treatment of intrinsically multiconfigurational atoms and molecules, especially transition-metal-containing compounds. In order to develop better density functional, we studied the 70 first-transition-row (3d) transition-metal-containing molecules (19 single-reference molecules and 51 multi-reference molecules) by 42 exchange-correlation functionals.[62]

It is observed that adding HF exchange does not guarantee better accuracy for GGAs or for NGA, but inclusion of the kinetic energy densities can benefit the GGAs and NGA calculations. The metal hydrides and metal oxides are demonstrated to be the most difficult bond types to predict, and CrO_3, FeH, CrO, VH, and MnS are found to be the most difficult molecules to predict. The middle transition metals (V, Cr, and Mn) lead to larger errors on average than either the early or late transition metals. We did representative analysis separately for the single-reference subset and the multi-reference subset. Six molecules are selected from each of the subset since the percentage errors in representation (PEIR, see definition in ref. 63) resulted from them are only 15.0% and 11.3%, respectively. The single-reference representative database contains the following six molecules: ZnCl, ZnSe, $CrCl_2$, MnF_2, $FeCl_2$, and $CoCl_2$. The multi-reference representative database contains the following six molecules: TiCl, VF_5, CrCl, CrOF, $(FeBr_2)_2$, and $Co(CO)_4H$. In another paper we publish recently, we compared the DFT calculations and Coupled Cluster calculations against best available experimental data for dissociation energies of bonds to 3d transition metals.[64] We selected one single-reference system FeCl and four multi-reference systems CuH, VO, CuCl, and NiCl, and add them into our latest Minnesota Database 2015B.[65]

2.2.2 Palladium Complex Bond Energies

We studied $Pd(PH_3)_2$ and $Pt(PH_3)_2$ complexes with ethane and conjugated C_nH_{n+2} systems (n = 4, 5, 8, and 10).[66] We selected two complexes $Pd(PH_3)_2C_6H_8$ and $Pd(PH_3)_2C_{10}H_{12}$ and add them into the latest Minnesota Database 2015B.[65] As it is stated

in reference 66, there are two possible conformations for $Pd(PH_3)_2C_{10}H_{12}$ and here we chose the less planar conjugated conformation (denoted as 10b in reference 66) as it has an energy of about 2 kcal/mol lower than the other one (denoted as 10a in reference 66).

2.3 Atomic Excitation Energies

2.3.1 3d Transition Metal Atomic Excitation Energies

The 3d-series transition metal, Sc to Zn, are very important in industry and biology, but they provide unique challenges to computing the electronic structure of their compounds. We studied the 3d transition metal atoms and their cations.[67] We analyze the results using three ways to compute the energy of the open-shell states: the direct variational method, the weighted-averaged broken symmetry (WABS) method, and a new broken-symmetry method called the reinterpreted broken symmetry (RBS) method. By examining the overall accuracy in treating 18 multiplicity-changing excitations and 10 ionization potentials with the RBS method, we found 10 functionals that have a mean-unsigned error smaller than 5 kcal/mol, with ωB97X-D topping the list. Among these excitation energies we selected six 3d transition metal atoms or cations, namely, Sc, V, Mn^+, Fe, Ni^+, and Zn. Besides, Ca^+ is also selected because of its excitation from Ca^+(4s) state to Ca^+ (3d) state.[68]

2.3.2. 4d Transition Metal Atomic Excitation Energies

We studied all 4d transition metal atoms of groups 3-10 (Y to Pd) and their singly positive cations by 60 density functionals of 10 different types.[69] All 16 excitation

energies connecting the ground states to their first excited states of different multiplicities, and all eight ionization potentials are predicted by these 60 functionals. By analyzing the fractional subshell occupancies and spin contaminations, we are able to sort out the effects of s orbital vs. d orbital bias and high-spin vs. low-spin bias. We conclude that a reliable functional should have little or no bias of either type rather than succeeding for a limited subset of cases by cancellation of errors. The widely used correlations of spin splittings to percentage of HF exchange are not borne out by the data, and the correlation functional also play significant role. In order to develop a diverse database for training density functionals, we add five of these 4d transition metal atoms or cations, namely, Mo^+, Ru^+, Rh^+, Pd^+, and Y^+ to our latest Minnesota Database 2015B.[65]

2.3.3 p-block Atomic Excitation Energies

We studied a database containing 17 multiplicity-changing valence and Rydberg excitation energies of p-block elements by exchange-correlation functionals.[70] We consider only systems where both the low-spin and high-spin state are well described by a single Slater determinant, thereby avoiding complications due to broken-symmetry solutions. Most density functionals give mean unsigned errors (MUEs) larger 6 kcal/mol for valence excitations and MUEs larger than 3 kcal/mol for Rydberg excitations. We found out that the long-range corrected functionals, which have 100% HF exchange at large inter-electronic distance, do not improve the performance for Rydberg excitations. Among all tested density functionals, O3LYP, M08-HX, and OLYP give the best overall performance for both valence and Rydberg excitations, with MUEs of 2.1, 2.6, and 2.7

kcal/mol. From this database (17 excitation energies of p-block elements), we select F, Ar, C^+, Al, and Si^+ as the representative database and add them to Minnesota Database 2015B.[65]

2.4 Noncovalent Interactions

One of the advantages of the Minnesota Functionals is that they are able to capture the mid-range van der Waals interactions. It is because by design we optimized the functional against a diverse set of weak interactions, which make the functionals have built-in van der Waals interactions. In order to further improve the performance of our functionals, we add in the following two databases, noble gas dimer weak interactions and a representative database of S66x8 database.[71]

2.4.1 Noble Gas Dimer Weak Interactions

This database is composed of seven noble gas dimers, four of which are taken from the previous NCCE31/05 database from Database 2.0[1] and three of them are new dimers, He2, Ar2, and Kr2. For each dimer, three data points are selected from the potential energy curve,[72] where one of them is the equilibrium point and the other two points are 0.3 A away from the equilibrium point (on either side). This results in 21 data points.

2.4.2 The S66 and S66x8 Databases

The S66 and S66x8 databases[71] were developed primarily for the validation of new quantum chemical method. The S66 database contains accurate interaction energies

for 66 noncovalently bound complexes, and it is divided into three sub-databases: complexes that are damped-dispersion-dominated (DD23), hydrogen-bonding complexes (HB23), and complexes dominated by a mix of damped dispersion and electrostatics (Mix20). The S66x8 contains not only the S66 as a subset but also interaction energies of the 66 complexes at seven other intersubsystem distances, ranging from 0.9 times the van der Waals distance to 2.0 times van der Waals distance. From the S66x8 we select six complexes at six distances (0.90, 0.95, 1.00, 1.05, 1.10, and 1.25 times the van der Waals distance). The resulting subset is called S6x6, which is added to Minnesota Database 2015B.[65]

2.5 Alkyl Bond Dissociation Energy

In a recent paper, we studied bond dissociation enthalpies of unsaturated methyl esters and methyl linolenate with density functional theory and coupled cluster theory.[73] We found that several Kohn-Sham exchange-correlation functionals are very useful for modeling ester combustion, especially the global hybrid functionals M08-HX, M06-2X, M05-2X, M08-SO, and MPWB1K, range-separated-hybrid meta functionals M11 and MN12-SX, the range-separated hybrid gradient approximation functional ωB97, and the global-hybrid gradient approximation functional SOGGA11-X. Among the C-H and C-C bond dissociation of seven fragment molecules of methyl linolenate, we select 13 bond dissociation energies and add them into Minnesota Database 2015B.[65]

2.6 Main-Group Diatomic Molecules

In a recent paper, we studied various chemical properties of 15 main-group diatomic molecules with fifty-three exchange-correlation functionals of 11 types.[74] We divide these fifteen molecules into two groups based on various diagnostics,[74] multi-reference systems (MR7) and single-reference systems (SR8). Then we select four representative molecules CaO, LiO^-, KO^-, and MgS from MR7 and three representative molecules KOH, NaO, and LiO from SR8 and add them into the Minnesota Database 2015B.[65]

2.7 Other Tpyes of New Databases

Comparing to the database 2.0,[1] the above databases (from section 2.2 to 2.5) and the following data are added to form the Minnesota Database 2015B[65]: the bond energy of Fe_2,[75] the first vertical excitation energy of Fe_2,[75] the atomization energies of SO_3,[76] H_2S_2,[77] and H_2SO_4,[78] the isomerization energies of four molecules containing 2p block atoms (C, N, O, and F) and four molecules containing 4p block atoms (Ge, As, Se, and Br),[79] and diatomic geometries for molecules with one or more heavy atoms (ZnS,[80] HBr,[80] NaBr, [80] and Ag_2[81]).

2.8 Summary

Combining the chemical energy and chemistry geometries from Database 2.0 and all the above databases, we built the largest database from our group, called Minnesota Database 2015B. In Table 2.2 we showed all the databases with their acronyms and brief

descriptions. In order to compare the functionals for different categories of data, we used the following combinations of subdatabases explained more fully in Table 2.2:

- MGBE150: 150 main-group bond energies, in particular SR-MGM-BE9, SR-MGN-BE107, MR-MGM-BE4, MR-MGN-BE17, and ABDE13
- TMBE33: 33 transition metal bond energies, in particular SR-TM-BE17, MR-TM-BE13, and MR-TMD-BE3
- BH76: 76 reaction barrier heights, in particular HTBH38 and NHTBH38
- EE18: 18 excitation energies, in particular 3dEE8, 4dAEE5, and pEE5
- IsoE14: 14 isomerization energies, in particular IsoL6, 4pIsoE4, and 2pIsoE4
- HCTC20: 20 hydrocarbon thermochemical data, in particular πTC13 and HC7
- MS10: 10 molecular structures, in particular DGL6 and DGH4

2.9 References

[1] R. Peverati and D. G. Truhlar, *Phil. Trans. R. Soc. A* 2014, **372**, 20120476.
[2] B. J. Lynch and D. G. Truhlar, *J. Phys. Chem. A* 2003, **107**, 3898.
[3] B. J. Lynch, Y. Zhao, and D. G. Truhlar, *J. Phys. Chem. A* 2005, **109**, 1643.
[4] Y. Zhao, N. E. Schultz, and D. G. Truhlar, *J. Chem. Theory Comput.* 2005, **2**, 364.
[5] R. Peverati and D. G. Truhlar, *J. Chem. Phys.* 2011, **135**, 191102.
[6] A. Karton, E. Rabinovich, J. M. L. Martin, and B. Ruscic, *J. Chem. Phys.* 2006, **125**, 144108.
[7] A. Karton, P. R. Taylor, and J. M. L. Martin, *J. Chem. Phys.* 2007, **127**, 064104.
[8] J. A. Pople, M. Head-Gordon, K. Raghavachari, *J. Chem. Phys.* 1987, **87**, 5968.
[9] B. J. Lynch, Y. Zhao, and D. G. Truhlar, *J. Phys. Chem. A* 2003, **107**, 1384.
[10] R. Peverati, Y. Zhao, and D. G. Truhlar, *J. Phys. Chem. Lett.* 2011, **2**, 1991.
[11] R. Peverati and D. G. Truhlar, *J. Phys. Chem. Lett.* 2012, **3**, 117.
[12] N. E. Schultz, Y. Zhao, and D. G. Truhlar, *J. Phys. Chem. A* 2005, **109**, 4388.
[13] N. E. Schultz, Y. Zhao, and D. G. Truhlar, *J. Phys. Chem. A* 2005, **109**, 11127.
[14] A. Karton, A. Tarnopolsky, J-F. Lamere, G. C. Schatz, J. M. L. Martin, *J. Phys. Chem. A* 2007, **112**, 12868.

[15] F. Weigend, M. Haser, H. Patzelt, and R. Ahlrichs, *Chem. Phys. Lett.* 1998, **294**, 143.
[16] F. Weigend and R. Ahlrichs, *Phys. Chem. Chem. Phys.* 2005, **7**, 3297.
[17] R. Huenerbein, B. Schirmer, J. Moellmann, and S. Grimme, *Phys. Chem. Chem. Phys.* 2010, **12**, 6940.
[18] S. Luo, Y. Zhao, and D. G. Truhlar, *Phys. Chem. Chem. Phys.* 2011, **13**, 13683.
[19] R. A. Kendall, T. H. Dunning, and R. Harrison, *J. Chem. Phys.* 1991, **96**, 6796.
[20] G. Purvis and R. J. Bartlett, *J. Chem. Phys.* 1982, **76**, 1910.
[21] K. Raghavachari, G. W. Trucks, J. A. Pople, and M. Head-Gordon, *Chem. Phys. Lett.* 1989, **157**, 479.
[22] G. Knizia, T. B. Adler, and H-J. Werner, *J. Chem. Phys.* 2009, **130**, 054104.
[23] J. Noga, S. Kedžuch, J. Šimunek, and S. Ten-no, *J. Chem. Phys.* 2008, **128**, 174103.
[24] S. Grimme, *J. Comput. Chem.* 2006, **27**, 1787.
[25] A. Schäfer, C. Huber, and R. Ahlrichs, *J. Chem. Phys.* 1993, **100**, 5829.
[26] Y. Zhao and D. G. Truhlar, *J. Chem. Theory Comput.* 2008, **4**, 1849.
[27] R. Peverati and D. G. Truhlar, *Phys. Chem. Chem. Phys.* 2012, **14**, 13171.
[28] R. Li, R. Peverati, M. Isegawa, and D. G. Truhlar, *J. Phys. Chem. A* 2012, **117**, 169.
[29] W. J. Balfour, J. Cao, C.V.V. Prasad, and C.X.W. Qian, *J. Chem. Phys.* 1995, **103**, 4046.
[30] J.M.L. Martin and A. Sundermann, *J. Chem. Phys.* 2001, **114**, 3408.
[31] K. A. Peterson, D. Figgen, M. Dolg, and H. Stoll, *J. Chem. Phys.* 2007, **126**, 124101.
[32] M. Douglas and N.M. Kroll, *Ann. Phys.* 1974, **82**, 89.
[33] B.A. Hess, *Phys. Rev. A* 1986, **33**, 3742.
[34] G. Jansen and B. A. Hess, *Phys. Rev. A* 1989, **39**, 6016.
[35] Y. Zhao, N.E. Schultz, and D. G. Truhlar, *J. Chem. Phys.* 2005, **123**, 161103.
[36] Y. Zhao and D. G. Truhlar, *J. Phys. Chem. A* 2006, **110**, 10478.
[37] E. I. Izgorodina, M. L. Coote, and L. Radom, *J. Phys. Chem. A* 2005, **109**, 7558.
[38] Y. Zhao and D. G. Truhlar, *Org. Lett.* 2006, **8**, 5753.
[39] Y. Zhao and D. G. Truhlar, *Theor. Chem. Acc.* 2008, **120**, 215.
[40] W. J. Hehre, L. Radom, P. V. R. Schleyer, and J. A. Pople, *Ab initio molecular orbital theory* (New York, NY: Wiley, 1986)
[41] Y. Zhao and D. G. Truhlar, *J. Chem. Phys.* 2006, **125**, 194101.
[42] J. Zheng, Y. Zhao, and D. G. Truhlar, *J. Chem. Theory Comput.* 2009, **5**, 808.
[43] Y. Zhao, B. J. Lynch, and D. G. Truhlar, *Phys. Chem. Chem. Phys.* 2005, **7**, 43.
[44] Y. Zhao and D. G. Truhlar, *J. Chem. Theory Comput.* 2005, **1**, 415.
[45] Y. Zhao and D. G. Truhlar, *J. Phys. Chem. A* 2005, **109**, 5656.
[46] M. O. Sinnokrot and C. D. Sherril, *J. Phys. Chem. A* 2003, **108**, 10200.
[47] P. L. Fast and D. G. Truhlar, *J. Phys. Chem. A* 2000, **104**, 6111.
[48] S. Chakravorty, S. Gwaltney, E. R. Davidson, F. Parpia, and C. Fischer, *Phys. Rev. A* 1993, **47**, 3649.

[49] K. A. Peterson and T. H. Dunning, *J. Chem. Phys.* 2002, **117**, 10548.
[50] T. H. Dunning, *J. Chem. Phys.* 1988, **90**, 1007.
[51] Y. Zhao and D. G. Truhlar, *J. Chem. Phys.* 2008, **128**, 184109.
[52] V. N. Staroverov, G. E. Scuseria, J. Tao, and J. P. Perdew, *Phys. Rev. B* 2004, **69**, 075102.
[53] J. Heyd, J. E. Peralta, G. E. Scuseria, and R. L. Martin, *J. Chem. Phys.* 2005, **123**, 174101.
[54] R. Peverati and D. G. Truhlar, *J. Chem. Phys.* 2012, **136**, 134704.
[55] Y. Zhao and D. G. Truhlar, *J. Chem. Phys.* 2009, **130**, 074103.
[56] R. Matz and H. Lütz, *Appl. Phys.* 1979, **18**, 123.
[57] R. Peverati and D. G. Truhlar, *J. Chem. Theory Comput.* 2012, **8**, 2310.
[58] P. Haas, F. Tran, and P. Blaha, *Phys. Rev. B* 2009, **79**, 085104.
[59] L. Schimka, J. Harl, and G. Kresse, *J. Chem. Phys.* 2011, **134**, 024116.
[60] P. Hao, Y. Fang, J. Sun, G. I. Csonka, P. H. T. Philipsen, and J. P. Perdew, *Phys. Rev. B* 2012, **85**, 014111.
[61] R. R. Reeber, *J. Appl. Phys.* 1970, **41**, 5063.
[62] W. Zhang, D. G. Truhlar, and M. Tang, *J. Chem. Theory Comput.* 2013, **9**, 3965.
[63] J. Zhang, Y. Zhao, and D. G. Truhlar, *J. Chem. Theory Comput.* 2007, **3**, 569.
[64] X. Xu, W. Zhang, M. Tang, and D. G. Truhlar, *J. Chem. Theory Comput.* 2015, **11**, 2036.
[65] H. S. Yu, X. He, S. L. Li, and D. G. Truhlar, Chem. Sci. 2016, DOI: 10.1039/c6sc00705h
[66] B. Averkiev, Y. Zhao, and D. G. Truhlar, *J. Mol. Cata. A: Chem.* 2010, **324**, 80.
[67] S. Luo, B. Averkiev, K. R. Yang, X. Xu, and D. G. Truhlar, *J. Chem. Theory Comput.* 2014, **10**, 102.
[68] H. S. Yu and D. G. Truhlar, *J. Chem. Theory Comput.* 2014, **10**, 2291.
[69] S. Luo and D. G. Truhlar, *J. Chem. Theory Comput.* 2012, **8**, 4112.
[70] K. Yang, R. Peverati, D. G. Truhlar, and R. Valero, *J. Chem. Phys.* 2011, **135**, 044118.
[71] J. Řezáč, K. E. Riley, and P. Hobza, *J. Chem. Theory Comput.* 2011, **7**, 2427.
[72] K. T. Tang and J. P. Toennies, *J. Chem. Phys.* 2003, **118**, 4976.
[73] X. Li, X. Xu, X. You, and D. G. Truhlar, *J. Phys. Chem. A*, 2016, *Accepted*.
[74] H. Yu and D. G. Truhlar, *J. Chem. Theory Comput.* 2015, **11**, 2968.
[75] C. E. Hoyer, L. G. Manni, D. G. Truhlar, and L. Gagliardi, *J. Chem. Phys.* 2014, **141**, 204309.
[76] Sulfur Trioxide. National Institute of standards and Technology (NIST). http://webbook.nist.gov/cgi/cbook.cgi?ID= C7446119&Units=SI (accessed on July 26, 2015).
[77] HSSH. National Institute of standards and Technology (NIST). http://webbook.nist.gov/cgi/cbook.cgi?ID=C63344865&Units=SI (accessed on July

26, 2015).
[78] Sulfuric Acid. National Institute of standards and Technology (NIST). http://webbook.nist.gov/cgi/cbook.cgi?ID= C7664939&Units=SI&Mask=1#Thermo-Gas (accessed on July 26, 2015).
[79] T. Schwabe, *Phys. Chem. Chem. Phys.* 2014, **16**, 14559.
[80] http://cccbdb.nist.gov/expbondlengths1.asp, accessed on Oct. 29, 2014.
[81] A. Posada-Borbón and A. Posada-Amarillas, *Chem. Phys. Lett.* 2015, **618**, 66.

Table 2.1 Database 2.0

Subset	description	geometries
CE345		
MGAE109/11	Main-group atomization energies	QCISD/MG3
SRMBE13	Single-reference metal bond energies	experiment
MRBE10	Multi-reference bond energies	QCISD/MG3 and experiment
IsoL6/11	Isomerization energies of large molecules	B97-D/TZVP
IP21	Ionization potentials	QCISD/MG3 and experiment
EA13/03	Electron affinities	QCISD/MG3
PA8/06	Proton affinities	MP2/6-31G(d)
ABDE12	Alkyl bond dissociation energies	B3LYP/6-31G(d)
HC7/11	Hydrocarbon chemistry	MP2/6-311+G(d,p)
πTC13	Thermochemistry of π systems	MP2/6-31+G(d,p)
HTBH38/08	Hydrogen transfers barrier heights	QCISD/MG3
NHTBH38/08	Non-hydrogen transfers barrier heights	QCISD/MG3
NCCE31/05	Non-covalent complexation energies	MC-QCISD/3
DC9/12	Difficult cases	MP2/6-311+G(d,p)
AE17	Atomic energies	—
PE39		
SSCE8	Solid-state cohesive energies	Optimized
SBG31	Semiconductor band gaps	Optimized
CS20		
MGHBL9	Main-group hydrogenic bond lengths	Optimized
MGNHBL11	Main-group non-hydrogenic bond lengths	Optimized
PS47		
MGLC4	Main-group lattice constants	Optimized
ILC5	Ionic lattice constants	Optimized
TMLC4	Transition metal lattice constants	Optimized
SLC34	Semiconductor lattice constants	Optimized

Table 2.2 Database 2015B

n^a	Combined databases	Primary subsets	Secondary subset	Description
1-26	AME471			Atomic and Molecular Energies
1-4	MGBE150			Main-group bond energies
1		SR-MGM-BE9		Single-reference main-group metal bond energy
			SRM2	Single-reference main-group bond energies
			SRMGD5	Single-reference main-group diatomic bond energies
			3dSRBE2	3d single-reference metal-ligand bond energies
2		SR-MGN-BE120		Single-reference main-group non-metal bond energies
			SR-MGN-BE107	Single-reference main-group non-metal bond energies
			ABDE13	Alkyl bond dissociation energies
3		MR-MGM-BE4		Multi-reference main-group metal bond energies
4		MR-MGN-BE17		Multi-reference main-group non-metal bond energies
5-7	TMBE33			Transition metal bond energies
5		SR-TM-BE17		Single-reference TM^b bond energies
			3dSRBE4	3d single-reference metal-ligand bond energies
			SRMBE10	Single-reference metal bond energies
			PdBE2	Palladium complex bond energies
			FeCl	FeCl bond energy
6		MR-TM-BE13		Multi-reference TM bond energies
			3dMRBE6	3d multi-reference metal-ligand bond energies
			MRBE3	Multi-reference bond energies
			remaining	Bond energies of remaining molecules: CuH, VO, CuCl, NiCl
7		MR-TMD-BE3		Multi-reference TM dimer bond energies (Cr_2, and V_2)
				Multi-reference TM dimer bond energy (Fe_2)

8-9	BH76		Reaction barrier heights
8		HTBH38/08	Hydrogen transfer barrier heights
9		NHTBH38/08	Non-hydrogen transfer barrier heights
10-12	NC87		Noncovalent interactions
10		NCCE23	Noncovalent complexation energies (without charge transfer)
		CT7	Seven Charge transfer data
11		S6x6	Six dimers at six intermonomeric distances
12		NGDWI21	Noble gas dimer weak interaction
13-15	EE18		Excitation energies
13		3dEE8	3d TM atomic excitation energies and first excitation energy of Fe_2
14		4dAEE5	4d TM atomic excitation energies
15		pEE5	p-block excitation energies
16-18	IsoE14		Isomerization energies
16		4pIsoE4	4p isomerization energies
17		2pIsoE4	2p isomerization energies
18		IsoL6/11	Isomerization energies of large molecules
19-20	HCTC20		Hydrocarbon thermochemistry
19		πTC13	Thermochemistry of π systems
20		HC7/11	Hydrocarbon chemistry
21		EA13/03	Electron affinities
22		PA8	Proton affinities
23		IP23	Ionization potentials
24		AE17	Atomic energies
25		SMAE3	Sulfur molecules atomization energies
26		DC9/12	Difficult cases
27-29	MS10		Molecular structures

27	DGL6		Diatomic geometries of light-atom molecules
28-29	DGH4		
28		DGH3	Diatomic geometries of heavy-atom molecules: ZnS, HBr, NaBr
29		DGH1	Diatomic geometry of Ag_2

[a]In databases named X*n*, there are *n* data; in those named X*n*/*yy*, there are *n* data, and *yy* denotes the year of an update.
[b]TM denotes transition metal.

Chapter 3. The GAM Functional: "Nonseparable Exchange-Correlation Functional for Molecules, Including Homogeneous Catalysis Involving Transition Metals"

Adapted with permission from H. S. Yu, W. Zhang, P. Verma, and D. G. Truhlar, Phys. Chem. Chem. Phys. 2015, 17, 12146.

3.1 Introduction

Kohn-Sham (KS) density functional theory has been very successful for electronic structure calculations in both physics and chemistry.[1] The accuracy of KS calculations depends on the quality of the exchange–correlation functional. The quest for quantum mechanical methods that can be accurately applied to study atomic, molecular, and material properties has resulted in the design of exchange–correlation functionals with variety of ingredients, costs, and accuracies, where the accuracy may depend strongly on the kind of property that is calculated. Exchange–correlation functionals that depend only on spin-up and spin-down electronic densities (ρ_α and ρ_β) are known as local spin density approximations (LSDAs), and ones that depend on both the spin densities and spin density gradients are called gradient approximations (GAs, in particular GGAs and NGAs). More complicated functionals include ingredients calculated from the orbitals (which are functionals of the density), in particular spin-up and spin-down local kinetic energy densities (as in meta-GGAs and meta-NGAs), nonlocal Hartree–Fock exchange (as in hybrid functionals), and/or nonlocal correlation (as in doubly hybrid functionals, which have both nonlocal exchange and nonlocal correlation.). (One can also include nonlocal correlation without including nonlocal exchange.) Functionals depending only

on local variables, such as spin densities, their gradients, and spin-specific local kinetic energy densities, are often called local (especially in the chemistry literature, while the physics literature often labels them as semilocal if they include density gradients or spin kinetic energy densities).

Even though the meta and nonlocal functionals can give more accurate results than GGAs and LSDAs, GAs are still of great interest for four reasons. First, GAs are widely implemented in many programs because of their ease of coding. Second, GAs often have better self-consistent field (SCF) convergence and smaller grid requirements than meta functionals. Third, calculations employing GAs are less expensive than calculations involving nonlocal functionals, with the difference being more pronounced for extended and large systems and when geometries are optimized.

The fourth reason for special interest in GAs is that local functionals often have better performance than hybrid functionals, on average, for systems with high multi-reference character. Multi-reference character is the extent to which a wave function is inherently multi-configurational so that a single Slater determinant does not provide a good starting point (reference function) for approximating the complete wave function. Although KS theory does not calculate the wave function of the interacting system, it does use a Slater determinant to represent the density, and calculating the exchange from the Slater determinant, as in Hartree–Fock exchange, can introduce static correlation error, a result of which is that it is often more challenging to obtain good approximations for multi-reference systems when Hartree–Fock exchange is included. (The unknown

exact exchange–correlation energy functional includes nonlocal exchange effects and does not have static correlation error, but the problem just mentioned is not completely solved by currently available functionals). Multi-reference systems are sometimes called strongly correlated. Many open-shell systems and transition-metal systems have multi-reference character, and hence the ability to treat multi-reference systems is critical to the ability to treat many catalytic reaction mechanisms. Systems without high multi-reference character are called single-reference systems.

Most GAs have a form that separately approximates exchange and correlation, as first introduced by Langreth and Mehl[2] and usually called a generalized gradient approximation[3] (GGA); however, it has been shown that a nonseparable gradient approximation[4] (which has more flexibility at the cost of satisfying less exact constraints) is capable of performing well for a broader set of properties. The original NGA, called N12, was designed to give good predictions both of solid-state lattice constants and of cohesive energies and molecular atomization energies; it also gave good predictions of molecular bond lengths.[4] Here we show that we can get improved performance for barrier heights (which are important for studies of both uncatalyzed and catalyzed reactions) by relaxing the accuracy for lattice constants, which are not needed for molecular (as opposed to solid-state) processes. By diminishing the emphasis on obtaining good lattice constants we can obtain an exchange–correlation functional that may be more useful for treating many large and complex homogeneous and enzymatic catalysts that do not require the calculations on solid-state material.

A second goal of this work is to obtain improved results for compounds containing metal atoms, including transition metal compounds with high multi-reference character, by incorporating a greater amount of representative data for metal-ligand bond energies in the training set of a density functional. A third goal of the present work is to obtain a very smooth exchange–correlation functional by enforcing an unsmoothness penalty as part of the optimization process.

Combining these three goals, we have designed a new exchange–correlation functional called gradient approximation for molecules, or GAM, and this new functional is presented here. The GAM functional is an NGA, and so it depends only on spin densities and spin density gradients. The parameters of the GAM functional are optimized against a broad set of molecular and solid-state data in a new database called Minnesota Database 2015, which is also presented here. We will show that the resulting GAM functional yields good results for main group bond energies, chemical reaction barrier heights, transition-metal bond energies, weak interaction energies between noble gas atoms, and bond lengths of diatomic molecules.

Section 3.2 describes the computational details. Section 3.3 describes Minnesota Database 2015. Section 3.4 describes previously available functionals to be used for comparison. Section 3.5 describes the design and optimization of the GAM functional. Section 3.6 gives results; Section 3.7 provides discussion; and Section 3.8 summarizes the main conclusions.

3.2 Computational details

All the calculations in this paper were performed by a locally modified version[5] of the *Gaussian 09* program.[6] Ultrafine grids ("99,590") are used to evaluate the exchange–correlation energies of our new GAM functional. We use the stable=opt keyword in *Gaussian 09*[6] to find the stationary solution to the Kohn-Sham equations by allowing symmetry breaking in the wave function if the symmetry-constrained solution is unstable. The periodic boundary condition (PBC) algorithm[7] in *Gaussian 09*[6] is used to calculate the lattice constants, cohesive energies, and semiconductor band gaps in our new Minnesota Database 2015, which will be explained in the next section.

Besides testing the new functional on the training subset of Minnesota Database 2015, we made several tests outside the training set. First we tested the new functional on subdatabases SBG31 and SSCE8, which are in Minnesota Database 2015 but outside the training set. We also tested our functional against other data that is not in the training set. This data includes a recently published database WCCR for transition metal coordination reactions[8] (renamed here as WCCR10 for consistency with our general naming scheme), the enthalpies of binding of O_2 and N_2 to the metal organic framework Fe-MOF-74, the binding of C_2H_4 to $Pd(PH_3)_2$, and the Ar_2 potential energy curve.

For the WCCR database we use the same basis set (def2-QZVPP) and geometries as used in the original paper; these geometries, which were optimized by functional BP86.[9,10] are provided by the supporting information of the WCCR paper.[8]

For calculating the binding enthalpies of O_2 and N_2 bound to Fe-MOF-74, we used an 88-atom cluster model of the experimental structure of Fe-MOF-74 containing three iron centers. The details of this cluster and rationale for its design are described in our earlier work.[11] This cluster has three iron atoms, and here we studied binding at the central iron, which best represents the immediate environment around iron in the actual MOF. During optimization, the cluster of the MOF was frozen and the guest molecules (O_2 or N_2) were allowed to relax. The binding enthalpies were calculated using the formula given in eq. 1 of reference 11.

The binding energy of the $Pd(PH_3)_2C_2H_4$ complex were computed using four basis sets. In all four basis sets, Pd atom has 18 active electrons and 28 core electrons that are replaced by effective core potential. Basis set BS1 denotes Stuttgart-Dresden-Dunning (SDD) basis set for Pd [12] and the cc-pVTZ basis set for P,[13] C, and H.[14] Basis set BS2 denotes the def2-TZVP basis set for Pd[15] and the cc-pVTZ basis set for P, C, and H. Basis set BS3 denotes the def2-TZVP basis set for Pd, the cc-pV(T+d)Z basis set for P[16,17] and the cc-pVTZ basis set for C and H. Basis set BS4 denotes the def2-TZVP basis set for Pd, the maug-cc-pV(T+d)Z basis set for P,[18] the maug-cc-pVTZ basis set for C[18,19] and the cc-pVTZ basis set for H.

One basis set was used for Ag dimer, namely jun-cc-pVTZ-PP,[20,21,22] one basis set was used for homonuclear transition metal bond distance, namely LanL2DZ,[23,24,25,26] and two basis sets were used for Ar dimer, namely the aug-cc-pVQZ[13,27] and aug-cc-pV6Z[28] basis sets.

3.3 Minnesota Database 2015

Minnesota Database 2015 is our new database for optimizing and testing density functionals. Compared to Database 2.0 that we used in previous work[29] the following changes are made:

We divide the previous bond energy databases according to two types of classification: (i) whether the molecule contains only main-group nonmetal atoms or it also contains main-group-metal atoms or transition-metal atoms; (ii) whether the molecule has singe-reference character, i.e., can well described by a single configuration wave function, or multi-reference character, i.e., cannot be so described. Then we added additional data to the underpopulated classes. Accordingly we have six new subdatabases for bond energies. Theses subdatabases are as follows (their shorthand names are in parentheses, where the final number in the shorthand name of a subdatabase is the number of data):

- single-reference main-group-metal bond energies (SR-MGM-BE9),
- single-reference main-group-nonmetal bond energies (SR-MGN-BE107),
- single-reference transition-metal bond energies (SR-TM-BE17),
- multi-reference main-group-metal bond energies (MR-MGM-BE4),
- multi-reference main-group nonmetal bond energies (MR-MGN-BE17),
- multi-reference transition-metal bond energies (MR-TM-BE15).

A new subdatabase called NGDWI21 has been added for noble-gas-dimer weak interactions. It comprises both homodimers and heterodimers.

We have added three new subdatabases for atomic excitation energies, namely

- 3d transition metal atomic excitation energies (3dAEE7),
- 4d transition metal atomic excitation energies (4dAEE5),
- p-block excitation energies (pEE5).

Two new subdatabases for p-block isomerization energies are added:

- 2p isomerization energies (2pIsoE4)
- 4p isomerization energies (4pIsoE4).

A new subdatabase for molecular geometries has been added; it is called diatomic geometries for heavy atoms (DGH4).

The above points summarize the main changes made to our previous database,[29] called Database 2.0. A complete list of the subdatabases included in Minnesota Database 2015 is given in Table 3.1, which also shows the number of data in each category (the inverse weight column of this table will be explained in Section 3.5). The database is divided into primary subdatabases, and some of the primary subdatabases are further divided into secondary subdatabases.

3.4 Functional for comparison

We compare our results to 22 previously available exchange–correlation functionals. Since GAM depends only on spin densities and spin density gradients, we compare our results mainly to GAs, in particular to 14 GGAs and the one previously available NGA. In a practical sense, three of the GGAs are corrected to second order in the density gradient expansion for exchange, and the other 11 are not. Altogether we

compare to 20 local functionals of four types and to two hybrid functionals. The local functionals are an LSDA, namely GKSVWN5;[30,31,32] 14 GGAs, namely SOGGA,[33] PBEsol,[34] PBE,[35] BP86,[9,10] PW91,[36] BLYP,[10,37] mPWPW,[38] revPBE,[39] BPW91,[10,36] RPBE,[40] HCTH407,[41] SOGGA11,[42] OLYP[37,43] and OreLYP;[37,43,44] an NGA, namely N12;[4] and four meta-GGAs, namely TPSS,[45] revTPSS,[46] M06-L,[47] and M11-L.[48] For context we also compare to two popular hybrid functionals, namely a global-hybrid GGA, B3LYP;[43,49,50] and a range-separated hybrid GGA, HSE06.[51,52]All these functionals are listed in Table 3.2 with the type, the percentage of Hartree-Fock exchange, the year, and the original reference. A more complete comparison of gradient approximations to more advanced functionals of the meta-GGA, meta-NGA, and hybrid type is found elsewhere[29] and will not be repeated here, where our emphasis is on gradient approximations for the four reasons stated in the introduction, so comparisons to more advanced functionals are limited here to providing context.

3.5 Design and optimization of the GAM functional

The general functional form of GAM is the same as N12,[4] which has the flexibility to approximate both exchange and correlation effects in terms of spin density ρ_σ and reduced spin density gradient x_σ. In order to design a good functional, we use a broad molecular and solid-state database to optimize the parameters of the functional, and we also add smoothness constraints to our optimization. We will discuss the functional form in Sections 3.5.1, 3.5.2, and 3.5.3 and the optimization of the functional in Section 3.5.4.

3.5.1 Functional Form

The exchange–correlation energy E_{xc} of the GAM functional is the sum of nonseparable exchange-correlation component $E_{\mathrm{nxc}}^{\mathrm{NSGA}}$ and an additional term that is nominally treated as a correlation energy E_{c}. Typically one writes the first component as E_{x}, however, we label it as $E_{\mathrm{nxc}}^{\mathrm{NSGA}}$ to show that it is a nonseparable approximation involving both exchange and correlation. Since we optimize the functional empirically and do not enforce the factorable form on the first term, the first term also represents part of correlation energy, and similarly the second term is not purely correlation. Both terms must also include an empirical contribution required to account for the difference of the exact electronic kinetic energy from that computed from the orbitals of the Kohn-Sham determinant. The philosophy used in designing the functional form is consistent with the statement of Tozer and Handy that "The functionals represent exchange and correlation effects in a combined manner. Individual exchange and correlation terms cannot be isolated."[53] Our total exchange-correlation functional is

$$E_{\mathrm{xc}} = E_{\mathrm{nxc}}^{\mathrm{NSGA}} + E_{\mathrm{c}} \tag{3.1}$$

Where

$$E_{\mathrm{nxc}}^{\mathrm{NSGA}} = \sum_{\sigma=\alpha}^{\beta} \int dr \Gamma_{\mathrm{nxc}\sigma}^{\mathrm{NSGA}}(\rho_\sigma, x_\sigma) \tag{3.2}$$

$$E_{\mathrm{c}} = E_{c\alpha\beta} + \sum_{\sigma=\alpha}^{\beta} E_{c\sigma\sigma} \tag{3.3}$$

3.5.2 Nonseparable Exchange-Correlation Functional Form

In equation (3.2) the nonseparable energy density is written as

$$\Gamma_{\mathrm{nxc}\sigma}^{\mathrm{NSGA}} = \varepsilon_{x\sigma}^{\mathrm{UEG}}(\rho_\sigma) F_x(\rho_\sigma, x_\sigma) \tag{3.4}$$

Where F_x is the exchange enhancement factor, which in the present paper is defined as

$$F_x = \sum_{i=0}^{m} \sum_{j=0}^{m'} a_{ij} u_{x\sigma}^i v_{x\sigma}^j \tag{3.5}$$

Where ρ_σ stands for the spin density, $u_{x\sigma}$ and $v_{x\sigma}$ are finite variables defined by

$$u_{x\sigma} = \gamma_{x\sigma} x_\sigma^2 \big/ (1 + \gamma_{x\sigma} x_\sigma^2) \tag{3.6}$$

$$v_{x\sigma} = \omega_{x\sigma} \rho_\sigma^{1/3} \big/ (1 + \omega_{x\sigma} \rho_\sigma^{1/3}) \tag{3.7}$$

x_σ stands for reduced spin density gradient, for which we use the definition of Becke: [10]

$$x_\sigma = |\nabla \rho_\sigma| \big/ \rho_\sigma^{4/3} \tag{3.8}$$

$\varepsilon_{x\sigma}^{\mathrm{UEG}}$ stands for the uniform electron gas energy, which is calculated by[30,31]

$$\varepsilon_{x\sigma}^{\mathrm{UEG}} = -\frac{3}{2}\left(\frac{3}{4\pi}\right)^{1/3} \rho_\sigma^{4/3} \tag{3.9}$$

$\gamma_{x\sigma}$ and $\omega_{x\sigma}$ are unitless parameters taken to have the same values as the one in N12,[4] namely $\gamma_{x\sigma}$ = 0.004 and $\omega_{x\sigma}$ = 2.5, and a_{ij}, are unitless parameters to be determined. Since both ρ_σ and x_σ range over [0, ∞), the dependent variables $u_{x\sigma}$ and $v_{x\sigma}$ range over [0,1].

A GGA exchange functional can be written like equation (3.4) but where the enhancement factor F_{X} depends only on the reduced spin density gradient x_σ. For an NGA we allow the enhancement factor to depend also on the spin density ρ_σ.

3.5.3 Additional Correlation Functional Form

In equation (3.3), the correlation functional has two parts. One is the contribution $E_{c\alpha\beta}$ from opposite spins, and the other is the contribution $E_{c\sigma\sigma}$ from same spins. These two contributions are defined by

$$E_{c\alpha\beta} = \int dr \varepsilon_{c\alpha\beta}^{\mathrm{UEG}} \{ \sum_{i=0}^{n} b_i u_{c\alpha\beta}^{i} \} \tag{3.10}$$

$$E_{c\sigma\sigma} = \int dr \varepsilon_{c\sigma\sigma}^{\mathrm{UEG}} \{ \sum_{i=0}^{n'} c_i u_{c\sigma\sigma}^{i} \} \tag{3.11}$$

where b_i and c_i are unitless parameters to be determined,

$$u_{c\alpha\beta} = \frac{\gamma_{c\alpha\beta} x_{\mathrm{avg}}^2}{1 + \gamma_{c\alpha\beta} x_{\mathrm{avg}}^2} \tag{3.12}$$

$$u_{c\sigma\sigma} = \frac{\gamma_{c\sigma\sigma} x_\sigma^2}{1 + \gamma_{c\sigma\sigma} x_\sigma^2} \tag{3.13}$$

$\gamma_{c\alpha\beta}$ and $\gamma_{c\sigma\sigma}$ are unitless parameters given the same values as in N12,[4] namely, $\gamma_{c\alpha\beta}$ = 0.006 and $\gamma_{c\sigma\sigma}$ = 0.2, x_{avg}^2 is defined as the average of x_α^2 and x_β^2, and $\varepsilon_{c\alpha\beta}^{\mathrm{UEG}}$ and $\varepsilon_{c\sigma\sigma}^{\mathrm{UEG}}$ represent the correlation energy of the uniform electron gas. The uniform-gas functions

are taken from the Perdew-Wang parameterization[54] and the ansatz of Stoll, which is used to separate the correlation energy into same-spin and the opposite-spin contributions. [55,56]

3.5.4 Functional Optimization

In equations (3.5), (3.10), and (3.11) above, we see that a_{ij}, b_i, and c_i are linear parameters of the functionals, which will be optimized. We do not force the uniform-electron-gas limit to hold when we optimize the functional. In order to make our functional smooth, smoothness constraints are added to the optimization, which will be explained in detail in the last paragraph of this section. The values of *m, m′, n*, and *n′* are chosen as 3, 3, 4, and 4 respectively. We found that the performance of the functional is not significantly improved by increasing these values, which shows that one cannot obtain improved functionals simply by adding more parameters. Therefore, in order to design good density functionals we must pay more attention to the mathematical form of the functional and the diversity of the database we are optimizing against, instead of concentrating on the number of parameters.

We optimize our functional against 27 primary databases, including 24 molecular energy databases, two molecular structure databases, and one solid-state structure database. We optimize the GAM functional self-consistently by minimizing the following unfitness function:

$$U = \sum_{n=1}^{27} R_n / I_n + \lambda(a+b+c) \tag{3.14}$$

where R_n is the root mean squared error of database n, I_n is the inverse weight of database n, and the product of λ and $(a + b + c)$ is the smoothness constraint, which is explained by

$$a = \sum_{i=0}^{3} \sum_{j=0}^{2} (a_{i,j} - a_{i+1,j})^2 + (a_{03} - a_{10})^2 + (a_{13} - a_{20})^2 + (a_{23} - a_{30})^2 \tag{3.15}$$

$$b = \sum_{i=0}^{3} (b_i - b_{i+1})^2 \tag{3.16}$$

$$c = \sum_{i=0}^{3} (c_i - c_{i+1})^2 \tag{3.17}$$

We varied the value of λ from 0.001 to 0.1; finally we chose λ to be 0.001, which gives what we judged to be the best combination of overall accuracy, convergence, and smoothness of the density functional. The inverse weights are chosen as follows: first, the mean unsigned error (MUE) of 80 density functionals have been calculated against all the molecular database in Minnesota Database 2015, which show how well the conventional density functionals performs on these databases; second, we use these MUE as the inverse weights for our optimization; third, we modify the inverse weights according to our emphasis on different chemistry and physics properties. The main idea of this constraint is make the density functional a reasonably smooth function of the spin densities and their gradients.

In order to design a good across-the-board performance functional, we include various molecular and solid-state properties in our training set, such as, main-group bond

energies, transition metal bond energies, transition metal atomic excitation energies, barrier heights, ionization potentials, proton affinities, electron affinities, and lattice constants, etc. In Table 1, the inverse weight of each primary database is given. The smaller the inverse weight is, the more emphasis we put on that primary database.

Whereas the N12[4] functional involved 20 optimized linear coefficients and the constraint that it reduced to PBEsol at low density, the new GAM functional involves optimizing 26 linear coefficients in equations (5), (10), and (11) with no constraints. We use the same values as N12 for the nonlinear parameters $\omega_{x\sigma}$, $\gamma_{x\sigma}$, $\gamma_{c\alpha\beta}$, and $\gamma_{c\sigma\sigma}$. A key element in the optimization is the choice of weights. We do not choose them to minimize the overall error but rather to try to get small errors across the board, i.e., relatively small errors for each of the subdatabases, to the greatest extent possible. The final choice of weights was determined after considerable trial and error and is a subjective decision that cannot be justified by any numerical argument.

Table 3.3 lists the values for the optimized parameters of the GAM functional.

3.6 Table of Results

In Tables 3.4 and 3.5 we compare the performance of the new functional to that of 22 existing functionals for molecular energetic data, and in Table 3.6 we do the same for molecular bond distances.

Table 3.7 gives the performance for solid-state databases, but since B3LYP calculations with periodic boundary conditions are very expensive, we only compare 21 density functionals for the solid-state lattice constant and energetic data of Table 3.7.

Table 3.8 compares the performance of GAM to that of eight density functionals for the WCCR10 database of Weymuth et al.[57] Table 3.9 is a test for the binding of dioxygen and dinitrogen to Fe-MOF-74, which is also called Fe_2(dobdc), where we compare to experiments of Bloch et al.[58] Table 3.10 presents results for the binding of ethylene to $Pd(PH_3)_2$, where we compare the results of GAM to the best estimate computed using BCCD(T)[59] in our earlier work. [60] Table 3.11 presents results for the bond distance of homonuclear transition metal dimer, where we compare the results of GAM and N12 with 5 functionals in a recent paper. [61]

3.6.1 Molecular Energy Database

Tables 3.4 and 3.5 show the mean unsigned error (MUE) for molecular energy database ME417 and its subdatabases. Note that we always compute MUEs without weighting the data; it is a straight average over the absolute deviations from the reference data of the database. In order to compare the properties for the molecular catalysis, we also combine some of existing subdatabases to form three new databases, which are main-group bond energy (MGBE137), which includes SR-MGM-BE9, SR-MGN-BE107, MR-MGM-BE4, and MR-MGN-BE17 subdatabases; transition metal bond energy (TMBE32), which includes SR-TM-BE17, MR-TM-BE13, and MR-TMD-BE2 subdatabases; barrier heights (BH76), which includes HTBH38/08 and NHTBH38/08 subdatabases.

3.6.2 Molecular Structure Database

Table 3.6 shows the mean unsigned error for DGL6 and DGH4 subdatabases. The last column showed the MS10, which is the overall mean unsigned error of these two subdatabases.

3.6.3 Solid State Database

Table 3.7 shows the mean unsigned errors for solid-state databases, which include LC17, SBG31, and SSCE8. Lattice constants are related to nearest neighbor distances (NNDs), but the ratio of the lattice constant to the nearest-neighbor distance depends on the crystal structure. For our larger lattice constant database, SSS47,[29] we calculated an average value for this ratio of 2.15, and we use this as a typical conversion factor for discussion purposes. Therefore we also report the results for LC17 by dividing by 2.15 so that the reader can more easily compare the errors to the errors in molecular bond distances. These results are labeled NND and are discussed as mean unsigned errors in nearest neighbor distances, but the reader should keep in mind that a slightly different result would be obtained if we first converted to NND and then averaged. The rationale of having both columns in Table 3.7 is that the LC17 column can be directly compared to physics literature papers that report average errors in lattice constants, while the NND column allows a more physical comparison to average errors in molecular bond lengths.

3.6.4 WCCR10

We show mean unsigned errors for the WCCR10 database of transition metal coordination reactions in Table 3.8. The mean unsigned error of GAM against WCCR10

is 6.60 kcal/mol. This is larger than the mean unsigned error of GAM against TMB31 subdatabase, i.e. 5.73 kcal/mol, but still reasonable since it is the second best among the functionals tested in Table 3.8.

3.6.5 Separation of O_2 and N_2 on Fe_2(dobdc)

The performance of the newly designed functional, GAM was also tested for its ability to predict the separation of a mixture of O_2 and N_2 on a metal-organic framework (MOF), in particular Fe_2(dobdc). The binding enthalpies for O_2 and N_2 bound to Fe_2(dobdc) were computed using the GAM exchange–correlation functional with the def2-TZVP basis set, and then compared to experimental values[58] of isosteric heat of adsorption. The values for the Fe–O_2 and Fe–N_2 interacting systems in their ground spin states computed at 201 K were 10.8 and 3.9 kcal/mol, respectively, while the corresponding experimental values reported in ref. 58 are 9.8 kcal/mol and 8.4 kcal/mol, respectively. Later, a more accurate experimental adsorption enthalpy for N_2 bound to Fe-MOF-74 under different experimental conditions and with different procedures was reported to be 5.5 kcal/mol.[62] Table 9 also presents the binding enthalpies of higher energy spin states of the Fe–O_2 interacting system, which are predictions for which no experimental data is available (these calculations were necessary to be sure that the reported binding energy corresponds to lowest-energy spin state of the system).

3.6.6 Binding energy of $Pd(PH_3)_2C_2H_4$

The binding of C_2H_4 to $Pd(PH_3)_2$ was computed using GAM and compared to the best estimate of binding energy performed in our earlier work.[60] The binding energies calculated using various basis sets are reported in Table 3.10.

3.6.7 Bond length of homonuclear transition metal dimer

The equilibrium bond lengths of seven transition metal dimers are calculated by GAM and six other density functionals with the LanL2DZ basis set.[23,24,25,26] Table 11 shows the bond length and mean unsigned error calculated by each functional.

3.7 Other Results and Discussion

3.7.1 Convergence

In order to design a smooth functional, we add a smoothness constraint to the parameter optimization of the GAM functional. The linear coefficients optimized for GAM all have magnitudes in the range 0.8–23, which is a reasonably narrow range so there is no excessive cancellation between terms. The convergence of the new functional has been tested against our common Minnesota Database 2015. In the common Minnesota Database 2015, there are 483 data including ME417, MS10, SBG31, SSCE8, and LC17. If we also count the fragments that are used to calculate these data, there are more than one thousand data calculated by the GAM functional. Among the over-a-thousand data, only FeCl shows some SCF convergence issues; all other calculations converged without any problems. The smoothness of the exchange–correlation

enhancement factor of the GAM functional has also been examined in plots, and it will be discussed in Section 3.7.3.

3.7.2 Performance of the GAM Functional

Tables 3.4 and 3.5 show that the GAM functional gives especially good results for main group bond energies, transition metal bond energies, reaction barrier heights, molecular structures, and noble gas weak interactions. Furthermore, the GAM functional provides reasonably good results for the test sets including semiconductor band gaps, solid-state cohesive energies, and transition metal coordination reactions.

Table 3.4 shows that among LSDA, all the GGAs, and the previous NGA, the new functional GAM gives the smallest overall mean unsigned error for the entire molecular energy database ME417; the mean unsigned error is only 4.51 kcal/mol. We also show the overall error of ME400xAE, which is the average error for the molecular energy database when we exclude absolute atomic energies, and in this case too, the GAM functional GAM also gives the smallest error among GGAs, LSDA, and NGA. We emphasize that we could reduce these total errors more, if that were our goal, but that is not our goal. Our goal is rather to obtain good performance across a broad range of databases. In order to have a functional that is especially good for studying molecular catalysis, the functional should be good for main-group bond energy (MGBE137), which includes the SR-MGM-BE9, SR-MGN-BE107, MR-MGM-BE4, and MR-MGN-BE17 subdatabases, for transition metal bond energy (TMBE32), which includes the SR-TM-BE17, MR-TM-BE13, and MR-TMD-BE2 subdatabases, for barrier heights (BH76),

which includes the HTBH38/08 and NHTBH38/08 subdatabases, and for molecular structure (MS10), which includes DGL6 and DGH4 subdatabases. In Tables 3.4 and 3.5 we calculate the average error for each of these four categories by averaging the errors from each subdatabase. Among LSDA and all GGAs and NGAs, the GAM functional ranked the best for the MGBE137, TMBE32, and BH76 subdatabases. If we consider all the functionals in Tables 3.4 and 3.5, the GAM functional ranks the second best for TMBE32 subdatabase, for which M06-L is the best with an error 0.48 kcal/mol smaller than the GAM; the GAM functional ranks the second best for the MGBE137 subdatabase, for which M06-L is the best with an error 0.28 kcal/mol smaller than the GAM; and the GAM functional ranks the fifth best for BH76 subdatabase, for which M11-L is the best followed by M06-L, B3LYP, and HSE06. We note that M06-L is a meta functional, and therefore it should be better than a simpler gradient approximation, but we gave several reasons for optimizing a gradient approximation in the introduction.

In addition to the databases mentioned above, the GAM functional also provides good results for 3d transition metal atomic excitation energies, which are very hard for most available density functionals, but which we have recently shown[63] can be very important for understanding metal–metal bonding. The GAM functional ranks the fifth best for the 3dAEE7 subdatabase, behind M06-L, B3LYP, PBE, and RPBE.

Next we consider noble-gas weak interactions. From Tables 3.4 and 3.5 we can see that all the functionals tested except GAM give a mean unsigned error larger than 0.081 kcal/mol for the NGDWI21 subdatabase, for which GAM only gives 0.019 kcal/mol. The

average value of the all the noble gas weak interaction energies in our database is 0.160 kcal/mol, which means that most functionals give an average error that is larger than 50% of the average of the reference values. The GAM functional gives the best results for NCCE30 subdatabase as compared to all tested GGAs and N12.

The GAM functional also provides the second best results for MR-TMD-BE2 (Cr_2 and V_2, which are known to be very hard cases for density functional theory) among all functionals tested.

Table 3.6 shows that the relative performance of GAM for molecular structures is not quite as good as for energies. The GAM functional ranks the 13th for MS10 subdatabase with an MUE of 0.018Å, which is 0.002 Å larger than the average MUE of all functionals tested in Table 6. However, a more fair comparison in this case is to compare to the 12 GGAs excluding PBEsol and SOGGA (we exclude PBEsol and SOGGA at this point since their design is understood to make them better for structures than for energies, and so we do not consider them to be general-purpose functionals). As compared to the remaining group of 12 GGAs, only HCTH407 does better for DGL6 and only four of the 12 do better for MS10. The less than stellar performance of GAM on MS10 is primarily due to a large overestimate of the bond length of Ag dimer; this bond length behaves differently than other bond lengths in MS10, and success for this bond length is highly correlated to performance on lattice constants, which we downplayed. This downplay is evidenced in Table 3.7, which shows that the GAM functional does not give good results for the solid-state lattice constant database with a mean unsigned error

of 0.046 Å for the quantities we nominally call nearest neighbor distances (NND – see section 6.3); this error is 0.010 Å larger than the average mean unsigned error for NND. As discussed in the introduction, this results from a strategic decision to emphasize molecular energies over lattice constants in the creation of GAM. The "M" (for "molecules") at the end of GAM is primarily to indicate our awareness that we still do not have a universally good functional, which is so far unattainable by any functional containing only density and density gradient ingredients. Nevertheless, despite not being universal, the performance of the new functional developed here is very good if we consider *molecules* rather than solid-state lattice constants.

Next we turn to data not used for training.

Table 3.7 shows that the GAM functional also shows reasonably good results for the solid-state energies databases. Among the 17 LSDA, GGAs, and NGAs the GAM functional ranks the sixth best for the SGB31 database and fifth best for the SSCE8 database. These databases were not used for training.

In Table 3.8, the GAM functional ranks the second best among all functionals being tested, where the functionals tested are those chosen by the previous[8] authors. The WCCR10 database includes ten transition metal coordination reactions. The molecules involved in these reactions are very large and very different from the training sets in Minnesota Database 2015. The performance against these large molecules is slightly worse than that for the transition metal molecules in our training set, but within a reasonable range.

Table 3.9 presents the results for the performance of GAM on MOFs. We find that GAM gives good results when compared to experiments for the separation of O_2 and N_2 on Fe-MOF-74, with a deviation from experimental adsorption enthalpies of 1.0 kcal/mol for O_2 and 1.6 kcal/mol for N_2. It should be noted here that our training set has no data on MOFs or any other type of nanoporous materials. This average deviation from the latest experimental values is under 3 kcal/mol and is within experimental error. This indicates that the GAM functional shows good agreement with experimental data not used for training.

In Table 3.10, results for the binding of C_2H_4 to $Pd(PH_3)_2$ are presented. This datum is outside the training set. This is a difficult case for functionals; for example, BLYP gives a binding energy of 10.2 kcal/mol as compared to the best estimate of 17.6 kcal/mol. Table 3.10 shows good stability with respect to changes in the basis set and that the GAM functional deviates from the best estimate by 6.5 kcal/mol with the largest basis set used. This is comparable to the 6.3 kcal/mol mean unsigned error for single-reference transition metal bond energies of molecules in the training set, and therefore it is an example where we obtain comparable performance inside and outside of the training set.

A very recent paper, which we considered only after our training set weights were final, reported bond distance for eight transition metal dimers, only one of which (Ag_2) is in our training set. We therefore use the bond distances of the seven others as a test against data quite different from that used for training. These seven dimers, Cu_2, Au_2, Ni_2, Pd_2, Pt_2, Ir_2, and Os_2, include two 3d metals, one 4d metals, and four 5d metals. (No 5d

data were used for training.) The GAM functional gives the third best results all the functionals tested in Table 3.11, with an MUE of 0.05 Å; the only functionals that do better are LSDA, which is much better for bond lengths than for molecular energies, and N12, the only previous NGA. This is very encouraging performance well outside the training set.

We also tested our new functional against the experimental bond dissociation energies of Ag_2 and FeC, which are 38.0 kcal/mol and 88.32 kcal/mol respectively.[64,65] The GAM functional predicts these bond dissociation energies to be 39.21 kcal/mol and 86.49 kcal/mol. Li et al.[65] have tested the bond dissociation energy of FeC with various functionals, and in Table 3.12 we add our new result to their comparison. The results in Table 3.12 show that the GAM functional is the second best among all 18 functionals being tested, and that many of the previous functionals have large errors for this difficult case.

Recent studies pointed out that some density functionals give unstable results for large basis sets.[66] Figure 3.1 shows the potential curve of Ar_2 with our new GAM functional and the aug-cc-pVQZ and aug-cc-pV6Z basis sets. Figure 3.1 shows that our results are very close to the reference values[67] and there is no slow convergence issue with respect to the basis sets. Moreover, the excellent agreement with the reference plot shows that the GAM functional provides good results for noble gas weak interaction. This is consistent with Tables 3.4 and 3.5 showing that the GAM functional is the best for NGDWI21 basis set among all the functionals tested in the present paper.

3.7.3 Exchange–correlation Enhancement factor of the GAM Functional

The enhancement factor is defined by the following equations:

$$E_{\mathrm{xc}} = \int dr \varepsilon_{\mathrm{x}}^{\mathrm{UEG}}(\rho) F_{\mathrm{xc}}(r_s, s) \tag{3.18}$$

$$s = \frac{|\nabla \rho|}{2(3\pi^2)^{1/3} \rho^{4/3}} \tag{3.19}$$

$$r_s = \left(\frac{3}{4\pi\rho}\right)^{1/3} \tag{3.20}$$

where E_{xc} is the total exchange-correlation energy, $\varepsilon_{\mathrm{x}}^{\mathrm{UEG}}(\rho)$ is the exchange energy density of a uniform electron gas, ρ stands for the total density, s is the unitless reduced density gradient, and r_s is the Wigner-Seitz radius. For illustrating the enhancement factor in this section, we only consider the spin-unpolarized cases, which mean that $\rho = 2\rho_\alpha = 2\rho_\beta$. The exchange-correlation enhancement factor of the GAM functional is plotted in Figure 3.2. We choose four values of ρ to plot the enhancement factor F_{xc}, and these values corresponds to r_s = 0.5, 2.5, 4.5, 6.5 in atomic units. The region of *s* is chosen from 0 to 3, which is the key range for real systems. The enhancement factor for all 14 GGAs, for the previous NGA, namely N12, and for GAM are shown in Figure 3.2.

A key design element of the NGA functional form is that, unlike GGAs, we do not attempt to separately fit exchange and correlation. Therefore, unlike a GGA, we do not have a pure-exchange enhancement factor that depends only on *s*. However, Figure 3.2 shows that after we add correlation to exchange, the extent of dependence on ρ for closed-shell systems is not qualitatively different in GAM and in the GGAs.

3.8 Conclusions

The GAM functional has the following advantages over current GGAs and N12.

1. The GAM functional gives the smallest mean unsigned error for main group bond energies (MGBE137), transition metal bond energies (TMBE32), and reaction barrier heights (BH76).
2. The GAM functional gives the smallest mean unsigned error of 0.019 kcal/mol for the noble gas dimer weak interaction energies (NGDWI21), with all the other functionals tested here giving a mean unsigned error larger than 0.081 kcal/mol, which is about 50% of the reference value.
3. GAM is best of any LSDA, GGA, or NGA for both the overall mean unsigned error for molecular energies, either including total atomic energies (ME417) or excluding them (ME400xAE). OreLYP (which has not previously been widely tested) and OLYP are the second and the third best.
4. The GAM functional gives an MUE of 0.018Å for the molecular structure subdatabase (MS10), which is reasonable, although not outstanding.
5. Besides the training sets tested in the paper, we also test the performance of the GAM functional against band gaps (SBG31), solid-state cohesive energies (SSCE8), transition metal coordination reactions (WCCR10), the bond energies of Ag_2 and FeC, adsorption enthalpies of gases on MOFs, the binding of C_2H_4 to $Pd(PH_3)_2$, and the bond distances of homonuclear transition metal dimers (HTMD7). The last-named test includes four 5d transition metals, although no 5d transition metal data was used for training. The GAM functional does acceptably well in these tests. We conclude that the GAM functional we designed is transferable to molecular problems outside our training sets.

6. The linear coefficients optimized for GAM are in a narrow range of magnitude so there is no excessive cancellation between terms. The self-consistent-field convergence of the GAM functional has been tested against more than one thousand data; only one of them shows some convergence problems. The enhancement factor plot of the GAM functional is reasonably smooth.

With all these advantages over the GGAs and the previous NGA, with the advantage of an NGA requiring smaller grids than meta-GGAs or meta-NGAs, and with the advantage of an NGA requiring considerably less computation time for extended systems than hybrid functionals, we expect the GAM functional to be very useful for molecular catalysis and a wide variety of other applications to large and complex molecular systems.

3.9 References

[1] W. Kohn, A. D. Becke and R. G. Parr, *J. Phys. Chem.,* 1996, **100**, 12974.

[2] D. C. Langreth and M. J. Mehl, *Phys. Rev. B,* 1983, **28**, 1809.

[3] J. P. Perdew and Y. Yang, *Phys. Rev. B,* 1986, **33**, 8800.

[4] R. Peverati and D. G. Truhlar, *J. Chem. Theory Comput*., 2012, **8**, 2310.

[5] Y. Zhao, R. Peverati, K. Yang, S. Luo and D. G. Truhlar, *MN-GFM, version 6.4: Minnesota Gaussian Functional Module*; University of Minnesota: Minneapolis, MN, 2012.

[6] M. J. Frisch, *et al., Gaussian 09, Revision A.1*, Gaussian, Inc., 2009.

[7] K. Kudin and G. E. Scuseria, *Phys. Rev. B,* 2000, **61**, 16440.

[8] T. Weymuth, E. P. A. Couzijn, P. Chen and M. Reiher, *J. Chem. Theory Comput*., 2014, **10**, 3092.

[9] J. P. Perdew, *Phys. Rev. B,* 1986, **33**, 8822.

[10] A. D. Becke, *Phys. Rev. A,* 1988, **38**, 3098.

[11] P. Verma, X. Xu and D. G. Truhlar, *J. Phys. Chem. C,* 2013, **117**, 12648.

[12] D. Andrae, U. Häussermann, M. Dolg, H. Stoll and H. Preuss, *Theor. Chim. Acta,* 1990, **77**, 123.
[13] D.E. Woon and T.H. Dunning Jr., *J. Chem. Phys.,* 1993, **98**, 1358.
[14] T.H. Dunning Jr., *J. Chem. Phys.*, 1989, **90**, 1007.
[15] F. Weigend and R. Ahlrichs, *Phys. Chem. Chem. Phys*., 2005, **7**, 3297.
[16] T. H. Dunning, Jr., K. A. Peterson and A. K. Wilson, *J. Chem. Phys*., 2001, **114**, 9244.
[17] K. L. Schuchardt, B. T. Didier, T. Elsethagen, L. Sun, L., V. Gurumoorthi, J. Chase, J., J. Li and T. L. Windus, *J. Chem. Inf. Model.,* 2007, **47**, 1045.
[18] E. Papajak, H. R. Leverentz, J. Zheng and D. G. Truhlar, *J. Chem. Theory Comput.,* 2009, **5**, 1197.
[19] E. Papajak and D. G. Truhlar, *J. Chem. Theory Comput*., 2010, **6**, 597.
[20] K.A. Peterson and C. Puzzarini, *Theor. Chem. Acc.*, 2005, **114**, 283.
[21] D. Figgen, G. Rauhut, M. Dolg and H. Stoll, *Chem. Phys.*, 2005 **311**, 227.
[22] E. Papajak and D. G. Truhlar, *J. Chem. Theory Comput*., 2011, **7**, 10.
[23] T. H. Jr. Dunning and P. J. Hay, in *Modern Theoretical Chemistry*, Ed. H. F. Schaefer III, Vol. 3, Plenum: New York, 1977, pp. 1-28.
[24] P. J. Hay and W. R. Wadt, *J. Chem. Phys.*, 1985, **82**, 270.
[25] P. J. Hay and W. R. Wadt, *J. Chem. Phys.*, 1985, **82**, 284.
[26] P. J. Hay and W. R. Wadt, *J. Chem. Phys.*, 1985, **82**, 299.
[27] T. H. Jr. Dunning, *J. Chem. Phys*., 1989, **90**, 1007.
[28] T. van Mourik and T. H. Dunning, Jr., *Int. J. Quantum Chem.*, 2000, **76**, 205.
[29] R. Peverati and D. G. Truhlar, *Phil. Trans. R. Soc. A*, 2014, **372**, 20120476.
[30] W. Kohn and L. Sham, J. *Phys. Rev.,* 1965, **140**, A1133.
[31] (a) R. Gáspár, *Acta Phys. Hung*., 1954, **3**, 263. (b) R. Gáspár, *Acta Phys. Hung*., 1974, **35**, 213.
[32] S. H. Vosko, L. Wilk and M. Nusair, *Can. J. Phys.,* 1980, **58**, 1200.
[33] Y. Zhao and D. G. Truhlar, *J. Chem. Phys.,* 2008, **128**, 184109.
[34] J. P. Perdew, A. Ruzsinsky, G. I. Csonka, O. A. Vydrov, G. E. Scuseria, L. A. Constantin, X. Zhou and K. Burke, *Phys. Re.v Lett.*, 2008, **100**, 136406.
[35] J. P. Perdew, K. Burke and M. Ernzerhof, *Phys. Rev. Lett.,* 1996, **77**, 3865.
[36] J. P. Perdew, in *Electronic Structure of Solids '91*; P. Ziesche and H. Eschrig, Eds.; Akademie Verlag: Berlin, 1991; pp. 11–20.
[37] C. Lee, W. Yang and R. G. Parr, *Phys. Rev. B,* 1988, **37**, 785.
[38] C. Adamo and V. Barone, *J. Chem. Phys.,* 1997, **108**, 664.

[39] Y. Zhang and W. Yang, *Phys. Rev. Lett*., 1997, **80**, 890.

[40] B. Hammer, L. Hansen and J. Norskov, *Phys. Rev. B,* 1999, **59**, 7413.

[41] A. D. Boese and N. C. Handy, *J. Chem. Phys*., 2000, **114**, 5497.

[42] R. Peverati, Y. Zhao and D. G. Truhlar, *J. Phys. Chem. Lett.,* 2011, **2**, 1991.

[43] N. Handy and A. Cohen, *Mol. Phys*., 2001, **99**, 403.

[44] A. J. Thakkar and S. P. McCarthy, *J. Chem. Phys.,* 2009, **131**, 134109.

[45] J. M. Tao, J. P. Perdew, V. N. Staroverov and G. E. Scuseria, *Phys. Rev. Lett.,* 2003, **91**, 146401.

[46] J. P. Perdew, A. Ruzsinszky, G. I. Csonka, L. A. Constantin and J. Sun, *Phys. Rev. Lett.,* 2009, **103**, 026403.

[47] Y. Zhao and D. G. Truhlar, *J. Chem. Phys.,* 2006, **125**, 194101.

[48] R. Peverati and D. G. Truhlar, *J. Phys. Chem. Lett.,* 2011, **3**, 117.

[49] P. J. Stephens, F. J. Devlin, C. F. Chabalowski and M. J. Frisch, *J. Phys. Chem.,* 1994, **98**, 11623.

[50] A. D. Becke, *J. Chem. Phys*., 1993, **98**, 5648.

[51] J. Heyd, G. E. Scuseria and M. Ernzerhof, *J. Chem. Phys.,* 2003, **118**, 8027.

[52] T. M. Henderson, A. F. Izmaylov, G. Scalmani and G. E. Scuseria, *J. Chem. Phys.,* 2009, **131**, 044108.

[53] D. J. Tozer and N. C. Handy, *J. Phys. Chem*. *A*, 1988, **102**, 3162.

[54] J. P. Perdew and Y. Wang, *Phys. Rev. B,* 1992, **45**, 13244.

[55] H. Stoll and C. Pavlidou, *Theor. Chim. Acta,* 1978, **149**, 143.

[56] H. Stoll and E. Golka, *Theor. Chim. Acta,* 1980, **55**, 29.

[57] T. Weymuth, E. P. A. Couzijn, P. Chen and M. Reiher, *J. Chem. Theory Comput*., 2014, **10**, 3092.

[58] E. D. Bloch, L. J. Murray, W. L. Queen, S. Chavan, S. N. Maximoff, J. P. Bigi, R. Krishna, V. K. Peterson, F. Grandjean, G. J. Long, B. Smit, S. Bordiga, C. M. Brown and J. R. Long, *J. Am. Chem. Soc.,* 2011, **133**, 14814.

[59] N. C. Handy, J. A. Pople, M. Head-Gordon, K. Raghavachari and G. W. Trucks, *Chem. Phys. Lett.*, 1989, **164**, 185.

[60] B. Averkiev, Y. Zhao and D. G. Truhlar, *J. Mol. Cata A: Chem.,* 2010, 80.

[61] A. Posada-Borbón and A. Posada-Amarillas, *Chem. Phys. Lett.* 2015, **618**, 66.

[62] K. Lee, W. C. Isley III, A. L. Dzubak, P. Verma, S. J. Stoneburner, L.-C. Lin, J. D. Howe, E. D. Bloch, D. A. Reed, M. R. Hudson, C. M. Brown, J. R. Long, J. B. Neaton, B. Smit, C. J. Cramer, D. G. Truhlar and L. Gagliardi, *J. Am. Chem. Soc.,* 2014, **136**, 698.

[63] W. Zhang, D. G. Truhlar, and M. Tang, *J. Chem. Theory Comput.*, 2014, **10**, 2399.
[64] V. Beutel, H. G. Krämer, G. L. Bhale, M. Kuhn, K. Weyers and W. Demtröder, *J. Chem. Phys.,* 1993, **98**, 2699.
[65] R. Li, R. Peverati, M. Isegawa and D. G. Truhlar, *J. Phys. Chem. A*, 2012, **117**, 169.
[66] N. Mardirossian and M. Head-Gordon, *J. Chem. Theory Comput*., 2013, **9**, 4453.
[67] K. T. Tang and J. P. Toennies, *J. Chem. Phys.*, 2003, **118**, 4976.

Table 3.1 Databases included in Minnesota Database 2015[a,b]

n^a	Primary subsets	Secondary subset	Description	$I_n{}^c$
AME417			Atomic and Molecular Energies	
1	SR-MGM-BE9		Single-reference main-group metal bond energy	2.00
		SRM2	Single-reference main-group bond energies	
		SRMGD5	Single-reference main-group diatomic bond energies	
		3dSRBE2	3d single-reference metal-ligand bond energies	
2	SR-MGN-BE107		Single-reference main-group non-metal bond energies	0.20
3	SR-TM-BE17		Single-reference TM[d] bond energies	3.15
		3dSRBE4	3d single-reference metal-ligand bond energies	
		SRMBE10	Single-reference metal bond energies	
		PdBE2	Palladium complex bond energies	
		FeCl	FeCl bond energy	
4	MR-MGM-BE4		Multi-reference main-group metal bond energies	4.95
5	MR-MGN-BE17		Multi-reference main-group non-metal bond energies	1.25
6	MR-TM-BE13		Multi-reference TM bond energies	0.76
		3dMRBE6	3d multi-reference metal-ligand bond energies	
		MRBE3	Multi-reference bond energies	
		remaining	Bond energies of remaining molecules: CuH, VO, CuCl, NiCl	
7	MR-TMD-BE2		Multi-reference TM dimer bond energies (Cr_2, and V_2)	10.00
8	IP23		Ionization potentials	5.45
9	NCCE30		Noncovalent complexation energies	0.10
10	NGDWI21		Noble gas dimer weak interaction	0.01
11	3dAEE7		3d TM atomic excitation energies	0.40
12	4dAEE5		4d TM atomic excitation energies	6.90

13	PEE5	p-block excitation energies	1.74
14	4pIsoE4	4p isomerization energies	8.00
15	2pIsoE4	2p isomerization energies	7.81
16	IsoL6/11	Isomerization energies of large molecules	2.00
17	EA13/03	Electron affinities	2.96
18	PA8	Proton affinities	2.23
19	πTC13	Thermochemistry of π systems	5.75
20	HTBH38/08	Hydrogen transfer barrier heights	0.25
21	NHTBH38/08	Non-hydrogen transfer barrier heights	0.80
22	AE17	Atomic energies	10.22
23	HC7/11	Hydrocarbon chemistry	6.48
24	DC9/12	Difficult cases	10.00
MS10			
25	DGL6	Diatomic geometries of light-atom molecules	0.01
26	DGH4	Diatomic geometries of heavy-atom molecules: ZnS, HBr, NaBr	0.01
		Diatomic geometry of Ag_2	0.0013
SS17			
27	LC17	Lattice constants	0.013
SSE39			
28	SBG31	Semiconductor band gaps	NA[e]
29	SSCE8	Solid-state cohesive energies	NA
WCCR10			
30	WCCR10 [a]	Ligand dissociation energies of large cationic TM complexes	NA

[a]Databases 1-27 were used with various inverse weights in training, and databases 1-29 constitute Minnesota Database 2015. Database 30 is from T. Weymuth et al. (ref. 8), and – like databases 28 and 29 – it was used only for testing.

[b]In the name of a database or subdatabase, the number at the end of the name or before the solidus is the number of data. For example, ME417, SR-MGM-BE9, IsoL6/11, and DGH4 contain respectively 417, 9, 6, and 4 data.

[c] Inverse weights with units of kcal/mol per bond for databases 1–7, kcal/mol for databases 8–24, and Å for databases 25–27.

[d]TM denotes transition metal.

[e]NA denotes not applicable.

Table 3.2 Exchange–correlation functionals tested in this paper

Category	X [a]	Type	Year	Method	Ref.
local	0	LSDA	1980	GKSVWN5[b]	30, 31, 3
	0	GGA - correct to 2nd order in exchange	2008	SOGGA	33
	0		2008	PBEsol	34
	0		2011	SOGGA11	42
	0	GGA - other	1988	BP86	9, 10
	0		1988	BLYP	10, 37
	0		1991	PW91[c]	36
	0		1991	BPW91	10, 36
	0		1996	PBE	35
	0		1997	mPWPW	38
	0		1997	revPBE	39
	0		1999	RPBE	40
	0		2000	HCTH407	41
	0		2001	OLYP	37, 43
	0		2009	OreLYP	37, 43, 4
	0	NGA	2012	N12	4
	0		2015	GAM	present
	0	meta-GGA	2003	TPSS	45
	0		2006	M06-L	47
	0		2009	revTPSS	46
	0		2011	M11-L	48
nonlocal	20	global hybrid GGA	1994	B3LYP	43,49
	0-25	range-separated hybrid GGA	2009	HSE06	51, 52

[a] X is the percentage of nonlocal Hartree–Fock exchange. When a range is given, the first valu for small interelectronic distances, and the second value is for large interelectronic distances. Details of the functional form that joins these regions of interelectronic separation are given in references.

[b] GVWN5 denotes the Gáspár approximation for exchange and the VWN5 fit to the correlatio energy; this is an example of the local spin density approximation (LSDA), and it has the keyword SVWN5 in the *Gaussian 09* program. Note that Kohn-Sham exchange is the same as Gáspár exchange, but Slater exchange (not tested here) is greater by a factor of 1.5.

[c] PW91 formally satisfies the gradient expansion for exchange to second order but only at suc small values of the gradient that for practical purposes it should be grouped with functionals th do not satisfy the gradient expansion to second order.

Table 3.3 Optimized and inherited parameters of the GAM functional

	Exchange		Correlation
	Optimized parameters		
a_{00}	1.32730	b_0	0.860548
a_{01}	0.886102	b_1	-2.94135
a_{02}	-5.73833	b_2	15.4176
a_{03}	8.60197	b_3	-5.99825
a_{10}	-0.786018	b_4	-23.4119
a_{11}	-4.78787	c_0	0.231765
a_{12}	3.90989	c_1	0.575592
a_{13}	-2.11611	c_2	-3.43391
a_{20}	0.802575	c_3	-5.77281
a_{21}	14.4363	c_4	9.52448
a_{22}	8.42735		
a_{23}	-6.21552		
a_{30}	-0.142331		
a_{31}	-13.4598		
a_{32}	1.52355		
a_{33}	-10.0530		
	Inherited parameters		
$\omega_{x\sigma}$	2.5	$\gamma_{c\alpha\beta}$	0.006
$\gamma_{x\sigma}$	0.004	$\gamma_{c\sigma\sigma}$	0.2

Table 3.4 MUE (kcal/mol) for the Molecular Energy Database and its subdatabases: GAM compared to LSDA and other gradient approximations

Type	LSDA	GGA	GGA	GGA	GGA	GGA	GGA	GGA	GGA	GGA	GGA	GGA	GGA	GGA	GGA	NGA	**NGA**
Functional	GKSVWN	SOGG	PBEso	PBE	BP8	PW9	BLY	mPWP	revPB	BPW9	RPB	HCTH40	SOGGA1	OLY	OreLY	N12	**GA**
SR-MGM-BE9	11.64	4.43	4.47	2.72	3.10	2.57	5.07	2.87	4.26	3.20	4.57	3.52	8.79	4.67	4.06	5.92	**2.00**
SR-MGN-	16.21	7.27	7.28	3.40	4.06	3.51	2.78	2.80	2.99	2.49	3.35	2.55	2.77	2.32	2.56	2.38	**2.27**
SR-TM-BE17	20.89	11.59	11.33	7.20	7.39	8.76	6.52	6.73	6.22	7.34	6.24	8.36	11.44	9.32	7.15	8.31	**6.31**
MR-MGM-BE4	24.56	14.48	15.81	9.31	9.49	10.26	8.75	9.02	6.24	8.03	6.43	10.11	7.44	8.39	8.35	9.10	**7.76**
MR-MGN-BE17	36.89	21.29	23.16	14.8	13.8	14.80	6.67	12.45	5.94	10.74	5.51	5.24	8.57	5.15	4.25	6.93	**4.22**
MR-TM-BE13	34.07	22.03	21.24	12.7	12.1	13.25	10.64	11.67	8.55	10.81	7.73	19.70	18.79	5.77	5.10	12.5	**4.94**
IsoL6/11	2.05	1.89	1.55	1.98	2.28	1.92	3.73	2.16	2.82	2.38	2.99	3.02	1.73	3.44	3.39	1.73	**1.96**
IP23	9.59	4.84	5.82	6.19	8.44	7.29	6.52	6.85	5.00	6.30	4.92	6.81	5.92	3.12	3.03	4.36	**4.53**
EA13/03	5.70	2.70	2.16	2.27	4.21	2.60	2.68	2.31	2.40	2.26	2.37	3.70	5.23	3.60	2.32	4.12	**4.49**
PA8	5.07	2.33	2.10	1.34	1.41	1.30	1.58	1.52	2.00	1.88	1.98	2.84	2.11	2.40	1.70	1.35	**3.84**
πTC13	4.80	4.06	4.20	5.59	5.85	5.73	6.07	6.41	7.15	7.08	7.20	8.23	7.41	8.26	7.27	8.61	**8.59**
HTBH38/08	17.56	12.88	12.69	9.31	9.16	9.60	7.52	8.43	6.58	7.38	6.43	5.48	6.57	5.63	6.28	6.94	**5.35**
NHTBH38/08	12.42	9.68	9.86	8.42	8.72	8.80	8.53	8.03	6.82	7.26	6.82	6.29	4.32	5.25	5.57	6.86	**5.15**
NCCE30	3.61	2.12	2.07	1.46	1.53	1.60	1.64	1.42	1.71	1.74	1.61	1.32	1.48	2.52	2.68	1.38	**1.29**
AE17	421.13	283.06	245.90	47.2	16.9	4.63	8.68	12.55	10.88	11.95	9.39	16.80	10.06	10.13	2.37	14.2	**10.18**
HC7/11	21.45	17.88	13.31	3.97	9.95	4.55	27.39	8.08	13.65	10.77	14.96	14.97	6.26	17.01	16.34	4.27	**6.24**
3dAEE7	11.86	10.87	10.77	9.80	10.3	10.47	10.27	10.63	10.05	10.84	9.78	12.00	12.50	11.56	10.98	18.5	**9.82**
4dAEE5	14.10	4.77	8.48	4.70	5.07	4.73	5.73	4.89	4.49	5.03	4.27	7.75	7.60	5.94	6.42	10.2	**5.23**
pEE5	4.36	6.30	5.15	3.96	3.46	4.14	5.10	5.22	4.37	6.33	3.51	4.27	5.01	2.09	3.25	14.8	**2.99**
DC9/12	17.35	14.61	13.34	14.9	15.1	13.94	17.88	14.76	20.35	16.21	21.48	19.74	16.65	21.71	22.57	10.2	**23.07**
2pIsoE4	2.05	1.44	1.71	2.73	3.21	2.87	5.45	3.20	3.59	3.43	3.70	4.59	1.72	3.95	3.72	3.41	**5.02**
4pIsoE4	3.05	2.29	2.28	2.43	2.87	2.58	4.00	2.50	2.16	2.41	2.16	3.29	3.27	2.15	2.22	1.73	**3.57**
NGDWI21	0.212	0.082	0.081	0.10	0.52	0.165	0.385	0.220	0.282	0.587	0.179	0.246	0.650	0.323	0.389	0.38	**0.019**
MR-TMD-BE2	51.28	33.08	30.87	28.1	24.4	27.97	42.70	29.43	28.40	30.96	26.79	20.09	35.20	25.18	12.74	27.9	**10.67**

MGBE137[a]	18.72	9.04	9.31	4.94	5.38	5.05	3.58	4.18	3.54	3.73	3.79	3.17	4.02	3.00	3.04	3.37	**2.65**
TMBE32[b]	28.14	17.18	16.58	10.7	10.3	11.79	10.45	10.15	8.55	10.22	8.13	13.70	15.91	8.87	6.66	11.2	**6.03**
BH76[c]	14.99	11.28	11.27	8.87	8.94	9.20	8.02	8.23	6.70	7.32	6.62	5.88	5.44	5.44	5.92	6.90	**5.25**
ME417[d]	30.67	19.55	18.04	7.45	6.68	5.98	5.89	5.80	5.27	5.60	5.26	5.90	5.74	5.01	4.56	5.57	**4.51**
ME400xAE[d]	14.07	8.36	8.36	5.76	6.25	6.03	5.77	5.51	5.03	5.33	5.09	5.44	5.56	4.79	4.66	5.20	**4.27**

[a] The MGBE137 database consists of SR-MGM-BE9, SR-MGN-BE107, MR-MGM-BE4, and MR-MGN-BE17. [b] The TMBE32 database consists of SR-TM-BE17, MR-TM-BE13, and MR-TMD-BE2. [c] The BH76 database consists of HTBH38/08 and NHTBH38/08. [d] The ME417 database consists all the 24 subdatabases above and the ME400xAE consists all the subdatabases except AE17. The functionals arre listed in this table in order of decreasing ME400xAE.

Table 3.5 MUE (kcal/mol) for the Molecular Energy Database and its subdatabases: GAM compared to meta and hybrid functionals

Type Functional	**NGA GAM**	meta TPSS	meta revTPSS	meta M06-L	meta M11-L	hybrid B3LYP	hybrid HSE06
SR-MGM-BE9	**2.00**	2.55	2.91	3.40	7.24	4.58	3.47
SR-MGN-BE107	**2.27**	2.43	2.24	2.03	1.76	2.45	2.08
SR-TM-BE17	**6.31**	6.11	6.13	6.24	5.73	5.48	4.96
MR-MGM-BE4	**7.76**	6.69	5.98	6.15	13.50	7.76	8.52
MR-MGN-BE17	**4.22**	4.25	4.62	3.11	4.02	5.09	5.30
MR-TM-BE13	**4.94**	8.87	6.81	4.40	4.44	5.33	4.87
IsoL6/11	**1.96**	3.66	3.96	2.76	1.57	2.61	1.25
IP23	**4.53**	4.29	4.07	3.91	4.77	5.51	4.06
EA13/03	**4.49**	2.35	2.59	3.83	5.54	2.33	2.77
PA8	**3.84**	2.66	2.79	1.88	2.17	1.02	1.10
πTC13	**8.59**	8.12	7.85	6.69	5.14	6.03	6.20
HTBH38/08	**5.35**	7.71	6.96	4.15	1.44	4.23	4.23
NHTBH38/08	**5.15**	8.91	9.07	3.81	2.86	4.55	3.73
NCCE30	**1.29**	1.34	1.33	0.90	0.81	1.09	0.95
AE17	**10.18**	18.04	23.81	7.04	21.81	18.29	32.82
HC7/11	**6.24**	10.48	6.42	3.35	2.42	16.80	7.34
3dAEE7	**9.82**	10.78	10.47	7.84	14.03	8.47	10.62
4dAEE5	**5.23**	5.19	5.11	6.58	11.04	5.67	5.07
pEE5	**2.99**	2.25	2.31	7.50	10.39	2.87	5.70
DC9/12	**23.07**	14.20	14.94	10.67	5.90	12.02	9.08
2pIsoE4	**5.02**	3.54	2.53	3.16	3.32	4.69	2.44
4pIsoE4	**3.57**	2.60	3.27	2.88	5.03	4.24	2.64
NGDWI21	**0.019**	0.171	0.174	0.125	0.568	0.276	0.102
MR-TMD-BE2	**10.67**	26.21	26.59	7.22	22.18	31.21	45.13
MGBE137[a]	**2.65**	2.79	2.69	2.37	2.74	3.07	2.76
TMBE32	**6.03**	8.49	7.68	5.55	6.24	7.03	7.43
BH76	**5.25**	8.31	8.01	3.98	2.15	4.39	3.98
ME417	**4.51**	5.40	5.42	3.55	4.15	4.68	4.83
ME400xAE	**4.27**	4.86	4.64	3.41	3.40	4.10	3.64

[a] The MGBE137, TMBE32, BH76, ME417, and ME400xAE notations are explained in footnotes to Table 4.

Table 3.6 MUE (kcal/mol) for the Molecular Structure Database and its subdatabases

Functional	Type	DGL6	DGH4	MS10[a]
GKSVWN5	LSDA	0.011	0.031	0.019
SOGGA	GGA	0.009	0.013	0.010
PBEsol	GGA	0.010	0.007	0.009
PBE	GGA	0.013	0.020	0.016
BP86	GGA	0.015	0.021	0.018
PW91	GGA	0.012	0.019	0.015
BLYP	GGA	0.019	0.037	0.026
mPWPW	GGA	0.012	0.021	0.016
revPBE	GGA	0.015	0.034	0.023
BPW91	GGA	0.013	0.022	0.017
RPBE	GGA	0.016	0.038	0.025
HCTH407	GGA	0.004	0.033	0.015
SOGGA11	GGA	0.008	0.053	0.026
OLYP	GGA	0.009	0.036	0.020
OreLYP	GGA	0.011	0.034	0.020
N12	NGA	0.008	0.007	0.008
GAM	**NGA**	**0.007**	**0.034**	**0.018**
TPSS	meta	0.010	0.015	0.012
revTPSS	meta	0.011	0.009	0.010
M06-L	meta	0.006	0.018	0.011
M11-L	meta	0.012	0.033	0.021
B3LYP	hybrid	0.009	0.027	0.016
HSE06	hybrid	0.003	0.015	0.008

[a] The MS10 database consists of DGL6 and DGH4 subdatabases. The functionals are listed in the same order as in Tables 4 and 5.

Table 3.7 Mean unsigned errors for lattice constants and nearest neighbor distances in Å, band gaps in eV, and cohesive energies in eV/atom.

Functional[a]	Type	LC17	NND[b]	SBG31	SSCE8
GKSVWN5	LSDA	0.069	0.032	1.14	0.70
SOGGA	GGA	0.022	0.010	1.14	0.31
PBEsol	GGA	0.023	0.011	1.14	0.27
PBE	GGA	0.068	0.031	0.98	0.11
BP86	GGA	0.073	0.034	1.12	0.12
PW91	GGA	0.065	0.030	1.11	0.50
BLYP	GGA	0.111	0.052	1.14	0.37
mPWPW	GGA	0.075	0.035	1.11	0.10
revPBE	GGA	0.110	0.051	1.08	1.12
BPW91	GGA	0.083	0.038	1.10	0.20
RPBE	GGA	0.119	0.055	1.07	0.61
HCTH407	GGA	0.120	0.056	0.89	0.30
SOGGA11	GGA	0.125	0.058	0.89	0.07
OLYP	GGA	0.118	0.055	0.90	0.36
OreLYP	GGA	0.113	0.053	0.92	0.20
N12	NGA	0.027	0.012	0.99	0.13
GAM	**NGA**	**0.092**	**0.046**	**0.99**	**0.13**
TPSS	meta	0.055	0.025	0.85	0.22
revTPSS	meta	0.039	0.018	1.00	0.13
M06-L	meta	0.080	0.037	0.73	0.17
M11-L	meta	0.073	0.034	0.54	0.24
HSE06	hybrid	0.041	0.019	0.26	0.11

[a] The functionals are listed in the same order as in Tables 4 and 5.

[b] The values in this column are obtained by dividing the previous column by 2.15 (a standard factor determined in previous work – see text) so that the results may be compared more physically to errors in molecular bond lengths.

Table 3.8 Mean unsigned errors for the WCCR10 database in kcal/mol[a]

Functional	Type	WCCR10
PBE0	hybrid	6.40
GAM	NGA	**6.60**
PBE	GGA	7.58
TPSSh	hybrid	7.62
TPSS	GGA	7.84
B97-D-D2	GGA	8.59
B3LYP	hybrid	9.30
BP86	GGA	9.42
BP86-D3	GGA	10.62

[a]The GAM results are from the present calculations, but all other results in this table are from ref. 8

Table 3.9 Binding enthalpies (kcal/mol) of O_2 and N_2 bound to the 88-atom cluster model of Fe-MOF-74 calculated using GAM[a]

		ΔH^b	
	M_S(Fe, X_2)[c]	**GAM**[d]	Exp.[e]
Fe–N_2	2, 0	**3.9**	5.5
Fe–O_2	2, 1	**10.8**	9.8
	2, 0	**7.8**	NA
	2, -1	**5.0**	NA

[a] The basis set is def2-TZVP.

[b] The binding enthalpy (a positive value indicates exothermic binding)

[c] This column has the M_S values for the central Fe and the guest molecule in the initial iteration of self-consistent field calculations. The two peripheral Fe centers where no guest is bound were taken to have $M_S = 2$ for all the calculations.

[d] This column is calculated by eq. 1 of ref. 11.

[e] The most recent experimental value is shown, as discuss in the text.

[f] NA denotes not applicable.

Table 3.10 Binding energies (kcal/mol) of C_2H_4 bound to $Pd(PH_3)_2$ calculated using GAM and various basis sets.

Basis set[a]	**GAM**	Best estimate[b]
BS1	**11.0**	17.6
BS2	**11.1**	
BS3	**11.1**	
BS4	**11.1**	

[a]The various basis sets used are:
BS1 = SDD (Pd), cc-pVTZ (P, C, H);
BS2 = def2-TZVP (Pd), cc-pVTZ (P, C, H);
BS3 = def2-TZVP (Pd), cc-pV(T+d)Z (P), cc-pVTZ (C, H);
BS4 = def2-TZVP (Pd), maug-cc-pV(T+d)Z (P), maug-cc-pVTZ (C), cc-pVTZ (H).
[b] The best estimate was calculated in an earlier work using BCCD(T) and is described in ref. 60.

Table 3.11 Homonuclear transition metal dimers: equilibrium bond lengths (Å) and mean unsigned errors as compared to experiment.

	Cu_2	Au_2	Ni_2	Pd_2	Pt_2	Ir_2	Os_2	MUE
LSDA	2.215	2.495	2.118	2.373	2.353	2.271	2.354	0.038
PBE	2.278	2.552	2.135	2.397	2.391	2.302	2.384	0.062
B3LYP	2.292	2.577	2.099	2.411	2.392	2.301	2.387	0.071
B3PW91	2.288	2.552	2.095	2.367	2.375	2.287	2.373	0.068
mPWPW	2.293	2.549	2.088	2.359	2.369	2.282	2.369	0.068
N12	2.224	2.543	2.110	2.501	2.366	2.262	2.282	0.026
GAM	**2.306**	**2.543**	**2.189**	**2.536**	**2.408**	**2.283**	**2.292**	**0.050**
Exp.[a]	2.219	2.472	2.155	2.480	2.333	2.270	2.280	0.000

a. The experimental bond length is taken from reference 61

Table 3.12 Errors for Bond Dissociation Energy (kcal/mol) of FeC.

	M11-L	SOGGA11	τ-HCTHhyb	M06-L	BLYP	B3LYP	M05	M06
FeC	-4.60	10.81	-7.13	-7.36	12.88	-1.38	5.75	-20.93
	ωB97	ωB97X	ωB97X-D	M08-SO	M08-HX	M11	SOGGA11-X	GAM
FeC	-38.87	-20.01	21.39	-26.68	-35.65	-37.03	-67.16	1.83

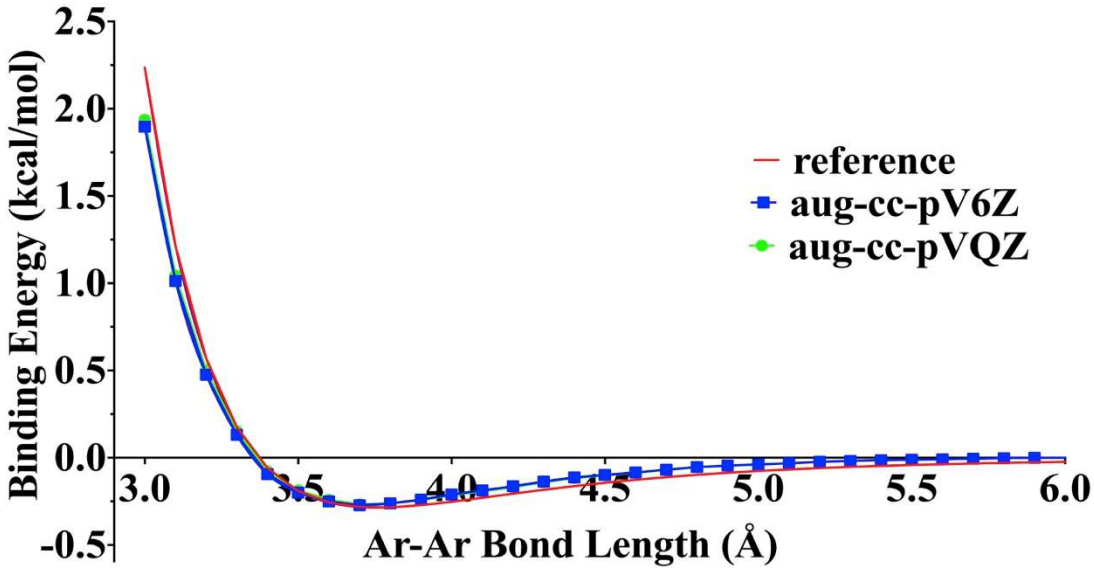

Figure 3.1. Ar-Ar Potential Curve, the bonding energies are calculated with GAM/aug-cc-pVQZ and GAM/aug-cc-pV6Z level of theory. The Reference is from the Tang-Toennies model.

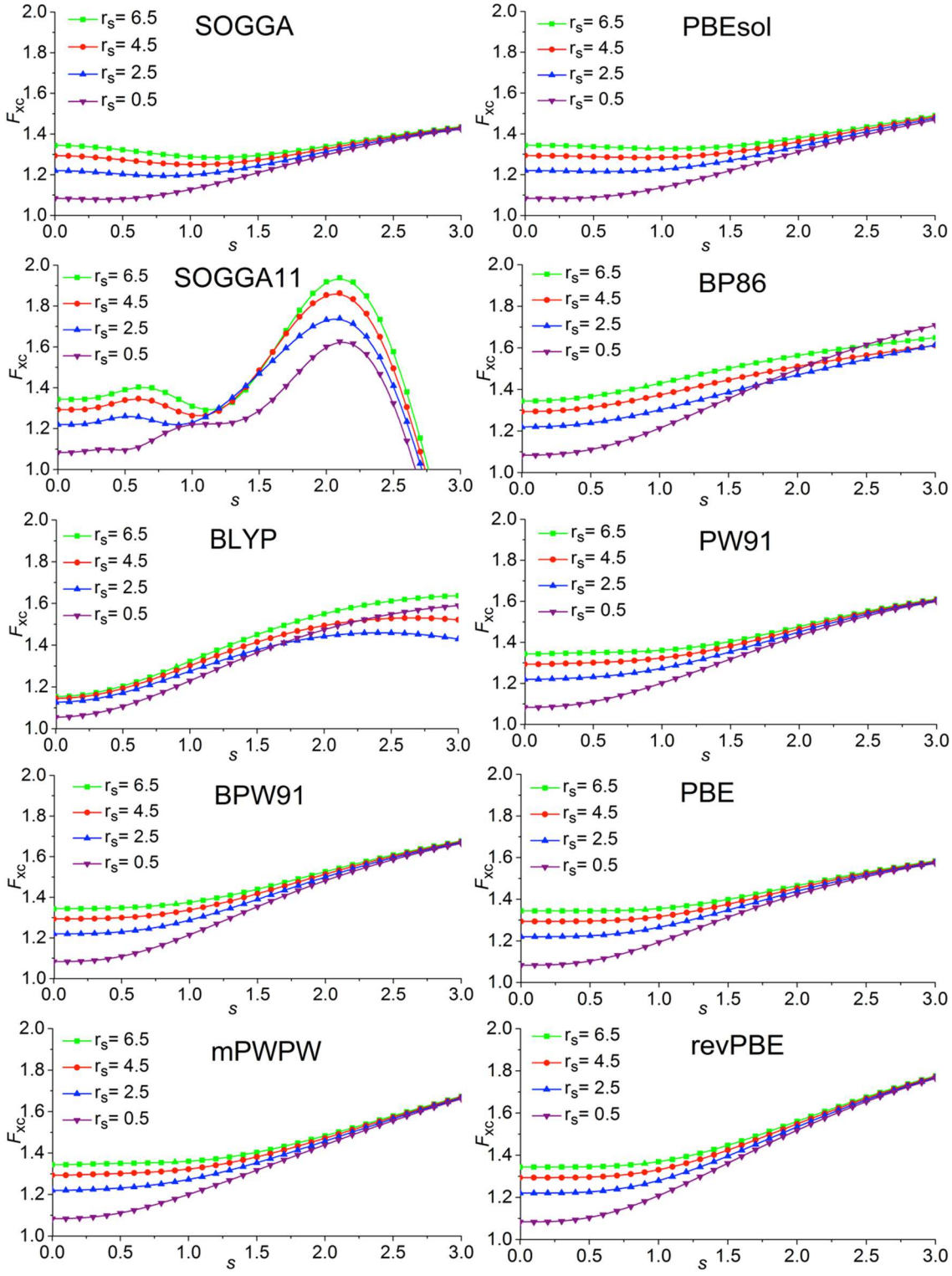
SOGGA
PBEsol
SOGGA11
BP86
BLYP
PW91
BPW91
PBE
mPWPW
revPBE
r_s= 6.5
r_s= 4.5
r_s= 2.5
r_s= 0.5
F_{xc}
s

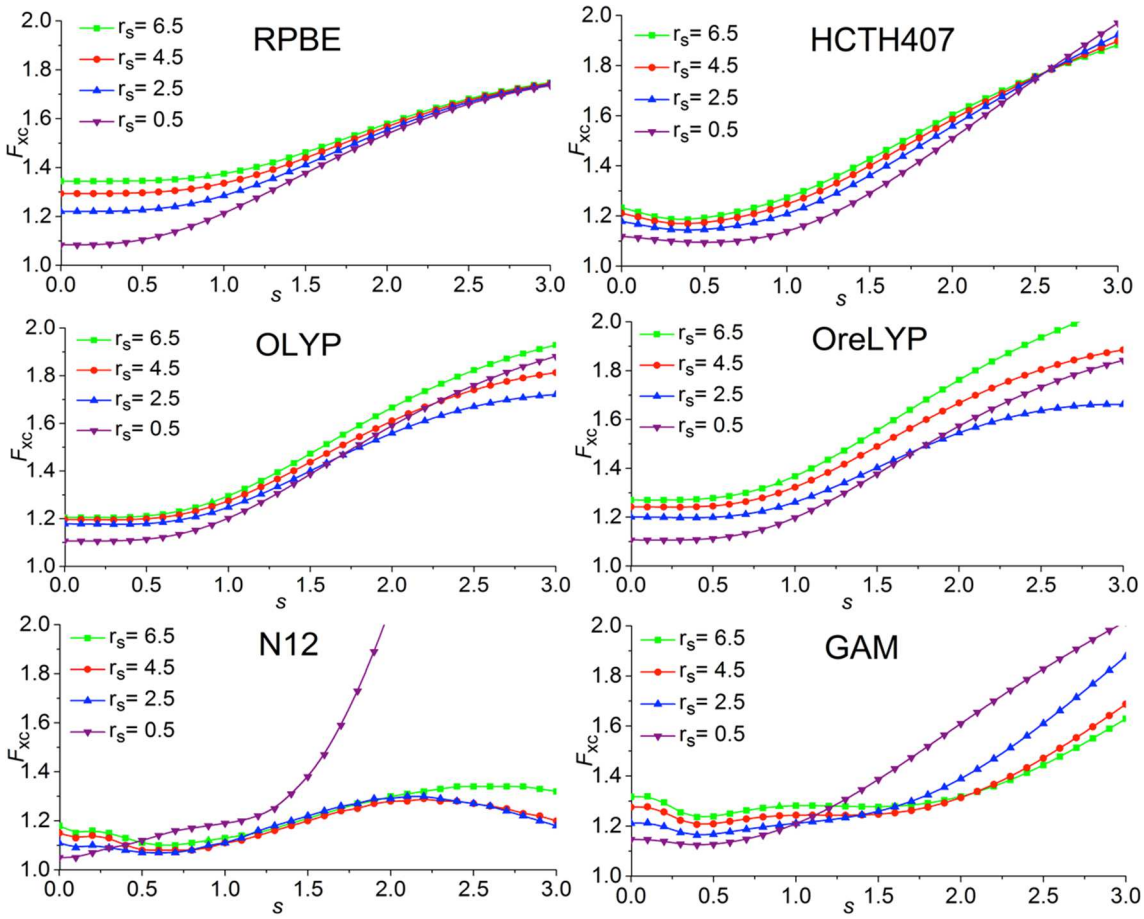

Figure 3.2 Enhancement Factor of 14 GGAs, N12, and GAM

Chapter 4. The MN15-L Functional: A New Local Exchange-Correlation Functional for Kohn-Sham Density Functional Theory with Broad Accuracy for Atoms, Molecules, and Solids

Adapted with permission from Haoyu S. Yu, Xiao He, Donald G. Truhlar, J. Chem. Theory Comput. 2016, 12, 1280-1293.

4.1 Introduction

Over the past 25 years, Kohn-Sham density functional theory has revolutionized the application of quantum mechanical electronic structure theory to complex problems in chemistry and physics.[1] The theory would be exact if we knew the exact exchange-correlation functional, which has been proven to exist but which is essentially unknowable. The accuracy of Kohn-Sham density functional theory therefore depends on our ability to develop good approximations to the exchange-correlation functional, which is often more simply called the density functional. Local functionals (e.g., those depending on only the local electron spin densities, local electron spin density gradients, and local electronic kinetic energy density for electrons of each spin) have been widely used in both chemistry and physics because (1) their computational cost, especially for extended systems, is lower than that of nonlocal functionals such as hybrid functionals depending on nonlocal Hartree-Fock exchange energy or doubly hybrid functionals depending on both nonlocal Hartree-Fock exchange energy and nonlocal correlation terms (for large systems this savings can be one to three orders of magnitude in cost), and

(2) local functionals have been more accurate for many problems containing transition metals. Yet local functionals have not been as accurate as hybrid functionals in general and especially for organic thermochemistry, chemical reaction barrier heights, and electronic spectroscopy.

A long-term goal of density functional development is to design functionals that are as accurate as possible for a set of applications that is as broad as possible, that is, to design a universal functional. Many workers have described difficulties in doing this,[2] for example, functionals that are better for thermochemistry have been less accurate for solid-state lattice constants.[3] In the present article we report significant progress by re-parameterizing the MN12-L functional against a broader database and employing smoothness restraints. The major goal for the new functional is broad accuracy for predictions of a wide range of chemical and physical properties. In designing the functional we have employed smoothness restraints that are simplifications of those introduced in a previous paper;[4] these restraints are designed to make the calculated results be smooth functions of molecular geometry and to reduce the grid sizes and number of self-consistent-field iterations as compared to those for a functional designed in the same way but without smoothness restraints.

Section 4.2 describes Minnesota Database 2015A, which is a slightly extended version of Minnesota Database 2015 presented previously;[4] part of this database is used for training, and the full database is used for testing and comparison to a large number of older exchange-correlation functionals. Although the two major divisions of Minnesota

Database 2015 were originally named chemistry database and physics database, better names are atomic and molecular database and solid-state database, respectively; therefore we change the notation in appropriate places here. In addition the new functional is tested against data not in Minnesota Database 2015A. Section 4.3 describes the computational details for computations on Minnesota Database 2015A. Section 4.4 describes previously available functionals to be used for comparison. Section 4.5 describes the design and optimization of the MN15-L functional.

Our goal was to design a functional that is smooth and has broad accuracy. Smoothness is important for rapid convergence of numerical steps and is believed to promote better transferability outside the training set, and accuracy is important for its own sake. The article proper is kept brief to promote readability by a broad readership; in particular Section 4.6 addresses smoothness, and Section 4.7 discusses accuracy. Section 4.8 summaries the main conclusions of the paper.

4.2 Minnesota Database 2015A and Test Data

The new database, designated 2015A, is obtained by extending Minnesota Database 2015[4] by the addition of twelve new pieces of data, which are the bond energy of Fe_2,[5] the first vertical excitation energy of Fe_2,[5] the atomization energies of SO_3,[6] H_2S_2,[7] and H_2SO_4,[8] and seven homonuclear transition metal bond lengths.[9] (Note that this brings the total number of homonuclear transition metal bond lengths in the database to eight.) Table 4.1 summarizes all the data in Minnesota Database 2015A. If data is used in training, it has an entry in the last column; if it is only used for testing it has "NA"

in the last column. Inverse weights in this table are explained in section 4.5. Figure 4.1 illustrates the composition of Minnesota Database 2015A pictorially.

Notice that the database includes not only relative energies, like bond energies, barrier heights, and ionization potentials, but also the absolute energies of the first 17 atoms in the periodic table (these are in database AE17) and geometrical parameters with units of length (the data in MS10 and LC17).

4.3 Computational Details

All the calculations are done by using a locally modified version of the *Gaussian 09* program.[10] All the basis sets and geometries for calculations on the Minnesota Database 2015 subset of Minnesota Database 2015A are the same as the ones used and fully explained in our work on the GAM functional.[4] The bond energy and first excitation energy of Fe_2 are treated with the def2-QZVP basis set,[11] and the atomization energies of SO_3, H_2S_2, and H_2SO_4, are treated with MG3S basis set.[12] The geometries of Ag_2 and Fe_2 are from references 9 and 5; the geometries of SO_3, H_2S_2, and H_2SO_4 are from reference 6, 7, and 8; the geometry of H_2SO_4 is calculated by M06-L/MG3S. The basis sets for transition metal bond length tests are LANL2DZ[13,14,15,16] and def2-TZVP.[11]

4.4 Density Functionals for Comparison

In Kohn-Sham density functional theory, the density is represented as that of a single Slater determinant with spin-orbitals $\psi_{i\sigma}$, where in the present work we make the usual collinear assumption that each spin orbital has the simple form $\phi_i\alpha$ or $\phi_i\beta$, where

ϕ_i is a spatial orbital; and the Born-Oppenheimer energy E (total electronic energy, which includes nuclear repulsion) is written a sum of the (i) kinetic energy of the Slater determinant, (ii) the classical Coulomb energy of the electron density, the interaction of the electron density with the nuclei, and the internuclear repulsion, and (iii) an exchange-correlation energy computed from the exchange-correlation (xc) functional F of the electron density:

$$E_{F\mathrm{xc}} = \int d\mathbf{r}\rho(\mathbf{r})F(\mathbf{r}) \tag{4.1}$$

where $\mathbf{r}$ is a point in space, and ρ is the density at that point, computed as

$$\rho = \sum_{\sigma=\alpha}^{\beta}\sum_{i=1}^{n_\sigma}\left|\psi_{i\sigma}\right|^2 = \rho_\alpha + \rho_\beta \tag{4.2}$$

where n_σ is the number of electrons of spin component σ, and ρ_α and ρ_β are spin densities. The XC functional may be local, which means it depends only on quantities evaluated at $\mathbf{r}$. Local functionals that depend only on ρ_α and ρ_β are called local spin density approximations (LSDAs); local functionals that also depend on their reduced gradients

$$x_\sigma = \rho_\sigma^{-4/3}\left|\nabla\rho_\sigma\right| \tag{4.3}$$

are called gradient approximations (generalized gradient approximation, GGAs,[17,18] or nonseparable gradient approximations, NGAs[19]); and functionals that also depend on local kinetic energy variables

$$\tilde{\tau}_\sigma = \sum_{i=1}^{n_\sigma}\left|\nabla\psi_{i\sigma}\right|^2 \tag{4.4}$$

are called[20,30] meta functionals (we consider meta-GGAs and meta-NGAs). The XC functional must account for three effects: the difference of the exact electron kinetic energy from that computed from the Slater determinant, electron exchange, and electron correlation. Nevertheless many functionals are written as a sum of two terms, called the exchange term and the correlation term. (NGAs are written as sum of a nonseparable exchange-correlation term and an additional correlation term.) Either exchange or correlation or both may be nonlocal, which means that the energy density at **r** depends on an integral over all **r**, not just on local quantities evaluated at **r**. Functionals with nonlocal correlation (sometimes called doubly hybrid functionals[21,22,23] or van der Waals functionals[24,25]) open many interesting possibilities for improvement but raise new levels of complication not associated with conventional Kohn-Sham theory and are not considered further in this article. Functionals with nonlocal exchange are called hybrid, nonlocal, or generalized Kohn-Sham. Hybrid functionals are usually defined by replacing a percentage of local exchange by nonlocal Hartree-Fock exchange; those in which the percentage is a constant are called global hybrids, and those in which the percentage depends on interelectronic separation are called range-separated hybrids. (Range separation may also be used in local functionals, as was done in the M11-L functional).

In order to evaluate the performance of the MN15-L functional, we tested a large number of previously developed density functionals for comparison. In the supporting information we show the performances of 47 previously developed density functionals of eight types and compare these to the performance of MN15-L. We selected only a subset

of these comparisons for presentation in Tables 4.3 and 4.4. We first selected the best-performing (on the basis of the MUEs for AME422, presented in full detail in the SI) gradient approximation (GA), namely GAM[4], the best-performing meta-GA, namely M06-L,[26] the best-performing hybrid-GA, namely B97-1,[27] and the best-performing hybrid meta-GA, namely, M06.[28] To these we added the most popular (as determined by citation counts) functional in each of these four categories, namely PBE[29] as a GA, TPSS[30] as a meta-GA, B3LYP[31,32,33] as a hybrid GA, and M06-2X[28] as a hybrid-meta-GA. These tables also include B97-3,[34] PBE0, [35] ωB97X-D, [36] HSE06,[37,38] and M11-L; [39] although somewhat arbitrarily selected for illustration, including them gives a better representation of various interesting types of functional.

For extended systems, by using the density-fitting algorithm, calculations with local functionals (GAs and meta-GAs) can be carried out with significantly less computational cost than hybrid functionals. Thus the comparison of the present new functional to previous local functionals is of special interest for judging functionals that are affordable for applications involving the most extended systems (large molecular systems and solid-state systems with periodic boundary conditions).

4.5 Design and Parameterization of the MN15-L Functional

One advantage of employing the kinetic energy density term is to differentiate regions (such as regions occupied mainly by a single electron or a singlet-coupled pair of electrons) where the density is dominated by a single spatial orbital; this allows one to diminish in those regions the errors in density functional theory due to the self-interaction

energy in the classical Coulomb interaction energy and due to self-correlation energy when correlation energy is written as a function of electron density without explicit electron correlation.[40,41] It can also distinguish regions of decaying density from bonding regions.[42,43] The MN15-L functional is a meta-NGA functional of the same functional form as used for the MN12-L functional. However, having learned from the experience of designing and using MN12-L, the new functional is trained over a broader training set and its parameters are determined with smoothness restraints.

The form of the MN15-L functional is that it is the sum of a nonseparable exchange-correlation energy term E_{nxc} plus an additional correlation energy term E_{c}. The dependence on ρ_σ ($\sigma = \alpha, \beta$) and x_σ is the same as employed in the N12 and GAM functionals, the dependence on $\tilde{\tau}_\sigma$ is the same as in MN12-L. For the additional correlation energy term E_{c}, we use the same mathematic form as we used in M08-SO,[44] M08-HX,[44] M11-L,[45] and M11.[46]

The exchange-correlation functional can be written as a sum of nonseparable exchange-correlation term $E_{\mathrm{nxc}}^{\mathrm{NSGA}}$ and a correlation term E_{c}. The former is

$$E_{\mathrm{nxc}} = \sum_{\sigma} \int d\mathbf{r} \rho_\sigma \left\{ \varepsilon_{\mathrm{x}\sigma}^{\mathrm{UEG}} \sum_{i=0}^{3} \sum_{j=0}^{3-i} \sum_{k=0}^{5-i-j} a_{ijk} v_{\mathrm{x}\sigma}^{i} u_{\mathrm{x}\sigma}^{j} w_{\sigma}^{k} \right\} \tag{4.5.1}$$

$$\varepsilon_{x\sigma}^{\mathrm{UEG}} = -\frac{3}{2}\left(\frac{3}{4\pi}\right)^{1/3} \rho^{1/3} \tag{4.5.2}$$

In eq. 4.5.1, $\varepsilon_{\mathrm{x}\sigma}^{\mathrm{UEG}}$ is the Gáspár-Kohn-Sham LSDA approximation[47] to the exchange energy per electron of a given spin and given density; this result would be correct for a

hypothetical system with a uniform density of electrons.[47,48] The nonseparable term is written as the product of powers of *v, u*, and *w*, which are defined as follows:

$$v_{\mathrm{x}\sigma} = \frac{\omega_{\mathrm{x}\sigma}\rho_\sigma^{1/3}}{1+\omega_{\mathrm{x}\sigma}\rho_\sigma^{1/3}} \tag{4.6.1}$$

$$u_{\mathrm{x}\sigma} = \frac{\gamma_{\mathrm{x}\sigma}x_\sigma^2}{1+\gamma_{\mathrm{x}\sigma}x_\sigma^2} \tag{4.6.2}$$

$$w_\sigma = \frac{y_\sigma - 1}{y_\sigma + 1} \tag{4.6.3}$$

$$y_\sigma = (3/5)\left(6\pi^2\right)^{2/3}\rho_\sigma^{5/3}/\tilde{\tau}_\sigma. \tag{4.6.4}$$

For the nonlinear coefficients of MN15-L, we use the same values as in the GAM functional, namely $\omega_{\mathrm{x}\sigma} = 2.5$ and $\gamma_{\mathrm{x}\sigma} = 0.004$. The kinetic energy density is introduced through eqs. 4.6.3 and 4.6.4.

The additional correlation energy is

$$E_c = \sum_\sigma \int dr \rho \varepsilon_c^{\mathrm{LSDA}}(\rho) \sum_{i=0}^{8} b_i w_\sigma^i + \int dr \rho H^{\mathrm{PBE}}(\rho, s) \sum_{i=0}^{8} c_i w_\sigma^i \tag{4.7}$$

where the function $\varepsilon_c^{\mathrm{LSDA}}$ is the correlation energy per electron of the uniform electron gas,[49] the function H^{PBE} is the PBE gradient correction for the correlation energy,[29] and the function w_σ is defined in eq. 6c.

With the functional form given by the sum of eqs 4.5.1 and 4.7, we optimized all the linear parameters against training data shown in Table 4.1. The MN15-L functional is optimized by minimizing

$$U = \sum_{n=1}^{28} R_n / I_n + \lambda(a+b+c) \tag{4.8.1}$$

with

$$R_n = \sqrt{\sum_{i}^{n} (E_i)^2 / N} \tag{4.8.2}$$

where R_n stands for the root mean squared error of a database or subset n in Table 4.1, E_i is the error of the ith data in database or subset n, N is the total number of data in database or subset n, and I_n stands for the inverse weight of database or subset n. The initial inverse weight of each database is chosen based on the average performance of 84 density functionals we tested against Minnesota Database 2015A. For example, we set the mean unsigned error for the noble gas dimer weak interaction database over the 81 other functionals studied (the 84 for which we had results for the full database but excluding GAM, MN12-L, and MN15-L) is 0.206 kcal/mol; therefore, we initially set the inverse weight I_{11} equal to 0.206 kcal/mol. Then, based on the performance of preliminary versions of the MN15-L functional, we decreased or increased the weights of the various databases and the smoothness restraint to try to obtain balanced across-the-board accuracy with a smooth functional. For example, we reduced I_{11} to be 0.005 kcal/mol, which gives us an MUE of 0.024 kcal/mol. Note that while iterating the weights (and hence iterating the trial density functionals determined from these weights), when the weights change appreciably, and hence the trial density functional changes appreciably, one must update the densities of all species in the database to be consistent with the current version of density functional. The sum in eq. 4.8.2 is over the rows of

Table 4.1 that have a value in the I_n column; notice that a smaller I_n corresponds to a larger weight.

The product of λ times the sum of *a*, *b*, and *c* controls the smoothness of the functional. The reasons for controlling the smoothness of the MN15-L functional by these restraints are to prevent the grid requirements from being unnecessarily large and to promote easier self-consistent-field (SCF) convergence. The formulas for *a*, *b*, and *c* are

$$a = \sum_{i=0}^{3} \sum_{j=0}^{3-i} \sum_{k=0}^{4-i-j} (a_{i,j,k} - a_{i,j,k+1})^2 \tag{4.9}$$

$$b = \sum_{i=0}^{7} (b_i - b_{i+1})^2 \tag{4.10}$$

$$c = \sum_{i=0}^{7} (c_i - c_{i+1})^2 \tag{4.11}$$

As we can see from these equations, when the coefficients become large or alternate in sign, the product of λ and the sum of *a*, *b*, and *c* increases as a penalty term in the minimization of function *U*. Based on our experience with SCF convergence, with grid requirements for converged frequencies (which will be discussed in section 7.3), with the smoothness of rare gas potential curves (which will be discussed in section 7.2), and with the effect of λ on the various R_n, we chose the value of λ to be 0.01.

The main purpose of our paper is to design a universal density functional; therefore, we include various atomic, molecular, and solid-state properties in our training set. The breadth of the training set is very important. The MN15-L functional is optimized against the most diverse database yet used for training a density functional, especially because of the broad inclusion of both main-group and transition metal data. Our training set includes quantities depending on relative energies like bond energies,

ionization potentials, electron affinities, proton affinities, barrier heights for chemical reactions, noncovalent van der Waals binding energies, atomic excitation energies, and isomerization energies, diatomic molecule geometry, and atomic energy; it includes absolute energies of atoms; and it includes solid-state properties like lattice constant.

We found, as we have found in previous work, that without a sufficiently powerful functional form, simply increasing the orders of the polynomials will not enable one to accurately reproduce a large amount of diverse data. When we increase the number of parameters, which means increasing the values of *i, j,* and *k*, the contributions of the higher-order terms of the polynomials in eq. 4.5 do not usually decrease the error by a large amount. We conclude that it is the lower-order terms of the polynomials that have the main effect on the accuracy. The design of the functional form is very important for parameterizing good density functionals. The MN15-L functional form is more flexible than most other functionals, and it has better near-universal performance than various other functional forms we have tried.

The values of all the linear parameters of MN15-L are shown in Table 4.2.

4.6 Properties of the New Exchange-Correlation Functional

4.6.1 Convergence Test

If a functional is not smooth, it may require especially fine grids to converge the integral in eq. 4.1.The next test we made was whether the new functional presented here requires exceptionally fine grids. Vibrational perturbation theory[50,51] calculations of frequencies are a good test of smoothness because they involve second, third, and fourth derivatives

of the energy. Therefore we tested smoothness by calculating harmonic and anharmonic frequencies of ethanol by the MN15-L and TPSSh[52] functionals with various grids. The TPSSh functional is chosen for this comparison because it is a well designed hybrid meta functional, which make the comparison to the MN15-L hybrid meta functional reasonable. We found (as shown in tables S12 and S13 in the SI of the MN15-L paper[53]) that the MN15-L harmonic frequencies converge better with respect to the increasing of the grids than do the frequencies computed by the TPSSh functional, and so we conclude that the new functional is smooth enough in this respect. The SI[53] also compares MN15-L frequencies to those calculated by second-order wave function perturbation theory (MP2)[54] and by six other functionals including M06-2X, M08-HX, ωB97X-D,[55] MPW1K,[56] B3LYP, and PBE0.[57] The results (the harmonic frequencies are shown in tables S14 and S8 of the S15) [53] show that MN15-L predicts very reasonable frequencies as compared to MP2 and other functionals.

4.6.2 Rare Gas Potential Curves

The potential curves calculated for rare gas Ar_2, by the nine density functionals including MN15-L with the aug-cc-pVQZ basis set and with a grid having 250 radial shells around each atom and 590 angular points in each shell, are shown in Figure 4.2. As we can see that the MN15-L and GAM give results close to the experimentally determined[58] potential curves over a reasonably wide range, even though the training set has only three points near the minimum. The B3LYP functional predicts repulsive energy

near the correct equilibrium geometry, and other functionals underestimate the attraction between Ar atoms.

In the supporting information[53] we also show the potential curves of Ne_2, Kr_2, and KrHe calculated by MN15-L, MGGA_MS2, and M06-L. These figures show that MN15-L gives the best potential curves even though there is no KrHe potential data in our training set. The supporting information also shows that the calculated curves are smooth if one converges the numerical integrations.

Figure S8[53] in the supporting information shows the Ar_2 potential curve calculated by MN15-L with aug-cc-pVQZ and aug-cc-pV6Z basis sets. This figure shows that the results are stable with respect to even unnecessarily large increases in the basis set.

4.7 Performance of the MN15-L Functional

In this section we consider tables and figures that compare the performance of the MN15-L functional to the performances of eight other density functionals (See section 4.4) for subdatabases (key subsets of the data discussed in Section 2). Figures 4.4, 4.5, and 4.6 present the main comparisons for nine combined atomic and molecular energy databases, and Table 4.3 shows the rankings of 12 selected functionals against 16 subdatabases. Figure 4.7 shows the performance of the MN15-L functional against molecular geometry databases. Figure 4.8 shows the performance of the MN15-L functional against solid-state energy and geometry databases. Figure 4.9 shows the performance against an additional molecular test set. Figure 4.10 shows the performance against the transition metal dimer bond length database. These figures and Table 4.3 are a

subset of the data considered in designing, parameterizing, and testing the functional. In the following subsections, we are mainly comparing MN15-L with eight other functionals, namely, PBE, GAM, TPSS, M06-L, B3LYP, B97-1, M06-2X, and M06.

4.7.1 Atomic and Molecular Energies

Figure 4.4 compares the performance for 33 transition metal bond energies (TMBE33) and 76 reaction barrier heights (BH76). Among the functionals shown in Figure 4.4, MN15-L gives the smallest mean unsigned error (MUE) for TMBE33. It has been well established in the literature that most of the density functionals cannot predict accurate results for both reaction barrier heights and transition metal bond energies – as one of these is improved, the other usually gets worse. As we can see from Figure 4.4, B97-1 and M06-L give fairly good results for TMBE33, but their performances on BH76 are respectively 3.9 and 4.0 kcal/mol, which are not very good. On the other hand, M06 and M06-2X gives relatively small MUEs for BH76, in particular 2.2 kcal/mol and 1.2 kcal/mol respectively, but have higher errors for transition metals. The MN15-L functional is the only functional that can predict relatively accurate results for both of these databases.

Figure 4.5 shows the performance of nine density functionals against main-group bond energies (MGBE137), main-group and transition-metal excitation energies (EE18), main-group isomerization energies (IsoE14), and hydrocarbon thermochemistry (HCTC) databases. The MN15-L functional gives the best results for MGBE137 and EE18. It is

also the only functional that gives an MUE smaller than 5.0 kcal/mol for all four databases.

Weak noncovalent interactions were traditionally difficult to predict by density functional theory, a problem that is truly satisfactorily resolved only by including nonlocal correlation, which is beyond the present scope; however, modern XC functionals with the right ingredients can predict reasonably accurate van der Waals binding energies. In Figure 4.6, MN15-L predicts the second best results among local functionals for the noncovalent interaction (NC51) database; it trails two of the hybrid meta functionals M06-2X and M06 and one of meta gradient approximations M06-L.

Figure 4.6 also shows that MN15-L gives the lowest MUE for the full set of 422 atomic and molecular energies (AME422). Some functionals are very poor for absolute energies, and to see if those functionals might fare better if we remove absolute energies from the comparison, we also computed the MUE for the 405 data remaining after excluding absolute energies; this is called database AME405xAE. Figure 4.6 shows that MN15-L remains the best functional even after this removal.

Although MN15-L is not the best functional in every category, as we have just seen, its strength is its high across-the-board accuracy. In Table 3, we show the rankings of 12 popular functionals against 16 subdatabases that form the MGBE137, TMBE33, BH76, NC51, EE18, and HCTC20 databases. The B97-1 functional is very good for both main-group and transition metal bond energies; however, it does not provide accurate reaction barriers and excitation energies. The ωB97X-D functional gives good single-

reference bond energies, better-than-average reaction barriers, and good noncovalent interaction energies, but it failed badly for multi-reference systems and atomic excitation energies.

The M06-2X functional gives good single-reference main-group bond energies, reaction barriers heights, and noncovalent interaction energies, but as was pointed out when it was originally presented, it was presented as a specialized functional for main-group chemistry and was not recommended for transition metal systems.

Since a practical application to a complex system may require calculations of a variety of properties – all in a single application, it can be very advantageous – even necessary – to use a functional designed to be universal. The MN15-L functional is the only functional that ranks in the top third of the 48 considered functionals in 15 of the 16 categories of Table 4.3. The average ranking of MN15-L in these 16 categories is no. 8, which is the best among all tested functionals by a reasonably large margin, with the second best average rank being no. 13. We list the rankings of all 48 density functionals against these 16 subdatabases in the supporting information.

Our database has 54 multi-reference systems, 300 single-reference systems, 51 noncovalent interactions, and 17 absolute energies, which makes the total 422 data. For the 300 single-reference data, MN15-L has an MUE of 1.85 kcal/mol, which may be compared to some values for hybrid functionals: 2.72 kcal/mol for M06, 2.16 kcal/mol for M06-2X, and 3.89 for B3LYP. For the 54 multi-reference data, MN15-L has an MUE of 4.35 kcal/mol, which may be compared to 5.43 kcal/mol for M06, 13.33 kcal/mol for

M06-2X, and 10.67 kcal/mol for B3LYP. Thus the performance of the new local functional is excellent compared to previous hybrid functionals.

For M06-2X, the very large mean unsigned error for multi-reference systems is mainly due to the bond energies of V_2 and Cr_2. The MUE of M06-2X for the 52 multi-reference systems excluding V_2 and Cr_2 is 7.96 kcal/mol. This is smaller, but still much larger than for single-reference systems, and this confirms our previous recommendations not to use M06-2X for transition metal systems or other multi-reference systems.

4.7.2 Molecular Geometries

Figure 4.7 shows the performance of MN15-L against the molecular geometry databases. The category labeled "DGL6" includes six light diatomic molecules (Cl_2, H_2, HF, MgS, N_2, and OH). The category labeled "DGH4" includes four diatomic molecules with one or more heavy atom (HBr, NaBr, ZnS, and Ag_2). The category labeled "MS10" is the average MUE over all ten molecules. The MN15-L functional gives the best results in all three categories.

The combination of these results with those in the previous subsection demonstrates that MN15-L provides good results for both atomic and molecular energies and molecular geometries.

4.7.3 Solid-State Databases

Figure 4.8 shows the MUE of various functionals against three solid-state databases: lattice constants (LC17), semiconductor band gaps (SBG31), and solid-state cohesive energies (SSCE8). The MN15-L gives the best results for LC17 and SSCE8 and

second best for SBG31. Therefore, the MN15-L functional is the best functional tested in our paper for both chemistry and physics databases.

4.7.4 Additional Test Sets

We also tested our new functional against the WCCR10 database,[59] which is a recently published database for large transition metal complex coordination energies. In Figure 4.9, we compare the performance of MN15-L with other functionals. The MN15-L functional is the best functional with an overall MUE of 5.46 kcal/mol for the WCCR10 database. All the other functionals tested in the figure provide an overall MUE larger than 6.00 kcal/mol.

For Figure 4.10, we applied 11 widely used functionals plus the new MN15-L functional and the recent GAM functional to calculate the bond lengths of homonuclear transition metal dimers. We used two basis sets namely, LANL2DZ[13,14,15,16] (which was used by previous workers[9] for this test set, and def2-TZVP, [11] which is a higher-quality basis set, to test the performance of these 11 functionals. The results are the MUE over two basis sets, and we expect this to be a more robust assessment of the density functionals than using a single basis set. The MN15-L functional gives the best result with an overall MUE of 0.030 Å. In summary, the performance of MN15-L again WCCR10 and this transition metal database show that the MN15-L functional performs very well for energy and geometry test sets outside the training set as well as within it.

4.7.5 Further Comparison of Results with MN15-L

Table 4.4 shows that the MN15-L density functional provides considerable improvement over MN12-L. In particular, MN15-L provides better performance than MN12-L for 17 of the 25 databases in in the table. The MN12-L functional provides good performance for hydrocarbons (HC7), with an MUE of 2.58 kcal/mol as compared to 3.98 kcal/mol for MN15-L; and MN12-L gives better noncovalent complexation energies (NCCE30) than MN15-L. For more general applications, we think that MN15-L should be preferred over MN12-L. Tale S19 in the SI53 shows that he MN12-L and MN15-L functionals give MUEs of 0.035 and 0.030 Å, respectively, for the transition metal dimer bond length (TMDBL7) database.

We also include eight other functionals in Table 4.5, in particular the eight functionals singled out in Section 4.4 for best performance in a class and most popular in a class. Table 4.5 shows that the MN15-L functional gives very good performance for reaction barrier heights and transition metal bond energies. We see that MN15-L also gives the best performance for excitation energies, which are mainly atomic excitation energies in this database. The GAM and MN15-L functionals are the only two functionals that give an MUE smaller than 0.03 kcal/mol for the noble gas dimer interactions. In the last two rows of Table 4.5, we show the MUEs of single-reference systems (SR300) and multi-reference systems (MR54). One of our goals in designing the MN15-L functional was decreasing the errors in multi-reference systems while keep the good performance for single-reference systems. The MN15-L functional is the only one that gives both an

MUE smaller than 4.5 kcal/mol for MR54 and an MUE smaller than 2.00 kcal/mol for SR300.

4.8 Conclusions

We have presented a meta-NGA exchange-correlation functional called MN15-L that provides across-the-board high accuracy for atoms, molecules, and solids. The convergence of the functional has been checked against all the data included in the Minnesota Database 2015A (only a portion of which is used for training) and in additional test sets. We ensured that the MN15-L functional provides smooth results for both rare-gas dimer potential energy curves and exchange-correlation enhancement factors and that the rare-gas potential energy curves converge well for large basis sets. As is well known, adding Hartree–Fock exchange can improve the performance of the functionals for reaction barrier heights, band gaps, electron affinities, atomic excitation energies, and proton affinities; but at the same time it usually increases the error of transition metal bond energies, brings in static correlation error, and increases the cost for extended systems. The present functional without Hartree-Fock exchange performs better on average (by a considerable amount) than all available functionals whether or not they have Hartree-Fock exchange. In particular, The MN15-L functional gives an overall mean unsigned error (MUE) of 2.32 kcal/mol for the AME422 database of energetic quantities for atoms molecules, with the second best functional (M06) having an MUE of 2.84 kcal/mol, and the popular B3LYP and PBE functionals have MUEs of 4.80 and 7.58 kcal/mol, respectively, on Minnesota Database 2015A. Moreover, the MN15-L functional

not only has small average errors across databases, it has uniformly good performance in that it gives the best results for main-group bond energies, transition metal bond energies, and atomic excitation energies, fourth best (out of 48 functionals tested) for noncovalent interactions, and seventh best for reaction barrier heights and for hydrocarbon energetics. In addition, the MN15-L functional is tied for the best results for diatomic molecule bond lengths. For the solid-state quantities we do not test functionals with nonzero Hartree-Fock exchange at large interelectronic distances because these are too expensive for most practical applications to solids, but out of 27 functionals with no Hartree-Fock exchange or screened Hartree-Fock exchange, MN15-L is third best for solid-state cohesive energies, fifth best for semiconductor band gaps, and eighth best for solid-state lattice constants. The MN15-L functional is the only functional that gives reasonably accurate results for all these properties. Since many applications in new energy, nanotechnology, functional materials, synthesis, understanding chemical dynamics and catalysis, biochemistry, and the drive toward a cleaner environment require good accuracy in two or several of the properties tested, we believe the good across-the-board performance will be useful for a variety of research areas in the future.

4.9 Reference

[1] W. Kohn, *Rev. Mod. Phys.* 1999, **71**, 1253.

[2] A. J. Cohen, P. Mori-Sánchez, and W. Yang, *Chem Rev.* 2012, **112**, 289.

[3] R. Peverati and D. G. Truhlar, *Phil. Trans. R. Soc. A* 2014, **372**, 20120476.

[4] H. S. Yu, W. Zhang, P. Verma, X. He, and D. G. Truhlar, *Phys. Chem. Chem. Phys.* 2015, **17**, 12146.

[5] C. E. Hoyer, G. L. Manni, D. G. Truhlar, and L. Gagliardi, *J. Chem. Phys*. 2014, **141**, 204309.

[6] http://webbook.nist.gov/cgi/cbook.cgi?ID=C7446119&Units=SI, accessed on Jul. 26, 2015.

[7] http://webbook.nist.gov/cgi/cbook.cgi?ID=C63344865&Units=SI, accessed on Jul. 26, 2015.

[8] http://webbook.nist.gov/cgi/cbook.cgi?ID=C7664939&Units=SI&Mask=1#Thermo-Gas, accessed on Jul. 26, 2015.

[9] A. Posada-Borbón and A. Posada-Amarillas, *Chem. Phys. Lett.* 2015, **618**, 66.

[10] Y. Zhao, R. Peverati, K. R. Yang, S. Luo, H. Yu, X. He, and D. G. Truhlar, *MN-GFM, version 6.5: Minnesota Gaussian Functional Module*; University of Minnesota: Minneapolis, MN, 2015.

[11] F. Weigend and R. Ahlrichs, *Phys. Chem. Chem. Phys.* 2005, **7**, 3297.

[12] B. J. Lynch, Y. Zhao, and D. G. Truhlar, *J. Phys. Chem. A*, 2003, **107**, 1384.

[13] T. H. Dunning Jr. and P. J. Hay, in *Modern Theoretical Chemistry*, ed. Schaefer III, Plenum, New York, 1977, vol.3, pp. 1-28.

[14] P. J. Hay and W. R. Wadt, *J. Chem. Phys.*, 1985, **82**, 270.

[15] P. J. Hay and W. R. Wadt, *J. Chem. Phys*. 1985, **82**, 284.

[16] P. J. Hay and W. R. Wadt, *J. Chem. Phys*. 1985, **82**, 299.

[17] D. C. Langreth and M. J. Mehl, *Phys. Rev. B* 1983, **28**, 1809.

[18] J. P. Perdew and Y. Wang, *Phys. Rev. B* 1986, **33**, 8800.

[19] R. Peverati and D. G. Truhlar, *J. Chem. Theory Comput.* 2012, **8**, 2310.

[20] J. P. Perdew, S. Kurth, A. Zupan, and P. Blaha, *Phys. Rev. Lett.* 1999, **82**, 2544.

[21] Y. Zhao, B. J. Lynch, and D. G. Truhlar, *J. Phys. Chem. A* 2004, **108**, 4786.

[22] I. Y. Zhang and X. Xu, *Int. Rev. Phys. Chem.* 2011, **30**, 115.

[23] M. Steinmetz, A. Hansen, S. Ehrlich, and T. Risthaus, Grimme, S. *Top. Curr. Chem*. 2015, **365***,* 1.

[24] M. Dion, H. Rydberg, E. Schröder, D. C. Langreth, and B. I. Lundqvist, *Phys. Rev. Lett.* 2004, **92**, 246401.

[25] O. A. Vydrov and T. Van Voorhis, *J. Chem. Phys.* 2010, **133**, 244103..

[26] Y. Zhao and D. G. Truhlar, *J. Chem. Phys.* 2006, **125**, 194101.

[27] F. A. Hamprecht, A. J. Cohen, D. J. Tozer, and N. C. Handy, *J. Chem. Phys.* 1988, **109**, 6264.

[28] Y. Zhao and D. G. Truhlar, *Theor. Chem. Acc.* 2008, **120**, 215.

[29] J. P. Perdew, K. Burke, and M. Ernzerhof, *Phys. Rev. Lett.* 1996, **77**, 3865.

[30] J. M. Tao, J. P. Perdew, V. N. Staroverov, and G. E. Scuseria, *Phys. Rev. Lett.* 2003, **91**, 146401.

[31] A. D. Becke, *Phys. Rev. A,* 1988, **38**, 3098.

[32] C. Lee, W. Yang, and R. G. Parr, *Phys. Rev. B,* 1988, **37**, 785.

[33] P. J. Stephens, F. J. Devlin, C. F. Chabalowski, and M. J. Frisch, *J. Phys. Chem*. 1994, **98**, 11623.

[34] T. W. Keal and D. J. Tozer, *J. Chem. Phys.* 2005, **123**, 121103.

[35] C. Adamo and V. Barone, *J. Chem. Phys.* 1999, **110**, 6158.

[36] J.-D. Chai and M. Head-Gordon, *Phys. Chem. Chem. Phys.* 2008, **10**, 6615.

[37] J. Heyd, G. E. Scuseria, and M. Ernzerhof, *J. Chem. Phys*. 2003, **118**, 8207.

[38] T. M. Henderson, A. F. Izmaylov, G. Scalmani, and G. E. Scuseria, *J. Chem. Phys*. 2009, **131**, 044108.

[39] R. Peverati and D. G. Truhlar, *J. Phys. Chem. Lett.* 2011, **3**, 117.

[40] A. D. Becke, *J. Chem. Phys.* 2000, **112**, 4020.

[41] Y. Zhao, N. E. Schultz, and D. G. Truhlar, *J. Chem. Phys.* 2005, **123**, 161103.

[42] R. Peverati and D. G. Truhlar, *Phys. Chem. Chem. Phys.* 2012, **14**, 13171.

[43] L. Ferrighi, B. Hammer, and G. K. H. Madsen, *J. Am. Chem. Soc.* 2009, **131**, 10605.

[44] Y. Zhao and D. G. Truhlar, *J. Chem. Theory Comput.* 2008, **4**, 1849.

[45] R. Peverati and D. G. Truhlar, *J. Phys. Chem. Lett.* 2011, **3**, 117.

[46] R. Peverati and D. G. Truhlar, *J. Phys. Chem. Lett.* 2011, **2**, 2810.

[47] (a) R. Gáspár, *Acta Phys. Hung*. 1954, **3**, 263-286. (b) R. Gáspár, *Acta Phys. Hung*. 1974, **35**, 213.

[48] W. Kohn and L. Sham, J. *Phys. Rev.,* 1965, **140**, A1133.

[49] J. P. Perdew and Y. Wang, *Phys. Rev. B* 1992, **45**, 13244.

[50] H. H. Nielsen, H. H. The vibration-rotation energies of molecules and their spectra in the infra-red. In *Handbuch der Physik*; Flügge, S., Ed.; Springer: Berlin, 1959; Vol. 37, pp. 173-313.

[51] Q. Zhang, P. N. Day, and D. G. Truhlar, *J. Chem. Phys.* 1993, **98**, 4948.

[52] V. N. Staroverov, G. E. Scuseria, J. Tao, and J. P. Perdew, *J. Chem. Phys*. 2003, **119**, 12129.

[53] H. S. Yu, X. He, and D. G. Truhlar, *J. Chem. Theory Comput.* 2016, **12**, 1280.

[54] J. A. Pople, J. S. Binkley, and R. Seeger, *Int. J. Quantum Chem. Symp.* 1976, **10**, 1–19.

[55] J.-D. Chai and M. Head-Gordon, *Phys. Chem. Chem. Phys.* 2008, **10**, 6615.

[56] B. J. Lynch, P. L. Fast, M. Harris, and D. G. Truhlar, *J. Phys. Chem. A* 2000, **104**, 4811.

[57] C. Adamo and V. Barone, *J. Chem. Phys.* 1999, **110**, 6158.

[58] K. T. Tang and J. P. Toennies, *J. Chem. Phys.* 2003, **118**, 4976.

[59] T. Weymuth, E. P. A. Couzijn, P. Chen, and M. Reiher, *J. Chem. Theory Comput.* 2014, **10**, 3092.

Table 4.1. Databases included in Database 2015A[a,b]

n	Combine	Primary[g]	Secondar	Description	I_n[c]
	AME422			Atomic and Molecular Energies	
	MGBE13			Main-group bonding energies	
		SR-MGM-BE9		Single-reference main-group metal bond energy	1.11
	_		SRM2	Single-reference main-group bond energies	
			SRMGD	Single-reference main-group diatomic bond energies	
			3dSRBE	3d single-reference metal-ligand bond energies	
2		SR-MGN-BE107		Single-reference main-group non-metal bond energies	0.11
3		MR-MGM-BE4		Multi-reference main-group metal bond energies	1.98
4		MR-MGN-BE17		Multi-reference main-group non-metal bond energies	1.67
	TMBE33			Transition metal bonding energies	
5		SR-TM-		Single-reference TM[d] bond energies	1.35
			3dSRBE	3d single-reference metal-ligand bond energies	
			SRMBE	Single-reference metal bond energies	
			PdBE2	Palladium complex bond energies	
			FeCl	FeCl bond energy	
6		MR-TM-BE1		Multi-reference TM bond energies	1.01
			3dMRB	3d multi-reference metal-ligand bond energies	
			MRBE3	Multi-reference bond energies	
			remainin	Bond energies of remaining molecules: CuH, VO, CuCl,	
7		MR-TMD-		Multi-reference TM dimer bond energies (Fe_2, Cr_2, and	1.51
	BH76			Reaction barrier heights	
8		HTBH38/08		Hydrogen transfer barrier heights	0.50

9		NHTBH38/0	Non-hydrogen transfer barrier heights	0.40
	NC51		Noncovalent interaction	
10		NCCE30	Noncovalent complexation energies	0.10
11		NGDWI21	Noble gas dimer weak interaction	0.005
	EE18		Excitation energies	
12		3dEE8	3d TM atomic excitation energies and first excitation	1.78
13		4dAEE5	4d TM atomic excitation energies	8.97
14		pEE5	p-block excitation energies	7.81
	IsoE19		Isomerization energies	
15		4pIsoE4	4p isomerization energies	8.00
16		2pIsoE4	2p isomerization energies	7.81
17		IsoL6/11	Isomerization energies of large molecules	2.00
	HCTC20		Hydrocarbon thermochemistry	
18		πTC13	Thermochemistry of π systems	5.75
19		HC7/11	Hydrocarbon chemistry	6.48
20		EA13/03	Electron affinities	2.96
21		PA8	Proton affinities	2.23
22		IP23	Ionization potentials	3.64
23		AE17	Atomic energies	3.41
24		SMAE3	Sulfur molecules atomization energies	5.00
25		DC9/12	Difficult cases	10.00
	MS10		Molecular structures	
26		DGL6	Diatomic geometries of light-atom molecules	0.01
		DGH4[f]		

27			DGH3	Diatomic geometries of heavy-atom molecules: ZnS,	0.01
	SS17			Solid-state structures	
29		LC17		Lattice constants	0.011
	SSE39			Solid-state energies	
30		SBG31		Semiconductor band gaps	NA[e]
31		SSCE8		Solid-state cohesive energies	NA
32		WCCR10[a]		Ligand dissociation energies of large cationic TM	NA

[a]Databases 1-29 were used with various inverse weights in training, and databases 1-33 constitute Database 2015A. Database 32 is from T. Weymuth et al. (ref. 59), database 33 is from A. Posada-Borbón et al. (ref.), and – like databases 30 and 31 – these databases were used only for testing.

[b]In the name of a database or subdatabase, the number at the end of the name or before the solidus is the number of data. For example, ME422, SR-MGM-BE9, IsoL6/11, and DGH4 contain respectively 422, 9, 6, and 4 data.

[c] Inverse weights with units of kcal/mol per bond for databases 1–7, kcal/mol for databases 8–25, and Å for databases 26–29.

[d]TM denotes transition metal.

[e]NA denotes not applicable.

[f]DGH4, with a total of four molecules (Ag_2, NaBr, HBr, and ZnS), contains two subsets with different inverse weights.

[g]The primary subsets are the ones that have inverse weights (except DGH4, which we have to optimize the Ag2 dimer separately), which are used for optimization. The secondary subsets are further decomposition of the primary subsets, which give the reader an idea of how we make our training sets, namely primary subsets.

Table 4.2. Optimized and inherited parameters of the MN15-L functional

Exchange				Correlation	
a_{000}	0.670864162	a_{102}	0.867791614	b_0	0.952058087
a_{001}	-0.822003903	a_{103}	-0.591190518	b_1	-0.756954364
a_{002}	-1.022407046	a_{104}	-0.295305435	b_2	5.677396094
a_{003}	1.689460986	a_{110}	-5.825759145	b_3	-5.017104782
a_{004}	-0.00562032	a_{111}	2.537532196	b_4	-5.10654071
a_{005}	-0.110293849	a_{112}	3.143390933	b_5	-4.812053335
a_{010}	0.972245178	a_{113}	2.939126332	b_6	3.397640087
a_{011}	-6.697641991	a_{120}	0.599342114	b_7	1.980041517
a_{012}	-4.322814495	a_{121}	2.241702738	b_8	10.1231046
a_{013}	-6.786641376	a_{122}	2.035713838		
a_{014}	-5.687461462	a_{200}	-1.525344043	c_0	0.819504932
a_{020}	9.419643818	a_{201}	-2.325875691	c_1	-7.689358913
a_{021}	11.83939406	a_{202}	1.141940663	c_2	-0.70532663
a_{022}	5.086951311	a_{203}	-1.563165026	c_3	-0.600096421
a_{023}	4.302369948	a_{210}	7.882032871	c_4	11.03332527
a_{030}	-8.07344065	a_{211}	11.93400684	c_5	5.861969337
a_{031}	2.429988978	a_{212}	9.852928303	c_6	8.913865465
a_{032}	11.09485698	a_{300}	0.584030245	c_7	5.74529876
a_{100}	1.247333909	a_{301}	-0.720941131	c_8	4.254880837
a_{101}	3.700485291	a_{302}	-2.836037078		

Table 4.3. Rankings[a] and Average Ranking of MN15-L Compared to Other Local Functionals.

Type Functional	GGA PBE	NGA GAM	meta-GGA TPSS	meta-GGA M06-L	meta-GGA M11-L	meta-NGA **MN15-L**
MGBE137						
SR-MGM-BE9	12	2	10	26	45	**13**
SR-MGN-BE107	43	26	31	19	16	**8**
MR-MGM-BE4	31	16	10	6	43	**1**
MR-MGN-BE17	44	7	9	2	5	**1**
TMBE43						
SR-TM-BE17	32	23	16	21	15	**2**
MR-TM-BE13	39	14	30	8	9	**3**
MR-TMD-BE3	21	3	11	1	22	**16**
BH76						
HTBH38/08	44	28	41	19	9	**5**
NHTBH38/08	40	28	44	23	15	**8**
NC51						
NCCE30	33	28	31	11	9	**12**
NGDWI21	10	1	23	16	45	**2**
EE18						
3dEE8	24	17	27	7	45	**1**
4dAEE5	7	18	17	29	45	**1**
pEE5	20	12	5	41	46	**27**
HCTC20						
πTC13	16	45	41	28	14	**13**
HC7/11	7	16	32	5	2	**8**
Average	27	18	24	16	24	**8**

[a] out of 48 functionals for which results are presented in detail in the SI.
[b]This functional also includes a molecular-mechanics damped dispersion term.

Table 4.4. Rankings[a] and Average Ranking of Local MN15-L Compared to Selected Hybrid Functionals.

Type Functional	meta- **MN15-**	hybrid B3LYP	hybrid PBE0	hybrid B97-1	hybrid B97-3	hybrid HSE06	hybrid ωB97X-D	hybrid M06	hybrid M06-2X
MGBE137									
SR-MGM-	**13**	38	25	3	17	28	8	27	1
SR-MGN-	**8**	32	18	10	15	21	6	4	1
MR-MGM-	**1**	17	28	5	12	25	33	2	38
MR-MGN-	**1**	18	20	3	17	22	28	6	24
TMBE43									
SR-TM-BE17	**2**	11	7	5	4	9	3	12	33
MR-TM-	**3**	19	11	2	27	12	5	6	43
MR-TMD-	**16**	26	40	18	39	38	36	33	47
BH76									
HTBH38/08	**5**	22	21	24	14	23	15	12	2
NHTBH38/08	**8**	26	19	18	6	21	22	10	3
NC51									
NCCE30	**12**	26	16	15	24	18	4	5	2
NGDWI21	**2**	34	14	4	42	11	20	27	13
EE18									
3dEE8	**1**	14	9	18	5	35	11	21	10
4dAEE5	**1**	20	6	33	32	14	34	37	42
pEE5	**27**	11	37	6	13	36	43	33	25
HCTC20									
πTC13	**13**	21	24	29	35	25	26	10	1

HC7/11	**8**	43	29	17	25	24	12	4	1
Average	**8**	24	20	13	20	23	19	16	18

[a] out of 48 functionals for which results are presented in detail in the SI.
[b]This functional also includes a molecular-mechanics damped dispersion term.

Table 4.5 MUE (kcal/mol) for the Molecular Energy Databases: MN12-L compared to MN15-L.

Functional	PBE	GAM	B3LYP	B97-1	TPSS	M06-L	M06	M06-2X	MN12-L	**MN15-L**
SR-MGM-BE9	2.72	2.00	4.58	2.17	2.55	3.40	3.42	1.91	3.07	**2.77**
SR-MGN-BE107	3.40	2.27	2.45	1.51	2.43	2.03	1.25	0.98	1.37	**1.39**
MR-MGM-BE4	9.31	7.76	7.76	6.05	6.69	6.15	5.00	10.45	19.21	**1.88**
MR-MGN-BE17	14.80	4.22	5.09	3.22	4.25	3.11	4.12	5.74	4.27	**2.08**
SR-TM-BE17	7.20	6.31	5.48	4.17	6.11	6.24	5.61	7.22	8.64	**3.65**
MR-TM-BE13	12.73	4.94	5.33	2.87	8.87	4.40	3.95	17.54	14.09	**3.63**
MR-TMD-BE3	23.71	11.53	26.41	21.79	18.94	5.59	34.74	118.02	18.54	**20.31**
HTBH38/08	9.31	5.35	4.23	4.39	7.71	4.15	1.98	1.14	1.31	**1.25**
NHTBH38/08	8.42	5.15	4.55	3.38	8.91	3.81	2.33	1.22	2.24	**2.06**
NCCE30	1.42	1.29	1.19	0.85	1.40	0.63	0.46	0.32	0.52	**0.75**
NGDWI21	0.102	0.019	0.276	0.080	0.171	0.125	0.190	0.110	0.370	**0.024**
3dEE8	11.88	10.45	9.46	10.49	12.41	8.55	10.84	8.94	21.07	**4.83**
4dAEE5	4.70	5.23	5.67	7.27	5.19	6.58	7.86	9.44	11.05	**0.88**
pEE5	3.96	2.99	2.87	2.25	2.25	7.50	5.23	4.55	22.39	**4.75**
4pIsoE4	2.43	3.57	4.24	2.51	2.60	2.88	2.31	2.71	3.19	**3.75**
2pIsoE4	2.73	5.02	4.69	2.90	3.54	3.16	1.60	1.77	2.79	**1.95**
IsoL6/11	1.98	1.96	2.61	1.82	3.66	2.76	1.27	1.53	1.07	**1.32**
πTC13	5.59	8.59	6.03	7.04	8.12	6.69	4.40	1.49	5.32	**4.84**
HC7/11	3.97	6.24	16.80	6.25	10.48	3.35	2.78	2.15	2.58	**3.98**
EA13/03	2.27	4.49	2.33	2.08	2.35	3.83	1.85	2.14	2.65	**2.17**
PA8	1.34	3.84	1.02	1.57	2.66	1.88	1.84	1.65	1.91	**2.17**
IP23	6.19	4.53	5.51	2.61	4.29	3.91	4.99	3.31	3.56	**2.32**
AE17	47.24	10.18	18.29	5.47	18.04	7.04	4.45	2.14	9.73	**6.85**
SMAE3	17.50	5.54	13.24	4.18	9.04	6.02	2.18	7.43	3.16	**3.33**
DC9/12	14.99	23.07	12.02	9.79	14.20	10.67	2.75	4.11	9.01	**3.47**
SR300	5.15	4.02	3.89	3.04	4.72	3.54	2.72	2.16	3.55	**1.85**

MR54	14.15	9.45	10.67	6.09	9.48	5.91	5.43	13.33	8.93	**4.35**

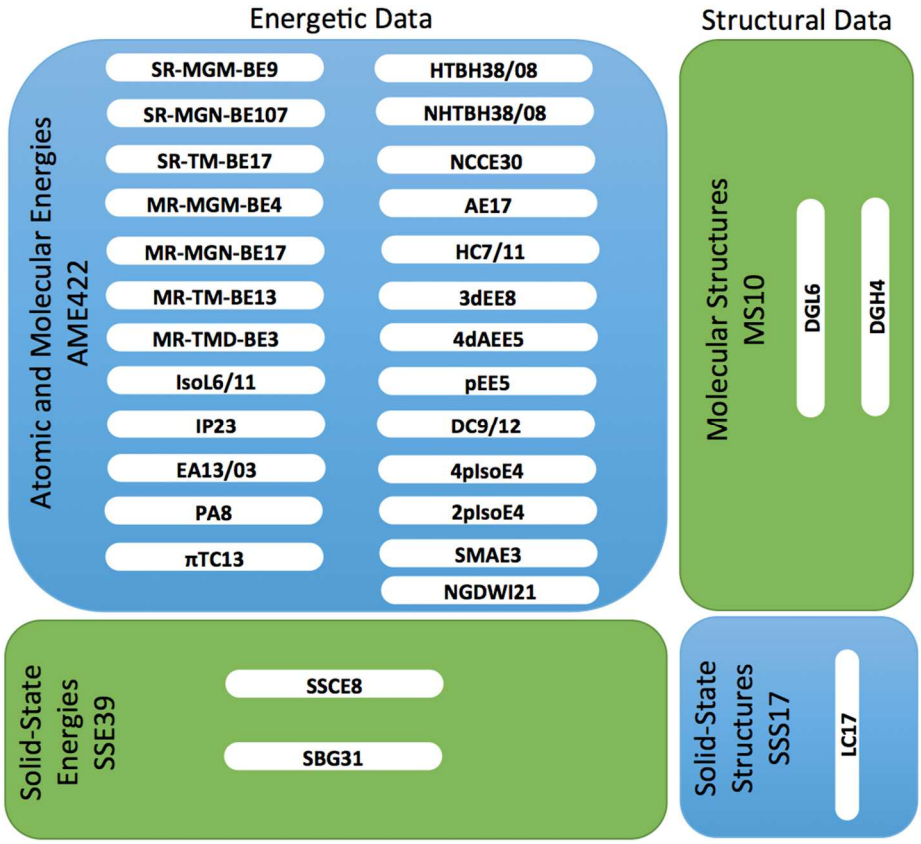

Figure 4.1 Minnesota Database 2015A

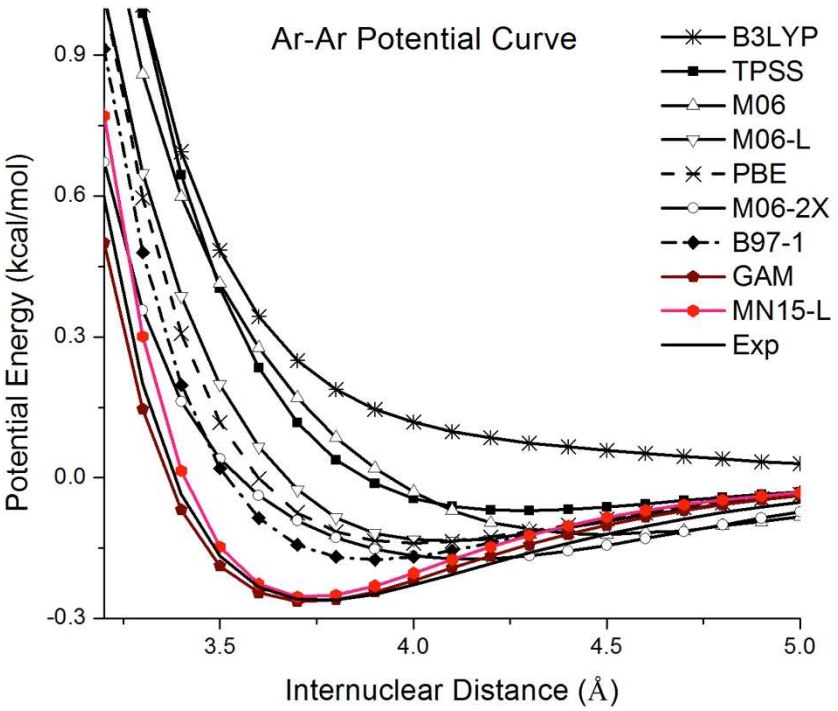

Figure 4.2 Ar-Ar potential curve calculated by M06-L, MGGA_MS2, and MN15-L with grids (250,590) compared to with the experimental value

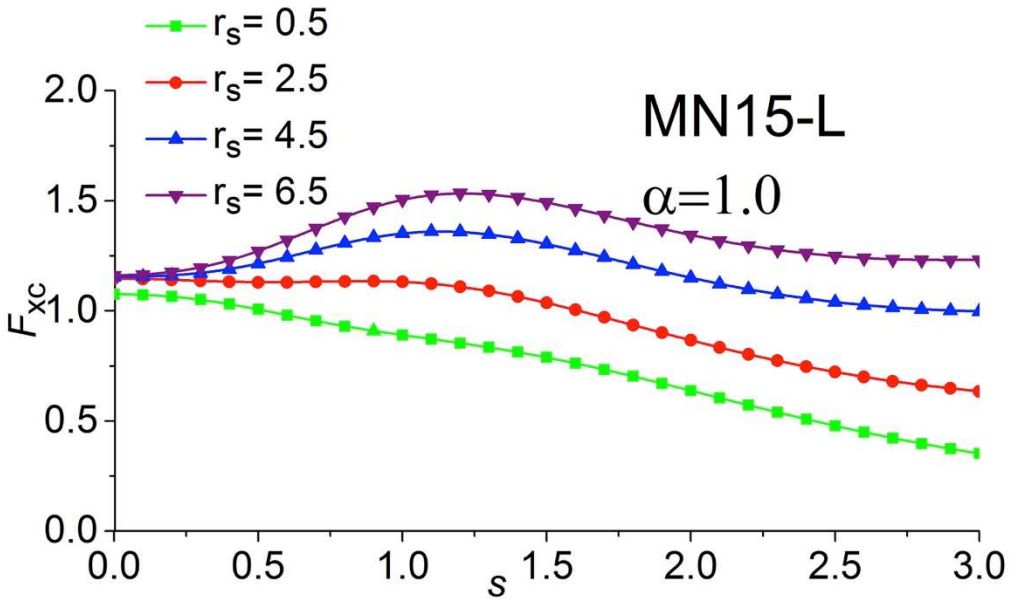

Figure 4.3 Enhancement factor of MN15-L verse reduced density gradient plot at α=1.0

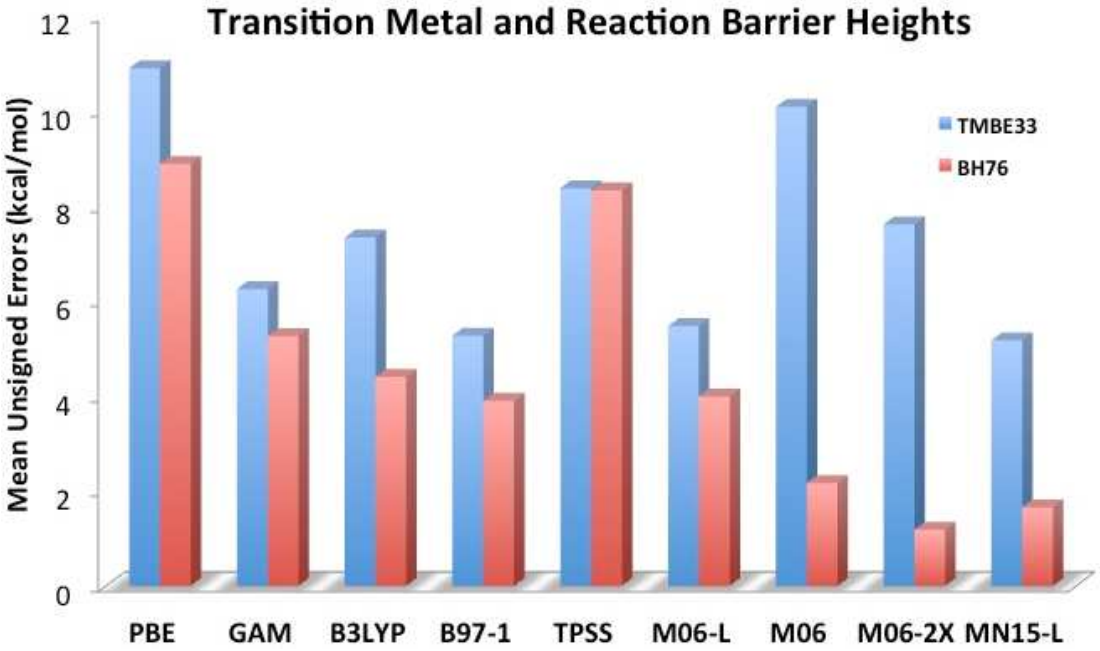

Figure 4.4 Mean unsigned errors (MUEs) for transition metal bond energies (TMBE33) and reaction barrier heights databases (BH76).

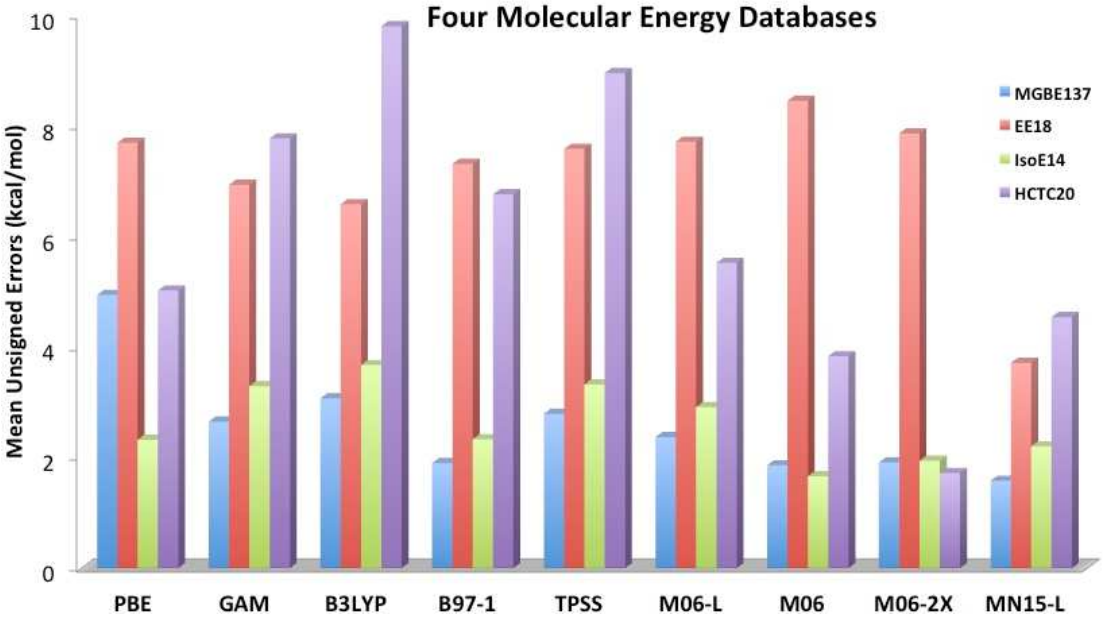

Figure 4.5 Mean unsigned errors for four databases, including main-group bond energies (MGBE137), excitation energy (EE18), isomerization energy (IsoE14), and hydrocarbon thermochemistry (HCTC20).

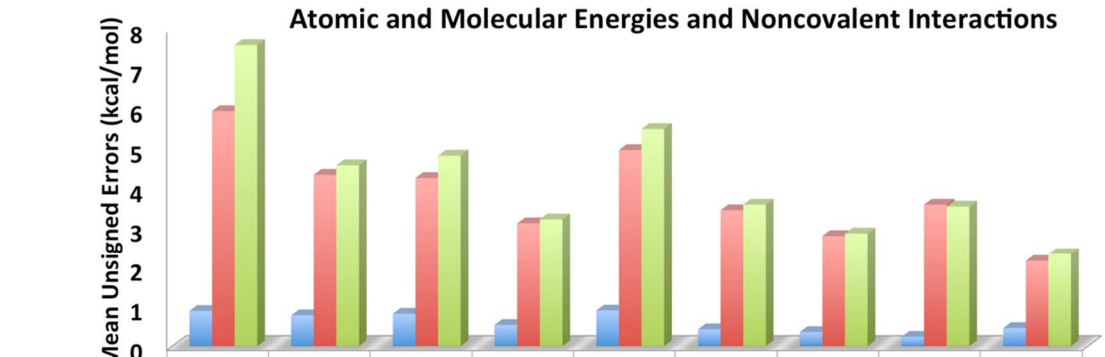

	PBE	GAM	B3LYP	B97-1	TPSS	M06-L	M06	M06-2X	MN15-L
NC51	0.88	0.77	0.81	0.53	0.89	0.42	0.35	0.23	0.45
AME405xAE	5.9	4.3	4.2	3.1	4.9	3.4	2.8	3.6	2.1
AME422	7.6	4.6	4.8	3.2	5.5	3.6	2.8	3.5	2.3

Figure 4.6 Mean unsigned errors for the noncovalent interaction database (NC51), the atomic and molecular energy database (AME422), and the atomic and molecular energy database without absolute energies (AME405xAE).

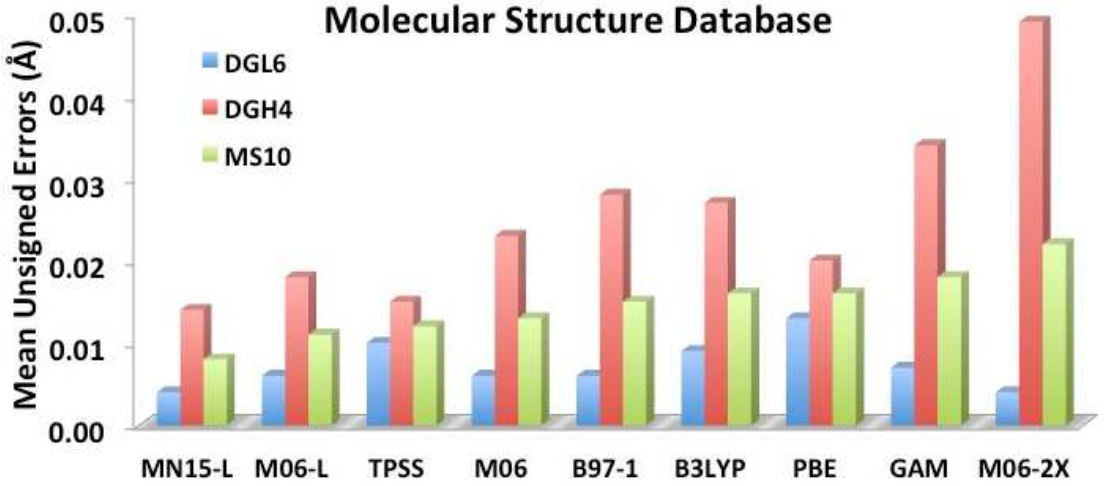

Figure 4.7 Mean unsigned errors for molecular structure databases (MS10) and its subdatabases (DG6L and DGH4).

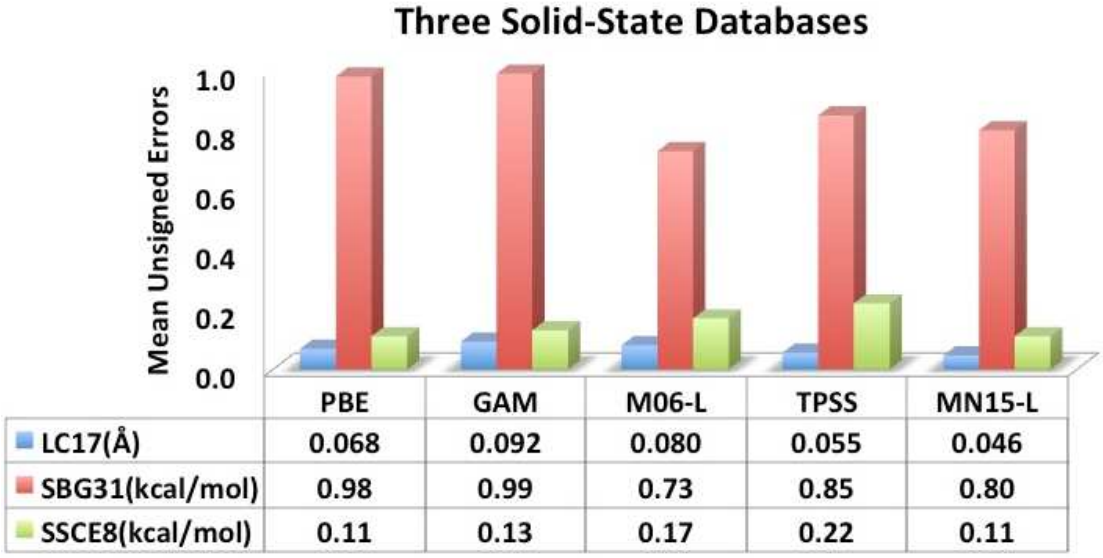

	PBE	GAM	M06-L	TPSS	MN15-L
LC17(Å)	0.068	0.092	0.080	0.055	0.046
SBG31(kcal/mol)	0.98	0.99	0.73	0.85	0.80
SSCE8(kcal/mol)	0.11	0.13	0.17	0.22	0.11

Figure 4.8 Mean unsigned errors for solid-state databases including lattice constants (LC17), semiconductor band gaps (SBG31), and solid-state cohesive energies (SSCE8).

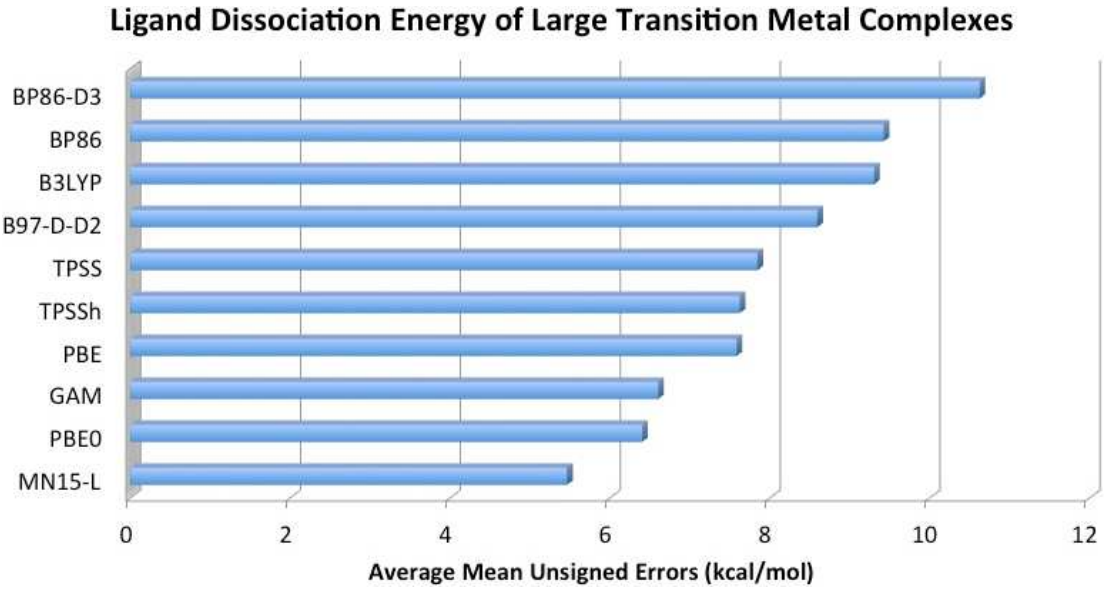

Figure 4.9 Mean unsigned error of 10 ligand dissociation energies of large transition metal complexes (WCCR10).

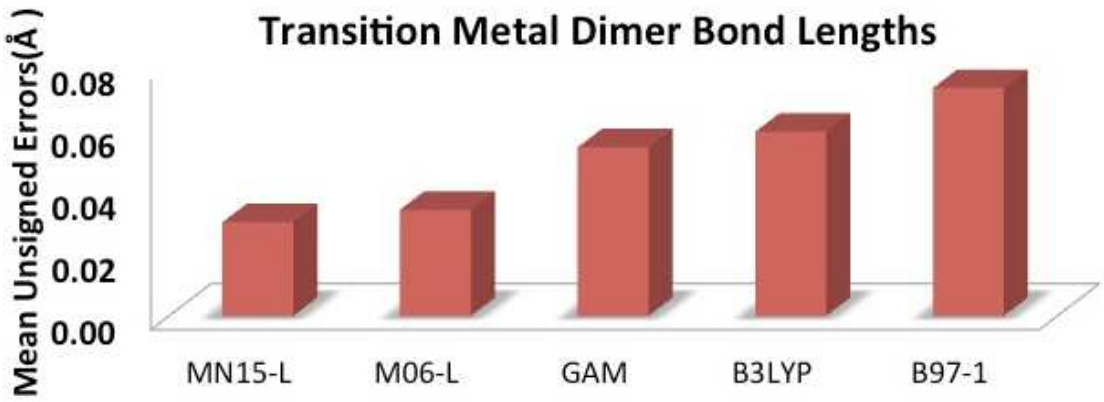

Figure 4.10 Mean unsigned error of seven transition metal dimer bond lengths (TMDBL7).

Chapter 5. The MN15 Functional: A Kohn-Sham Global-Hybrid Exchange-Correlation Density Functional with Broad Accuracy for Multi-Reference and Single-Reference Systems and Noncovalent Interactions

Adapted with permission from Haoyu S. Yu, Xiao He, Shaohong L. Li and Donald G. Truhlar, Chemical Science, DOI: 10.1039/c6sc00705h

5.1 Introduction

In 1927-30, Thomas, Fermi, and Dirac proposed treating the energies of systems of many electrons by a statistical model of the electron density ρ.[1,2,3] However, Teller proved that no such model can predict the existence of stable molecules.[4] In 1951 Slater[5] proposed a set of self-consistent-field (SCF) equations involving effective local potentials defined in terms of ρ by the free-electron gas model, and these equations do predict molecular binding. In 1964, Hohenberg and Kohn proved that the ground-state energy of a system can be written as a universal functional F of ρ,[6] and in 1965 Kohn and Sham[7] represented the density as the square of a Slater determinant and provided an SCF scheme for using the Hohenberg-Kohn theorem to calculate the energies of atoms, molecules, and solids. These equations resemble Slater's equations but the new derivation shows that SCF equations with local potentials are not just an approximation scheme but can be exact if Slater's approximation to exchange is replaced by a local potential derived from

the so called exact exchange-correlation functional (XCF), which is a functional of ρ. Unfortunately, this exact XCF is unknown and is essentially unknowable.[8] Progress in density functional theory is therefore dominated by attempts to obtain better approximations to this functional; although somewhat unsystematic, this progress has revolutionized the practice of modern chemistry.

We will discuss Kohn-Sham theory in the spin-unrestricted form in which the XCF is generalized to depend not just on total density but on the spin-up and spin-down densities ρ_α and ρ_β (where α and β denote spin-up and spin-down electrons).[9,10] The original approximations to the XCF involved separate approximations to exchange energy density and correlation energy density, at given points in space, that are explicit functionals of the local electron spin densities ρ_α and ρ_β. These are called local-spin-density approximations (LSDAs).[11,12,13] Later work added dependence of exchange and correlation energy densities on the magnitudes s_α and s_β of the reduced gradients of ρ_α and ρ_β, leading to generalized gradient approximations (GGAs)[14,15,16] and on the local kinetic energy densities τ_α and τ_β of spin-up and spin-down electrons,[17] leading to meta-GGAs. The partition of the electronic energy into exchange and correlation in exchange-correlation functionals is different than the partition usually used in wave function theory; and in Kohn-Sham theory one can also approximate exchange and correlation together, without separating them, leading to nonseparable gradient approximations (NGAs)[18] and meta-NGAs.[19] Note that the local kinetic energies are local functionals of the occupied Kohn-Sham orbitals.[20] It can easily be shown[21] though that the unknown exact functional

is not a local functional of the orbitals or the densities; therefore the search for improved approximations must also consider nonlocal energy densities such as some percentage of the Hartree-Fock energy, leading to so called hybrid functionals,[22] and/or nonlocal approximations to electron correlation, leading to so called van der Waals functionals[23] or doubly hybrid functionals.[24,25] There are various kinds hybrid functionals, but we especially distinguish global hybrids, where the percentage X of Hartree-Fock exchange is a constant, and range-separated (RS) hybrids, where it is a nonconstant function of interelectronic distance.

Many research groups have proposed approximations to the XCF containing some or all of the elements reviewed in the previous paragraph, and we will give references to many of these below. Here we mention though that the new functional presented here builds on previous work in our group, especially the GAM[26] functional, which is an NGA, the M06-L[27] functional, which is a meta-GGA, the MN12-L[28] and MN15-L[29] functionals, which are meta-NGAs, the PW6B95,[30] M06,[31] M06-2X,[31] and M08-HX[32] functionals, which are global-hybrid meta-GGAs, and the MN12-SX[33] functional, which is a range-separated-hybrid meta-NGA. Even though these and many functionals from other groups (many of which are listed in section 5.5 and discussed in section 5.6) have had considerable success, there are still some important and challenging areas where exchange-correlation functionals can be improved, and we particularly single out the difficulty of finding a single functional that is accurate both for inherently multi-configuration systems, such as many systems containing transition metals, and for barrier

heights. (We will follow the common convention of labeling inherently multi-configurational systems as "multireference" systems; such systems include those with near-degeneracy correlation, also called static correlation. Systems that are qualitatively well described by a single configuration state function will be called "single-reference" systems.)

In the present article, building on the work summarized above, we present a global-hybrid meta-NGA, called MN15, that is able to achieve better simultaneous accuracy for these two properties (energies of multireference systems and barrier heights) than any previous functional and also has especially good performance for noncovalent interactions and excitation energies. Such a functional should be useful for a wide variety of application areas, including catalysis, the quest for new energy, nanotechnology, functional materials, synthesis, biochemistry, the drive toward a cleaner environment, and understanding chemical dynamics.

5.2 Databases

The largest database we consider in the present paper is called Database 2015B, which has 481 data and is a combination of databases AME471 and MS10. Database AME471 contains 471 atomic and molecular energies. It is obtained by extending a previous database, AME422,[29] by the addition of 49 new data, of which 36 are noncovalent interactions (subdatabase S6x6 , which means six dimers at six intermonomer distances taken from the S66x8 database[34]) and 13 alkyl bond dissociation energies from a recent paper of our group.[35] The distribution of data in AME471 across

its various subdatabases is illustrated in Figure 1, which shows that is a very diverse database. Minnesota Database 2015B also includes database MS10, which has ten molecular structure data, as used in a previous work.[29] All the data in Database 2015B are shown in Table 5.1 with their acronyms, brief descriptions, and inverse weights for training (which are explained in Section 4).

Minnesota Database 2015B was used for both training and testing of the MN15 functional, and we calculated this full database for 82 other functionals for comparison. In Table 5.2, we list additional databases that we used only for testing the performance of the new MN15 functional and for more limited comparisons to other functionals. These data are not used for parameterization, except for the 36 data (out of 528) in S66x8 that are also in S6x6 .

For testing the performance of functionals on electronic excitation energies, another database, EE69 was used.[36] It contains the experimental vertical excitation energies of 30 valence and 39 Rydberg excitations of 11 organic molecules. These data are not used for parameterization.

5.3 Computational Details

All the calculations are performed by a locally modified version[37] of the *Gaussian 09*[38] program. Vertical electronic excitation energies of the molecules in the EE69 database were calculated by linear-response time-dependent density functional theory (TDDFT).[39] Twenty excitation energies were computed for each molecule. To compare

the computed values with experiment, we made the assignments based on state symmetry as used and discussed in previous work.[40,41,42]

5.4 Design and Parameterization of the MN15 Functional

The LSDA exchange-correlation energy is a starting point for the MN15 functional. It can be written as:

$$E_{\mathrm{xc}}^{\mathrm{LSDA}} = E_{\mathrm{x}}^{\mathrm{LSDA}} + E_{\mathrm{c}}^{\mathrm{LSDA}} = \int dr \sum_{\sigma=\alpha}^{\beta} \rho_\sigma \varepsilon_{\mathrm{x}\sigma}^{\mathrm{UEG}}(\rho_\sigma) + \int dr \rho \varepsilon_{\mathrm{c}}^{\mathrm{UEG}}(\rho_\alpha, \rho_\beta) \tag{5.1}$$

where $E_{\mathrm{x}}^{\mathrm{LSDA}}$ is the LSDA exchange energy, $E_{\mathrm{c}}^{\mathrm{LSDA}}$ is the LSDA correlation energy, $\varepsilon_{\mathrm{x}\sigma}^{\mathrm{UEG}}$ is the exchange energy per electron with spin σ, and $\varepsilon_{\mathrm{c}}^{\mathrm{UEG}}$ is the correlation energy per electron for which we use the parameterization of Perdew and Wang.[10] The MN15 functional is

$$E_{\mathrm{xc}}^{\mathrm{MN15}} = \frac{X}{100} E^{\mathrm{HF}} + E_{\mathrm{nxc}} + E_{\mathrm{c}} \tag{5.2}$$

where $E_{\mathrm{x}}^{\mathrm{HF}}$ is the nonlocal Hartree-Fock exchange energy computed from the Kohn-Sham orbitals, X is the percentage of Hartree-Fock exchange, E_{nxc} is the nonseparable local exchange-correlation energy, and E_{c} is the additional correlation energy. The local terms are given by

$$E_{\mathrm{nxc}} = \int d\mathbf{r} \sum_{\sigma=\alpha}^{\beta} \rho_\sigma \left\{ \varepsilon_{\mathrm{x}\sigma}^{\mathrm{LSDA}}(\rho_\sigma) \sum_{i=0}^{3} \sum_{j=0}^{3-i} \sum_{k=0}^{5-i-j} a_{ijk} \{v_{\mathrm{x}\sigma}(\rho_\sigma)\}^i \{u_{\mathrm{x}\sigma}(s_\sigma)\}^j \{w_\sigma(\rho_\sigma, \tau_\sigma)\}^k \right\} \tag{5.3}$$

where the variables $v_{x\sigma}$, $u_{x\sigma}$, and w_{σ} are the same functions as we used in the MN15-L functional,[29] and

$$E_c = \sum_{\sigma} \int dr \rho \varepsilon_c^{\mathrm{LSDA}}(\rho_\alpha, \rho_\beta) \sum_{i=0}^{8} b_i \{w(\rho,\tau)\}^i + \int dr \rho H^{\mathrm{PBE}}(\rho_\alpha, \rho_\beta, s) \sum_{i=0}^{8} c_i \{w(\rho,\tau)\}^i \quad (5.4)$$

where w is a function defined in a previous paper,[32] and H^{PBE} is the PBE gradient correction[43] for the correlation energy. Equation (3) is the same form as used in the MN12-L functional,[28] and eq. (4) is the same as introduced[32] for M08-HX except that the upper limits of sums have been reduced to 8. We optimized the value of X along with the parameters a_{ijk}, b_i, and c_i in equations (3) and (4) by minimizing

$$U = \sum_{n=1}^{32} R_n / I_n + \lambda(a+b+c) \quad (5.5)$$

where R_n and I_n are respectively the root mean squared error and inverse weight of database or subset n in Table 5.1. Each term in the sum of eq. (5) corresponds to one of the 32 rows of the table that has an entry in the inverse weight column. The product of λ and $(a+b+c)$ is a smoothness restraint, which has the same form as used previously.[26,29] In particular, we have

$$a = \sum_{i=0}^{3} \sum_{j=0}^{3-i} \sum_{k=0}^{4-i-j} (a_{i,j,k} - a_{i,j,k+1})^2 \quad (5.6)$$

$$b = \sum_{i=0}^{7} (b_i - b_{i+1})^2 \quad (5.7)$$

$$c = \sum_{i=0}^{7} (c_i - c_{i+1})^2 \tag{5.8}$$

We choose the same value, namely 0.01, of λ as we used in the MN15-L parametrization.[29] All the optimized parameters are shown in Table 5.3.

The final functional is not overly sensitive to the relative number of data in each subdatabase because the inverse weights are changed manually (by trial and error) to try to obtain balanced performance across the full collection of data.

5.5 Density Functionals for Comparison

In order to evaluate the performance of the new MN15 functional, we compare the results obtained with the MN15 functional to those obtained with 82 previously developed density functional approximations for the entire Minnesota Database 2015B. The results for 48 of the previous functionals are compared to the results for the new MN15 functional in the article proper, and the results for the remaining 34 functionals are in Electronic Supplementary Information (ESI). The 49 functionals considered in the article proper are sorted into nine types as follows:

- LSDA: GKSVWN5 [7,44,45]
- GGA: SOGGA,[46] PBEsol,[47] SOGGA11,[48] BP86, [14,49] BLYP,[14,50] PW91,[51] BPW91,[14,51] PBE,[20] mPWPW,[52] revPBE,[53] RPBE,[54] HCTH407,[55] OLYP,[50,56] and OreLYP[50,56,57]
- NGA: N12[18] and GAM[26]
- meta-GGA: VSXC,[58] τ-HCTC,[59] TPSS,[60] M06-L,[27] revTPSS,[61] M11-L,[62] MGGA_MS2[63]
- meta-NGA: MN12-L[19] and MN15-L[29]

- global-hybrid GGA: B3LYP,[64,65,66] PBE0,[67] B98,[68] B97-1,[69] O3LYP,[70] B97-3,[71] and SOGGA11-X[72]
- range-separated hybrid GGA: CAM-B3LYP,[73] LC-ωPBE,[74,75,76,77] HSE06,[78,79] ωB97,[80] ωB97X,[80]
- range-separated hybrid GGA plus molecular mechanics: ωB97X-D[81]
- global-hybrid meta-GGA: TPSSh,[82] τ-HCTHhyb,[83] BB1K,[14,17,84] BMK,[85] PW6B95,[30] M06,[31] M06-2X,[31] M08-HX[32]
- global-hybrid meta-NGA: MN15
- range-separated hybrid meta-GGA: M11[86]

For each of the functionals in the above list, Table 5.4 shows the percentage of nonlocal Hartree-Fock exchange, the year that the functional was published, and the original reference or references.

We do not consider the more expensive doubly hybrid functionals (functionals with nonlocal correlation) in this article, except in Section 5.6.2 on noncovalent interactions.

5.6 Performance of the MN15 Functional

The performance of the new MN15 functional and the 48 other functionals in Table 5.4 has been evaluated for the entire Database 2015B. The results of these tests are given in Tables 5-7 for the energetic part of Database 2015B and in Table 5.8 for the structural portion of Database 2015B. In addition we compared MN15 against results in the literature for the following additional test sets: the noncovalent interactions of the S66 and S66x8 databases,[34] the excitation energies of selected organic molecules in the EE69

database,[40] transition metal reaction barrier heights in the TMBH21 database,[87,88,89] transition metal coordination energies in the WCCR10 database,[90] semiconductor band gaps in the SBG31 database,[91] transition metal dimer bond lengths in the TMBDL7 database,[92] and geometrical parameters of 47 selected organic molecules.[93] These evaluations and comparisons are discussed in the following subsections.

All energetic quantities in this paper are calculated from Born-Oppenheimer energies without including vibrational energies. Therefore when the reference data are from experiment, we removed zero-point vibrational energy and thermal vibration-rotational energies, if present in the original data. For example, bond energies are equilibrium dissociation energies (D_e), not ground-state dissociation energies (D_0). Most of the bond energies in the databases are average bond energies calculated as atomization energy per bond. Even when all bonds are not atomized, we calculate bond energies on a per bond basis. For example one of the bond-breaking processes in subdatabase PdBE2 is the dissociation of $Pd(PH_3)_2C_6H_8$ into $Pd(PH_3)_2$ and C_6H_8. As shown in Figure 5.2, this involves breaking two bonds, so the energy of dissociation is divided by 2. Further details of the molecules in the databases, the bonds broken, and the removal of vibrational energy from experiment are given in Ref. 26 and in the references in Tables 5.1 and 5.2.

In evaluating performance, we always use the unweighted mean unsigned error (MUE) over the data in a database, subdatabase, or specified collection of subdatabases. Thus, even though the MN15 functional was optimized using root-mean-square errors and weights, performance is measured with unweighted MUEs.

5.6.1 Performance of Minnesota Database 2015B

In order to compare the functionals for different categories of data, we used the following combinations of subdatabases explained more fully in Table 5.1:

- MGBE150: 150 main-group bond energies, in particular SR-MGM-BE9, SR-MGN-BE107, MR-MGM-BE4, MR-MGN-BE17, and ABDE13
- TMBE33: 33 transition metal bond energies, in particular SR-TM-BE17, MR-TM-BE13, and MR-TMD-BE3
- BH76: 76 reaction barrier heights, in particular HTBH38 and NHTBH38
- NC87: 87 noncovalent interactions, in particular NCCE30, NGDWI21, and S6x6
- EE18: 18 excitation energies, in particular 3dEE8, 4dAEE5, and pEE5
- IsoE14: 14 isomerization energies, in particular IsoL6, 4pIsoE4, and 2pIsoE4
- HCTC20: 20 hydrocarbon thermochemical data, in particular πTC13 and HC7
- MS10: 10 molecular structures, in particular DGL6 and DGH4

Minnesota Database 2015B has 481 data: 10 structural data (MS10) and 471 energetic data (AME471). If we exclude 87 noncovalent interactions (NC87) and 17 absolute energies (AE17) from AME471, we have 367 data that can be classified as either single-reference data or multi-reference data. We classified these based on the generalized B1[94,95,96] diagnostic, which separates these data into 54 multi-reference data (MR54) and

313 single-reference data (SR313). Therefore we also consider the following three other ways to combine related data:

- AME454xAE: 454 atomic and molecular energies, in particular AME471 without AE17 (which denotes 17 absolute energies from H to Cl)
- SR313: 313 single-reference systems
- MR54: 54 multi-reference systems

We show the performance of the MN15 functional for ME471 and the 11 combined energetic subdatabases delineated above in Tables 5.5, 5.6, and 5.7. Table 5.5 has the performance of a local spin density approximation (LSDA) and 16 gradient approximations (GAs); Table 5.6 has the performance of nine meta gradient approximations (meta-GAs) and seven global-hybrid gradient approximations (hybrid GAs); and Table 5.7 has the performance of six range-separated hybrid gradient approximations (RS-hybrid GAs), nine global-hybrid meta gradient approximations (hybrid meta-GAs), and one range-separated-hybrid meta gradient approximations (RS-hybrid meta-GAs).

Tables 5.5–5.7 show that the MN15 functional gives the best result for main-group bond energies (MGBE150) with an MUE of 1.36 kcal/mol, followed by MN15-L, M06-2X, and M06 with MUEs of 1.84, 1.87, and 1.90 kcal/mol respectively. The MN15 functional gives the fourth best result for transition metal bond energies (TMBE33) with an MUE of 5.54 kcal/mol, with B97-1, MN15-L and M06-L being the top three with

MUEs of 5.04, 5.16, and 5.29 kcal/mol, respectively. The other functional that gives an MUE smaller than 6.0 kcal/mol is τ-HCTHhyb, with an MUE of 5.62 kcal/mol.

We found that it is hard to get simultaneously good accuracy for certain pairs of databases, even when both are present in the training set. For example, a functional that gives good results for transition metal bond energies does not usually work very well for reaction barrier heights, and vice versa. Incorporating Hartree-Fock exchange usually improves the performance on hydrocarbons, weak interactions, and barrier heights, but it usually worsens the results for multi-reference systems. Therefore, the mathematical form of the functional and a carefully selected set of diverse databases are very important for the design of a universal and highly transferable functional like MN15. For the reaction barrier heights database (BH76), the top six best functionals are M08-HX, M06-2X, BMK, BB1K, M11, and MN15, which all have an MUE smaller than 1.50 kcal/mol.

The MN15 functional gives the second best results for the isomerization energies database (IsoE14), with an MUE of 1.41 kcal/mol, following only M08-HX with an MUE of 1.26 kcal/mol. The MN15 functional gives the fourth best results for the hydrocarbon thermochemistry database (HCTC20), with an MUE of 3.59 kcal/mol. The top three functionals for HCTC20 are M06-2X with an MUE of 1.72 kcal/mol, M11 with an MUE of 2.77 kcal/mol, and M08-HX with an MUE of 2.93 kcal/mol.

The MN15 functional gives the best results for the noncovalent interactions (NC87), with an MUE of 0.25 kcal/mol, followed by ωB97X-D, M06-2X, M08-HX,

M11, ωB97, M06-L, ωB97X, and M06, which have MUEs of 0.30, 0.35, 0.37, 0.39, 0.55, 0.57, 0.64, and 0.67 kcal/mol, respectively.

For the excitation energies database (EE18), the top six functionals are MN15-L, SOGGA11-X, PW6B95, M08-HX, MN15, and O3LYP, which are the only functionals that have MUEs for EE18 smaller than 6.30 kcal/mol. It is especially noteworthy that MN15-L gives an MUE of only 3.71 kcal/mol and the other five give MUEs in the range 5.00–6.30 kcal/mol.

The MN15 functional is the only one that gives MUEs no larger than 2.10 kcal/mol for both ME471 with 471 energetic data and ME454xeAE with 454 energetic data excluding absolute energies (AE17). For the SR313 database of 313 single-reference data, the top five functionals are MN15, M06-2X, MN15-L, M08-HX, and BMK with MUEs of 1.85 kcal/mol, 2.13 kcal/mol, 2.15 kcal/mol, 2.29 kcal/mol, and 2.30 kcal/mol respectively. For the MR54 database of 54 multi-reference data, MN15-L and MN15 are the only two functionals that give an MUE smaller than 5.00 kcal/mol, and M06 and M06-L are the only two functionals with MUEs in the range of 5.00 kcal/mol and 6.00 kcal/mol.

Table 5.8 shows the performance of 49 functionals including MN15 for the molecular structure database MS10 and its subdatabases DGL6 and DGH4. The MN15 functional is the tenth best for DGL6 with an MUE of 0.005 Å and the third best for DGH4 with an MUE of 0.008 Å. Because it is rare for a functional do well on both databases, MN15 is the best overall when these databases are combined into MS10. We

conclude that the MN15 functional gives good results not only for energies but also for geometries.

Some functionals that are good for one property (like main-group bond energies, transition metal bond energies, noncovalent interactions, etc.), as seen for certain databases in Table 5.5-7 and 9, fail badly for other properties. Parameterizing a functional that is good for several properties is the challenge of designing and parameterizing a universal functional. Average errors over diverse databases like ME471 are one way gauge the universality of a functional, but such mean errors are sensitive to the number of data of each type and can underweight performance in categories with intrinsically smaller errors (like noncovalent interactions) unless those categories have a compensatingly large number of data, but the amount of compensation is arbitrary. A better measure, at least for relative success compared to other functionals, is to look at the ranking of the mean unsigned error in each category. To illustrate the high universality of the MN15 functional, we consider Table 5.9, which lists the rankings for 27 subdatabases of 12 selected functionals among the set of 83 functionals that were tested for the entire Minnesota Database 2015B. The table also shows the average ranking, which is a way to summarize combined performance on diverse databases that does not suffer from the two deficiencies mentioned at the start of this paragraph, and it also shows the lowest ranking. The MN15 functional gives the best average ranking, which is 9, with MN15-L being second with an average ranking of 17. The average ranking of the other functionals is in the range of 22–52. Furthermore, every other functional in the list has at least one ranking

of 62 or lower, whereas MN15 ranks lower than 29th in none of the 27 categories. MN12-L, M06-2X, and M06 rank lower than 29th in 8-10 categories, and the other functionals in the table rank lower than 29th in 14–22 categories.

5.6.2 Performance for S66 and S66x8 databases

Next we consider the S66 and S66x8 databases. These databases[34] were developed primarily for the validation of new quantum chemical methods. The S66 database contains accurate interaction energies for 66 noncovalently bound complexes at the equilibrium van der Waals geometry of the complex, and it is divided into three subdatabases, damped-dispersion-dominated (DD23), hydrogen bonding (HB23), and dominated by a mix of damped dispersion and electrostatics (Mix20). DD23 contains stacked and unstacked aromatic complexes and complexes containing aliphatic molecules; HB23 contains both singly H-bonded and doubly H-bonded complexes. Examples of mixed systems are benzene...water and pentane...acetic acid. The S66x8 database contains not only S66 as a subset but also interaction energies of the 66 complexes at seven other intersubsystem distances, ranging from 0.9 times the van der Waals distance to 2.0 times the van der Waals distance. The average interaction energy in S66 is 5.46 kcal/mol, and the average interaction energy in S66x8 is 4.15 kcal/mol. Georigk et al.[97] choose to benchmark several methods against the S66 and S66x8 databases, choosing methods based mainly on their good performance relative to other functionals of the same class in previous tests, but also including three functionals based on their widespread use or general interest. In this section we compare the performance of MN15 to the

performance of the functionals they chose. The functionals they chose included functionals with nonlocal correlation terms, which are more expensive but often favored for treating noncovalent complexes because dispersion interactions in the long-range region where the subsystems have no overlap can only be treated by nonlocal correlation. The comparison is shown in Table 5.10, were we have classified functionals based on whether or not they contain nonlocal correlation or damped-dispersion molecular mechanics terms or both. Although the table includes all the functionals without molecular mechanics that were selected by the authors of ref. 97, it includes only two examples including molecular mechanics (the best for S66 with local correlation and one with nonlocal correlation that was specifically designed for use with molecular mechanics terms), since molecular mechanics corrections are not the focus of our article. There are four doubly hybrid functionals included in Table 5.10, in particular B2-LYP,[98] B2GP-PLYP,[99] DSD-BLYP-D3,[97,100] and PWPB95[101].

Before considering Table 5.10, we provide background contextual comments on dispersion. Dispersion interactions were originally modeled by London, and his formulas apply only at long range where the subsystems have no charge cloud penetration.[102] In the strict meaning of the term, "dispersion force" applies only in such regions. As subsystems begin to overlap there is no unique way to partition the interaction energy into dispersion and the remainder, although there are reasonable ways to do so in an approximate sense.[103] However, when doing this, the dispersion component of the interaction energy no longer satisfies the inverse power laws of long-range dispersion;

rather it is damped by overlap. This overlap also leads to Pauli repulsion, and when the intersubsystem distance is reduced to the van der Waals distance, since that represents an equilibrium geometry, the repulsive force exactly cancels the attractive force. Functionals with local correlation, such as MN15 and the other functionals to which we compare in the other sections of this article, cannot treat the inverse power dependence of long-range dispersion, but in principle they can treat attractive noncovalent interactions at the van der Waals geometry, as tested by S66 and its subdatabases, and in principle they can even provide reasonable results at large distances in the range tested by S66x8. Table 5.10 tests how well this is done by various functionals.

Table 5.10 shows that the MN15 functional gives the best results for S66x8 database, even though the other functionals in the table were selected[97] mainly for their good performance on this kind of problem. The MN15 functional gives the second best results for the dispersion-dominated (DP23), mixed (Mix20) and S66 databases, with M06-2X being the best. The MN15 functional gives the fourth best results for hydrogen bond (HB23) database with M06-2X, M05-2X and B2GP-PLYP being the first, second, and third. It is especially remarkable that MN15 does better than all three functionals with nonlocal correlation but without molecular mechanics dispersion. Functionals with empirical molecular mechanics terms are the best for noncovalent interactions, but they are not necessarily well balanced when one consider properties more general than noncovalent interactions.

S66 has 66 data and S66x8 has 528; of these we used only six of the data in S66 and only 36 (which is 7%) of the data in S66x8 in training MN15. We conclude that MN15 performs well for noncovalent data not used for training.

5.6.3 Performance for excitation energy database

Because of its modest computational cost and often-useful accuracy, TDDFT is now the workhorse for calculating energies and properties of electronically excited states of large molecules. However, one of the typical problems of TDDFT combined with many functionals is the difficulty of achieving high accuracy for valence and Rydberg excitation with the same functional.[40] Local functionals are well-known to underestimate Rydberg excitations severely due to the incorrect asymptotic behavior of the exchange-correlation potential.[104] Hybrid functionals alleviate this problem by incorporating a fraction of the Hartree-Fock exchange, whose derived exchange potential has the correct asymptotic behavior. However, a high percentage of Hartree-Fock exchange, while helpful for Rydberg excitations, often compromises the accuracy for valence states. A good overall design and balance in the functional, instead of simply raising the fraction of Hartree-Fock exchange, is therefore required to obtain simultaneous accuracy for valence and Rydberg excitations. Range-separated hybrid functionals[74] are a popular way to achieve a better balance of accuracy for valence and Rydberg excitations. A local exchange enhancement scheme has also been proposed for this purpose.[42]

The general trends discussed in the preceding paragraph can be seen in Table 5.11, where we compare the performance of MN15 with 60 other methods reported in

references 36 and 40 for the calculation of valence and Rydberg excitation energies of selected organic molecules (EE69). (References of the listed methods are also given in the table.[105,106,107,108,109,110,111,112,113,114,115,116,117]) The table shows that MN15 gives the best results for all states and is the only one that gives an error smaller than 0.3 eV for both valence and Rydberg states. The runners-up with an error smaller than 0.4 eV for both types of excitations include M06-2X, BMK, M05-2X, which are hybrid functionals with a high percentage of Hartree-Fock exchange, and ωB97X-D and CAM-B3LYP, which are range-separated hybrid functionals.

We emphasize that in our training set, we only have excitation energies for atoms and for the first excitation energy of the Fe_2 molecule. No TDDFT calculations were used in training (the few excitation energies in the training set were calculated as the difference in SCF energies, which is possible when the excited state has a different symmetry than the ground state.

5.6.4 Performance for transition metal barrier height database

Table 5.12 tests the performance of the MN15 functional for the transition metal reaction barrier heights published by Chen et al.[87,88,89] The transition metals involved are Mo, W, Zr, and Re. This is a good test for MN15 because the training set involved no W or Re data, only one Zr datum (the Zr_2 bond energy in SR-TM-BE17), and only three data for Mo (all for monatomic species: Mo and Mo^+ in IP23 and the quartet-to-sextet transition energy of Mo in 4dAEE5). The results for MN15, MN15-L, and GAM were calculated by the present authors, and the other results in the table are the calculations of

Chen et al. The functionals they selected for testing include two doubly hybrid functionals (both of which were also included in Section 6.2), B2GP-PLYP, which gives the best results, and B2-PLYP, which gives the fourth best results. Among the 20 functionals without nonlocal correlation in Table 5.12, the MN15 functional gives the second best results, behind M06. We conclude that the MN15 functional provides good results for transition metal reaction barrier heights, even though there were no transition metal barrier heights in the training set.

5.6.5 Performance for transition metal coordination database

Table 5.13 shows the performance of 11 density functionals for the transition metal coordination database (WCCR10).[90] The results for MN15, MN15-L, and GAM were calculated by the present authors, and the other results in the table are calculations from Ref. 90. The molecules that used for training are relatively small comparing to all the molecules in the WCCR10 database. We find that the MN15 functional gives the best results for the WCCR10 database with an MUE of 5.04 kcal/mol. The MN15 functional gives the fourth best results for TMBE33 in Tables 5–7, with an MUE of 5.54 kcal/mol, which is close to the MUE that MN15 gives for the WCCR10 database. Therefore, the good performance of the MN15 functional for transition metal bond energies in TMBE33 does transfer well to other databases.

5.6.6 Performance for semiconductor band gap database

Table 5.14 shows the performance of 28 density functionals for the semiconductor band gap database (SBG31).[91] The functionals included in the table are the same as those

in Table S17 of our previous paper[29] plus MN15. The band gaps in this table are calculated, as is widely done,[118] as the orbital energy of the lowest unoccupied crystal orbital minus the orbital energy of the highest occupied crystal orbital. When calculated this way, the MN15 functional gives the eleventh best results for the SBG31 database, with an MUE of 0.92 eV.

This kind of a test of an XCF suffers from the fact that the orbital energies are not physically observable quantities like the quasiparticle energies appropriate for interpreting optical excitation, photoemission, and inverse photoemission experiments. A better way to calculate the observable band gap for a single-reference system is to use the Green's function–screened potential (GW) method to calculate true quasiparticle energies from the Kohn-Sham single-particle orbitals and orbital energies.[119] It would be interesting to carry out such a calculation with the MN15 potential, but it is beyond the scope of the present paper.

5.6.7 Performance for transition metal bond length database

Table 5.15 shows the performance of 14 density functionals for the homonuclear transition metal dimer bond length database (TMBDL7).[92] The functionals included in the table are the same as those in Table S17 of our previous paper[29] plus MN15. The MN15 functional gives the seventh best results for the TMBDL7 database with an MUE of 0.045 Å. Interestingly, local functionals often give more accurate bond lengths and vibrational frequencies than nonlocal ones, and this trend is seen for the bond lengths in Table 5.15. Of the six nonlocal functionals in Table 5.15 (HSE06, MN15, B3PW91,

B3LYP, B97-1, and ωB97X-D), MN15 gives the second best MUE, and its MUE of 0.045 Å may be compared to an average MUE for the five other nonlocal functionals of 0.063 Å.

5.6.8 Performance for organic molecule geometry database

Table 5.16 shows the performance of 13 density functionals for a recently published structural database called SE47, which denotes semi-experimental structures of 47 organic molecules.[93] The functionals included in this table are those selected as the best ranking functionals in Table 5.9. The SE47 database consists of 193 bond lengths of the 47 organic molecules. In this case MN15 gives the best bond lengths with an MUE of only 0.0033 Å. In Table 5.15 the nonlocal functionals (hybrid functionals) do better, on average, than the nonlocal ones. Since we only have ten molecular structure data (MS10) in our training set, the good performance of the MN15 functional against these 193 bond length shows that our functional is highly transferable to quantities not in our training set.

5.7 Concluding remarks

The new functional presented in this article is the culmination of a large body of work. Our group various kinds of properties one at a time and added the knowledge so gained to earlier databases. Some of our small databases were built by selecting representative data from large databases by statistical processes. In the current round of functional optimization, we first worked out the best gradient approximation (comparing all the functionals in Table 5.5), the GAM functional.[26] Next we made the MN15-L functional[29] by adding kinetic energy density to the ingredients in the GAM functional.

As we can see from Table 5.6, averaged over all 471 energetic data in Minnesota Database 2015B, MN15-L is the best functional among all the local approximations, and it even does better than all of the hybrid functionals in Tables 6 and 7 except for the MN15 functional presented here. The MN15 functional adds a portion of Hartree-Fock exchange to the ingredients of the MN15-L functional, and improves the mean unsigned error on the 471 data from 2.36 kcal/mol to 2.08 kcal/mol. It also has the best performance for the ten bond distances in the MS10 database. Perhaps most significantly f all, it improves the average ranking over 27 diverse energetic databases from 17 to 9.

In order to test the transferability of the functionals even more broadly, we tested them on the following databases: S66x8, EE69, TMBH21, WCCR10, SBG31, TMBDL7, and SE47 with a total of 859 pieces of data. The S6x6 subdatabase is from S66x8, there will be 823 pieces of data being tested (there are 481 pieces of data in our training set).

We develop a new global-hybrid exchange-correlation functional, called MN15, which gives good results for various chemistry proprieties. Most importantly, the MN15 functional is the only functional that gives best results for single-reference systems (SR313) and second best results for multi-reference systems (MR54). The average ranking of MN15 among 84 density functionals being tested for 27 atomic and molecular databases is 9, which is the best and which therefore shows that the MN15 functional is a very universal functional that can be used for a variety of applications. Since various applications like designing new energy material, catalysts, and understanding chemistry

dynamics require more than one property being tested, the universality of MN15 can be very useful for studying these applications in the near future.

A common question is which functional should one use for studying a given system. The answer has always depended on what properties you are studying. Now the MN15 functional gives relatively accurate results for most of these the properties, and we believe the MN15 functional provides a general answer to the question.

5.8 References

[1] L. H. Thomas, *Proc. Cambridge Philos. Soc.* 1927, **23**, 542.
[2] E. Fermi, *Rend. Accad. Naz. Lincei*, 1927, **6**, 602.
[3] P. A. M. Dirac, *Math. Proc. Cambridge. Phil. Soc*. 1930, **26**, 376.
[4] E. Teller, *Rev. Mod. Phys.* 1962, **34**, 627.
[5] J. C. Slater, *Phys. Rev.* 1951, **81**, 385.
[6] P. Hohenberg, W. Kohn, *Phys. Rev.* 1964 **136**, B864.
[7] W. Kohn, L. J. Sham, *Phys. Rev*. 1965, **140**, A1133.
[8] N. Schuch, F. Verstraete, *Nature Phys.* 2009, **5**, 732.
[9] U. von Barth, L. Hedin, *J. Phys. C: Solid State Phys.* 1972, **5**, 1629.
[10] C. R. Jacob, M. Reiher, *Int. J. Quantum Chem*. 2012, **112**, 3661.
[11] J. P. Perdew, A. Zunger, *Phys. Rev. B* 1981, **23**, 5048.
[12] S. H. Vosko, L. Wilk, M. Nusair, *Can. J. Phys.* 1980, **58**, 1200.
[13] J. P. Perdew, Wang, Y. *Phys. Rev. B* 1992, **45**, 13244.
[14] D. C. Langreth, M. J. Mehl, *Phys. Rev. B* 1983, 28**,** 1809.
[15] J. P. Perdew, Y. Wang, *Phys. Rev. B* 1986, **33**, 8800.
[16] A. D. Becke, *J. Chem. Phys*. 1986, **84**, 4524.
[17] A. D. Becke, *J. Chem. Phys.* 1996, **104**, 1040.
[18] R. Peverati and D. G. Truhlar, *J. Chem. Theory Comput.*, 2012, **8**, 2310.
[19] R. Peverati, D. G. Truhlar, *Phys. Chem. Chem. Phys.* 2012, **14**, 13171.

[20] J. P. Perdew, S. Kurth, *Lecture Notes Phys*. 2003, **55**, 1.

[21] J. P. Perdew, A. Ruzsinszky, J. Tao, V. N. Staroverov, G. E. Scuseria, G. I. Csonka, *J. Chem. Phys.* 2005, **123**, 062201.

[22] A. D. Becke, *J. Chem. Phys.,* 1993, **98**, 5648.

[23] Y. Andersson, D. C. Langreth, B. I. Lundqvist, Phys. Rev. Lett. 1996, **76**, 102.

[24] Y. Zhao, B. J. Lynch, D. G. Truhlar, *J. Phys. Chem. A* 2004, **108**, 4786.

[25] L. Goerigk, L., Grimme, S. *Wiley Interdis. Rev. Comp. Mol. Sci.* 2014, **4**, 576.

[26] H. S. Yu, W. Zhang, P. Verma, H. Xiao, D. G. Truhlar, *Phys. Chem. Chem. Phys.* 2015, **17**, 12146.

[27] Y. Zhao, D. G. Truhlar, *J. Chem. Phys.* 2006, **125**, 194101.

[28] R. Peverati, D. G. Truhlar, *Phys. Chem. Chem. Phys.* 2012, **14**, 13171.

[29] H. S. Yu, H. Xiao, D. G. Truhlar, MN15-L: A New Local Exchange-Correlation Functional for Kohn-Sham Density Functional Theory with Broad Accuracy for Atoms, Molecules, and Solids. *J. Chem. Theory Comput*. 2016, available online as Article ASAP. DOI: 10.1021/acs.jctc.5b01082

[30] Y. Zhao, D. G. Truhlar, *J. Phys. Chem. A* 2005, **109**, 5656.

[31] Y. Zhao, D. G. Truhlar, *Theor. Chem. Acc.* 2008, **120**, 215.

[32] Y. Zhao, D. G. Truhlar, *J. Chem. Theory Comput.* 2008, **4**, 1849.

[33] R. Peverati, D. G. Truhlar, *Phys. Chem. Chem. Phys.* 2012, **14**, 16187.

[34] J. Řezáč, K. E. Riley, P. Hobza, *J. Chem. Theory Comput*. 2011, **7**, 2427.

[35] X. Li, X. Xu, X. Yu, D. G. Truhlar, Benchmark Calculations for Bond Dissociation Enthalpies of Unsaturated Methyl Esters. 2016, *J. Phys. Chem A*, accepted.

[36] M. Caricato, G. W. Trucks, M. J. Frisch and K. B. Wiberg, *J. Chem. Theory Comput.*, 2010, **6**, 370.

[37] Y. Zhao, R. Peverati, K. Yang, S. Luo, H. S. Yu, and D. G. Truhlar, *MN-GFM, version 6.6: Minnesota Gaussian Functional Module*; University of Minnesota: Minneapolis, MN, 2015.

[38] M. J. Frisch, et al., *Gaussian 09, Revision C.1*, Gaussian, Inc., 2009.

[39] M. E. Casida, in *Recent Advances in Density Functional Methods, Part I*, ed. D. P. Chong, World Scientific: Singapore1995, pp. 155-193.

[40] M. Isegawa, R. Peverati and D. G. Truhlar, *J. Chem. Phys.*, 2012, **137**, 244104.

[41] S. L. Li and D. G. Truhlar, *J. Chem. Phys.*, 2014, **141**, 104106.

[42] S. L. Li and D. G. Truhlar, *J. Chem. Theory Comput.*, 2015, **11**, 3123.

[43] J. P. Perdew, K. Burke, M. Ernzerhof, *Phys. Rev. Lett*. 1996, **77**, 3865.

[44] (a) R. Gáspár, *Acta Phys.* Hung., 1954, **3**, 263-286. (b) R. Gáspár, *Acta Phys.* Hung., 1974, **35**, 213.

[45] S. H. Vosko, L. Wilk and M. Nusair, *Can. J. Phys.*, 1980, **58**, 1200.

[46] Y. Zhao and D. G. Truhlar, *J. Chem. Phys.*, 2008, **128**, 184109.

[47] J. P. Perdew, A. Ruzsinsky, G. I. Csonka, O. A. Vydrov, G. E. Scuseria, L. A. Constantin, X. Zhou and K. Burke, *Phys. Re.v Lett.*, 2008, **100**, 136406.

[48] R. Peverati, Y. Zhao and D. G. Truhlar, *J. Phys. Chem. Lett.*, 2011, **2**, 1991.

[49] J. P. Perdew, *Phys. Rev. B*, 1986, **33**, 8822.

[50] C. Lee, W. Yang and R. G. Parr, *Phys. Rev. B*, 1988, **37**, 785.

[51] J. P. Perdew, in *Electronic Structure of Solids '91*; P. Ziesche and H. Eschrig, Eds.; Akademie Verlag: Berlin, 1991; pp. 11–20.

[52] C. Adamo and V. Barone, *J. Chem. Phys*., 1997, **108**, 664.

[53] Y. Zhang and W. Yang, *Phys. Rev. Lett*., 1997, **80**, 890.

[54] B. Hammer, L. Hansen and J. Norskov, *Phys. Rev. B*, 1999, **59**, 7413.

[55] A. D. Boese and N. C. Handy, *J. Chem. Phys.*, 2000, **114**, 5497.

[56] N. Handy and A. Cohen, *Mol. Phys.*, 2001, **99**, 403.

[57] A. J. Thakkar and S. P. McCarthy, *J. Chem. Phys.*, 2009, **131**, 134109.

[58] T. V. Voorhis, G. E. Scuseria, *J. Chem. Phys.* 1998, **109**, 400.

[59] A. D. Boese, N. C. Handy, *J. Chem. Phys*. 2002, **116**, 9559.

[60] J. M. Tao, J. P. Perdew, V. N. Staroverov, G. E. Scuseria, *Phys. Rev. Lett.* 2003, **91**, 146401.

[61] J. P. Perdew, A. Ruzsinszky, G. I. Csonka, L. A. Constantin and J. Sun, *Phys. Rev. Lett.*, 2009, **103**, 026403.

[62] R. Peverati and D. G. Truhlar, *J. Phys. Chem. Lett*., 2011, **3**, 117.

[63] J. Sun, R. Haunschild, B. Xiao, I. W. Bulik, G. E. Scuseria, J. P. Perdew, *J. Chem. Phys.* 2013, **138**, 044113.

[64] A. D. Becke, *Phys. Rev. A*, 1988, **38**, 3098.

[65] C. Lee, W. Yang, R. G. Parr, *Phys. Rev. B*, 1988, **37**, 785.

[66] P. J. Stephens, F. J. Devlin, C. F. Chabalowski, M. J. Frisch, *J. Phys. Chem*. 1994, **98**, 11623.

[67] C. Adamo, V. Barone, *J. Chem. Phys.* 1999, **110**, 6158.

[68] H. L. Schmider, A. D. Becke, *J. Chem. Phys.* 1998, **108**, 9624.

[69] F. A. Hamprecht, A. J. Cohen, D. J. Tozer, N. C. Handy, *J. Chem, Phys.* 1988, **109**, 6264.

[70] W.-M. Hoe, A. J. Cohen, N. C. Handy, *Chem. Phys. Lett.* 2001, **341**, 319.

[71] T. W. Keal, D. J. Tozer, *J. Chem. Phys.* 2005, **123**, 121103.

[72] R. Peverati, D. G. Truhlar, *J. Chem. Phys.* 2011, **135**, 191102.

[73] T. Yanai, D. Tew, N. Hanyd, *Chem. Phys. Lett*. 2004, **393**, 51.

[74] Y. Tawada, T. Tsuneda, S. Yanagisawa, T. Yanai, K. Hirao, *J. Chem. Phys*. 2004, **120**, 8425.

[75] O. A. Vydrov, G. E. Scuseria, *J. Chem. Phys.* 2006, **125**, 234109.

[76] O. A. Vydrov, J. Heyd, A. V. Krukau, G. E. Scuseria, *J. Chem. Phys.* 2006, **125**, 074106.

[77] O. A. Vydrov, G. E. Scuseria, J. P. Perdew, *J. Chem. Phys.* 2007, **126**, 154109.

[78] J. Heyd, G. E. Scuseria, M. Ernzerhof, *J. Chem. Phys.* 2003, **118**, 8027.

[79] T. M. Henderson, A. F. Izmaylov, G. Scalmani, G. E. Scuseria, *J. Chem. Phys.* 2009, **131**, 044108.

[80] J.-D. Chai, M. Head-Gordon, *J. Chem. Phys.* 2008, **128**, 084106.

[81] J-D. Chai, M. Head-Gordon, *Phys. Chem. Chem. Phys.* 2008, **10**, 6615.

[82] V. N. Staroverov, G. E. Scuseria, J. Tao, J. P. Perdew, *J. Chem. Phys.* 2003, **119**, 12129.

[83] A. D. Boese, N. C. Handy, *J. Chem. Phys.*, 2002, **116**, 9559.

[84] Y. Zhao, B. J. Lynch, D. G. Truhlar, *J. Phys. Chem. A* 2004, **108**, 2715.

[85] A. D. Boese, M. L. Martin, *J. Chem. Phys.* 2004, **121**, 3405.

[86] R. Peverati, D. G. Truhlar, *J. Phys. Chem. Lett.* 2011, **2**, 2810.

[87] L. Hu, H. Chen, *J. Chem. Theory Comput.* 2015, **11**, 4601.

[88] Y. Sun, H. Chen, *J. Chem. Theory Comput.* 2014, **10**, 579.

[89] Y. Sun, H. Chen, *J. Chem. Theory Comput.* 2013, **9**, 4735.

[90] T. Weymuth, E. P. A. Couzijn, P. Chen and M. Reiher, *J. Chem. Theory Comput.*, 2014, **10**, 3092.

[91] R. Peverati and D. G. Truhlar, *Phil. Trans. R. Soc. A*, 2014, **372**, 20120476.

[92] A. Posada-Borbón and A. Posada-Amarillas, *Chem. Phys. Lett.* 2015, **618**, 66.

[93] M. Piccardo, E. Penocchio, C. Puzzarini, M. Biczysko, V. Barone, *J. Phys. Chem. A* 2015, **119**, 2058.

[94] N. E. Schultz, Y. Zhao, D. G. Truhlar, *J. Phys. Chem. A* 2005, **109**, 11127.

[95] O. Tishchenko, J. Zheng, D. G. Truhlar, *J. Chem. Theory Comput.* 2008, **4**, 1208.

[96] Y. Zhao, O. Tishchenko, J. R. Gour, W. Li, J. J. Lutz, P. Piecuch, D. G. Truhlar, *J. Phys. Chem. A* 2009, **113**, 5786.

[97] L. Goerigk, H. Kruse, S. Grimme, *ChemPhysChem* 2011, **12**, 3421.

[98] S. Grimme, *J. Chem. Phys.* 2006, **124**, 034108.

[99] A. Karton, A. Tarnopolsky, J. F. Lamère, G. C. Schatz, J. M. L. Martin, *J. Phys. Chem. A* 2008, **112**, 12868.

[100] S. Kozuch, D. Gruzman, J. M. L. Martin, *J. Phys. Chem. C* 2010, **114**, 20801.

[101] L. Goerigk, S. Grimme, *J. Chem. Theory Comput.* 2011, **13**, 6670.

[102] F. London, *Trans. Faraday Soc.* 1937, **33**, 8.

[103] K. Szalewicz, *Wiley Interdis. Rev. Comp. Mol. Sci.* 2012, **2**, 254.

[104] M. E. Casida and M. Huix-Rotllant, *Annu. Rev. Phys. Chem.*, 2012, **63**, 287.

[105] D. C. Comeau and R. J. Bartlett, *Chem. Phys. Lett.*, 1993, **207**, 414.

[106] Y. Zhao, N. González-García, and D. G. Truhlar, *J. Phys. Chem. A*, 2005, **109**, 2012.

[107] Y. Zhao and D. G. Truhlar, *J. Phys. Chem. A*, 2005, **109**, 5656.

[108] B. J. Lynch, P. L. Fast, M. Harris, and D. G. Truhlar, *J. Phys. Chem. A*, 2000, **104**, 4811.

[109] Y. Zhao and D. G. Truhlar, *J. Phys. Chem. A*, 2004, **108**, 6908.

[110] Y. Zhao, N. E. Schultz, and D. G. Truhlar, *J. Chem. Theory Comput.*, 2006, **2**, 364.

[111] Y. Zhao and D. G. Truhlar, *J. Chem. Theory Comput.*, 2008, **4**, 1849.

[112] M. Head-Gordon, R. J. Rico, M. Oumi, and T. J. Lee, *Chem. Phys. Lett.*, 1994, **219**, 21.

[113] Y. Zhao and D. G. Truhlar, *J. Phys. Chem. A*, 2006, **110**, 13126.

[114] J. Heyd, G. E. Scuseria, and M. Ernzerhof, *J. Chem. Phys.*, 2003, **118**, 8207.

[115] Y. Zhao, N. E. Schultz, and D. G. Truhlar, *J. Chem. Phys.*, 2005, **123**, 161103.

[116] R. McWeeny, *Methods of Molecular Quantum Mechanics*, 2nd Edition; Academic Press: London, 1992; pp 435-438.

[117] J. B. Foresman, M. Head-Gordon, J. A. Pople, and M. J. Frisch, *J. Phys. Chem.*, 1992, **96**, 135.

[118] J. Paier, M. Marsman, K. Hummer, G. Kresse, I. C. Gerbr, and J. G. Ángyán, *J. Chem. Phys.* 2006, **124**, 154709.

[119] P. Rinke, M. Winkelnkemper, A. Qteish, D. Bimberg, J. Neugebauer, and M. Scheffler, *Phys. Rev. B* 2008, **77**, 075202.

Table 5.1 Databases included in Database 2015B[a]

n	Combined databases	Primary	Secondary	Description	I_n[b]
1–26	AME471			Atomic and Molecular Energies	
1–4	MGBE150			Main-group bond energies	
1		SR-MGM-BE9		Single-reference main-group metal bond energy	0.91
			SRM2	Single-reference main-group bond	
			SRMGD5	Single-reference main-group diatomic	
			3dSRBE2	3d single-reference metal-ligand bond	
2		SR-MGN-BE120		Single-reference main-group non-metal	
			SR-MGN-BE107	Single-reference main-group non-metal	0.10
			ABDE13	Alkyl bond dissociation energies	2.00
3		MR-MGM-BE4		Multi-reference main-group metal bond	0.66
4		MR-MGN-BE17		Multi-reference main-group non-metal	1.00
5–7	TMBE33			Transition metal bond energies	
5		SR-TM-BE17		Single-reference TM[c] bond energies	1.18
			3dSRBE4	3d single-reference metal-ligand bond	
			SRMBE10	Single-reference metal bond energies	
			PdBE2	Palladium complex bond energies	
			FeCl	FeCl bond energy	
6		MR-TM-BE13		Multi-reference TM bond energies	0.72
			3dMRBE6	3d multi-reference metal-ligand bond	

			MRBE3	Multi-reference bond energies
			remaining	Bond energies of remaining molecules:
				CuH, VO, CuCl, NiCl
7		MR-TMD-BE3		Multi-reference TM dimer bond energies 1.61
				Multi-reference TM dimer bond energy 1.25
8–9	BH76			Reaction barrier heights
8		HTBH38/08		Hydrogen transfer barrier heights 0.14
9		NHTBH38/08		Non-hydrogen transfer barrier heights 0.13
10–12	NC87			Noncovalent interactions
10		NCCE23		Noncovalent complexation energies (23 0.10
		CT7		Seven Charge transfer data 0.03
11		S6x6		Six dimers at six intermonomeric 0.013
12		NGDWI21		Noble gas dimer weak interaction 0.003
13–15	EE18			Excitation energies
13		3dEE8		3d TM atomic excitation energies and 0.94
14		4dAEE5		4d TM atomic excitation energies 2.99
15		pEE5		p-block excitation energies 0.74
16–18	IsoE14			Isomerization
16		4pIsoE4		4p isomerization 0.64
17		2pIsoE4		2p isomerization 3.12
18		IsoL6/11		Isomerization 2.00
19–20	HCTC20			Hydrocarbon

19		πTC13	Thermochemistry	3.90
20		HC7/11	Hydrocarbon	1.44
21		EA13/03	Electron affinities	0.54
22		PA8	Proton affinities	0.45
23		IP23	Ionization	2.73
24		AE17	Atomic energies	2.38
25		SMAE3	Sulfur molecules	2.00
26		DC9/12	Difficult cases	10.00
27–29	MS10		Molecular	
27		DGL6	Diatomic	0.009
28–29		DGH4		
28		DGH3	Diatomic	0.008

[a]All the databases in this table are used for both training and testing. In databases named X*n*, there are *n* data; in those named X*n*/*yy*, there are *n* data, and *yy* denotes the year of an update.
[b]Inverse weights with units of kcal/mol per bond for databases 1-7, kcal/mol for databases 8-26, and Å for databases 27
[c]TM denotes transition metal

Table 5.2 Multi-reference systems and single-reference systems in Database 2015[a]

Name	Number of multi-reference systems	Number of single-reference systems
SR-MGM-BE9	0	9
SR-MGN-BE120	0	120
MR-MGM-BE4	4	0
MR-MGN-BE17	17	0
SR-TM-BE17	0	17
MR-TM-BE13	13	0
MR-TMD-BE3	3	0
HTBH38/08	1	37
NHTBH38/08	3	35
NCCE30	0	0
S6x6	0	0
NGDWI21	0	0
3dEE8	0	8
4dAEE5	0	5
pEE5	0	5
4pIsoE4	0	4
2pIsoE4	0	4
IsoL6/11	0	6
πTC13	0	13
HC7/11	3	4
EA13/03	0	13
PA8	0	8
IP23	0	23
AE17	0	0
SMAE3	2	1
DC9/12	8	1
Total	54	313

[a] The 26 energetic databases from Table 1 are shown here with the number of multi-reference systems and single-reference systems defined by generalized B1 diagnostics.[94,95,96]

Databases for testing only

ase	Description	Reference(s)
1[a]	Semiconductor band gaps (31 data)	91
R10	Ligand dissociation energies of large cationic TM complexes (10 data)	90
[b]	Interaction energies relevant to bimolecular structures (528 data)	34
I21	TM reaction barrier heights (21 data)	87,88,89
	Excitation energies of 30 valence and 39 Rydberg states of 11 organic molecules (69 data)	40
BL7	Bond lengths of homonuclear TM dimers (7 data)	92
	Semi-experimental structures of 47 organic molecules (193 data)[c]	93

s a solid-state database computed with periodic boundary conditions; all other databases in this article are nd/or molecular databases.

x8 includes the database S6x6 , which is used for training as well

e 859 data in this table, but 36 are also in the S6x6 subdatabase of Minnesota Database 2015B; therefore the f tested data that were not used for training equals 823.

Table 5.4 Optimized parameters of the MN15 functional

Exchange				Correlation		X^a
a_{000}	0.073852235	a_{102}	6.89391326	b_0	1.093250748	44
a_{001}	-0.839976156	a_{103}	2.489813993	b_1	-0.269735037	
a_{002}	-3.082660125	a_{104}	1.454724691	b_2	6.368997613	
a_{003}	-1.02881285	a_{110}	-5.054324071	b_3	-0.245337101	
a_{004}	-0.811697255	a_{111}	2.35273334	b_4	-1.587103441	
a_{005}	-0.063404387	a_{112}	1.299104132	b_5	0.124698862	
a_{010}	2.54805518	a_{113}	1.203168217	b_6	1.605819855	
a_{011}	-5.031578906	a_{120}	0.121595877	b_7	0.466206031	
a_{012}	0.31702159	a_{121}	8.048348238	b_8	3.484978654	
a_{013}	2.981868205	a_{122}	21.91203659			
a_{014}	-0.749503735	a_{200}	-1.852335832	c_0	1.427424993	
a_{020}	0.231825661	a_{201}	-3.4722735	c_1	-3.57883682	
a_{021}	1.261961411	a_{202}	-1.564591493	c_2	7.398727547	
a_{022}	1.665920815	a_{203}	-2.29578769	c_3	3.927810559	
a_{023}	7.483304941	a_{210}	3.666482991	c_4	2.789804639	
a_{030}	-2.544245723	a_{211}	10.87074639	c_5	4.988320462	
a_{031}	1.384720031	a_{212}	9.696691388	c_6	3.079464318	
a_{032}	6.902569885	a_{300}	0.630701064	c_7	3.521636859	
a_{100}	1.657399451	a_{301}	-0.505825216	c_8	4.769671992	
a_{101}	2.98526709	a_{302}	-3.562354535			

[a] X stands for the percentage of Hartree-Fock exchange

Table 5.5 Exchange–correlation functionals tested against Database 2015B in the article pro

Category	Type	X^a	Year	Method	Ref
local	LSDA	0	1980	GKSVWN5[b]	7,44,
	GGA - exchange correct to 2nd order	0	2008	SOGGA	46
		0	2008	PBEsol	47
		0	2011	SOGGA11	48
	GGA - other	0	1988	BP86	14,1
		0	1988	BLYP	14,5
		0	1991	PW91[c]	51
		0	1991	BPW91	14,5
		0	1996	PBE	20
		0	1997	mPWPW	52
		0	1997	revPBE	53
		0	1999	RPBE	54
		0	2000	HCTH407	35
		0	2001	OLYP	50,5
		0	2009	OreLYP	50,56,
	NGA	0	2012	N12	18
		0	2015	GAM	26
	meta-GGA	0	1998	VSXC	58
		0	2002	τ-HCTH	34
		0	2003	TPSS	60
		0	2006	M06-L	27
		0	2009	revTPSS	61
		0	2011	M11-L	62
		0	2013	MGGA_MS2	63
	meta-NGA	0	2012	MN12-L	19
		0	2015	MN15-L	29
nonlocal	global-hybrid GGA	20	1994	B3LYP	64,65,
		25	1996	PBE0	67
		21.98	1998	B98	68
		21	1998	B97-1	69
		11.61	2001	O3LYP	70
		26.93	2005	B97-3	71
		35.42	2011	SOGGA11-X	72

range-separated hybrid GGA	19-65	2004	CAM-B3LYP	73
	0-100	2006	LC-ωPBE	74,75,76,77
	0-25	2006	HSE06	78,79
	0-100	2008	ωB97	80
	15.77-100	2008	ωB97X	80
range-separated hybrid GGA+MM[d]	22.2-100	2008	ωB97X-D	81
global-hybrid meta-GGA	10	2002	TPSSh	82
	15	2002	τ-HCTHhyb	83
	42	2004	BB1K	14,17,84
	42	2004	BMK	85
	28	2005	PW6B95	30
	27	2006	M06	31
	54	2006	M06-2X	31
	52.23	2008	M08-HX	32
global-hybrid meta-NGA	44	2015	MN15	present
range-separated hybrid meta-GGA	42.8-100	2011	M11	86

[a] *X* is the percentage of nonlocal Hartree–Fock exchange. When a range is given, the first value is for small interelectronic distances, and the second value is for large interelectronic distances. Details of the functional form that joins these regions of interelectronic separation are given in the references.

[b] GVWN5 denotes the Gáspár approximation for exchange and the VWN5 fit to the correlation energy; this is an example of the local spin density approximation (LSDA), and it has the keyword SVWN5 in the *Gaussian 09* program. Note that Kohn-Sham exchange is the same as Gáspár exchange, but Slater exchange (not tested here) is greater by a factor of 1.5.

[c] PW91 formally satisfies the gradient expansion for exchange to second order but only at such small values of the gradient that for practical purposes it should be grouped with functionals that do not satisfy the gradient expansion to second order.

MM denotes molecular mechanics, which in this case corresponds to atom-atom pairwise damped dispersion terms added post-SCF to the calculated energy

Table 5.6 MUE (kcal/mol) for the AME471 database and its subdatabases: LSDA and other gradient approximations

Type	LSDA	GGA														NGA	
Functional	GKSVWN	SOGG	PBEso	SOGGA1	BP86	BLY	PW9	BPW9	PBE	mPWP	revPB	RPB	HCTH40	OLY	OreLY	N12	**GA**
MGBE150[a]	18.36	8.63	8.81	4.01	5.55	4.34	5.04	4.23	4.96	4.47	4.25	4.53	3.80	3.75	3.73	3.42	**2.98**
TMBE33[b]	25.20	15.00	14.50	14.00	9.05	9.85	10.26	9.19	9.33	8.82	7.64	7.34	13.31	8.42	6.48	9.36	**5.85**
BH76[c]	14.99	11.28	11.28	5.45	8.94	8.03	9.20	7.32	8.87	8.23	6.70	6.63	5.89	5.44	5.93	6.90	**5.25**
NC87[d]	2.48	1.61	1.63	2.29	2.43	2.78	1.49	3.07	1.61	2.15	3.04	2.83	2.41	4.32	4.53	2.30	**1.08**
EE18[e]	10.81	8.08	8.81	9.63	7.32	8.31	7.41	9.31	7.06	7.80	7.15	6.74	9.80	7.56	8.18	16.2	**6.91**
IsoE14[f]	2.34	1.88	1.80	2.17	2.71	4.30	2.38	2.69	2.32	2.55	2.85	2.96	3.55	3.22	3.15	2.21	**3.29**
HCTC20[g]	10.63	8.90	7.39	7.01	7.29	13.53	5.32	8.37	5.02	6.99	9.43	9.92	10.59	11.32	10.44	7.09	**7.77**
AME454xAE	13.59	7.90	7.88	5.39	6.13	5.92	5.70	5.47	5.49	5.43	5.26	5.33	5.57	5.25	5.18	5.05	**4.14**
AME471[h]	28.30	17.83	16.47	5.56	6.52	6.02	5.66	5.70	7.00	5.68	5.47	5.48	5.98	5.43	5.08	5.38	**4.36**
MR54	35.04	22.32	21.92	13.51	14.0	14.08	14.25	12.66	14.1	13.32	11.44	11.58	14.01	11.03	10.22	9.35	**9.45**
SR313	13.03	7.22	7.25	4.96	5.86	5.46	5.46	5.03	5.14	5.05	4.88	5.01	5.06	4.59	4.56	5.20	**4.11**

[a] The MGBE150 database consists of SR-MGM-BE9, SR-MGN-BE107, MR-MGM-BE4, MR-MGN-BE17, and ABDE13. [b] The TMBE33 database consists of SR-TM-BE17, MR-TM-BE13, and MR-TMD-BE3. [c] The BH76 database consists of HTBH38/08 and NHTBH38/08. [d] The NC87 database consists of NGDWI21, S66x8_6x6, NCCE23 and CT7. [e] The EE18 database consists of 3dEE8, 4dAEE5, and pEE5. [f] The IsoE14 consists of 2pIsoE4, 4pIsoE4, and IsoL6/11. [g] The HCTC20 consists of HC7/11, ABDE13, and πTC13. [h] The ME471 database consists all the 27 subdatabases (from 1 to 27 in Table 1) and the ME454xAE consists all the subdatabases except AE17.

Table 5.7 MUE (kcal/mol) for the AME471 database and its subdatabases: meta-GGAs, MN12-L, MN15-L, and global-hybrid GGAs.

Type	meta-GGA							meta-NGA		hybrid						
Functional	VSXC	τ-HCTH	TPSS	M06-L	revTPSS	M11-L	MGGA_MS2	MN12-L	**MN15-L**	B3LYP	PBE0	B98	B97-1	O3LYP	B97-3	SOGGA11-X
MGBE150[a]	3.02	3.40	3.49	2.63	3.26	2.81	3.93	2.35	**1.84**	3.58	2.82	2.71	2.09	3.51	2.50	2.62
TMBE33[b]	7.77	7.83	7.11	5.29	7.36	7.02	7.92	11.20	**5.16**	8.83	10.18	6.92	5.04	10.49	9.85	15.26
BH76[c]	4.91	6.39	8.31	3.99	8.02	2.15	6.22	1.78	**1.66**	4.39	3.83	3.74	3.89	3.85	1.83	1.48
NC87[d]	4.23	2.22	1.92	0.57	1.83	0.97	1.11	0.74	**0.98**	2.05	1.33	1.51	1.32	3.61	2.10	1.50
EE18[e]	7.63	14.02	6.96	8.37	6.71	14.44	10.77	18.65	**3.71**	6.47	6.85	7.16	7.31	6.04	6.20	5.14
IsoE14 [f]	4.27	3.52	3.32	2.91	3.35	3.06	2.75	2.17	**2.19**	3.67	1.87	2.55	2.33	2.98	2.56	2.22
HCTC20[g]	10.56	10.71	8.95	5.52	7.35	4.19	10.38	4.36	**4.54**	9.80	7.26	7.60	6.76	9.58	7.44	6.50
AME454xAE[h]	4.71	5.00	4.88	3.28	4.70	3.45	4.96	3.52	**2.19**	4.45	3.72	3.50	3.07	4.73	3.44	3.58
AME471[h]	6.34	5.44	5.35	3.42	5.39	4.11	5.36	3.75	**2.36**	4.95	4.98	3.55	3.15	4.76	3.57	3.63
MR54	8.66	9.37	9.48	5.91	9.39	6.74	10.76	8.93	**4.35**	10.67	10.37	8.26	6.09	10.19	9.92	12.84
SR313	4.23	5.10	4.96	3.61	4.74	3.71	5.07	3.49	**2.15**	4.09	3.28	3.28	3.08	4.13	2.70	2.56

[a] The MGBE150, TMBE33, BH76, NC87, EE18, IsoE14, HCTC20, AME454xAE, and AME471 notations are explained in footnotes to Table 5.5.

Table 5.8 MUE (kcal/mol) for the AME471 database and its subdatabases: range-separated-hybrid GGAs, global-hybrid meta-GGAs, MN15

Type	RSH GGA					RSH GGA	GH mGGA								RSH	**GH**
Functional	CAM-B3LYP	LC-ωPBE	HSE06	ωB97	ωB97X	ωB97X-D	TPSSh	τ-HCTHhyb	BB1K	BMK	PW6B95	M06	M06-2X	M08-HX	M11	**MN15**
MGBE150[a]	3.09	3.47	2.97	2.46	2.42	2.23	3.76	2.37	2.37	2.06	2.65	1.90	1.87	2.74	2.36	**1.36**
TMBE33[b]	10.75	12.43	9.92	10.31	10.57	8.70	6.78	5.62	5.62	13.02	9.50	7.10	19.11	17.59	14.36	**5.54**
BH76[c]	2.90	1.77	3.98	2.15	2.45	3.05	6.39	4.88	4.88	1.21	2.98	2.16	1.18	0.97	1.29	**1.36**
NC87[d]	1.35	1.56	1.31	0.55	0.64	0.30	1.92	1.61	1.61	1.68	1.03	0.67	0.35	0.37	0.39	**0.25**
EE18[e]	6.20	8.46	8.09	11.51	8.94	8.30	6.46	9.00	9.00	6.74	5.34	8.45	7.86	5.78	8.99	**6.28**
IsoE14[f]	2.89	1.55	1.99	1.42	1.79	1.75	3.02	2.50	2.50	1.54	2.01	1.66	1.94	1.26	1.74	**1.41**
HCTC20[g]	4.57	8.96	6.60	6.58	5.21	5.68	7.65	7.25	7.25	5.09	5.24	3.83	1.72	2.93	2.77	**3.59**
AME454xAE[h]	3.59	4.02	3.85	3.39	3.20	2.99	4.52	3.57	3.57	3.07	3.21	2.59	3.11	3.25	3.20	**1.88**
AME471[h]	3.85	4.79	4.89	3.49	3.29	3.09	4.91	3.66	3.66	3.57	6.65	2.66	3.08	3.28	3.41	**2.08**
MR54	9.64	11.81	10.18	10.26	9.72	8.89	9.41	6.38	6.38	10.03	8.95	5.43	13.33	13.62	10.35	**4.75**
SR313	3.20	3.39	3.54	3.05	2.84	2.77	4.43	3.68	3.68	2.30	2.86	2.71	2.13	2.29	2.80	**1.85**

[a] The MGBE150, TMBE33, BH76, NC87, EE18, IsoE14, HCTC20, AME454xAE, and AME471 notations are explained in footnotes to Table 5.

Table 5.9 MUE (kcal/mol) of top ten best functionals for charge transfer database (CT7)[a]

Name	SOGGA11-X	MPWB1K	MN15-L	MN15	MGGA_MS2	PWB6K	ωB97X-D	M11	M06-HF	M06-2X
CT7	0.21	0.23	0.25	0.25	0.26	0.26	0.28	0.30	0.35	0.37

[a] There are seven intermolecular charge transfer systems included in the database, which are C_2H_4…F_2, NH_3…F_2, C_2H_2…ClF, HCN…ClF, NH_3…Cl_2, H_2O…ClF, and NH_3…ClF.

Table 5.10 MUE (Å) for the Molecular Structure 10 Database and its Subdatabas

Functional	Type	DGL6	DGH4	MS10[a]
MN15	**GH mNGA**	**0.005**	**0.008**	**0.006**
N12	NGA	0.008	0.007	0.008
MN15-L	mNGA	0.004	0.014	0.008
PBE0	GH GGA	0.003	0.014	0.008
HSE06	RSH GGA	0.003	0.015	0.008
PBEsol	GGA	0.010	0.007	0.009
CAM-B3LYP	RSH GGA	0.008	0.010	0.009
TPSSh	GH mGGA	0.006	0.013	0.009
PW6B95	GH mGGA	0.004	0.016	0.009
SOGGA	GGA	0.009	0.013	0.010
revTPSS	mGGA	0.011	0.009	0.010
τ-HCTHhyb	GH mGGA	0.006	0.017	0.010
BB1K	GH mGGA a	0.009	0.011	0.010
τ-HCTH	mGGA	0.006	0.019	0.011
M06-L	mGGA	0.006	0.018	0.011
M11	RS-hybrid-meta	0.007	0.017	0.011
TPSS	mGGA	0.010	0.015	0.012
MGGA_MS2	mGGA	0.005	0.022	0.012
MN12-L	mGGA	0.005	0.022	0.012
LC-ωPBE	RSH GGA	0.013	0.011	0.012
ωB97X	RSH GGA	0.008	0.017	0.012
ωB97X-D	RSH GGA-D	0.005	0.023	0.012
VSXC	mGGA	0.006	0.022	0.013
M06	GH mGGA	0.006	0.023	0.013
O3LYP	GH GGA	0.004	0.030	0.014
SOGGA11-X	GH GGA	0.004	0.029	0.014
ωB97	RSH GGA	0.011	0.018	0.014

PW91	GGA	0.012	0.019	0.015
HCTH407	GGA	0.004	0.033	0.015
B98	GH GGA	0.007	0.026	0.015
B97-1	GH GGA	0.006	0.028	0.015
BMK	GH mGGA	0.007	0.027	0.015
PBE	GGA	0.013	0.020	0.016
mPWPW	GGA	0.012	0.021	0.016
B3LYP	GH GGA	0.009	0.027	0.016
B97-3	GH GGA	0.004	0.034	0.016
BPW91	GGA	0.013	0.022	0.017
BP86	GGA	0.015	0.021	0.018
GAM	NGA	0.007	0.034	0.018
GKSVWN5	LSDA	0.011	0.031	0.019
OLYP	GGA	0.009	0.036	0.020
OreLYP	GGA	0.011	0.034	0.020
M11-L	mGGA	0.012	0.033	0.021
M06-2X	GH mGGA	0.004	0.049	0.022
M08-HX	GH mGGA	0.005	0.047	0.022
revPBE	GGA	0.015	0.034	0.023
RPBE	GGA	0.016	0.038	0.025
SOGGA11	GGA	0.008	0.053	0.026
BLYP	GGA	0.019	0.037	0.026

[a] The MS10 database consists of DGL6 and DGH4 subdatabases. The functionals are listed in the order of increasing value in the last column.

Table 5.11 The rankings (out of 83 functionals) of 12 selected functionals for 28 atomic and molecular databases

Name	BP86	PBE	B3LYP	TPSS	HSE06	M06-L	τ-HCTHhyb	ωB97X-D	M06-2X	M06	MN15-L	MN15
SR-MGM-BE9	24	18	58	16	39	35	10	12	3	37	19	**29**
SR-MGN-BE107	75	69	48	46	33	29	20	10	2	8	12	**1**
SR-TM-BE17	52	49	20	22	11	37	38	3	58	18	2	**6**
MR-MGM-BE4	48	46	23	13	33	7	4	49	57	3	2	**1**
MR-MGN-BE17	73	75	30	13	34	3	15	44	37	10	1	**2**
MR-TM-BE13	61	64	15	43	25	20	2	8	69	5	11	**7**
IsoL6/11	51	44	57	75	10	61	32	5	20	11	12	**28**
IP23	75	63	55	38	32	29	27	7	15	52	3	**2**
EA13/03	72	27	30	31	45	67	6	9	19	8	22	**2**
PA8	21	17	2	66	8	44	47	61	35	40	55	**9**
πTC13	33	27	37	67	44	49	61	45	1	16	20	**9**
HTBH38/08	76	77	39	70	40	37	47	25	5	21	8	**3**
NHTBH38/08	72	70	43	75	37	39	42	38	3	21	15	**12**
NCCE30	65	57	46	56	33	19	39	7	2	11	22	**9**
AE17	57	73	60	59	70	23	17	16	1	5	22	**19**
ABDE13	40	35	45	55	33	36	31	10	9	19	30	**15**
HC7/11	48	11	68	49	37	8	35	19	1	6	12	**7**
3dEE8	47	32	20	44	54	27	66	18	17	41	2	**1**
4dAEE5	24	13	36	28	25	51	63	58	70	62	1	**3**
pEE5	19	31	11	6	56	66	29	69	40	50	42	**28**
DC9/12	62	60	46	54	33	40	36	20	8	3	9	**1**
2pIsoE4	47	36	74	58	31	43	48	18	16	13	20	**1**
4pIsoE4	50	27	75	37	38	51	48	29	40	23	68	**19**
S6x6	39	23	34	33	19	6	29	1	4	9	13	**2**
NGDWI21	80	16	66	42	18	26	44	39	24	52	3	**2**
MR-TMD-BE3	17	31	50	12	59	1	13	56	75	46	23	**26**
SMAE3	67	65	62	45	49	21	15	24	35	1	6	**4**
MS10	54	46	50	29	9	2	18	33	66	35	7	**1**
Lowest	80	77	75	75	70	67	66	69	75	62	68	**29**
Average	52	43	43	42	34	31	32	26	26	22	17	**9**

Table 5.12 The performance (kcal/mol) of 18 selected density functionals for the S60 and S492 databases and subdatabases.

DFT	Dd21[a]	HB20[b]	Mix19[c]	S60	S492
without nonlocal correlation or molecular mechanics (also called empirical dispersion correction)					
MN15	**0.59**	**0.39**	**0.31**	**0.46**	**0.32**
M06-2X	0.33	0.27	0.23	0.26	0.34
M05-2X	1.04	0.09	0.42	0.56	0.46
M06-L	0.68	0.26	0.74	0.54	0.48
PW6B95	2.43	0.59	1.41	1.57	1.06
MPW1B95	2.82	0.70	1.64	1.83	1.24
PBE	3.73	-0.05	2.00	2.05	1.41
LC-ωPBE	3.95	0.71	2.18	2.43	1.69
TPSS	4.95	0.46	2.83	2.95	1.98
B3LYP	5.30	0.50	3.08	3.15	2.25
BLYP	6.26	1.14	3.82	3.99	2.80
revPBE	6.42	2.02	3.90	4.42	2.91

[a]Dd21 is the dispersion-dominated subdatabase

[b]HB20 is the hydrogen bonding subdatabase

[c]Mix19 is the mixed subdatabase

Table 5.13 The performance (kcal/mol) of 18 selected density functionals for the S66 and S66x8 databases and subdatabases.

DFT	Dd23[a]	HB23[b]	Mix20[c]	S66	S66x8
without nonlocal correlation or molecular mechanics (also called empirical dispersion correction)					
MN15	**0.57**	**0.36**	**0.32**	**0.42**	**0.32**
M06-2X	0.35	0.24	0.25	0.28	0.34
M05-2X	1.03	0.27	0.43	0.58	0.49
M06-L	0.69	0.39	0.73	0.60	0.51
PW6B95	2.39	0.99	1.40	1.60	1.13
MPW1B95	2.76	1.13	1.62	1.85	1.31
PBE	3.63	0.74	1.94	2.11	1.51
LC-ωPBE	3.85	1.35	2.14	2.46	1.78
TPSS	4.83	1.38	2.77	3.00	2.11
B3LYP	5.17	1.47	3.00	3.22	2.37
oTPSS	5.99	2.17	3.55	3.92	2.72
BLYP	6.15	2.22	3.77	4.06	2.97
revPBE	6.35	3.03	3.91	4.45	3.13
with nonlocal correlation					
B2GP-PLYP	1.88	0.32	1.01	1.07	0.81
PWPB95	1.81	0.95	1.09	1.29	0.92
B2-PLYP	2.66	0.61	1.51	1.60	1.19
with molecular mechanics (also called empirical dispersion correction) added					
PW6B95-D3(BJ)	0.16	0.23	0.15	0.18	0.21
ωB97X-D	0.47	0.28	0.22	0.32	0.23
with nonlocal correlation and molecular mechanics (also called empirical dispersion correction)					
DSD-BLYP-D3	0.23	0.36	0.14	0.21	0.16

[a]Dd23 is the dispersion-dominated subdatabase

[b]HB23 is the hydrogen bonding subdatabase

[c]Mix20 is the mixed subdatabase

Table 5.14 The mean unsigned errors (MUE, in eV) of 60 selected methods for the vertical excitation energies of 30 valence, 39 Rydberg, and all 69 transitions

Name	X^a	Valence	Rydberg	All states	Ref. for	Ref. for
MN15	44	**0.29**	**0.24**	**0.26**	**present**	**present**
EOM-CCSD	WFT	0.47	0.11	0.27	36	105
M06-2X	54	0.36	0.26	0.30	40	31
ωB97X-D	22.2–100	0.32	0.28	0.30	40	81
MPWKCIS1	41	0.40	0.27	0.32	40	106
PWB6K	46	0.43	0.24	0.32	40	107
CAM-B3LYP	19–65	0.31	0.35	0.33	36	73
MPW1K	42.8	0.45	0.23	0.33	40	108
MPWB1K	44	0.40	0.28	0.33	40	109
ωB97X	15.77–100	0.40	0.28	0.33	40	80
BMK	42	0.33	0.39	0.36	36	85
M05-2X	52	0.37	0.35	0.36	36	110
LC-ωPBE	0–100	0.41	0.32	0.36	36	74,75,76,77
B3P86	20	0.19	0.53	0.38	36	15,64,66
SOGGA11-X	40.15	0.46	0.34	0.39	40	72
BH&H	50	0.49	0.33	0.40	36	36
ωB97	0–100	0.45	0.39	0.41	40	80
M08-SO	56.79	0.35	0.49	0.43	40	111
BH&HLYP	50	0.56	0.36	0.44	36	36
LC-BLYP	0–100	0.49	0.41	0.45	36	64,50,74
M08-HX	52.23	0.38	0.51	0.46	40	32
M11	42.8–100	0.37	0.54	0.47	40	86
CIS(D)	WFT	0.50	0.49	0.49	36	112
M06-HF	100	0.56	0.44	0.49	40	113
PBE0	25	0.22	0.80	0.55	36	67
HSE	25–0	0.21	0.82	0.56	36	114
B3P86(VWN	20	0.19	0.87	0.57	36	45,15,64,66
N12-SX	25–0	0.26	0.85	0.59	40	33
M05	26	0.24	0.90	0.62	36	115
LC-HCTH/93	0–100	0.53	0.70	0.63	40	74,35
B3LYP	20	0.20	1.03	0.67	36	64, 50,66
τ -HCTHhyb	15	0.18	1.04	0.67	36	83

LC-	0–100	0.53	0.85	0.71	40	74,35
LC-	0–100	0.53	0.85	0.71	40	74,35
LC-B97-D	0–100	0.53	0.84	0.71	40	74,Error!
M06-L	0	0.28	1.08	0.73	40	27
TPSSh	10	0.18	1.27	0.80	36	82
LC-τ -HCTH	0–100	0.54	1.00	0.80	40	74,83
LSDA	0	0.45	1.20	0.88	36	7,44,45
HCTH/147	0	0.38	1.26	0.88	40	35
M06	27	0.30	1.33	0.88	40	31
O3LYP	11.61	0.20	1.47	0.92	36	70
B97-D	0	0.39	1.35	0.93	40	117
VSXC	0	0.24	1.54	0.97	36	58
HCTH/93	0	0.38	1.45	0.99	40	35
HCTH/407	0	0.34	1.51	1.00	36	35
τ -HCTH	0	0.32	1.53	1.00	36	83
TDHF	WFT	1.19	0.88	1.01	36	116
LC-M06-L	0–100	0.57	1.35	1.01	40	74,27
TPSS	0	0.26	1.63	1.03	36	60
CIS	WFT	1.29	0.91	1.07	36	117
BP86	0	0.38	1.62	1.08	36	15,64
BP86(VWN5)	0	0.38	1.62	1.08	36	45,15,64
PBE	0	0.40	1.70	1.13	36	20
BLYP	0	0.40	1.88	1.23	36	50,64
MN12-L	0	0.49	1.80	1.23	40	19
M11-L	0	0.35	1.93	1.24	40	62
MN12-SX	25–0	0.38	1.90	1.24	40	33
N12	0	0.44	1.88	1.25	40	18
OLYP	0	0.36	1.97	1.27	36	50,56
SOGGA11	0	0.62	2.40	1.62	40	48

[a]WFT indicates wave function theory; other rows are density functional theory, and *X* is the percentage of Hartree–Fock exchange. When a range of *X* is indicated, the first value corresponds to small interelectronic separations, and the second to large interelectronic separations.

Table 5.15 The mean unsigned errors (MUE in kcal/mol) of transition metal reaction barrier heights[a]

Reactions[a]	MUE(Mo)	MUE(W)	MUE(Zr)	MUE(Re)	AMUE[b]
B2GP- PLYP	0.80	0.99	2.62	0.80	1.20
M06	1.12	1.19	0.75	1.87	1.25
MN15	**2.30**	**2.82**	**1.51**	**0.85**	**1.95**
B2-PLYP	1.43	1.32	3.77	2.03	1.99
TPSSh	2.12	1.77	3.36	1.08	2.01
MN15-L	**1.47**	**2.60**	**1.19**	**2.67**	**2.03**
PBE0	2.68	2.66	2.66	1.07	2.29
M06- 2X	3.56	2.68	0.23	2.75	2.48
M06-L	2.57	2.32	1.22	4.12	2.61
TPSS	3.70	2.60	3.12	1.56	2.77
B3LYP	1.69	2.31	7.58	1.42	2.92
CAM- B3LYP	3.46	2.28	5.78	1.78	3.16
RPBE	2.55	2.37	6.42	2.44	3.21
B1LYP	2.37	2.77	7.09	1.66	3.21
GAM	2.71	2.43	4.37	4.15	3.29
PBE	3.79	3.74	2.63	2.98	3.36
ωB97X	5.40	3.05	3.22	1.53	3.39
BP86	4.35	2.90	4.21	2.62	3.50
BLYP	3.02	3.29	7.09	2.14	3.66
BMK	4.13	3.98	5.16	1.72	3.71
OLYP	3.76	3.12	13.29	2.51	5.09
LC-ωPBE	6.24	4.34	NA	1.72	NA

[a]There are respectively 6, 6, 4, and 5 reactions in the database for Mo, W, Zr and Re reaction barrier heights

[b]The average mean unsigned error for all 21 barrier heights

Table 5.16 Mean unsigned errors (kcal/mol) for the WCCR10 database

Functional[a]	Type	WCCR10
MN15	hybrid meta-NGA	**5.04**
MN15-L	meta-NGA	**5.46**
PBE0	hybrid GGA	6.40
GAM	NGA	6.60
PBE	GGA	7.58
TPSSh	hybrid meta-GGA	7.62
TPSS	GGA	7.84
B97-D-D2	GGA + MM[b]	8.59
B3LYP	hybrid GGA	9.30
BP86	GGA	9.42
BP86-D3	GGA + MM[b]	10.62

[a]The MN15, MN15-L, and GAM results are from the present calculations, but all other results in this table are from reference 90.

[b]MM denotes molecular (also called empirical dispersion correction), which in this case corresponds to atom-atom pairwise damped dispersion terms added post-SCF to the calculated energy.

Table 5.17 Mean unsigned errors for the SBG31 database in eV

Functional[a]	Type	SBG31
HSE06	RS-hybrid GGA	0.26
M11-L	meta-GGA	0.54
MGGA_MS2	meta-GGA	0.66
M06-L	meta-GGA	0.73
MN15-L	**meta-NGA**	**0.80**
MN12-L	meta-NGA	0.84
TPSS	meta-GGA	0.85
SOGGA11	GGA	0.89
HCTH407	GGA	0.89
OLYP	GGA	0.90
MN15	**hybrid meta-NGA**	**0.92**
OreLYP	GGA	0.92
τ-HCTH	meta-GGA	0.92
VSXC	meta-GGA	0.97
PBE	GGA	0.98
N12	NGA	0.99
GAM	NGA	0.99
revTPSS	meta-GGA	1.00
RPBE	GGA	1.07
revPBE	GGA	1.08
BPW91	GGA	1.10
mPWPW	GGA	1.11
PW91	GGA	1.11
BP86	GGA	1.12
PBEsol	GGA	1.14
SOGGA	GGA	1.14
BLYP	GGA	1.14
GKSVWN5	LSDA	1.14

Table 5.18 Homonuclear transition metal dimers: equilibrium bond lengths (Å) and mean unsigned errors as compared to experiment.

	Cu_2	Au_2	Ni_2	Pd_2	Pt_2	Ir_2	Os_2	MUE(1) [b]	MUE(2) [b]
N12	2.224	2.543	2.110	2.501	2.366	2.262	2.282	0.026	0.028
MGGA_MS2	2.210	2.527	2.080	2.493	2.359	2.254	2.275	0.028	0.028
MN15-L	**2.274**	**2.540**	**2.138**	**2.520**	**2.346**	**2.232**	**2.257**	**0.028**	**0.030**
M06-L	2.214	2.555	2.101	2.500	2.380	2.274	2.294	0.033	0.034
LSDA	2.215	2.495	2.118	2.373	2.353	2.271	2.354	0.038	0.043
HSE06	2.258	2.258	2.551	2.078	2.514	2.358	2.250	0.041	0.043
MN15	**2.277**	**2.501**	**2.045**	**2.468**	**2.301**	**2.182**	**2.204**	**0.041**	**0.045**
PBE	2.278	2.552	2.135	2.397	2.391	2.302	2.384	0.062	0.047
mPWPW	2.293	2.549	2.088	2.359	2.369	2.282	2.369	0.068	0.050
GAM	2.306	2.543	2.189	2.536	2.408	2.283	2.292	0.050	0.054
B3PW91	2.288	2.552	2.095	2.367	2.375	2.287	2.373	0.068	0.056
B3LYP	2.292	2.577	2.099	2.411	2.392	2.301	2.387	0.071	0.059
B97-1	2.278	2.566	2.391	2.617	2.368	2.259	2.279	0.082	0.073
ωB97X-D	2.214	2.555	2.101	2.500	2.380	2.274	2.294	0.083	0.085
Exp.[a]	2.219	2.472	2.155	2.480	2.333	2.270	2.280	0.000	0.000

[a]The experimental values are from reference 92.

[b]The bond lengths in the table and MUE(1) are calculated with the LANL2DZ basis set for comparison with previous work, and MUE(2) is averaged over this basis set and also over the higher-quality def2-TZVP basis set.

Table 5.19 Mean unsigned errors for the SE47 database in Å

Functionals	Types	MUE of SE47 [a]
MN15	**hybrid meta-NGA**	**0.0033**
B3LYP	hybrid GGA	0.0037
M06-2X	hybrid meta-GGA	0.0040
ωB97X-D	RS-hybrid GGA + MM[b]	0.0043
M06-L	meta-GGA	0.0044
GAM	NGA	0.0044
HSE06	RS-hybrid GGA	0.0046
τ-HCTHhyb	hybrid meta-GGA	0.0046
M06	hybrid meta-GGA	0.0063
TPSS	meta-GGA	0.0078
MN15-L	meta-NGA	0.0098
PBE	GGA	0.0103
BP86	GGA	0.0112

[a]The SE47 is a new geometry database published by M. Piccardo et al.[93] There are 193 bond length from 47 organic molecules being calculated by 13 functionals above. The original database SE47 includes both bond lengths and bond angles, however, in the present paper we only compare the bond lengths.

[b]MM denotes molecular mechanics (also called empirical dispersion correction), which in this case corresponds to atom-atom pairwise damped dispersion terms added post-SCF to the calculated energy.

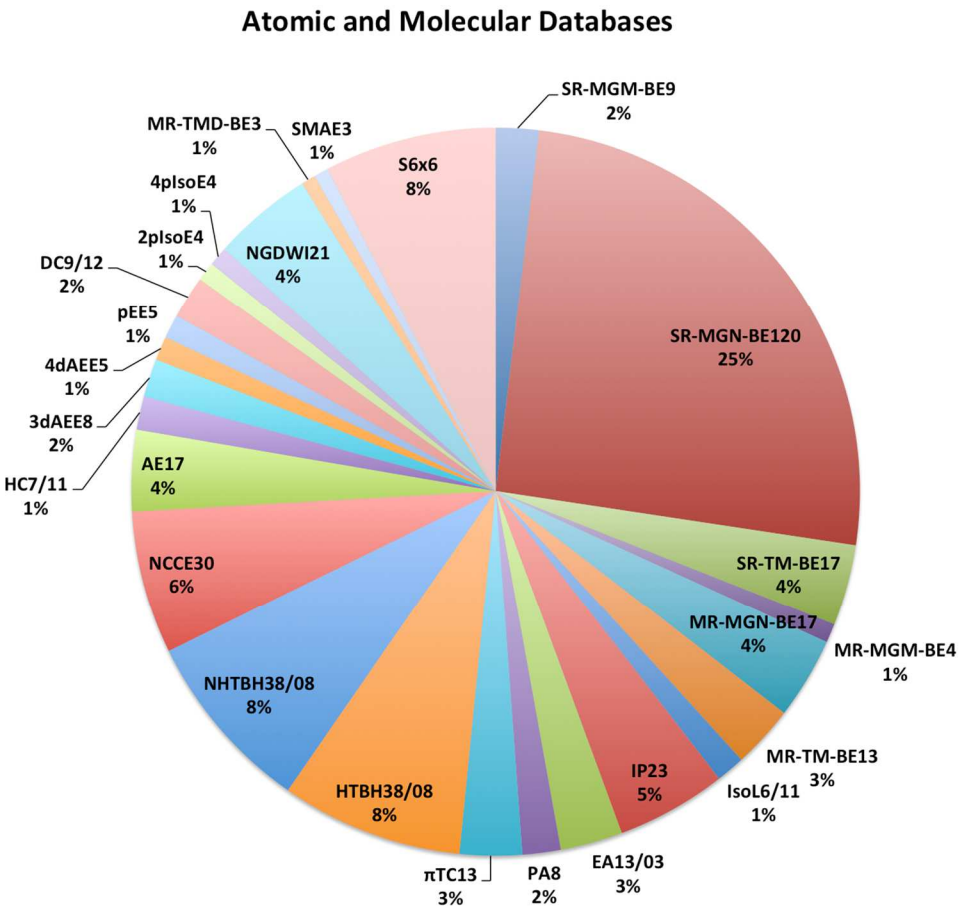

Figure 5.1. The percentage of all atomic and molecular databases (AME471), the number after a name means the number of data in this database, for example, SR-MGM-BE9 mean 9 pieces of bonding energy data in this database. The explanation of the these names are shown in Table 5.1.

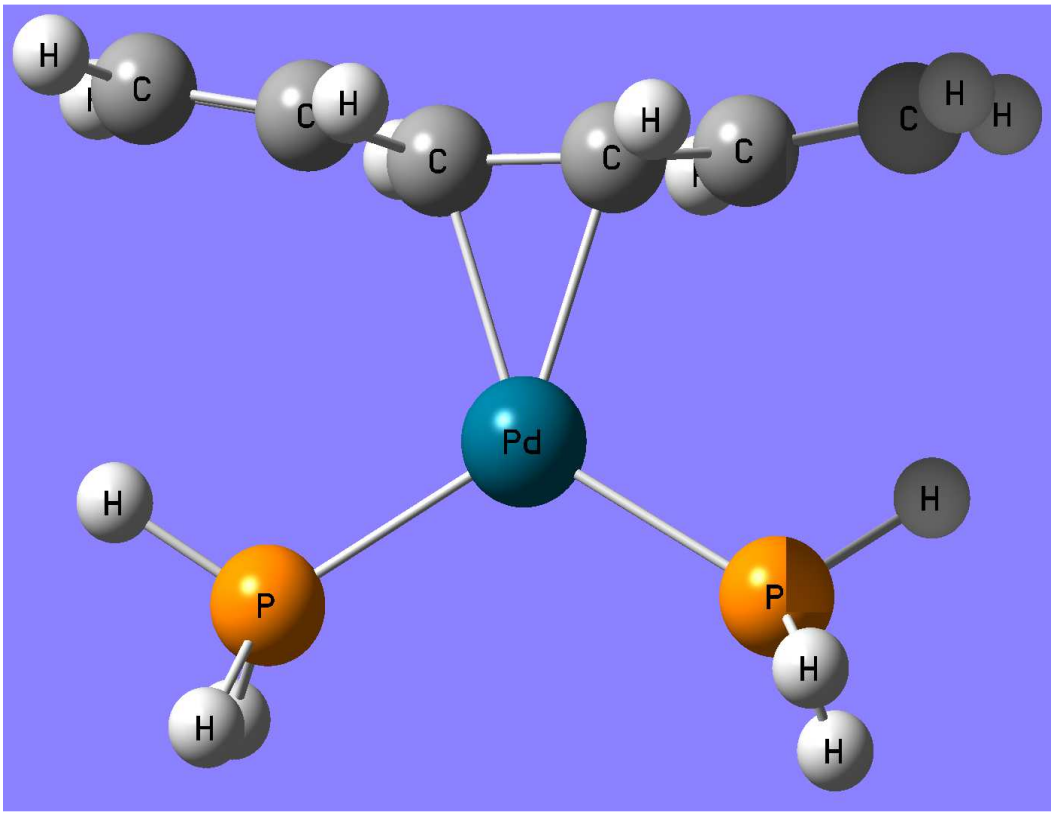

Figure 5.2 The structure of $Pd(PH_3)_2C_6H_8$ in subdatabase PdBE2.

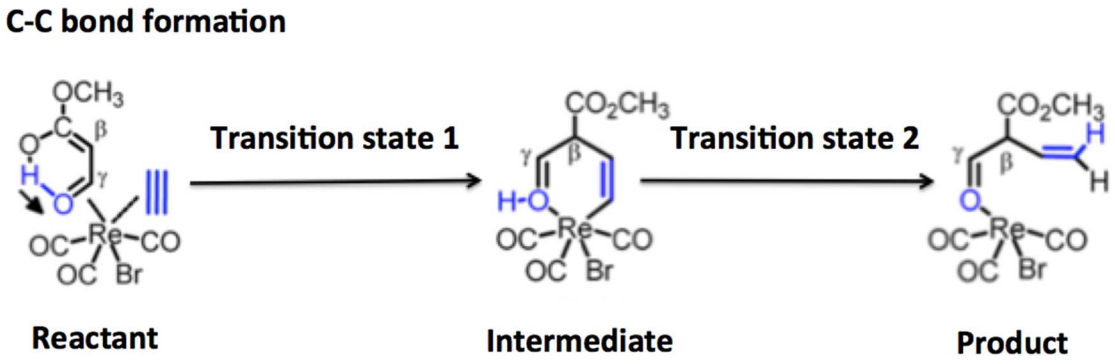

Unsigned errors (kcal/mol)

Name	ωB97-X	PBE0	M06-2X	MN15
Barrier Height 1	1.90	0.17	1.37	0.15
Barrier Height 2	1.37	2.51	1.47	0.10

Figure 5.3 Reaction barrier heights of Rhenium catalyzed reaction

Chapter 6. Applications of Kohn-Sham Density Functionals

Adapted with permission from:

Haoyu S. Yu and Donald G. Truhlar, J. Chem. Theory Comput. 2014, 10, 2291-2305.

Haoyu S. Yu and Donald G. Truhlar, J. Chem. Theory Comput. 2015, 11, 2968-2983.

Haoyu S. Yu and Donald G. Truhlar, Angewandte Chemie, 2016, Accepted.

Joachim Friedrich, Haoyu S. Yu, Hannah R. Leverentz, Peng Bai, J. Ilja Siepmann, and D. G. Truhlar, J. Phys. Chem. Lett. 2014, 5, 660-670.

Junwei Lucas Bao, Haoyu S. Yu, Kaining Duanmu, Maxim A. Makeev, Xuefei Xu, and D. G. Truhlar, ACS Catal. 2015, 5, 2070-2080.

James M. Lownsbury, Iván A. Santos-López, Wei Zhang, Charles T. Campbell, Haoyu S. Yu, Wei-Guang Liu, Christopher J. Cramer, Donald G. Truhlar, Timothy Wang, Joseph T. Hupp, and Omar K. Farha, J. Chem. Phys. in preparation.

Haoyu S. Yu, Lucas J. Fiedler, I. M. Alecu, and Donald G. Truhlar, Computer Physics Communications, 2016, submitted.

6.1 Introduction

We have discussed three density functionals we developed in the last three chapters. In the present chapter, we are going to study the applications of density functionals, especially for GAM, MN15-L, and MN15. We will discuss the following topics below: bond energy of CaO, bond energies of main-group molecules, highest oxidation states of existing metal compounds, water 26-mer simulation, water splitting on Fe(0) surface,

calcium metal adsorption on the metal-organic framework NU-1000, and scaling factors for vibration frequencies obtained from electronic model chemistries.

6.2 What Dominates the Error in the Bond Energy of CaO Predicted by Various Approximation Exchange-Correlation Functionals

In order to understand what governs the accuracy of approximate exchange–correlation functionals for intrinsically multiconfigurational systems containing metal atoms, the properties of the ground electronic state of CaO have been studied in detail. We first applied the T1, TAE(T), B1, and M diagnostics to CaO and confirmed that CaO is an intrinsically multiconfigurational system. Then we compared the bond dissociation energies (BDEs) of CaO as calculated by 49 exchange–correlation functionals, three exchange-only functionals, and the HF method. To analyze the error in the BDEs for the various functionals, we decomposed each calculated BDE into four components, in particular the ionization potential, the electron affinity, the atomic excitation energy of the metal cation to prepare the valence state, and the interaction energy between prepared states. We found that the dominant error occurs in the calculated atomic excitation energy of the cation. Third, we compared dipole moments of CaO as calculated by the 53 methods, and we analyzed the dipole moments in terms of partial atomic charges to understand the contribution of ionic bonding and how it is affected by errors in the calculated ionization potential of the metal atom. We then analyzed the dipole moment in terms of the charge distribution among orbitals, and we found that the orbital charge distribution does not correlate well with the difference between the calculated ionization

potential and electron affinity. Fourth, we examined the potential curves and internuclear distance dependence of the orbital energies of the lowest-energy CaO singlet and triplet states to analyze the near-degeneracy aspect of the correlation energy. The most important conclusion is that the error tends to be dominated by the error in the relative energies of s and d orbitals in Ca^+, and most popular density functionals predict this excitation energy poorly, so even if they were to predict the BDE reasonably well, it would be due to cancellation of errors. The effect of the cation excitation energy can be understood in terms of an orbital picture, as follows. For most functionals the predicted cation excitation energy is too small, so it is too easy to delocalize charge from the oxygen 2p orbital to the Ca^+ d orbital; this overestimates the covalency and explains why most functionals overestimate the bond energy.

6.2.1 Computational details

All calculations of CaO (except the potential energy curves and orbital energies as functions of internuclear distance R) are carried out at the experimental equilibrium value of R, which is R_e = 1.821 Å.[1] We always set the molecule CaO on the z-axis. We use the aug-cc-pCVQZ basis set for O and cc-pCVQZ for Ca for all the calculations in this paper.[2,3]

All calculations are nonrelativistic. For the M06-L density functional, we checked that the calculated bond energy increases from 113.32 kcal/mol to 114.39 kcal/mol (an 0.9% increase) when scalar relativistic effects are included by the second-order Douglas-Kroll-Hess[4,5,6,7] approximation. We also considered the spin-orbit effect of O, which

decreases the bond energy of CaO by -0.22 kcal/mol.[8] If we consider scalar relativistic effects and spin-orbit effect together, the calculated BDE of CaO by M06-L should be changed from 113.32 kcal/mol to 114.17 kcal/mol (an 0.7% increase). This is small enough that it does not affect our conclusions, so all calculations presented in the rest of this paper are nonrelativistic without spin-orbit effects.

There are two kinds of broken-symmetry aspects to our calculations. First we use unrestricted Hartree–Fock theory or spin-polarized KS-DFT (the latter is sometimes called unrestricted KS); these treatments involve different spatial orbitals for α and β electrons so the Kohn-Sham determinant is not an eigenfunction of the multi-electron operator S^2, where S is total electron spin. After the unrestricted Hartree–Fock or spin-polarized KS-DFT calculation has apparently converged, the solution is analyzed for stability with respect to further symmetry breaking by using the stable=opt keyword of *Gaussian 09*[9] to search for variations that lower the energy. The SCF optimization is then carried to convergence to a stable solution. None of the CaO calculations break symmetry at $R = R_e$, that is, the restricted Hartree-Fock solution is stable to breaking either spin symmetry (which would yield a so called unrestricted solution) or spatial symmetry. However, at large R the oxygen atom becomes a spin-polarized triplet, and we also find spin polarization in the potential-energy-curve and orbital-energy calculations at large R., that is the restricted solution is unstable with restrict to allowing it to be unrestricted.

We applied four multi-reference diagnostics to CaO at its equilibrium geometry. The T_1, TAE(T), and B_1 diagnostics[10,11,12,13,14] were calculated by using *Gaussian 09*; the

M diagnostic[13] was calculated by using *Molpro*.[15] CASSCF calculations[16] with an active space of 8 electrons in 10 orbitals are employed to calculate the M diagnostic. All the diagnostics are explained below.

A benchmark value for the dipole moment of CaO was calculated by the CCSDT method[17] with *NWChem*.[18]

6.2.2 Diagnostics of CaO

First, we apply the T_1 diagnostic to our system. Lee and Taylor proposed that the norm of the vector of single-excitation amplitudes (t_1 amplitudes) in a closed-shell coupled-cluster singles and doubles (CCSD) wave function could be used as a diagnostic for the prediction of the reliability of results obtained from a single-reference-based electron correlation procedure.[10] The T_1 diagnostic is

$$T_1 = \frac{\|t_1\|}{N_{\text{elec}}^{1/2}} \tag{6.1}$$

where N_{elec} is the number of the electrons of a system, and t_1 is the vector of single-excitation amplitudes in a CCSD calculation. If T_1 is smaller than 0.02, the system under consideration is considered to be a single-reference system; if T_1 is larger than 0.02, the system is a multi-reference system. Although it is well known that this diagnostic is sometimes small for multi-reference systems (and so it is not a reliable diagnostic in general), when it large it is a reasonably reliable indicator of multi-reference character.

We calculated $T_1 = 0.037$ for CaO. Therefore, CaO is a multi-reference system according to the T_1 diagnostic.

Second, we apply the *%TAE[T]* diagnostic to CaO; it is defined as[11]

$$\%TAE[T] = 100\left(\frac{AE[CCSD(T)] - AE[CCSD]}{AE[CCSD(T)]}\right) \tag{6.2}$$

where AE[CCSD] is the atomization energy of the system calculated with the coupled cluster method including single and double excitations, and AE[CCSD(T)] is the atomization energy of the system calculated with CCSD plus a quasiperturbative treatment of connected triple excitations. If *%TAE[T]* is smaller than 2%, the system under consideration is considered to be a single-reference system; if it is larger than 2% and smaller than 10%, the system is a moderate multi-reference system; and if it is larger than 10%, then the system is a multi-reference system.[11] We calculated that *%TAE(T)* = 11.7%. Therefore CaO is a multi-reference system according to the *%TAE(T)* diagnostic.

Third, we apply the B_1 diagnostic[12,13,14] to the CaO bond. This diagnostic is defined for a single bond as

$$B_1 = [D_e(\text{BLYP}) - D_e(\text{B1LYP//BLYP})] \tag{6.3}$$

where D_e is the energy required to break the bond, BLYP is the combination of the Becke (B) 1988 local exchange functional (B88X)[19] and the Lee-Yang-Parr (LYP) correlation functional,[20] B1LYP stands for an exchange–correlation functional in which the Hartree–Fock exchange and B88X exchange are mixed in the ratio ¼ and in which the correlation functional is LYP,[21] and B1LYP//BLYP denotes a B1LYP calculation

using the BLYP equilibrium geometries for the molecule and the fragments. The B_1 diagnostic is based on the realization that the Hartree-Fock exchange approximation fails badly for multi-reference systems because it introduces static correlation error. The criterion that has been adopted[12] is that if B_1 is larger than 10 kcal/mol, then the system is classified as a multi-reference system; otherwise, it is classified as a single-reference system. (Sometimes the B_1 diagnostic is better interpreted as a diagnostic of a "difficult case," but here we use it as a multi-reference diagnostic.) We calculated that B_1 equals 21.7 kcal/mol for CaO; therefore CaO is a multi-reference system according to the B_1 diagnostic.

Finally, we apply the M diagnostic to CaO. For a system like CaO at the equilibrium geometry with no singly occupied molecular orbitals in the dominant configuration, the M diagnostic is defined as[13]

$$M = \frac{1}{2}\Big(2 - n(MCDONO) + n(MCUNO)\Big) \tag{6.4}$$

where $n(j)$ is a natural orbital occupation number (which we here evaluate, as usual, as an eigenvalue of the first-order density matrix of a CASSCF wave function), and n(MCDONO) and n(MCUNO) are respectively the natural orbital occupation numbers of the most correlated doubly occupied natural orbital (MCDONO) and the most correlating unoccupied natural orbital (MCUNO). If M is larger than 0.04, then the system is considered to be a multi-reference system; otherwise, it is considered to be a single-reference system.[13]

To calculate the M diagnostic of CaO, we carried out a complete active space self-consistent field calculations at the equilibrium geometry with an active space of eight electrons in ten orbitals (2s and 2p orbitals from oxygen, 4s and 3d orbitals from calcium). The natural orbital occupation numbers are 1.9828, 1.9585, 1.9551, 1.9551, 0.0434, 0.0434, 0.0414, 0.0148, 0.0028, and 0.0028, listed in order of decreasing occupation number. The symmetry of the ground state is $^1\Sigma_g^+$. There are 16 electrons in σ orbitals and 12 electrons in π orbitals. This calculation yields the following order of the orbitals in the active space, listed in order of increasing energy, identified by the dominant atomic orbital or orbitals and with the molecular orbital ordering in each symmetry in parentheses: O2s(7σ), O2pσ(8σ), $O2p_xCa3d\pi(3\pi_x)$, $Op_yCa3d\pi(3\pi_y)$, Ca4s(9σ), $O2p\pi(4\pi_y)$, $O2p\pi(4\pi_x)$, Ca3dσ(10σ), $Ca3d\delta(1\delta_{x^2-y^2})$, $Ca3d\delta(1\delta_{xy})$ orbitals. (When two atomic orbitals are listed, the one listed first makes the greater contribution.) The HOMO orbital of a Hartree–Fock calculation would be O2pCa3dπ(3π), and the LUMO orbital would be Ca4s(9σ). In the present case, the MCDONO turns out to be the HOMO with 1.955 electrons, and the MCUNO turns out to be the LUMO with 0.043 electrons; consequently *M* is 0.044, and CaO is a multi-reference system according to the M diagnostic.

In summary, CaO is a multi-reference system according to all four diagnostics.

6.2.3 Results and discussions

CaO is a multi-reference system according to the T_1, TAE(T), B_1, and M diagnostics. We found that the predicted BDE is anticorrelated with the predicted dipole moment, with a larger dipole moment leading to a smaller BDE. At the equilibrium distance CaO is made up of Ca^{+}(d) and O^{-}. The partial charges we calculated from the experimental dipole moment are $Ca^{+0.998}$ and $O^{-0.998}$. By comparing dipole moments and orbital makeups predicted by different density functionals, we found that the valence-orbital charge distributions between the two centers can be used to explain the trends in the predicted dipole moment. Even if we have a good dipole moment (i.e., a good first moment of the density), we cannot guarantee good results for all the contributions to the bond energy of CaO. The error of the BDE of CaO was partitioned into errors from four sources: the ionization potential (IP), the electron affinity (EA), the atomic excitation energy (EE) of the metal cation to prepare the valence state, and the interaction energy between prepared states (IE). The more components a functional can predict accurately, the less likely that accurate results come from fortuitous cancellation of error. Typically the excitation energy and the interaction energy contribute more to the errors than other components, with the error in the excitation energy of Ca^{+} being the largest factor.

The excitation energy error is dominated to a large extent by near-degeneracy angular correlation of the s and d orbitals of Ca^{+}; a lower excitation energy leads to less delocalization of the σ bonding orbital (and hence a smaller dipole moment) and a higher bond energy. This is confirmed by Table 6.1, which shows that the usual trend is that

lower excitation energy (EE) leads to higher bond dissociation energy (BDE), anticorrelated with higher partial atomic charge on Ca. To get an accurate bond energy for the right reason, one must balance the localization and delocalization tendencies.

Combining what we learned from the orbital analyses with the data in Table 6.2, we infer that the important factors controlling the calculated bond energy and calculated dipole moment are the extent of delocalization, the amount of charge transfer, and the covalent bonding in the 8σ orbital, $3\pi_x$, and $3\pi_y$ orbitals. If functional A predicts that the 8σ, $3\pi_x$, and $3\pi_y$ orbitals are more delocalized than the ones predicted by functional B, then the dipole moment predicted by functional A is smaller than the dipole moment predicted by functional B. But the increased delocalization increases the calculated bond energy. From the NBO analysis, we found that MPWB1K predicts the 8σ orbital, the $3\pi_x$ orbital, and the $3\pi_y$ orbital to be more delocalized than the ones predicted by M05. Therefore, MPWB1K predicts a larger dipole moment than M05, but a smaller bond energy.

The present analysis suggests that a good approach toward making exchange–correlation functionals more accurate is try to design functionals that predict well all five of the properties studied here and especially to place more emphasis than previous work on atomic excitation energies. We found here that one way to get a more accurate atomic excitation energy is to increase the amount of HF exchange for each functional, but it is well known that there is a tradeoff in this kind of parameterization because high Hartree–Fock exchange often brings in static correlation error for many systems; therefore a

broader strategy is warranted. It will be interesting to carry out this kind of analysis for more molecules to further guide future density functional design.

6.3 Components of the Bond Energy in Polar Diatomic Molecules, Radicals, and Ions by Group-1 and Group-2 Metal Atoms

Although many transition metal complexes are known to have high multi-reference character, the multireference character of main-group closed-shell singlet diatomic molecules like BeF, CaO, and MgO is less studied. However, many group-1 and group-2 diatomic molecules do have multi-reference character, and they provide informative systems for studying multi-reference character because they are simpler than transition metal compounds. The goal of the present work is to understand these multi-reference systems better so that ultimately we can apply what we learn to more complicated multi-reference systems and to the design of new exchange-correlation functionals for treating multi-reference systems more adequately. Fourteen main group diatomic molecules and one triatomic molecule (including radicals, cations, and anions, as well as neutral closed-shell species) have been studied for this article. Eight of these molecules contain a group-1 element, and six contain a group-2 element. Seven of these molecules are multi-reference systems, and eight of them are single-reference systems. Fifty-one exchange-correlation functionals of 11 types [local spin-density approximation (LSDA), generalized gradient approximation (GGA), nonseparable gradient approximation (NGA), global-hybrid GGA, meta-GGA, meta-NGA, global-hybrid meta GGA, range-separated hybrid GGA, range-separated hybrid meta-GGA, range-separated hybrid meta-

NGA, and DFT augmented with molecular mechanics damped dispersion (DFT-D)] and the Hartree Fock method have been applied to calculate the bond distance, dissociation energy (BDE), and dipole moment of these molecules. All the calculations are converged to a stable solution by breaking the symmetry of the system. A reliable functional should not only predict an accurate BDE, but also predict accurate components of the BDE, so each bond dissociation energy has been decomposed into ionization potential (IP) of the electropositive element, electron affinity of the electronegative bonding partner (EA), atomic excitation energy (EE) to prepare the valence states of the interacting partners, and interaction energy (IE) of the valence-prepared states. Adding Hartree-Fock exchange helps getting better results for atomic excitation energy, and this to improvements in getting the right answer for the right reason. The following functionals are singled out for reasonably good performance on all three of bond distance, BDE, and dipole moment: B97-1, B97-3, MPW1B95, M05, M06, M06-2X, M08-SO, N12-SX, O3LYP, TPSS, τ-HCTHhyb, and GAM; all but two (TPSS and GAM) of these functionals are hybrid functionals.

6.3.1 Decomposition of bond energies

Multi-reference systems are systems for which accurate wave function calculations require a multi-configurational reference state because the system is inherently multi-configurational. These systems are also called strongly correlated. With the exact exchange-correlation functional, Kohn-Sham density functional theory (KS DFT) is exact for both single-reference and multi-reference systems, even though the density is

represented by a single Slater determinant. However, the exact functional is unknown and probably unknowable, and with currently available functionals, KS DFT is more accurate for single-reference systems than for multi-reference ones.

Transition metals and their complexes are well known to often have multi-reference character because many interesting systems (for example, bare atoms and molecules with less than eighteen valence electrons) have unfilled valence-shell orbitals, and the near degeneracies of the s and d electrons can lead to multiple low-energy electron configurations. However, main group diatomic molecules can also have multi-reference character, and their electronic structure, is in principle easier to understand. So they provide a testing ground for theory, which lies between main-group nonmetallic chemistry and transition metal chemistry. Understanding main-group diatomic molecules is therefore a useful complement to direct study of transition metal systems, as well as being of interest in its own right. Main-group molecules are usually easier to study than transition metals not only because their atoms do not have incomplete d subshells but also because they have fewer electrons than typical transition metal compounds.

Diatomic molecules contain only one chemical bond, and we can draw more unambiguous conclusions about their treatment than we can for polyatomic molecules. For this reason, and because Ca is the main-group metal most similar to a 3d transition metal, in a very recent article, we studied the CaO molecule in detail.[22] In our study of CaO, not only did we study the bond dissociation energy but also we partitioned the bond

dissociation energy into physical components. We did this be envisioning the bond forming process to occur in several steps, as follows:

1. Ca is ionized by losing an electron; the energetic cost is the ionization potential (IP) of Ca.
2. O attaches the electron; this process releases energy equal the electron affinity (EA).
3. $Ca^+(s)$ is excited to $Ca^+(d)$, which is its valence state, i.e., a description of the orbital occupancy that it has after the bond is formed; the cost for this is the corresponding excitation energy (EE) of Ca^+. Now the partners are both in their valence states – ready to interact.
4. The interaction of $Ca^+(d)$ and O^- releases energy; this is called the interaction energy between two prepared states (IE).

A theory that predicts the correct bond dissociation energy (BDE) for the right reason, rather than by cancellation of errors, should not only predict an accurate value for the BDE, but also it should predict correct values for these four components. We will use the same strategy to ascertain the reliability of exchange-correlation functionals for 15 molecules in the present article, and this broader test set should allow us to draw more robust conclusions.

In order to fully understand why exchange-correlation functionals often fail for multi-reference systems, we will study the BDE and dipole moments of 14 diatomic molecules and one triatomic molecule in this paper. Fourteen of the molecules contain a

main-group metal, and we also include the HF molecule for comparison. In particular, in the present article we study BeF radical, BeO, BeO^+ radical cation, HF, KF, KO^-, KOH, LiF, LiO radical, LiO^- , MgO, MgS, NaO radical, and NaO^- and we will include the previously studied CaO in our 15-molecule test set. Some of these 15 molecules have been studied by Martin using the W4 method.[23,24] The heats of formation and structures of BeO, MgO, KOH, and CaO have been studied with CCSD(T),[25] B3LYP,[26] and MP2 methods.[27,28] Martin concluded that core-correlation should be included, which requires additional basis functions as compared to the usual basis sets that are extended only for valence electrons, and that the molecules BeO, MgO, and CaO have multi-reference character that provides a challenge for the high level ab initio methods.[29] Some other studies of various chemical properties of BeO have also been reported; for example the valence band gap of BeO has been studied by Soulé de Bas et al.,[30] the valence states of BeO have been study by Sorensen et al.,[31] and the low-lying states of BeO have been studied by Irisawa et al.[32] The partial atomic charges and dipole moment of LiF, KF, BeO, and MgO have been studied by Nakazato et al.[33] In the present paper, we will study the BDE, IP, EA, EE, IE, and dipole moments for fourteen main-group diatomic molecules and one triatomic molecule (KOH).

6.3.2 Results and Discussions

We calculated the bond dissociation energies of 15 main group molecules, fourteen of which contain group-1 and group-2 metal atom, by employing 54 methods, in particular the Hartree–Fock method and 53 exchange-correlation functionals for Kohn-Sham

density functional theory. The T1, TAE, B1, and M diagnostics are used to classify these molecules into eight single-reference systems and seven multi-reference systems. Furthermore, we decomposed the bond dissociation energy into four components to better understand the sources of the errors in the bond dissociation energies. We calculated ionization potential, electron affinity, atomic excitation energy, interaction energy between two prepared valence states, and dipole moment by using 54 methods in particular Hartree-Fock method and 53 exchange-correlation functionals for Kohn-Sham density functional theory.

In order to predict the correct bond dissociation energy of 15 main group molecules, the method should predict the smallest average unsigned error of all the components that contribute to the energy change upon forming a bond. Whereas M08-HX, ωB97X-D, TPSS, PW6B95-D3(BJ), OreLYP, PW6B95-D3(0), and PW6B95 give the smallest mean unsigned errors for bond dissociation energy, PW6B95-D3(BJ), revTPSS, TPSS, PW6B95-D3(0), PW6B95, M08-HX, PW6B95-D3(0), M05-2X, and B97-1 give the smallest values for average unsigned error of all energetic data over 15 diatomic molecules.

The PW6B95 functional predicts these main-group molecules very well. The new GAM functional is the best gradient approximation for these main group molecules, and it is also the best functional for seven multi-reference systems. The best meta-GGA for these15 main group diatomic is revTPSS and it is also the best meta-GGA for eight single-reference systems. The best three functionals in predicting dipole moment are

MPWLYP1M, PBE and O3LYP. Multi-reference molecules are harder to predict than single-reference molecules because they have a larger mean unsigned error over all functionals. The hardest molecule for energetic predictions is LiO^{-}, which gives an overall MUE of 9.5 kcal/mol. This study shows the multi-reference character of main group diatomic molecules and importance of getting the correct components for each molecule so as to get the correct bond dissociation energy. These molecules including their components can be used for exchange-correlation functional development. A good functional should predict all five components correctly, otherwise the small errors may come from cancellation of error. The only functional tested in our paper that is able to predict all five components correctly is M06-2X. The MUE of bond distances tested in our paper have a very small correlation with the MUE of dipole moment and AUE of overall energies. The best functionals for bond distance are B3LYP*, revB3LYP and revTPSSh with an error of 0.011 Å for both of them. Over a half of the functionals tested in the paper give an error no larger than 0.015 Å for the bond distances.

A number of the findings of this study were unexpected. For example, the errors for bond energies involving main group metals are usually larger than typical errors for bonds between main-group nonmetals. For other examples, some functionals with high percentages of Hartree-Fock exchange do well for multireference systems, and the ability to predict electron affinities of ligands correlates well with the ability to predict accurate metal-ligand bond energies. If we compare Table 6.3 and Table 6.4 together, we find that there are some functionals that give small errors for both energy and geometry. For

example, B97-1, B97-3, MPW1B95, M05, M05-2X, M06, M06-2X, M08-HX, M08-SO, N12-SX, O3LYP, TPSS, GAM, and τ-HCTHhyb give an MUE for bond distance no larger than 0.015 Å and an overall AUE for energetic quantitates no larger than 5.20 kcal/mol. Of these functionals, Table 6.5 shows that the following functionals also give a mean unsigned error in dipole moments of 0.85 D or less: B97-1, B97-3, MPW1B95, M05, M06, M06-2X, M08-SO, N12-SX, O3LYP, TPSS, GAM, and τ-HCTHhyb. As we and others attempt to develop improved density functionals for systems containing metal atoms, the data presented here – which gives a snapshot of the current status – provides a standard against which one can measure whether success is being achieved; and this data provides a challenge in that we should try to reduce the errors.

6.4 Oxidation State 10 Exists

In a recent paper, Wang et al. found an iridium-containing compound with a formal oxidation state of 9 (Nature, 2014, 514, 475). This is the highest oxidation state ever found in a stable compound. In order to learn if this is the highest chemical oxidation state possible, we used Kohn-Sham density functional theory to study various compounds, including PdO_4^{2+}, PtO_4^{2+}, $PtO_3F_2^{2+}$, PtO_4OH^+, PtO_5, and PtO_4SH^+, in which the metal has an oxidation state of 10. We found that PtO_4^{2+} has a metastable state that is kinetically stable with a barrier height for decomposition of 31 kcal/mol and a calculated lifetime of 0.9 years. All other compounds studied will readily decompose to lower oxidation states.

6.4.1 Computational Details

The method employed is electronic structure calculations by Kohn-Sham density functional theory with the M06-L exchange-correlation functional,[34] the aug-cc-pVTZ basis set[35] for H, O, and F, the aug-cc-pV(T+d)Z basis set[36] for S, and the aug-cc-pVTZ-PP basis set[37,38] for Pd, Ir, and Pt. The M06-L functional has been well validated for transition metal energetics.[39] Calculated Born-Oppenheimer energies of reaction (ΔE) were converted to enthalpies of reaction (ΔH) and free energies of reaction (ΔG) by the rigid-rotator, quasiharmonic-oscillator-approximation with a vibrational scale factor[40] of 0.980. We used the same functional, basis sets, and vibrational approximation to calculate the enthalpy of activation, and we used conventional transition state theory[41] to calculate the unimolecular rate constant rate constant k for one reaction; the unimolecular lifetime is $1/k$. All calculations are for thermally equilibrated gas-phase species at 298.15 K and 1 bar. The *Gaussian 09*[42] software is used for all the electronic structure calculations.

6.4.2 Results and Discussions

"One of the major goals of inorganic chemistry is to prepare compounds of elements in unusual oxidation states."[43] As of 2009, the range of known oxidation states was -4 to +8.[44,45] In 2010, Himmel et al. showed the existence of IrO_4^+ by electronic structure calculations;[46] they studied the stability of cationic species $[MO_4]^+$ (M = Rh, Ir, Mt) and showed that IrO_4^+ is the only one that is stable to decomposition to MO_2^+ and O_2 or to MO_2 and O_2^+. The existence of IrO_4^+ shows that oxidation state 9 exists. This was confirmed in 2014 by Wang et al. by matrix-isolation experiments.[47] Pyykkö and Xu[48]

reviewed the status and noted "for many new exotic species, prediction precedes production." The question we pose here is: does oxidation state 10 exist? Here we predict that it does, in the species PtO_4^{2+}.

In order to answer the question posed in the first paragraph, we studied compounds containing Pd, Pt, and Ds, which are located in the tenth column of the periodic table. We found that Pt is the one most likely to have an oxidation state of 10. In 2014, Srivastava and Misra studied compounds with the formula of PdO_n (n = 1–5).[49] One of their conclusions is that Pd can bind stably to four oxygen atoms, indicating an oxidation state of Pd as high as 8. In the present paper, we studied the stability of six transition metal compounds (PdO_4^{2+}, PtO_4^{2+}, $PtO_3F_2^{2+}$, PtO_4OH^+, PtO_5, and PtO_4SH^+) of Pt that have a formal oxidation state of 10.

Reaction energies, enthalpies, and free energies were calculated (see methods) for the following reactions:

$PdO_4^{2+} \rightarrow PdO_2^{2+} + O_2$ (1) … ΔH = -68.4 kcal/mol

$PtO_4^{2+} \rightarrow PtO_2^{2+} + O_2$ (2) … ΔH = 28.7 kcal/mol

$PtO_4^{2+} \rightarrow PtO_2^{+} + O_2^{+}$ (3) … ΔH = -124.6 kcal/mol

$PtO_4^{2+} \rightarrow PtO_3^{+} + O^{+}$ (4) … ΔH = 55.6 kcal/mol

$PtO_4^{2+} \rightarrow PtO_3^{2+} + O$ (5) … ΔH = 83.2 kcal/mol

$PtO_4^{2+} \rightarrow PtO_3 + O^{2+}$ (6) … ΔH = 627.5 kcal/mol

$PtO_3F_2^{2+} \rightarrow PtOF_2^{+} + O_2^{+}$ (7) … ΔH = -217.4 kcal/mol

$PtO_4OH^{+} \rightarrow PtO_2OH^{+} + O_2$ (8) … ΔH = -94.8 kcal/mol

$PtO_4OH^+ \rightarrow PtO_2OH + O_2^+$ (9) … ΔH = -41.6 kcal/mol

$(PtO_4OH)^+ \rightarrow PtO_5 + H^+$ (10) … ΔH = 184.4 kcal/mol

$PtO_5 \rightarrow PtO_4 + O$ (11) … ΔH = -9.2 kcal/mol

$PtO_5 \rightarrow PtO_3 + O_2$ (12) … ΔH = -93.7 kcal/mol

$PtO_4SH^+ \rightarrow PtO_2SH^+ + O_2$ (13) … ΔH = -99.6 kcal/mol

The reaction enthalpies, energies and Gibbs free energies are shown in Table 6.6; these results show that none of the six compounds is thermodynamically stable because they all have at least one decomposition reaction that gives negative ΔE, ΔH, and ΔG. In particular PtO_4^{2+} can decompose to PtO_2^+ and O_2^+, $PtO_3F_2^{2+}$ can decompose to $PtOF_2^+$ and O_2^+, PtO_4OH^+ can decompose to PtO_2OH^+ and O_2, PtO_5 can decompose to PtO_3 and O_2, and PtO_4SH^+ can decompose to PtO_2SH^+ and O_2.

However, for PtO_4^{2+} all the possible reactions give positive reaction energies, enthalpies, and free energies except for reaction (3): $PtO_4^{2+} \rightarrow PtO_2^+ + O_2^+$. The energy profile and optimized structure of stationary points for reaction (3) are shown in Figure 6.1, which starts with the T_d structure. IrO_4^+ also has a Td structure, and in the T_d structures, the IrO_4^+ bond length is 1.689 Å, and the PtO_4^{2+} bond length is 1.712 Å. These may be compared to standard values (all in Å):[50,51] Ir–O, 1.85, Pt–O, 1.86, Ir=O, 1.72, Pt=O, 1.69; on this basis, all the metal oxo bonds in the T_d structures are double bonds. The T_d structure of PtO_4^{2+} decomposes through transition state TS1 to the C_{2v} structure; the C_{2v} structure goes to the C_s structure through transition state TS2 and then through TS3 to the products PtO_2^+ and O_2^+. The PtO_4^{2+} species is kinetically stable because it

needs to go through a 30.7 kcal/mol energy barrier in the first step. We calculated an enthalpy of activation for this step of 29.2 kcal/mol and a free energy of activation of 27.6 kcal/mol. The transition state theory rate constant is 3.7×10^{-8} s^{-1}. This gives a unimolecular lifetime of 2.7×10^{7} seconds, which is 0.86 years. We conclude that PtO_4^{2+} is kinetically stable to decomposition.

IrO_4^{+} and PtO_4^{2+} are isoelectronic, and their orbitals are very similar as illustrated in Figure 6.2 for the HOMO and in supporting information for more orbitals. However, the orbital energies are quite different as would be expected from the differing net charges; for example the HOMO orbital energy of IrO_4^{+} is –16.3 eV, whereas that of PtO_4^{2+} is –23.6 eV.

In order to understand the charge distribution in the high-oxidation-state compounds, we calculated partial atomic charges on the metal by both CM5[52] and Hirshfeld[53,54] charge analyses. The results for the T_d structure are in Table 6.7. For both IrO_4^{+} and PtO_4^{2+}, the T_d structure gives the highest positive charge on the metal. The CM5 charge of the metal is higher than the Hirshfeld charge for all three structures (T_d, C_{2v}, and C_s). The charge difference between PtO_4^{2+} and IrO_4^{+} is significant in that Pt has a charge about 0.2 higher than Ir. In Table 6.8 we also compared the dipole moments of the polar structures as calculated by CM5 charges, Hirshfeld charges, and the DFT density. As we can see, the Hirshfeld dipole moment is closer than the CM% dipole moment to the DFT dipole moment.; thus the Hirshfeld charges give the best estimates of the partial atomic charges in these molecules.

In summary, we predict that oxidation state 10 exists in the T_d structure of PtO_4^{2+}. The energy profile shows that in order to decompose, PtO_4^{2+} needs to pass a high barrier – so high that the lifetime is calculated to be 0.86 years. Comparing to the previously found highest oxidation state (oxidation number 9 in IrO_4^{+}), PtO_4^{2+} shows a similar charge distribution and electron densities, but the partial atomic charge on the metal is about 0.2 higher.

6.5 Water 26-mers Drawn from Bulk Simulations: Benchmark Binding Energies for Unprecedentedly Large Water Clusters and Assessment of the Electrostatically Embedded Three-Body and Pairwise Additive Approximations

It is important to test methods for simulating water, but small water clusters for which benchmarks are available are not very representative of the bulk. Here we present benchmarks calculations, in particular CCSD(T) calculations at the complete basis set limit, for water 26-mers drawn from Monte Carlo simulations of bulk water. These clusters are large enough that each water molecule participates in 2.5 hydrogen bonds on average. The electrostatically embedded three-body approximation with CCSD(T) embedded dimers and trimers reproduces the relative binding energies of eight clusters with a mean unsigned error (MUE, kcal per mole of water molecules) of only 0.013 and 0.022 for relative and absolute binding energies, respectively. Using only embedded dimers (electrostatically embedded pairwise approximation) and computing the energies with the M11 exchange-correlation functional, which is very economical, yields errors of only 0.030 and 0.021.

6.5.1 Computational Methods

Quantum mechanical electronic structure calculations are now being applied to calculate energies and forces for larger and more complex problems. However, the cost of accurate calculations on large systems increases as a high power of system size, for example, as the seventh power for calculations on large systems by the widely used and generally highly accurate CCSD(T) method (this acronym denotes coupled cluster theory with single and double excitations and a quasiperturbative treatment of connected triple excitations[55]). One way to circumvent the cost is to use fragment methods, where one breaks up the system into monomers, out of which one forms fragments (e.g., dimers, trimers, ...), and the energy and forces of the entire system are approximated by a series of calculations on the fragments.

Fragment methods hold great promise for extending accurate quantum mechanical calculations to larger systems because for large enough systems the cost scales as a low power of the number of monomers rather than with the intrinsic scaling power of the quantum mechanical method. By omitting interactions between distant monomers, one can make the number of fragments to be considered and hence the amount of computational work to be done on large systems scale only linearly ($N \ln N$) with system size. For systems of moderate size, where the saving from neglecting long-range interactions is not fully realized, the scaling power is higher, for example quadratic scaling for pairwise additive methods or cubic scaling for methods including all trimers.

Fragment methods are so appealing that a large number of different fragment methods have been proposed.[56,57,58,59,60,61,62,63,64,65,66,67,68,69] It is important to test them to learn which methods give the highest accuracy for a given cost and to validate the more accurate methods so that one has an idea about how reliable applications employing them may be. But here we run into a difficulty. The natural domain of application of fragment methods is very large systems, but accurate results are usually not available for validation on large systems; however, validation on small systems might be unrepresentative of performance in applications to large and complex systems. Consider, for example, fragment methods designed for studying processes in aqueous solution. Fragment methods were tested against CCSD(T) calculations on hexamers,[67] which have interesting hydrogen bond structures, but every water molecule in a hexamer is on the surface and is unrepresentative of the bulk.

Coupled cluster calculations were not affordable for larger clusters, but more approximate calculations were used were used for testing by asking whether a fragment method with a given electronic structure method reproduces a calculation on the entire system with the same method. In this way, we made tests using Møller-Plesset second order perturbation theory (MP2) on clusters as large as $(H_2O)_{20}$[68] and especially on optimized $(H_2O)_{16}$ and $(H_2O)_{17}$ clusters,[69] which are just at the border of size where one begins to find tetra-coordinated water molecules. These tests are valuable but have three characteristics upon which one would like to improve: (i) the water clusters are still not large enough to contain several tetra-coordinated water molecules; (ii) optimized clusters

are less representative of the structures found in the bulk than are clusters sampled from a molecular dynamics or Monte Carlo simulation of a thermal ensemble of the bulk liquid, and (iii) it is less reliable to make tests with a method like MP2 than to test against the more accurate standard of CCSD(T) with a complete basis set (CBS). In the present paper we circumvent all three drawbacks. In particular we report calculations on larger clusters, $(H_2O)_{26}$, that are drawn from bulk simulations, and we test against CCSD(T)/CBS calculations. These dramatically improved tests are made possible by recent advances in electronic structure calculations that allow CCSD(T)/CBS calculations for much larger systems than previously possible. In particular, we present CCSD(T)/CBS results obtained by a fully automated implementation[70] of the incremental scheme proposed by Stoll.[71]

There are two ways to test fragment methods. (1) One is to see if the fragment method can reproduce a full calculation at the same level of theory. (2) The other is to compare fragment calculations that are inexpensive enough to be affordable for lengthy simulations to accurate results obtain by any method (experiment or benchmark-quality theory). In the past, we and others have presented both kinds of comparisons, and both are valuable. The present paper emphasizes type-2 comparisons. The reason that type-2 comparisons are especially interesting at the present time is that the CCSD(T)/CBS benchmarks we present are for an unprecedentedly large water cluster, so that this paper pushes the boundary of available type-2 validations.

6.5.2 Results and Discussions

Test systems. We consider clusters selected from a snapshot of an equilibrated simulation (T = 300 K and p = 1 atm) with 1024 rigid water molecules (bond length 0.957 Å, bond angle 104.5 deg), using the TIP4P force field[72] with periodic boundary conditions and Ewald summation. Eight $(H_2O)_{26}$ clusters were carved from this snapshot. Each cluster contains the 26 water molecules whose centers of mass were closest to the center of each of the eight octants of the simulation cell.

Results and discussion. The bonding energy of each cluster was calculated by the incremental CCSD(T)(F12*)|MP2-F12 method[73] with the cc-pVTZ-F12[74] basis set. This method essentially yields the complete basis set limit of CCSD(T), and so we denote it as CCSD(T)/CBS.

We define the binding energy as cluster electronic energy (including nuclear repulsion) relative to the energy of separated monomers. With this definition, the clusters studied here have binding energies of −111.3 to −151.8 kcal/mol (i.e., per mole of $(H_2O)_{26}$). The average binding energy is −130.6 kcal/mol with a standard deviation of 13.9 kcal/mol. To facilitate comparison with bulk water and other clusters, all energies in the rest of this letter will be stated per mole of water molecules. Making this conversion yields an average binding energy of −5.02 kcal/mol with a standard deviation of 0.54 kcal/mol.

The first thing we notice about the values in the preceding paragraph is that clusters drawn from simulations have much less negative binding energies than optimized

clusters of the kind usually used for testing theory, and they are much more diverse. Consider for example the five optimized $(H_2O)_{16}$ clusters of our previous cluster study.[69] Those clusters have an average binding energy of −10.67 kcal/mol with a standard deviation of 0.014 kcal/mol. Thus even though the present clusters have a much higher fraction of interior monomers, their condition of not being optimized means that they are much more weakly bound.

To further characterize the $(H_2O)_{26}$ clusters, we counted the hydrogen bonds. Using the definition of a hydrogen bond suggested by Wernet et al.[75] we found 33–37 such hydrogen bonds per cluster, corresponding to an average of 1.35 hydrogen bonds per monomer with a standard deviation of 0.065. Since each hydrogen bond involves two monomers, this implies that each monomer participates on average in 2.7 hydrogen bonds, somewhat smaller than the value of 3.3 of bulk liquid water because the clusters contain a significant fraction of exterior molecules. We also counted the number of water monomers in these clusters with various numbers of hydrogen bonds and found, on average, 7%, 15%, 31%, 34% and 13% are involved in five, four, three, two and one hydrogen bond.

In the present article we use the benchmark results to test the standard many-body expansion, which can be truncated at the two-body level (callede pairwise additive or PA approximation) or the three-body level (called the three-body or 3B approximation) and also to test electrostatically embedded (EE) PA and 3B approximations.[3-5] In EE-PA and EE-3B calculations, each monomer and dimer is calculated in a background of point

charges at the nuclei of the other monomers, and in the latter the trimers are also embedded. The background charges for these calculations are taken from CHelpG analysis[76] of rigid monomer calculations carried out with Kohn-Sham density functional theory[77] (KS theory) using the M06-2X exchange-correlation functional[78] and the 6-311+G(2df,2p) basis set[79]; this yields $q_H = 0.361158$ for the charge on H and $-2q_H$ for the charge on O. (For H and O, the 6-311+G(2df,2p) basis set is the same as the MG3S basis set,[80] and henceforth we will use the shorter name.)

In testing the approximate methods we consider both relative binding energies and absolute binding energies. With eight clusters, we have $8\times7/2 = 28$ *pairs* of structures and hence 28 relative binding energies, and we compute the mean unsigned error (MUE) by averaging the absolute deviation from the benchmark results over all of them. For absolute binding energies, we compute both the MUE and the mean signed error (MSE).

Table 6.9 shows the errors for electrostatically embedded many-body calculations where the fragments are calculated by coupled cluster theory, either CCSD(T)-F12b[81] or CCSD-F12b,[82] both with a cc-pVDZ-F12 basis set. The MUEs of the relative binding energies are pleasingly small, ranging from 0.009 kcal/mol for CCSD(T)-F12b:EE-3B calculations to 0.054 kcal/mol for CCSD-F12b:EE-PA calculations. These mean errors are 43 to 7 times smaller than the mean relative binding energy and 23 to 4 times smaller than the standard deviation of the relative binding energies. In the classical rigid-molecule approximation, a free water molecule would have $3RT$ of thermal energy, and 0.009 kcal is only 0.6% of $3RT$ at 298 K. Clearly the electrostatically embedded many-

body theory is a success, and this is the best evidence yet that EE-PA and EE-3B should provide useful results for calculations on bulk water.

Table 6.9 shows that CCSD(T)-F12b:EE-3B errors in absolute binding energies are only slightly larger than those in the relative binding energies. The difference is larger for CCSD(T)-F12b:EE-PA and large for CCSD-F12b-based calculations. However, since the absolute binding energies are an order of magnitude larger than the relative binding energies, the errors are still encouragingly small, especially for CCSD(T)-F12b where they are 333 (EE-3B) or 73 (EE-PA) times smaller than the average binding energy.

Table 6.10 shows relative computer times for applying these methods to an $(H_2O)_{26}$ cluster. (Computer times, even relative ones, depend significantly on the size of the system, the basis set, the software, the machine and its load, and the compiler and operating system; thus one should not draw conclusions based on small difference, but when used with caution, they provide perspective in evaluating the potential usefulness of various methods.) For CCSD(T)-F12b fragments, EE-3B is two orders of magnitude more demanding in computer time than is EE-PA. The table also shows timings for KS theory with three different methods, where a KS method is a combination of basis set (MG3S or maug-cc-pVTZ[83]) and exchange-correlation functional (M06-2X or M11[84]). KS theory reduces the cost ratio of EE-3B to EE-PA from two orders of magnitude to one. Thus it is useful to also consider employing KS theory for the fragments.

The timings show the negligible cost of the EE operation. Although the number of point charges grows with the size of the system, the cost of the EE operations remains

negligible because it simply involves adding inexpensive analytic one-electron integrals into the energy calculations.

Before considering the KS theory results, we summarize the nature of the exchange-correlation functionals considered here. M06-2X and M11 are hybrid meta-GGAs. M06-2X has 54% Hartree-Fock exchange (HFE) as a global constant. M11 has range-separated exchange with 42.8% HFE at small interelectronic separations and 100% HFE at long interelectronic separations. Both functional have good accuracy on broad databases of chemical properties.[85] Hybrid functionals are orders of magnitude more expensive than less accurate local functionals for periodic calculations, but the cost difference is much smaller for the fragments of the present calculations.

For KS theory, we consider both straight many-body calculations and electrostatically embedded ones. The mean errors are in Table 6.11. For KS fragments, we see no advantage in going to EE-3B; one can always obtain better answers with either EE-PA or 3B, sometimes with both. Averaging over the three methods, over EE-PA and EE-3B, and over relative and absolute binding energies, the KS fragment calculations have roughly the same accuracy as the CCSD ones, but at much lower cost for EE-3B, and $(H_2O)_{26}$ is already large enough the cost is also significantly lower for EE-PA. The newer M11 functional is more accurate than M06-2X for this application; the results with M11/MG3S are uniformly excellent for both the 3B and EE-PA approximations for both relative and absolute binding energies. The less costly EE-PA approximation is more accurate than the 3B approximation.

Possible improvements. We also examined some possible improvements on the EE-PA method, in particular, EE-PA for the correlation energy,[67,68] EE-PA for the nonlocal energy,[69] and EE-PA for a higher-level energy,[69] but the errors did not go down enough for the present application to merit the additional complications. We also found that the jun-cc-pVTZ basis[86] did not offer significant improvement over maug-cc-pVTZ.

Conclusions. The CCSD(T)-F12b:EE-3B approximation reproduces the CCSD(T)/CBS results for $(H_2O)_{26}$ with a mean unsigned error of only 0.009 kcal (per mole of water molecules) for relative energies and 0.015 kcal for absolute binding energies. The EE-PA approximation has MUEs of respectively 0.038 and 0.070 kcal for these quantities. Using KS theory with M11/MG3S for the EE-PA dimers lowers the cost for $(H_2O)_{26}$ by a factor of 300 with respect to CCSD(T)-F12b:EE-3B and a factor of 3 with respect to CCSD(T)-F12b:EE-PA (the factors would be larger for bigger clusters), but the errors remain encouragingly small at respectively 0.029 and 0.042 kcal for relative and absolute binding energies.

6.6 Density Functional Theory of the Water Splitting Reaction on Fe(0): Comparison of Local and Nonlocal Correction Functionals

Metal clusters have broad applicability in catalysis due to their unique reactivity and chemical selectivity, and density functional theory has become an important method for understanding catalysis and attempting to design better catalysts. In the present section, we tested the reliability of the Kohn-Sham density functional theory with local correlation functionals and with the nonlocal random phase approximation (RPA)

correlation functional for the water splitting reaction on monatomic Fe(0) and, by implication, for transition-metal-catalyzed reactions more generally. We computed four barrier heights and six energies of reaction in the catalytic mechanism. If the results are judged by deviation from CCSD(T) calculations, it is found that many modern exchange-correlation (xc) functionals (about half of the functionals tested) with local correlation perform better than using RPA nonlocal correlation; for example, the PWB6K, B97-3, ωB97X-D, MPW1K, M06-2X, and M05-2X hybrid xc functionals with local correlation have overall mean unsigned deviations of 1.9 kcal/mol or less from the CCSD(T) results, as compared to a mean unsigned deviation of 3.5 kcal/mol for EXX-RPA@PBE. We also find significant differences between the predictions for catalysis at the Fe (100) surface. This work provides guidance and challenges for future theoretical investigations of transition metal catalysis.

6.6.1 Introduction

Kohn-Sham density functional theory[87,88] (DFT) has been an indispensible tool in modern catalytic, organometallic, and functional materials research due to its excellent performance-to-cost ratio. With the exact exchange-correlation (xc) functional in hand, the method would provide an exact treatment of all the complicated many-body electronic interactions while retaining the computational simplicity of an independent-particle method like the Hartree–Fock approximation. However, the accurate functional form of the exchange-correlation energy remains an enigma. Therefore, approximations of the xc functionals have to be made in order to provide practical predictions via DFT

calculations. Some xc functionals have a set of parameters which are fitted over selected training sets (including experimental and/or high-level wave function data) with functional forms incorporating some pre-defined constraints, others are based on an empirical choice of constraints and functional forms, and variations on these themes are also possible — a variety of approaches to approximating the xc functional are available. Essentially all the xc functionals possess some empirical and ad hoc ingredients, and their accuracy for practical problems can only be ascertained by testing them against reliable experimental data or reliable theoretical data, with the latter only available for a limited number of very small systems.

Metal clusters and single-metal-atom clusters[89,90,91,92,93,94,95,96,97,98,99,100,101] play an increasingly important role in catalytic chemistry due to their high selectivity and chemical reactivity combined with experimental advances in the preparation of well characterized, size-selected metal clusters. For instance, it has been shown that an encapsulated copper cluster can be a catalyst for hydrogenation with renewability and highly chemoselectivity.[100] Electronic structure computations, such as DFT or wave function methods like coupled cluster theory and multi-reference calculations, can contribute significantly to our understanding of the mechanisms of metal-cluster catalysis at the molecular level, and they can eventually lead us to the next generation of catalysts. However, reliable wave function methods remain impractically expensive for all but the simplest systems, and, because of the multi-reference open-shell character of catalysts containing transition metals, it is a very challenging task to develop computationally

efficient xc functionals that can make reliable predictions. The first step towards achieving this goal is to ascertain the accuracy of existing xc functionals for systems small enough to obtain reliable benchmark results by wave function theory, for example, small metal clusters or monatomic metallic systems of the first-row transition metals, such as iron, cobalt, nickel, and copper, and to learn from both the successes and the failures.

Exchange-correlation functionals may be local (by which we mean that they depend only on local variables such as the local spin densities, their gradients, and the spin-resolved local kinetic energy densities) or nonlocal, where the latter, until recently, has usually meant that nonlocal Hartree-Fock exchange is included. One motivation for including nonlocal Hartree-Fock exchange is that the original local xc functionals like PW91[102] significantly and systematically underestimated barrier heights and overestimated bond energies,[103,104] although these problem have been ameliorated and to some extent overcome with modern local functionals.[105,106,107] More recently some workers have begun to include nonlocal correlation.[108,109,110,111,112,113,114,115] (Functionals with nonlocal correlation are often called hybrid, and functionals that also have nonlocal correlation have been called doubly hybrid.) Recently Karlický and coworkers[116] studied the water splitting reaction on zero-valent iron with a few local-correlation xc functionals with both local and nonlocal approximations to exchange and compared the results to non-self-consistent random phase approximation (RPA) calculations that involved two steps, first a calculation with the local PBE[117] exchange-correlation functional to get

orbitals and then a post-SCF calculation employing these orbitals with nonlocal Hartree-Fock exchange and nonlocal random phase approximation[109,110,114,115,118,119,120] (RPA) correlation. The latter calculation has been labeled EXX-RPA,[121] and the combination with the first step has been called EXX-RPA@PBE, and we will follow that naming convention here. Karlický and coworkers judged the density functional theories by comparison of their results to values obtained by coupled cluster wave function theory and concluded that EXX-RPA provides a systematic improvement over methods with local correlation and therefore should serve as an accurate and efficient (compared with coupled cluster calculations) method in metallic catalytic studies and surface chemistry.

The theoretical foundations of the EXX-RPA method and applications to various material systems have recently been reviewed, and the reader is directed to those reviews for background.[122,123] Karlický and coworkers concluded that the RPA "provides a physically correct description of adsorption and systematically improved reaction barriers" as compared to local functionals, whose performance was gauged by the PW91 local xc functional. and even as compared to hybrid functionals that have nonlocal exchange. This conclusion could give the impression that using RPA nonlocal correlation is inherently more accurate or more accurate at the current state of development than using DFT with local correlation functionals. If true, this would be an important conclusion because DFT with nonlocal functionals is more expensive than DFT with local functionals, especially for extended systems. One goal of the present work is to test whether this conclusion is justified. We therefore compare the results of DFT calculations

with RPA correlation against DFT calculations with local correlation and against DFT calculations with both exchange and correlation local.

Previous work[124] has reported calculations for the reaction $Fe + H_2O \rightarrow FeO + H_2$. The first step of this reaction, i.e. $Fe + H_2O \rightarrow HFeOH$, is the same as the reaction we consider in this work. The role of the diffuse functions has been reported for the first step of the reaction we consider in the current work,[124] but the previous coupled cluster calculations[116] for the following steps in the presently studied reaction did not include diffuse functions, whose effect is tested here.

Filip and coworkers have carried out experimental work using Fe Mössbauer spectroscopy and computational work to investigate the mechanism and kinetics of the Fe(0) nanoparticle – water reactions.[125] Theoretical modeling of zero-valent iron nanoparticles is of great importance for their increasingly practical applications, and predicting their nanoscale chemistry via computational tools with a high performance-to-cost ratio is very challenging.[126] Eder *et al*. carried out periodic density functional calculations to study the initial stage of the iron (100) and (110) surface – water oxidation reaction, which involves the dissociation of the water molecule;[127] the dissociation of water on an iron surface has also been investigated using GGA functionals and range-separated hybrid functionals.[128]

The water splitting reaction on Fe(0), which results in the production of molecular hydrogen, has five elementary steps as summarized in Table 6.12; these processes

involve both transition metal reaction chemistry and physisorption, and hence they provide a broad testing ground.

We computed the classical (zero-point-energy exclusive) barrier heights and classical energies of reaction for all these reactions, and all our comparisons of theoretical results are made on a consistent basis of including electronic energies and nuclear repulsion but not vibration.

6.6.2 Computational Details

In the present study, a relatively broad range of density functionals is employed to compute the barrier heights and energies of reaction for the five-step zero-valent atomic iron–water reaction. We classified the density functionals tested in the current work into five groups as delineated in Table 6.13. We note that functionals labeled as "range-separated hybrid ...", "range-separated meta-GGA", and "screened exchange" are all range-separated, but in different ways. Range-separated hybrids have a percentage (called *X*) of Hartree-Fock exchange that increases as a function of internuclear distance (called r_{12}), screened-exchange functions have an x that decreases to 0 at large , and a range-separate meta-GGA is local for both small and large r_{12}, although it is a different local form.

In order to perform a consistent comparison, all these density functional calculations on atoms and molecules are carried out with the cc-pVQZ[129,130] basis based on the geometries optimized by B97-1/cc-pVTZ.[129,130] These geometries are taken from the previous work[116] for a consistent comparison. In all density functional calculations on

atomic and molecular systems, stability tests[131,132] of the Slater determinant have been carried out in order to find the most stable broken-symmetry solution.

The treatment of transition metal systems is sometimes troubled by spin contamination of the Kohn-Sham determinant due to intrinsically multidimensional character of the wave function and static correlation effects. Although one could anticipate that the systems studied here are high-spin systems with little spin contamination, we double-checked this as follows. The M06-L xc functional has been found to be able to predict correct spin multiplicity for a variety of transition metal systems,[133] and we used this functional to find the lowest spin state for the systems considered here. In all species considered, Fe(0) is found to be in the high-spin state, i.e., the quintet state. The computed $\langle S^2 \rangle$ values by M06-L/cc-pVQZ//B97-1/cc-pVTZ level are 6.018, 6.023, 6.021, 6.019, 6.030, 6.022, 6.016, and 6.016 for Fe(0), Fe...H_2O, TS1, HFeOH, HFeOH...H_2O, TS2, $Fe(OH)_2$...H_2 and $Fe(OH)_2$, respectively. Because these values are close to he correct quintet value of 6.000, we conclude that spin contamination is not important in the reactions we investigated here.

Spin-orbit coupling is not negligible for many problems in transition metal chemistry, especially for 4d and 5d elements, but sometimes also for 3d elements like Fe. However, the main quantitative comparisons in the present paper involve comparing density functional energies to coupled cluster calculations and to one another, and the spin-orbit effects would largely cancel in such comparisons, so we did not include them in these comparisons. However in the comparisons of coupled cluster and density functional

theory calculations to experiment for diatomic molecules (discussed below), we do include spin-orbit effects for both atoms and molecules.

Reference values have been computed for the barrier heights and energies of reaction by coupled cluster theory with single and double excitations and a quasiperturbative treatment of connected triple excitations[134] with the second order Douglas-Kroll-Hess scalar relativistic method[135,136,137,138] and valence plus outer-core 3*s*3*p* electronic correlations, and with the two-point extrapolated complete basis set (CBS),[139,140,141,142] which we may abbreviate as CCSD(T)-3*s*3*p*-DKH/CBS. As for the density functional calculations, all coupled cluster calculations are single-point energies at the geometries optimized by B97-1/cc-pVTZ. The reference values for the barrier heights and energies of reaction are obtained by extrapolating the aTZ and aQZ data points; these are the CBS-limit results in Table 6.14. In order to investigate the basis set effects in the coupled cluster calculations, triple-zeta (TZ), augmented-triple-zeta (aTZ) and augmented-quadruple-zeta (aQZ) basis sets are utilized. Specifically, cc-pwCVTZ-DK for Fe[130], cc-pVTZ for O[129], cc-pVTZ for H[129] in TZ calculations; cc-pwCVTZ-DK for Fe, aug-cc-pVTZ for O, cc-pVTZ for H in aTZ calculations; cc-pwCVQZ-DK for Fe, aug-cc-pVQZ for O, cc-pVQZ for H in aQZ calculations.

All the electronic structure calculations on molecular and atomic systems were performed with a locally modified *Gaussian 09*[143] program, except that the data for FeH and FeCl in Table 6.15 were carried out with *Molpro*2010.1.[144]

The problem of a single water molecule on the (100) iron surface was treated using

the Vienna *ab initio* simulation package (VASP).[145,146] The interactions between the valence electrons and core electron orbitals are described using the projector augmented wave (PAW) method,[147] as implemented by Kresse and Joubert.[148] The size of the basis set is determined by a cut-off energy, which was fixed at E_c = 400 eV throughout the calculations. In all the cases reported on here, spin-polarized atomic configurations (ISPIN = 2, in the keyword convention of VASP) are considered.

Three classes of exchange correlation functionals were tested for heterogeneous catalysis: (b) the M06-L and revTPSS meta-GGA functionals, (b) the HSE06 and N12-SX screened-exchange gradient approximations, and (c) EXX-RPA@PBE, defined above as the combination of Hartree-Fock exchange and RPA correlation in a post-SCF calculation with PBE orbitals. The EXX-RPA@PBE calculations were carried out using the adiabatic-connection fluctuation–dissipation theorem formulation of the RPA method, as implemented in the VASP code.[121] The methodology of calculations, adopted in this work, has previously been used to study CO adsorption on Cu(111)[149] and CO adsorption on Cu, 4d metals and Pt.[114]

The six stationary points (four minima and two saddle points) were optimized using the PBE functional, and these geometries were used for the subsequent calculations with M06-L, revTPSS, HSE06, N12-SX, and EXX-RPA@PBE. All the heterogeneous catalysis calculations use these PBE geometries, and PBE orbitals are used as the initial guess for the self-consistent-field cycles of both the meta-GGA and screened exchange calculations.

The Fe(100) surface was described by a repeated slab, with the size in the direction perpendicular to the (100) surface being three times that in the lateral directions (the vacuum spacing thus being ~12.0 Å). The lateral dimensions of the slab correspond to *p*(3x3) surface structure (comprised of a total of 27 Fe atoms positioned in the calculation cell of parallelepiped-type geometry, stretched in the *Z*-direction to accommodate the vacuum gap). The Brillouin zone integrations to obtain total energies were performed on Γ-centered grids of sizes 3×3×1 **k** points. The ionic relaxation was performed using the conjugate-gradient algorithm with the convergence criterion for the forces set to 10^{-4} eV/Å. The partial occupancies of orbitals were determined using Methfessel-Paxton method,[150] which is known to perform well for metallic systems. The dissociation barriers were determined using the climbing image nudged elastic band method (CI-NEB),[151,152] as implemented[153] in the VASP program. For the M06-L calculations we used a very fine grid of 10 points per Å.

6.6.3 Results and Discussion

6.6.3.1 Utility of coupled cluster calculations to serve as reference data

A recent test[154] against experimental bond energies for 20 diatomic molecules that contain a 3d transition metal and that have estimated experimental errors of 2 kcal/mol or less showed that – on average – CCSD(T) with a minimally augmented multiply polarized triple zeta basis set has errors comparable to, but not smaller than, the errors of the best Kohn-Sham density functionals. Two of the 20 diatomics, in particular FeH and FeCl, contain an iron atom, and in Table 6.15 [Table 6.15 lists the calculated errors

(kcal/mol) at CCSD(T)-3*s*3*p*-DKH/CBS level for bond dissociation energies of FeH and FeCl as compared to the experimental data], we present tests for these two molecules showing that increasing the basis set toward to complete-basis-set (CBS) limit does not systematically remove the discrepancy of CCSD(T) from experiment. It was concluded[154] on the basis of the results for the 20 diatomics that CCSD(T) cannot *in general* serve as a benchmark for testing Kohn-Sham density functional theory, and these additional basis set tests do not change that conclusion.

The 20 diatomic molecules in the previous study comprise a diverse set of molecules, but in the present study the only transition metal element is iron. We therefore analyzed the previous study from another point of view, considering results from 41 exchange-correlation functions plus the MP2 and CCSD methods. For each diatomic molecule, we "ranked" each of these 43 approximate methods in terms of the magnitude of the deviation from CCSD(T)-3s3p-DKH/apTZ calculations [apTZ denotes aug-cc-pwCVTZ-DK basis sets for transition metal elements and aug-cc-pVTZ-DK basis sets for other elements], and we also ranked them in terms of the magnitude of their deviation from experiment. We then did a Spearman rank correlation analysis of the two ranks. For some molecules, the correlation is good (as high as 0.992), and for others it is very bad (the lowest being –0.62; the average being 0.75). However, for FeH the Spearman correlation coefficient is 0.989, and for FeCl it is 0.982. Therefore, since both of these values are reasonably high, and although we should be cautious not to overinterpret the results, we conclude that we can tentatively use the CCSD(T)/CBS results in the present paper as

reference values for judging the relative accuracy of other methods for the Fe-atom mechanism.

6.6.3.2 Basis set effects in CCSD(T) calculations

The present section has two purposes: (i) test the effect of diffuse basis functions on the reference results; (2) test the effect of different methods of extrapolation to the complete basis set (CBS) limit.

Table 6.14 shows the computed relative energies of all the species involved in the iron–water reaction at CCSD(T)-3*s*3*p*-DKH level. The rows labeled CBS are obtained by separately extrapolating the Hartree-Fock and correlation energies to the complete basis set limit. The last column shows the mean unsigned deviation (MUD) relative to the most complete calculation, which is called the final reference value. For the final reference values, the CBS limits are based on the following equations[155]

$$E_{\mathrm{CBS}}^{\mathrm{corr}} = \frac{X^3 E_X^{\mathrm{corr}} - (X-1)^3 E_{X-1}^{\mathrm{corr}}}{X^3 - (X-1)^3} \tag{6.5}$$

$$E_{\mathrm{CBS}}^{\mathrm{HF}} = \frac{E_{\mathrm{X\text{-}1}}^{\mathrm{HF}} - \lambda E_{\mathrm{X}}^{\mathrm{HF}}}{1-\lambda} \tag{6.6}$$

where

$$\lambda = \frac{X}{X+1}\exp[9(\sqrt{X} - \sqrt{X-1})] \tag{6.7}$$

In the above equations, X and $X-1$ represent a pair of basis sets with successive cardinalities, which are aQZ ($X = 4$) and aTZ ($X - 1 = 3$) respectively in our study; "corr" stands for correlation energies and "HF" represents Hartree-Fock energies. Equation (6.7)

is derived from the Karton−Martin two-point formula,[141] which has also been employed in the extrapolation of CCSD(T) results to the CBS limits.[155] The final extrapolated CCSD(T) energy, denoted as CBS(aTZ, aQZ)-3, is computed as the summation of the correlation energy and the Hartree-Fock energy.

For comparison, we also carried out two other extrapolations, which were performed with the following equation[140]

$$E_{\mathrm{CBS}}^{\mathrm{CCSD(T)}} = \frac{X^{\alpha} E_X^{\mathrm{HF}} - (X-1)^{\alpha} E_{X-1}^{\mathrm{HF}}}{X^{\alpha} - (X-1)^{\alpha}} + \frac{X^{\beta} E_X^{\mathrm{corr}} - (X-1)^{\beta} E_{X-1}^{\mathrm{corr}}}{X^{\beta} - (X-1)^{\beta}} \qquad (6.8)$$

The CBS limits obtained with aTZ and aQZ data points using parameters $\alpha = 3.4$, $\beta = 2.4$, are denoted by CBS(aTZ, aQZ)-1. These two parameters are fitted for extrapolating DZ and TZ to CBS limits.[140] Another set of parameters, $\alpha = 4.93$, $\beta = 2.13$, which are fitted for extrapolating aDZ and aTZ to CBS limits,[156] can also be used to extrapolate aTZ and aQZ data points. The obtained CBS limits are denoted by CBS(aTZ, aQZ)-2. The CBS limits extrapolated from TZ and QZ data points, denoted by CBS(TZ, QZ), as reported in ref 116 are also included in Table 6.16.

The mean unsigned deviation of CBS(TZ,QZ) is 0.12 kcal/mol, which is insignificant compared to the relative energy of each species. Therefore, adding diffuse functions on oxygen atoms does not have a noticeable impact on the CCSD(T) results for this system. The CBS limits from the four different approaches are very close to each other, the standard deviations of these four extrapolated methods for the relative energies of all the species are all smaller than 0.30 kcal/mol.

6.6.3.3 Barrier heights and energies of reaction by density functional theory for catalysis at the bare metal atom

Figure 6.3 shows the schematic energy profile of all the steps involved in the water splitting reaction on Fe(0). M06-L functional is found to be able to predict correct spin multiplicity for a variety of transition metal systems.[133] For the system we studied in the current work, Fe (0) in all the species are in the high spin state, i.e., the quintuple state. The computed $<S^2>$ values at M06-L/cc-pVQZ//B97-1/cc-PBTZ level for Fe(0), Fe...H_2O, TS1, HFeOH, HFeOH...H_2O, TS2, $Fe(OH)_2$...H_2 and $Fe(OH)_2$ are 6.0175, 6.0234, 6.0207, 6.0186, 6.0300, 6.0216, 6.0162, 6.0163 respectively. Therefore, spin contamination is not important in the reactions we investigated here.

Table 6.16 lists the classical (zero-point-energy exclusive) forward and reverse barrier heights for reactions R2 and R4 (four barrier heights) and the classical energies of reaction for R1–R5 and the overall reaction R_O (six reaction energies). The mean unsigned deviations (MUDs) and mean signed deviations (MSDs) are computed with respect to the final reference value explained above. In each group of xc functionals in Table 6.16, the functionals are ordered with respect to their overall MUDs for the ten data; these MUDs are labeled TK for "thermochemical kinetics." Table 6.17 shows the percentage of Hartree-Fock exchange in the hybrid functionals we tested in the present work.

As we can see from the last column of Table 6.16, the overall MUDs depend strongly on the ingredients of the xc functional, being 5.6 to 8.7 kcal/mol for GGAs, 6.2 kcal/mol

for the NGA, 3.8 to 7.8 kcal/mol for meta-GGAs, 4.15 kcal/mol for the meta-NGA, 3.5 for the functional with nonlocal correlation, and 1.2–6.8 kcal/mol for hybrid functionals. However, most hybrid functionals yield errors closer to the lower end than the higher end of that range, with 21 of 23 hybrid functionals having MUDs in the range 1.2 to 3.8, and the other two having MUDs of 6.0 and 6.8 kcal/mol. Table 6 shows that the two hybrid functionals with largest overall MUDs are among those with the highest percentages of Hartree-Fock exchange.

The EXX-RPA@PBE calculations have an overall MUD lower than all 18 local functionals, but their overall MUD is lower than only two of the 23 hybrid functionals, which have nonlocal exchange.

If we consider the mean unsigned deviations of the four barrier, eight of the density functionals developed in our, namely MPW1K, SOGGA11-X, MN12-SX, M05, M06, M06-2X, M08-SO and PWB6K, provide – on average – more accurate predictions than EXX-RPA@PBE, and three density functionals developed elsewhere (B97-3, ωB97X-D, ωB97X) also do so. If we consider the overall performances for both the barrier heights and the energies of reaction, 11 density functionals developed in our group (MPW1K, SOGGA11-X, MN12-SX, M05, M05-2X, M06, M06-2X, M08-HX, M08-SO, PWB6K, and PW6B95) and eight density functionals developed elsewhere (B97-3, ωB97X-D, B97-2, ωB97X, B97-1, B3LYP, PBE0, and PW6B95-D3(BJ)) have smaller overall mean unsigned deviations than the nonlocal-correlation method EXX-RPA@PBE.

Among all these tested functionals, five have mean unsigned deviations in the range

1.2–1.7 kcal/mol. This is an encouraging result for this very challenging transition metal system, which not only involves the multi-reference characteristic character, but also includes physisorption that is sensitive to noncovalent interactions.

The averaged overall MUD of the GGA/NGA, meta-GGA/meta-NGA, hybrid GGA/hybrid NGA, hybrid meta-GGA/ hybrid meta-NGA, and RPA functionals examined in the current work are respectively 6.7, 5.2, 2.5, 3.0, and 3.5 kcal/mol. Therefore, the hybrid functionals give the best predictions for this system. From the MSD values listed in Table 6.16, we found that most of the density functional methods underestimate the barrier heights. The averaged MSD for the GGA, meta-GGA, hybrid GGA, and hybrid meta-GGA functionals are respectively -9.56, -4.99, -2.39, 0.33 kcal/mol. Therefore, the hybrid meta-GGA functionals provide the best prediction for the barrier heights for this system. RPA gives an overall MUD of 3.48 kcal/mol and has an error of 7.26 kcal/mol for the energy of reaction of R1.

PWB6K gave the smallest overall mean unsigned deviation from CCSD(T) for this system; ωB97X-D gave the smallest mean unsigned deviation for all the reaction barrier heights.

Another way to put the present findings in perspective is to note that Scuseria and coworkers[157] showed that the RPA is identical to an approximation to coupled cluster theory with only double excitations (CCD) in which only the ring diagrams are retained (ring-CCD). In this context it is notable that even full coupled cluster theory with both single and double excitations (CCSD without the approximation of being restricted to

ring diagrams) has been shown to be less accurate than many local-correlation exchange-correlation density functionals for barrier heights.[158] For the most complete basis set tested in each case, the mean unsigned error on 24 diverse barrier heights (for reactions involving only nonmetal elements) was found to be 0.5 kcal/mol for CCSD(T), 2.2 kcal/mol for CCSD, and 0.9 kcal/mol for M06-2X.[158] However, as a possible path to future improvement, we note that CCSD is well suited to the introduction of semiempirical improvements, and the mean unsigned error on the same data set for the BMC-CCSD method,[159] which is based on CCSD with five empirical parameters, reduced the error on the same dataset (which was not used in its parameterization) to 0.7 kcal/mol. The QCISD ("quadratic configuration interaction with single and double excitations") method, which consists of a subset of the terms in CCSD (but a different subset than those used in ring-CCD), has also been incorporated in a doubly hybrid density functional (with five empirical parameters) that reduced the error on a different barrier height database to 0.6 kcal/mol (as compared to 2.8 kcal/mol for straight QCISD).[160]

6.6.3.4 Barrier heights and energies of reaction by density functional theory for catalysis at the solid-vacuum interface

In the preceding section, it is shown that several density functionals provide an adequate description of the water dissociation on Fe(0) reactions in the gas phase, and a variety of local-correlation functionals correlate better with CCSD(T) than does EXX-RPA@PBE. However, the question as to what extent these conclusions are applicable to

the problem of chemical reactions on metal surfaces remains to be addressed.

Chemical reactions on metal surfaces are sufficiently different from those in the gas phase that it is imperative to assess the influence of extended metal surfaces on the mechanisms and energetics of chemical reactions and on the validity of various theoretical approaches that may be applied to them.

Here we compare the predictions of several methods of describing adsorption and dissociation of a water molecule on the iron (100) surface. Two kinds of structures are considered, namely four equilibrium adsorption structures and two transition structures, where the latter are first-order saddle points. The relative energies for the structures were computed by

$$\Delta E_{\text{structure}} = E_{\text{FeH}_2\text{O}} - \left(E_{\text{slab}} + E_{\text{H}_2\text{O}} \right) \tag{6.9}$$

where $E_{\text{FeH}_2\text{O}}$ is the total energy of the structure on the metal surface, E_{slab} is the energy of the bare iron slab, and $E_{\text{H}_2\text{O}}$ is the energy of a gas-phase water molecule.

Figure 6.4 illustrates the water dissociation reaction mechanism on the Fe (100) surface. Following Ref. 116 and a reference therein, we optimized six stationary points: four minima labeled C0–C3 and two saddle points labeled B1 and B2. The first stationary point, C0, corresponds to the bare surface with a water molecule infinitely separated. The second, C1, is the physisorbed water flat on the surface, with the oxygen atom over an iron atom, i.e., at an on-top site labeled T in fig. 6.4. Water dissociation at 250 K results in formation of p(1×2)-OH monolayer on the surface, with O-H bonds being tilted with

respect to the surface normal. Correspondingly, the third minimum-energy structure, C2, corresponds to OH located at the bridge site (B) and H chemisorbed on adjacent hollow site (H). The fourth minimum-energy structure, C3, corresponds to the OH moiety also having dissociated with all three atoms now at separate hollow sites. Saddle point B1 connects C1 to C2, and saddle point B2 connects C2 to C3. The trends of the energetics of these steps are summarized in Fig. 6.5, where the relative energies defined by Eq. 6.9 are presented.

First we note that our EXX-RPA@PBE calculations give similar results to those of Karlický et al.,[116] but show some quantitative differences that may be due to a different sample relaxation methodology and slab size used in our calculations (see above), as well as to different density functionals used to optimize geometries. Similarly our HSE06 calculations are quantitatively similar to the ones reported in Ref. 116, showing that the present use of PBE geometries leads to only minor differences from their calculations with PW91 geometries.

One interesting trend in fig. 6.5, where all results are for the same size slab, is that, as functions of the reaction coordinate, the two screened exchange functionals, HSE06 and N12-SX, give flatter potentials than EXX-RPA@PBE, and the two meta functionals, M06-L and revTPSS, give more widely varying potentials. A set of five energies, as in fig. 6.5, has 15 pairs of energies (1-2, 1-3, 1,-4, 1-5, 2-3, etc.), and we can compare various pairs of functionals with one another by computing the average difference in these 15 relative energies. Doing this shows that revTPSS and N12-SX both agree with

EXX-RPA@PBE within 4–5 kcal/mol, on average, while M06-L and HSE06 differ from EXX-RPA@PBE by 6 kcal/mol, on average.

Further studies are needed to understand which of the five sets of results in Fig. 6.5 is the most accurate, but since HSE06, N12-SX, and M06-L have only slightly larger deviations than EXX-RPA@PBE from CCSD(T) results for the single-atom catalytic mechanism, where CCSD(T) results are available, it is quite possible that these less expensive and simple calculations can be a fair alternative to the RPA approach. Further understanding will require a direct comparison to quantitatively accurate experimental or theoretical results, neither of which is available for the heterogeneous catalysis case.

6.6.4 Conclusion

In the current work, we first re-examined the reference CCSD(T) results for a zero-valent atomic iron for the water splitting reaction. We found that adding diffuse basis functions on oxygen does not have a noticeable impact on the coupled cluster results for all the reaction steps involved, which is consistent with the conclusion obtained previously[124] for the first step of the reaction.

Then, continuing with the zero-valent atomic iron catalyst for the water splitting reaction, forty-one density functionals with local correlation and one (EXX-RPA@PBE) with nonlocal correlation were tested against the reference results for six reaction energies and four barrier heights involved in the mechanism. We found that 19 of the functionals with local correlation had smaller average absolute errors than the one with nonlocal correlation. This indicates that previous conclusions[116] that there is a systematic

improvement in the accuracy of density functional theory from the generalized gradient approximation, to hybrid functionals, to the random phase approximation, are incorrect. Based on our investigation, the hybrid GGA functionals give the best overall mean unsigned deviation from the reference values for barrier heights and reaction energies combined, whereas hybrid meta-GGA functionals offer the best prediction if one only considers barrier heights. Most of the density functionals, including RPA, underestimate the barrier heights of this system. Only a few functionals, namely ωB97X, SOGGA11-X, MN12-SX, and PWB6K give a mean unsigned deviation for barriers that is smaller than 1.0 kcal/mol.

Finally we present a smaller study of the water splitting reaction on the (100) surface of iron. However, lack of enough solid experimental data or benchmark wave function data on the mechanism of water dissociation and, particularly, barrier heights prevent quantitative evaluation of the performance for this heterogeneous case. This presents a challenge for future work.

6.7 Calcium Metal Adsorption on the Metal-Organic Framework NU-1000: Interface Structure and Energetics

6.7.1 Computational Methods

The experimental crystal structure of NU-1000[161] was used as the initial structure in our study. We also built a cluster model ($Zr_6C_{56}O_{32}H_{56}$, see Figure 6.6) that has one Zr_6 core and eight benzoates attached to it; the geometry of the cluster was optimized with all carbons fixed to their positions that were optimized in the periodic calculation from the

previous work.[162] The *Gaussian 09*[163] and *CRYSTAL14*[164] software were used for the cluster and periodic calculations respectively. All theoretical calculations, both cluster and periodic calculations were performed with Kohn-Sham density functional theory (DFT) with atom-centered Gaussian basis functions. We used the M06-L[165] exchange-correlation functional for geometry optimization (and Hessian calculation if it is cluster calculation), followed by a single-point energy with the M06-2X[166] functional, which has been validated as giving an accurate energy for the formation of a Ca-O bond.[167] We used the 6-31G(d,p)[168,169,170,171,172] basis set for H, C, and O. The SDD effective core potential and corresponding basis set were used for Zr[173,174] and Ca.[175]

An ultrafine integration grid was used for all cluster calculations. Enthalpies were calculated at 300 K. The vibrational contributions were calculated by the quasiharmonic approximation, which means using the harmonic oscillator formulas but with scaled frequencies that account for anharmonicity and systematic errors in the density functional calculations, as explained elsewhere.[176] The scale factor used was 0.978 for M06-L, as calculated by the *Freqscale* program.[177]

In periodic calculations, the lattice constants and atomic positions were both optimized except in the slab calculations, in which the lattice constants were fixed to values optimized in the bulk calculations. For geometry optimization in the periodic model, the Gaussian basis functions with exponents smaller than 0.06 and the polarization p function of H were removed. In the following single-point calculation, the basis functions of Ca with exponent smaller than 0.06 but greater than 0.03 and the

polarization p functions of H were added back to better describe the reactions involving H and Ca. Default settings were used in *CRYSTAL14* except that `ITol5` was increased to 35 to facilitate convergence of the M06-2X calculations. All enthalpies from periodic calculations are approximated by adding the Born-Oppenheimer energy from the periodic calculation to the difference between 300 K enthalpy of reaction and the energy of reaction from the cluster calculation.

6.7.2 Results and Discussions

In this section we discuss the results from periodic and cluster calculations and compare them to experiment. To make the presentation unambiguous and easier to follow, we adopt the convention of following each numerical value by "[C]" if it is an enthalpy from a cluster calculation and by "[P]" if it is an approximated enthalpy from a periodic calculation, and "[T]" if it is an enthalpy from tabulated numbers in references.

As a strong reducing agent, Ca reacts with acidic hydrogens to produce H_2. In the absence of protons, Ca can also react with H_2 to give calcium hydride.[178] In NU-1000, the possible sources of protons are uncoordinated benzoic acid on the surface, $–OH_2$ or –OH groups of the Zr_6 nodes, and residual water that is molecularly bound to the nodes. We calculated the energies and enthalpies of these protons reacting with Ca, as listed in Table 6.18.

Since there are terminal uncoordinated carboxylic acid sites at the edges of NU-1000, the following reaction between Ca and carboxylic acid groups of the linkers may occur:

$$Ca(g) + 2\ RCOOH \rightarrow (RCOO)_2Ca + H_2(g) \quad (1)$$

The calculated enthalpy of reaction in the gas phase is -531 kJ/mol [C]. To calculate the reaction between Ca and uncoordinated benzoic acid on the surface, we built a periodic slab model of [001] surface of NU-1000 containing a single layer of three Zr_6 nodes (1 unit cell), terminating with 12 pyrene linkers in total, each of which has two benzoic acids on either top or bottom surface, as shown in Figure 6.7A. We considered the Ca reacts with different percentages of surface benzoic acid to form H_2: 50% (one benzoic acid was reacted per pyrene) and 100% (two benzoic acids were reacted per pyrene). For the 50% case, we found two benzoate and one unreacted benzoic acid coordinating Ca^{2+}, as shown in Figure 6.7B, and the reaction energy per Ca is -538 kJ/mol [P]. The extra coordination from the C=O bond of unreacted benzoic acid to Ca^{2+} may account for the even larger magnitude of the enthalpy of reaction as compared to the gas-phase reaction. The large exothermicity also agrees with the high initial enthalpy release measured experimentally, because the surface of NU-1000 makes contact with Ca first. For the 100% case, we found that each Ca^{2+} is chelated by two benzoates, as shown in Figure 6.7C. The enthalpy of reaction (-500 kJ/mol [P]) is not only lower than the 50% case but also lower than the enthalpy of Ca reacting with two free benzoic acids, i.e. benzoic acids in the gas phase (-531 kJ/mol [C]); this may be attributed to the more constrained geometry for two benzoates binding to Ca at the surface.

The Zr_6 node in NU-1000 has 16 protons distributed on four faces: two faces in the large pore (diameter d = 31 Å) and two in the small pore (d = 10 Å).[25] Each face has

the most stable proton topology[31] as shown in Figure 6.8 To model Ca reacting with an OH_x groups on a Zr_6 node, we replaced different numbers of H of OH_x on the Zr_6 node by Ca in the unit cell by using the reaction shown in Figure 6.8 to make the following cases: (A and B) one Ca in the large or small pore, (C, D, E, and F) two Ca in the large or small pore, (G and H) four Ca, one Ca per face or two Ca per face in the large or small pore, and (I, J, K, L, and M) eight Ca replacing all H on the node. To reduce the computational cost, C_2 or C_i node symmetry is imposed on these geometries where possible; further differentiation of the cases is provided in the caption of Figure 6.9, which shows the optimized structures.

The calculated enthalpies of reaction per Ca for the reactions leading to the products in Figure 6.9 are given in Table 6.18. The first Ca has similar exothermicity to react with the OH_x in the large pore or small pore (-421 kJ/mol [P]), and it slightly greater than the cluster calculation (-395 kJ/mol [C]), indicating the further relaxation of linkers that are fixed in the cluster calculation. A higher enthalpy of reaction (-436 kJ/mol [P]) is found for placing two Ca in the large pore with C_i symmetry. In this optimized structure, two benzoates dissociate from a Zr ion and coordinate on two Ca ions with the PhC(O)O–Ca distance being 2.23 Å. The dissociation and re-coordination of benzoate are more prominent for cases with C_i symmetry, such as two Ca in the large or small pore, as shown in Figure 8C and 8E, and for cases with high Ca loading (equal to or greater than 4 Ca per node). The most exothermic case is when four Ca react with the most acidic proton ($-OH_2$) and μ^3-OH on each face (-459 kJ/mol [P]); Ca reacting with the remaining

protons releases less enthalpy, as reflected by the smaller enthalpy of reaction per Ca in the case of 8 Ca per node (393 kJ/mol[P]). This type of reaction should account for the middle range of the experimentally measured enthalpies of reaction as Ca diffuses into the pores of NU-1000.

Another proton source is from the residual weakly-bonded water that may remain within the NU-1000 samples after outgassing. We estimated the reaction enthalpy between Ca and residue water by checking the tabulated heats of formation for the following reaction at 298 K:[72]

$$Ca(g) + 2\ H_2O(g) \rightarrow Ca(OH)_2(s) + H_2(g) \quad (2)$$

, which has reaction enthalpy -679 kJ/mol [T]. However assuming the physisorbed water is in equilibrium with the atmosphere at 1 bar and 300 K before outgassing, the ultrahigh vacuum condition (2×10^{-9} mbar) and the elevated temperature (348K) in the preparation chamber provides 87 kJ/mol free energy driving force to remove residual water based on the ideal gas law. We estimate that most of binding site between water and the surface of NU-1000 has the bond strength less than 87 kJ/mol, therefore not so much residual water exists under the UHV condition, rendering reaction 2 less important.

In the absence of other protons, Ca might react with an –OH group in single step to form hydride (in the form of –O-Ca-H). This hydride can exist as a reaction intermediate for Ca reacting with –OH group, or as a stable product when protons are almost depleted. We calculated the enthalpy of reaction for one representative case to form a Ca-H bond, as shown in Figure 6.9N; this gives an enthalpy of reaction of -311

kJ/mol [P], which is less than the one to produce H_2 but still comparable. Ca gas can also react with gaseous H_2 to produce calcium hydride with an enthalpy of -359 kJ/mol [T] based on standard enthalpies of formation.[72]

Once all protons are consumed, the incoming Ca nucleates and grows in a pore of NU-1000; therefore the reaction enthalpy approaches the negative of the enthalpy of sublimation of Ca. To study the nucleation step, we first placed two Ca on 1,3,6,8-tetrakis(phenyl)pyrene in the cluster model. After optimization, the flat pyrene becomes slightly bent toward two Ca, and the enthalpy of reaction per Ca is -62 kJ/mol [C]. The CM5 charge[78] on each Ca in this case is 0.37 and the Mulliken charge[79] is 0.39; these values indicate that Ca dimer donates electrons to pyrene to form a charge-transfer complex [Ca_2^+···pyrene$^-$]. To study how the geometry constraint of pyrene in NU-1000 affects the enthalpy or reaction, we also placed two Ca on pyrene in a periodic calculation (inside or outside the triangular channel, as shown in Figures 6.10A and 6.10B). For the in-channel and out-of-channel configurations, the Ca–Ca distance is 3.81 and 3.87 Å, respectively, with Mulliken charges on each Ca of 0.52 and 0.46, respectively, indicating more charge transfer in the condensed phase. The enthalpies of reaction for both conformations are slightly lower (-49 and -45 kJ/mol [P]) than the ones in the gas-phase calculations (see Table 6.18), reflecting the condition that both linker conformations in the periodic calculation are constrained. When protons are depleted, this reaction can make the first Ca–Ca bond for the nucleation step.

6.8 Computational Thermochemistry: Automated Generation of Scale Factors for Vibrational Frequencies Calculated by Electronic Structure Model Chemistries

We present a Python program, Freqscale, for calculating the optimal scale factors for calculating harmonic vibrational frequencies, fundamental vibrational frequencies, and zero-point vibrational energies from electronic structure calculations. The program utilizes a previously published scale factor optimization model [I. M. Alecu, J. Zheng, Y. Zhao, D. G. Truhlar, J. Chem. Theory Comput. 6 (2010) 2872] to efficiently obtain all three scale factors from a set of computed vibrational harmonic frequencies. In order to obtain the three scale factors, the user only needs to provide zero point energies of 15 or 6 selected molecules. If the user has access to the *Gaussian09* or *Gaussian03* program, we provide the option for the user to run the program by entering the keywords for a certain method and basis set in the *Gaussian09* or *Gaussian03* program. Four other Python programs, input.py, input6, pbs.py, and pbs6.py are also provided for generating *Gaussian 09* or *Gaussian 03* input and pbs files.

6.8.1 Introduction

Computational electronic structure theory is used to predict many useful properties of molecules. The harmonic vibrational frequencies obtained from such quantum chemical computations are widely employed to estimate spectroscopic, thermochemical, and dynamical properties of molecules. At the molecular level, computed harmonic vibrational frequencies can be used to approximate the spectroscopic energy differences associated with energetic transitions between various vibrational states

of a molecule as well as to provide a measure of the molecule's vibrational zero-point energy (ZPE). In addition, within the harmonic oscillator approximation, the molecular vibrational partition function, which is the fundamental quantity underlying molecular statistical mechanics for vibrational degrees of freedom and which links molecular properties to bulk thermochemical properties, can be conveniently estimated via a simple analytical expression utilizing the computed vibrational frequencies; these partition functions can then be used for a variety of calculations of thermochemistry and thermochemical kinetics.

The harmonic approximation is very practical because it only requires the quadratic force constants, which can be obtained from electronic structure calculations in the Born-Oppenheimer approximation. Although the practicality of the harmonic oscillator approximation has made this method very popular for computing vibrational frequencies, vibrational properties derived from computed harmonic vibrational frequencies can often disagree considerably with their experimentally-determined counterparts. This discrepancy between computed and observed vibrational properties has two origins. The first is the neglect of anharmonicity in the harmonic oscillator approximation. The second is the deviation of the electronic structure treatment from complete configuration interaction, which would correspond to the exact solution of the electronic Schrödinger equation. The deviation from complete configuration interaction is due to the incomplete treatment of electron correlation in the level of theory as well as the incompleteness of the one-electron basis set used to expand the orbitals used to construct

configuration state functions. The errors resulting from these effects are usually found to be systematic. The error due to anharmonicity can be minimized either by calculating and applying anharmonic corrections or – at least for the higher frequencies – by scaling the computed harmonic frequencies, and the error due to incompleteness of the electronic structure calculation can be partially overcome by selecting a level of theory that accounts well for electron correlation and pairing it with a well-balanced one-electron basis set. Systematic progress on the latter aspect is possible by identifying theoretical model chemistries,[179] which are well-defined general methods, such as the combination of Hartree-Fock theory or a particular Kohn-Sham exchange-correlation functional with a particular basis set. From this point onward, building on the language of Pople,[179] we will denote a combination of a level of theory (or choice of density functional) and a one-electron basis set as an electronic model chemistry.

In addition to the quadratic force constants needed in the computation of harmonic frequencies, the evaluation of anharmonic corrections also requires higher-order (e.g., cubic and quartic) force constants. The calculation of vibrational energy levels by including higher force constants can be accomplished by perturbative approaches[180,181,182,183,184,185,186] or by variational methods[187,188,189,190,191,192,193,194,195,196,197]. However, the higher-order force constants required as input for such calculations are expensive to compute. Consequently, the procedure of scaling the computed harmonic vibrational frequencies to compensate for the neglect of anharmonicity has become commonplace, and scale factors have been

devised for numerous electronic model chemistries. In fact, a recent study[198] has shown that it is beneficial to scale even the anharmonic vibrational frequencies obtained from second-order perturbation theory.

As previously explained,[199,200,201] scale factors are property-specific, and in the past, they have been predominantly optimized to accurately reproduce true harmonic vibrational frequencies, observed fundamental vibrational frequencies, and/or vibrational ZPEs; although, scale factors customized to better reproduce vibrational contributions to various thermodynamic quantities have also been proposed.[200] Although *applying* scale factors to correct for the systematic errors that arise from using harmonic vibrational frequencies to estimate vibrational properties of interest is convenient, the *optimization* of such scale factors can be a tedious and time-consuming process, especially if scale factors are needed for several electronic model chemistries and for more than one property. In a recent article,[201] we introduced a practical method for efficiently evaluating the optimal scale factors for reproducing the true harmonic vibrational frequencies, fundamental vibrational frequencies, and ZPEs from a set of computed harmonic vibrational frequencies. The subject of the present article is to introduce and describe FREQ, a program that further increases the efficiency of scale factor optimization through automation.

6.8.2 The Scale Factor Optimization Process

The use of harmonic oscillator formulas with effective frequencies is called the quasiharmonic approximation. Scale factors are empirically-derived factors to be applied

to computed harmonic frequencies in order to improve the accuracy of properties being modeled by the quasiharmonic approximation. For a given electronic model chemistry, the first step toward deriving the scale factor for the property of interest is computing this property for a set of molecules for which this property is accurately known from either experiments or high-level calculations. Then, operating under the assumption that the computed and actual properties are proportional to one another, it is customary to equate the scale factor (which we will call λ) to the optimal value for the proportionality constant, in particular the value that minimizes the root mean squared (RMS) deviation between the computed and accurate data sets. In previous work from our group, scale factors for harmonic vibrational frequencies were optimized against the 38 accurate harmonic frequencies compiled in the F38/06 database,[202] scale factors for fundamental vibrational frequencies were optimized to best reproduce the 38 accurate fundamental frequencies in the F38/10 database,[201] and scale factors for ZPEs were optimized to best reproduce the ZPVE13/99,[203] ZPVE15/06,[202] and ZPVE15/10[201] databases consisting of 13, 15, and 15 ZPEs, respectively.

Obtaining three property-specific scale factors for even one electronic model chemistry by fitting computed data against such extensive databases is already a laborious task, and if scale factors are needed for a multitude of electronic model chemistries, optimizing these can quickly become extensively time-consuming and computationally intensive. We therefore proposed[201] a scale factor optimization model to obtain the scale factors for true harmonic frequencies (λ^{H}), fundamental frequencies (λ^{F}

), and ZPEs (λ^{ZPE}) for a given electronic model chemistry from a set of harmonic frequencies computed with that same electronic model chemistry. Specifically, this model entails explicitly deriving just λ^{ZPE} , and then obtaining λ^{H} and λ^{F} through the relations

$$\lambda^{\mathrm{H}} = \alpha^{\mathrm{H/ZPE}} \lambda^{\mathrm{ZPE}} \tag{6.10}$$

$$\lambda^{\mathrm{F}} = \alpha^{\mathrm{F/ZPE}} \lambda^{\mathrm{ZPE}} \tag{6.11}$$

where the proportionality constants $\alpha^{\mathrm{H/ZPE}}$ and $\alpha^{\mathrm{F/ZPE}}$ are called the universal scale factor ratios[201] in light of the fact that they should be independent of the electronic model chemistry. The values of $\alpha^{\mathrm{H/ZPE}}$ and $\alpha^{\mathrm{F/ZPE}}$ have been determined to be 1.014 ± 0.002 and 0.974 ± 0.002, respectively, based on a test set of forty electronic model chemistries[201].

The ZPVE15/10 database is employed here to calculate λ^{ZPE} . The 15 ZPEs in this database are those for C_2H_2, CH_4, CO_2, CO, F_2, H_2CO, H_2O, H_2, HCN, HF, N_2O, N_2, NH_3, OH, and Cl_2, and accurate values for these have been tabulated previously[201] (the reference values are from Irikura et al.[204], Grev et al.[205], and Martin[206]) and are given in Table 6.19 The optimal scale factor for ZPEs, λ^{ZPE} , is obtained by minimizing the quantity

$$\mathrm{RMSE}\left(\mathrm{ZPE}\right) = \left\{ \left[\sum_{m=1}^{15} \left(\lambda^{\mathrm{ZPE}} \varepsilon_{\mathrm{vib},m}^{\mathrm{G,input}} - \varepsilon_{\mathrm{vib},m}^{\mathrm{G}} \right)^2 \right] \Big/ 15 \right\}^{1/2} \tag{6.12}$$

where $\varepsilon_{\mathrm{vib},m}^{\mathrm{G}}$ is the ZPE of the m^{th} molecule in the ZPE15 database, $\varepsilon_{\mathrm{vib},m}^{\mathrm{G,input}}$ is the harmonic approximation to it obtained via

$$\varepsilon_{\mathrm{vib},m}^{\mathrm{G,input}} \equiv \frac{hc}{2}\sum_{i}\omega_i \tag{6.13}$$

where ω_i a computed harmonic frequencies of the molecule in units of cm^{-1}, h is Planck's constant, and c is the speed of light. The value of λ^{ZPE} which minimizes RMSE(ZPE) in Eq. 6.12 is obtained analytically from the expression

$$\lambda^{\mathrm{ZPE}} = \frac{\sum_{m=1}^{15}\left(\varepsilon_{\mathrm{vib},m}^{\mathrm{G,input}}\,\varepsilon_{\mathrm{vib},m}^{\mathrm{G}}\right)}{\sum_{m=1}^{15}\left(\varepsilon_{\mathrm{vib},m}^{\mathrm{G,input}}\right)^2} \tag{6.14}$$

In order to save additional computational cost (which may be a consideration if one wishes to find the scale factor for an expensive, high-level method) , we also developed a model called the "Reduced Scale Factor Optimization Model", in which a subset from the original ZPE15 database of just 6 molecules is utilized in the optimization of λ^{ZPE} instead of the full set of 15 molecules comprising ZPE15. The six molecules used in the Reduced Scale Factor Optimization Model are C_2H_2, CH_4, H_2CO, H_2O, N_2O, and NH_3. This subset of molecules was selected based on the finding that the mean absolute deviation between the λ^{ZPE} values obtained from these molecules and the λ^{ZPE} values obtained from the full set of 15 molecules was only 0.0007 for the 40 electronic model chemistries tested.[201]

6.8.3 Program Descriptions

The FREQ program is made up of two basic components: (1) a Python program called Freqscale.py that calculates and outputs the optimal values for λ^{ZPE}, λ^{H}, and λ^{F} from a set of user-provided harmonic ZPEs, and (2), the Python scripts called input.py and pbs.py that instead allow the user to generate *Gaussian 09* or *Gaussian 03* input files and pbs files that calculate the ZPEs and provide them to Freqscale.py as a when the user cannot provide the harmonic frequencies a priori. Once the ZPEs are obtained by using the input.py and pbs.py, the final step of the calculation of λ^{ZPE}, λ^{H}, and λ^{F} is carried out by Freqscale.py. In the following two sections (6.8.3.1 and 6.8.3.2), we give detailed descriptions of these programs.

6.8.3.1 Freqscale.py

Freqscale.py is a Python program that computes the scale factors for zero-point energies, harmonic frequencies, and fundamental frequencies. The operation of this program requires an input file listing the computed ZPEs for the 15 molecules in Table 6.19, in units of kcal/mol, in the order: C_2H_2, CH_4, CO_2, CO, F_2, H_2CO, H_2O, H_2, HCN, HF, N_2O, N_2, NH_3, OH, and Cl_2. We call this input file FREQ_com.txt, which will be generated by running the following two programs “input.py” and “pbs.py”. Once these data are provided, the program calculates λ^{ZPE}, λ^{H}, and λ^{F} from eqs. 5, 1, and 2, respectively, and it prints the values for these scale factors to the screen. The code is provided below:

Freqscale.py

```
# This is a program for computing various scale factors based on
# a scale factor optimization model.
#
# The citation for the scale factor optimization model is:
# Alecu, I.M., Zheng, J., Zhao, Y., and Truhlar, D.G. J. Chem. Theory Comput.
# 2010, 6, 2872.
#
# The computed values for the ZPEs of C2H2, CH4, CO2, F2, H2CO, H2O, H2, HCN,
# HF, N2O, N2, NH3, OH, and Cl2.
# correspond to the tuple elements zpecom(0:15), respectively.
#
# The experimental values for the ZPEs of C2H2, CH4, CO2, F2, H2CO, H2O, H2,
# HCN, HF, N2O, N2, NH3, OH, and Cl2 correspond to the tuple elements
# zpeexp(0:15), respectively.
#
! The scale factor for accurately reproducing the ZPEs is called LAMBDA, and is
! derived from equation sum(zpecom(i)*zpeexp(i))/sum(zpecom(i)**2), or NUMER /
! DENOM below, where i = 1:15.
!
! To obtain the scale factors for harmonic and fundamental frequencies, LAMBDA
! is multiplied by the universal scale factor ratios 1.014 and 0.974,
! respectively.
!
import random
import sys
import os

NUMER = 0.0
DENOM = 0.0
LAMBDA = 0.0

with open('freqcom.txt') as f:
   f=[x.strip() for x in f if x.strip()]
   data=[tuple(map(float,x.split())) for x in f[0:]]
   zpecom=[x[0] for x in data]

zpeexp = (16.490, 27.710, 7.3, 3.0929144, 1.302, 16.1, 13.26, 6.231, 10.000, 5.864, 6.770, 3.3618, 21.200,
5.2915,   0.7983)

for i in range(0,15):
   NUMER = NUMER + zpecom[i]*zpeexp[i]
   DENOM = DENOM + zpecom[i]**2.0
LAMBDA = NUMER/DENOM

print('Freqscale: A PROGRAM FOR OPTIMIZING SCALE FACTORS\n')
print('                                written by                                \n')
print('Haoyu S. Yu, Lucas J. Fiedler, I.M Alecu, and Donald G.Truhlar\n')
print('Department of Chemistry and Supercomputing Institute\n')
print('University of Minnesota, Minnesota 55455-0431\n')
print('Scale Factor for Zero-Point Energies     =',LAMBDA,'\n')
print('Scale Factor for Harmonic Frequencies    =',LAMBDA*1.014,'\n')
```

```
print('Scale Factor for Fundamental Frequencies =',LAMBDA*0.974,'\n')
print('CITATIONS:\n')
print('1. Alecu, I.M., Zheng, J., Zhao, Y., and Truhlar, D.G. J. Chem. Theory Comput. 2010, 6, 2872\n')
        print('2. Yu, H. S., Fiedler, L.J., Alecu, I.M., and Truhlar, D.G. Comput. Phys. Commun, submitted

2016\n')
```

6.8.3.2 input.py and pbs.py

The input.py and pbs.py scripts allow the user to *directly* obtain *Gaussian 03*[207] or *Gaussian 09*[208] input files for computing the frequencies of C_2H_2, CH_4, CO_2, CO, F_2, H_2CO, H_2O, H_2, HCN, HF, N_2O, N_2, NH_3, OH, and Cl_2 with the specified electronic model chemistry, and it submits these files to a queuing system. Once the frequency calculations have finished, the run.sh script will automatically grep the ZPEs listed in the *Gaussian 09* output files as into freqcom.txt file which is used to run Freqscale.py program.

The python program will ask the user three questions, namely, “Which method are you going to choose?”, then “Which basis set are you going to choose?”, and lastly “What is the path of your basis set?” There are two choices when you choose the basis set. Here are two examples, one for using a basis set built into *Gaussian 09* and one for a user-defined basis set:

1. For a built-in basis set and the BLYP[209,210] functional as an example:
    a. Which method are you going to choose? “BLYP”
    b. Which basis set are you going to choose? “6-311G”
    c. What is the path of your basis set? Hit the enter key
2. For a user-defined basis set and BLYP[209] functional as an example:
    a. Which method are you going to choose? “BLYP”

b. Which basis set are you going to choose? “gen”

c. What is the path of your basis set?

“home/truhlar/user1/basis_set/MG3S.gbs”

In the above examples, the calculation of the harmonic frequencies of C_2H_2, CH_4, CO_2, CO, F_2, H_2CO, H_2O, H_2, HCN, HF, N_2O, N_2, NH_3, OH, and Cl_2 are using the BLYP[209] density functional paired with a particular basis set. If the basis set to be used is one that is already available in *Gaussian 09*, e.g., 6-311G[211,212], then the user can just type the keyword of this basis set. If the basis set to be used is not available in *Gaussian 09*, e.g., MG3S, the user can type “gen” and then the path of the external basis set. In addition, in the example above, all the other keywords for calculating the ZPEs of these 15 molecules are provided by input.py and pbs.py. The codes of these two programs are provided in the CPC Program Library. In the following two pages, we are going to show a representative part of the code, which is the creation of input and PBS files of C_2H_2 molecule.

input.py

```
import sys
import string
import os

functional = str(input('Which method are you going to choose? '))
basis = str(input('Which basis set are you going to choose? '))
path = str(input('What is the path of your basis set? '))

#c2h2.com
file = open("c2h2.com","w")
file.write("%mem=420mb\n")
file.write("# opt=(vtight,Maxcycle=200) scf=(xqc,maxcycle=400,tight) Freq integral=ultrafine\n")
file.write(functional + "/" + basis + "\n")
```

```
file.write("\nt\n")
file.write("0,1\n")
file.write("C\n")
file.write("C,1,CC\n")
file.write("X,2,1.,1,90.\n")
file.write("H,2,CH,3,90.,1,180.,0\n")
file.write("X,1,1.,2,90.,3,180.,0\n")
file.write("H,1,CH,5,90.,2,180.,0\n\n")
file.write("CC=1.203142\n")
file.write("CH=1.062605\n")
file.write("\n" + path + "\n")
file.write("\n")
file.close()
```

input.py

```
import sys
import string
import os

file = open("c2h2.pbs","w")
file.write("#!/bin/bash -l\n")
file.write("#\n")
file.write("# job: c2h2 \n")
file.write("\n")
file.write("# qg09 version 1.0.10\n")
file.write("\n")
file.write("#To submit this script to the queue type:\n")
file.write("#   qsub c2h2.pbs\n")
file.write("\n")
file.write("#PBS -m n\n")
file.write("#PBS -l nodes=1:ppn=24\n")
file.write("#PBS -l walltime=1:00:00\n")
file.write("#PBS -l mem=60000mb\n")
file.write("#PBS -e c2h2.e\n")
file.write("#PBS -e c2h2.o\n")
file.write("#PBS -q mesabi\n")
file.write("#\n")
file.write("\n")
file.write("cd $PBS_O_WORKDIR\n")
file.write("\n")
file.write("module load gaussian/g09.d01\n")
file.write("/usr/bin/time g09 < c2h2.com >& c2h2.out\n")
file.write("\n")
file.close()
```

6.8.4 Discussion

A few cautionary remarks are in order. First, because zero point energies are dominated by the higher frequencies, the scale factors determined by this method are especially appropriate for larger frequencies and for the whole zero-point energy; they may not be appropriate for, for example, low-frequency torsions or low-frequency bends. Second, since empirical scale factors are based on "normal" molecules they might be inappropriate for a molecule with an unusual bonding pattern. Third, the quasiharmonic approximation with scaled frequencies can be accurate for a molecule with a single conformation or for a single conformation of a molecule with multiple conformations if the barriers between conformational minima are high compared to the available thermal energy, but they do not treat multiple-structure contributions to partition functions. Other methods are available for multiple-structure anharmonicity[213,214,215,216], but the scaled vibrational frequencies determined the computer program presented here may be used to obtain vibrational frequencies to be used as input for the multiple-structure treatment, especially for the higher-frequency modes[217].

6.8.5 Concluding Remarks

Empirically scaling computed harmonic frequencies using appropriate scale factors is a widely employed and practical method for improving vibrational frequencies and zero-point energies from electronic structure calculations. Here we provide a program, Freqscale.py that automates the scale factor optimization process. In the current version

of FREQ, vibrational harmonic frequencies can be obtained by using the *Gaussian 09* or *Gaussian 03* input and pbs files provided by two python programs, input.py and pbs.py.

6.9 References

[1] M. Yoshimine, *J. Phys. Soc. Jpn*. 1968, 25, 1100.
[2] D. E. Woon and T. K. J. Dunning, *J. Chem. Phys*. 1995, **103**, 4572.
[3] J. Koput and K. A. Peterson, *J. Phys. Chem. A* 2002, **106**, 9595.
[4] M. Douglas and N. M. Kroll, *Ann. Phys*. 1974, **82**, 89.
[5] B. A. Hess, *Phys. Rev. A*. 1985, **32**, 756.
[6] B. A. Hess, *Phys. Rev. A*. 1986, **33**, 3742.
[7] G. Jansen and B. A. Hess, *Phys. Rev. A*. 1989, **39**, 6016.
[8] M. Vasiliu, D. Feller, J. L. Gole, and D. A. Dixon, *J. Phys. Chem. A* 2010**, 114**, 9349.
[9] M. J. Frisch, G. W. Trucks, H. B. Schlegel, G. E. Scuseria, M. A. Robb, J. R. Cheeseman, G. Scalmani, V. Barone, B. Mennucci, G. A. Petersson, H. Nakatsuji, M. Caricato, X. Li, H. P. Hratchian, A. F. Izmaylov, J. Bloino, G. Zheng, J. L. Sonnenberg, M. Hada, M. Ehara, K. Toyota, R. Fukuda, J. Hasegawa, M. Ishida, T. Nakajima, Y. Honda, O. Kitao, H. Nakai, T. Vreven, J. A. Montgomery, Jr., J. E. Peralta, F. Ogliaro, M. Bearpark, J. J. Heyd, E. Brothers, K. N. Kudin, V. N. Staroverov, R. Kobayashi, J. Normand, K. Raghavachari, A. Rendell, J. C. Burant, S. S. Iyengar, J. Tomasi, M. Cossi, N. Rega, J. M. Millam, M. Klene, J. E. Knox, J. B. Cross, V. Bakken, C. Adamo, J. Jaramillo, R. Gomperts, R. E. Stratmann, O. Yazyev, A. J. Austin, R. Cammi, C. Pomelli, J. W. Ochterski, R. L. Martin, K. Morokuma, V. G. Zakrzewski, G. A. Voth, P. Salvador, J. J. Dannenberg, S. Dapprich, A. D. Daniels, Ö. Farkas, J. B. Foresman, J. V. Ortiz, J. Cioslowski, and D. J. Fox, Gaussian 09, revision C01; Gaussian, Inc., Wallingford CT, 2009.
[10] T. J. Lee and P. R. Taylor, *Int. J. Quantum Chem. Symp*. 1989, **23**, 199-207.
[11] A. Karton, E. Rabinovich, J. M. L. Martin, and B. J. Ruscic, *Chem. Phys.* 2006, **125**, 144108.
[12] N. E. Schultz, Y. Zhao, and D. G. Truhlar, *J. Phys. Chem. A* 2005, **109**, 11127-11143.
[13] O. Tishchenko, J. Zheng, and D. G. Truhlar, *J. Chem. Theory. Comput.* 2008, **4**, 1208.
[14] Y. Zhao, O. Tishchenko, J. R. Gour, W. Li, J. J. Lutz, P. Piecuch, and D. G. Truhlar, *J. Phys. Chem. A* 2009, **113**, 5786.
[15] H.-J. Werner, P. J. Knowles, G. Knizia, F. R. Manby, M. Schu¨tz, P. Celani, T. Korona, R. Lindh, A. Mitrushenkov, G. Rauhut, K. R. Shamasundar, T. B. Adler, R. D. Amos, A. Bernhardsson, A. Berning, D. L. Cooper, M. J. O. Deegan, A. J. Dobbyn, F. Eckert, E. Goll, C. Hampel, A. Hesselmann, G. Hetzer, T. Hre- nar, G. Jansen, C. Ko¨ppl, Y. Liu, A. W. Lloyd, R. A. Mata, A. J. May, S. J. McNicholas, W. Meyer, M. E. Mura, A. Nicklass, D. P. O'Neill, P. Palmieri, K. Pflu¨ger, R. Pitzer, M. Reiher, T. Shiozaki, H. Stoll, A. J. Stone, R. Tarroni, T. Thorsteinsson, M. Wang, and A. Wolf, *Molpro*, version 2010.1; University of Birmingham: Birmingham, 2010.
[16] B. O. Roos, P. R. Taylor, and P. E. M. Siegbahn, *Chem. Phys.* 1980, **48**, 157.

[17] T. Helgaker, P. Jorgensen, and J. Olsen, *Modern Electronic Structure Theory*; Wiley: Chichester, 2000; p. 188.
[18] M. Valiev, E. J. Bylaska, N. Govind, K. Kowalski, T. P. Straatsma, H. J. J. van Dam, D. Wang, J. Nieplocha, E. Apra, T. L. Windus, and W. A. de Jong, *Comput. Phys. Commun.* 2010, **181**, 1477.
[19] A. D. Becke, *Phys. Rev. A*. 1988, **38**, 3098.
[20] C. Lee, W. Yang, and R. P. Parr, *Phys. Rev. B.* 1988, **37**, 785.
[21] C. Adamo and V. Barone, *Chem. Phys. Lett.* 1997, **274**, 242.
[22] H. Yu and D. G. Truhlar, *J. Chem. Theory Comput*. 2014, **10**, 2291.
[23] A. Karton, E. Rabinovich, J. M. L. Martin, B. Ruscic, *J. Chem. Phys*. 2006, **125**, 144108.
[24] A. Karton, P. R. Taylor, and J. M. L. Martin, *J. Chem. Phys*. 2007, *127*, 064104.
[25] K. Raghavachari, G. W. Trucks, J. A. Pople, and M. Head-Gordon, *Chem. Phys. Lett*. 1989, **157**, 479.
[26] P. J. Stephens, F. J. Devlin, C. F. Chabalowski, and M. J. Frisch, *J. Phys. Chem.* 1994, **98**, 11623.
[27] C. Møller and M. S. Plesset, *Phys. Rev*. 1934, **46**, 618.
[28] M. Head-Gordorn, J. A. Pople, and M. J. Frisch, *Chem. Phys. Lett*. 1988, **153**, 503.
[29] A. Karton and J. M. L. Martin, *J. Chem. Phys.* 2010, **133**, 144102.
[30] B. Soulé de Bas. H. E. Dorsett, and M. J. Ford, *J. Phys. Chem. Solids* 2003, **64**, 495.
[31] T. E. Sorensen and W. B. England, *Int. J. Quant. Chem*. 2000, **76**, 259.
[32] J. Irisawa and S. Iwata, *Theor. Chim. Acta.* 1992, **81**, 223.
[33] D. T. I. Nakazato, E. L. De Sá, and R. L. A. Haiduke, *Int. J. Quant. Chem*. 2010, **110**, 1729.
[34] Y. Zhao, and D. G. Truhlar, *J. Chem. Phys*. 2006, **125**, 194101.
[35] T. H. Dunning, Jr., *J. Chem. Phys.* 1989, **90**, 1007.
[36] T. H. Dunning, Jr., K. A. Peterson, and A. K. Wilson, *J. Chem. Phys.* 2001, **114**, 9244.
[37] K. A. Peterson, D. Figgen, M. Dolg, and H. Stoll, *J. Chem. Phys.* 2009, **130**, 163108.
[38] D. Figgen, K. A. Peterson, M. Dolg, and H. Stoll, *J. Chem. Phys.* 2009, **130**, 164108.
[39] R. Peverati and D. G. Truhlar, *Phil. Trans. Roy. Soc. A* 2014, **372**, 20120476.
[40] I. M. Alecu, J. Zheng, Y. Zhao, and D. G. Truhlar, *J. Chem. Theory Comp.* 2010, **6**, 2872.
[41] M. M. Kreevoy and D. G. Truhlar, *Tech. Chem.* (N.Y.), 4th ed., **1986**, *6*/Pt. 1, 13.
[42] M. J. Frisch, *et al*., *Gaussian 09*, revision C01 (Gaussian, Inc., Wallingford CT, 2009).
[43] C. K. Jørgensen, *Naturwiss.* 1976, **63**, 292.
[44] S. Sima, *Found. Chem.* 2009, **11**, 135.
[45] S. Reidel and M. Kaupp, *Coord. Chem. Rev.* 2009, **253**, 606.
[46] D. Himmel, C. Knapp, M. Patzschke and S. Riedel, *ChemPhysChem* 2010*,* **11**, 865.

[47] G. Wang, M. Zhou, J. T. Goettel, G. J. Schrobilgen, J. Su, J. Li, T. Schlöder, and S. Riedel, *Nature* 2014, **514,** 475.
[48] P. Pyykkö and W.-H., Xu, *Angew. Chem. Int. Ed.* 2015*,* **54**, 1080.
[49] A. K. Srivastava and N. Misra, *Int. J. Quantum Chem.* 2014, **114**, 328.
[50] P. Pyykkö and M. Atsumi, *Chem. Eur. J.* 2009, **15**, 186.
[51] P. Pyykkö and M. Atsumi, *Chem. Eur. J.* 2009, **15**, 12770.
[52] A. V. Marenich, S. V. Jerome, C. J. Cramer, and D. G. Truhlar, *J. Chem. Theory Comp.* 2012, **8**, 527.
[53] F. L. Hirshfeld, *Theor. Chem. Acc.,* 1977, **44,** 129.
[54] J. P. Ritchie and S. M. Bachrach, *J. Comp. Chem.* 1987, **8,** 499.
[55] K. Raghavachari, G. W. Trucks, J. A. Pople, and M. Head-Gordon, *Chem. Phys. Lett.* 1989, **157**, 479.
[56] A. P. Rahalkar, B. K. Mishra, V. Ramanathan, and S. R. Gadre, *Theor. Chem. Acc.* 2011, **130**, 491.
[57] R. M. Richard and J. M. Herbert, *J. Chem. Phys.* 2012, **137**, 06411.
[58] N. J. Mayhall and K. Raghavachari, *J. Chem. Theory Comput.* 2012, **9**, 2669.
[59] T. Nagata, D. G. Fedorov, and K. Kitaura, *Chem. Phys. Lett.* 2012, **544**, 87.
[60] S. Wen, K. Nanda, Y. Huang, and G. J. O. Beran, *Phys. Chem. Chem. Phys.* 2012, **14**, 7562.
[61] S. R. Pruitt, M. A. Addicoat, M. A. Collins, and M. S. Gordon, *Phys. Chem. Chem. Phys.* 2012, **14**, 7752.
[62] Y. Wang, C. P. Sosa, A. Cembran, D. G. Truhlar, and J. Gao, *J. Phys. Chem. B* 2012, **116***,* 6781.
[63] M. Isegawa, B. Wang, and D. G. Truhlar, *J. Chem. Theory Comput.* 2013, *9,* 1381-1393.
[64] X. Jia, X. Wang, J. Liu, J.Z.H. Zhang, Y. Mei, and X. He, *J. Chem. Phys*. 2013, **139**, 214104.
[65] S. Hua, W. Li, and S. Li, *ChemPhysChem.* 2013, **14**, 108.
[66] A. W. Lange and G. A. Voth, *J. Chem. Theory Comput.* 2013, **9**, 4018.
[67] E. E. Dahlke, H. R. Leverentz, and D. G. Truhlar, *J. Chem. Theory Comput.* 2008, **4**, 33.
[68] E. E. Dahlke and D. G. Truhlar, *J. Chem. Theory Comput.* 2007, **3**, 1342.
[69] H. W. Qi, H. Leverentz, and D. G. Truhlar, *J. Phys. Chem. A* 2013, **117**, 4486.
[70] J. Friedrich, M. Hanrath, and M. Dolg, *J. Chem. Phys*. 2007, **126**, 154110.
[71] H. Stoll, *Chem*. *Phys*. *Lett*. 1992, **191**, 548.

[72] W. Jorgensen, J. Chandrasekhar, J. D. Madura, R. W. Impey, and M. L. Klein, *J. Chem. Phys.* 1983, **79**, 926.

[73] J. Friedrich and J. Hänchen, *J. Chem. Theory Comput*. 2013, **9**, 5381.

[74] K. Peterson, T. Adler, and H.-J. Werner, *J. Chem. Phys.* 2008, **128**, 084102.

[75] P. Wernet, D. Nordlund, U. Bergmann, M. Cavalleri, M. Odelius, H. Ogasawara, L. A. Naslund, T. K. Hirsch, L. Ojamae, and P. Glatzel, *et al*. *Science* 2004, **304**, 995.

[76] L. E. Chirlian and M. M. Francl, *J. Comp. Chem.* 1987, **8**, 894.

[77] W. Kohn, A. D. Becke, and R. G. Parr, *J. Phys. Chem*. 1996, **100**, 12974.

[78] Y. Zhao and D. G. Truhlar, *Theor*. *Chem*. *Acc*. 2008, **120**, 215.

[79] M. J. Frisch, J. A. Pople, and J. S. Binkley, *J. Chem. Phys.* 1984, **80**, 3265.

[80] B. J. Lynch, Y. Zhao, and D. G. Truhlar, *J. Phys. Chem. A* 2003, **107**, 1384.

[81] G. Knizia, T. B. Adler, and H.-J. Werner, *J. Chem. Phys*. 2009, **130**, 054104.

[82] T. B. Adler, G. Knizia, and H.-J. Werner, *J. Chem. Phys.* 2007, **127**, 221106.

[83] E. Papajak, H. R. Leverentz, J. Zheng, and D. G. Truhlar, *J. Chem. Theory Comput.* 2009, **5**, 1197. Errata and addendum: 2009, **5**, 3330.

[84] R. Peverati and D. G. Truhlar, *J. Phys. Chem. Lett*. 2011, **2**, 2810.

[85] R. Peverati and D. G. Truhlar, *Phil. Trans. Roy. Soc. A* 2013, dx.doi.org/10.1098/rsta.2012.0476 [also published online at http:// http://arxiv.org/abs/1212.0944 (accessed Dec. 29, 2013)].

[86] E. Papajak and D. G. Truhlar, *J. Chem. Theory Comput*. 2011, **7**, 10.

[87] P. Hohenberg and W. Kohn, *Phys. Rev.* 1964, **136**, B864.

[88] W. Kohn and L. J. Sham, *Phys. Rev*. 1965, **140**, A1133.

[89] A. Uzun, V. Ortalan, N. D. Browning, and B. C. Gates, *Chem. Comm.* 2009, **31**, 4657.

[90] K. Shimizu, K. Ohshima, and A. Satsuma, *Chem. Eur. J.*. 2009*,* **15**, 9977.

[91] G. E. Johnson, R. Mitrić, V. Bonačić-Koutecký, A. Castleman, Jr. W. *Chem. Phys. Lett.* 2009*,* **475**, 1.

[92] Lopez-Acevedo, O.; Kacprzak, K. A.; Akola, J.; Häkkinen, H. *Nat. Chem.* 2010*,* **2**, 329.

[93] D. Yardimci, P. Serna, and B. C. Gates, *ACS Catalysis* 2012**,** **2**, 2100.

[94] C. Aydin, J. Lu, N. D. Browning, and B. C. Gates, *Angew. Chem. Int. Ed.* 2012*,* **51**, 5929.

[95] M. Flytzani-Stephanopoulos and B. C. Gates, *Annu. Rev. Chem. Biomol. Eng.* 2012*,* **3**, 545.

[96] K. An and G. A. Somorjai, *ChemCatChem* 2012*,* **4**, 1512.

[97] Y. Lu and W. Chen, *Chem. Soc. Rev.* 2012*,* **41**, 3594.
[98] A. Dhakshinamoorthy and H. Garcia, *Chem. Soc. Rev.* 2012*,* **41**, 5262.
[99] V. Dal Santo, M. Guidotti, R. Psaro, L. Marchese, F. Carniato, and C. Bisio, *Proc. R. Soc. A* 2012**, 468**, 1904.
[100] P. Maity, S. Yamazoe, and T. Tsukuda, *ACS Catal.* 2013, **3**, 182.
[101] A. Taketoshi and M. Haruta, *Chem Lett.* 2014*,* **43**, 380.
[102] J. P. Perdew, in *Electronic Structure of Solids '91*, Ziesche, P, Eschrig, H., Eds.; Akademie Verlag: Berlin, 1991; p. 11.
[103] Y. Zhao, J. Pu, B. J. Lynch, and D. G. Truhlar, *Phys. Chem. Chem. Phys*. 2004, **6**, 673.
[104] J. Zheng, Y. Zhao, and D. G. Truhlar, *J. Chem. Theory Comput*. 2007, **3**, 569.
[105] Y. Zhao and D. G. Truhlar, *J. Chem. Phys.* 2006, **125**, 194101.
[106] R. Peverati and D. G. Truhlar, *J. Phys. Chem. Lett*. 2012, **3**, 117.
[107] R. Peverati and D. G. Truhlar, *Phys. Chem. Chem. Phys*. 2012, **14**, 13171.
[108] Y. Andersson, D. C. Langreth, and B. I. Lundqvist, *Phys. Rev. Lett.* 1996, **76**, 102.
[109] Z. Yan, J. P. Perdew, and S. Kurth, *Phys. Rev. B* 2000, **61**, 16430.
[110] F. Furche, *Phys. Rev. B* 2001*,* **64***,* 1951201.
[111] Y. Zhao, B. J. Lynch, and D. G. Truhlar, *J. Phys. Chem. A* 2004, **108***,* 4786.
[112] S. Grimme, *J. Chem. Phys.* 2006, **124**, 034108.
[113] O. A. Vydrov and T. Van Voorhis, *J. Chem. Phys*. 2009, **130**, 104105.
[114] L. Schimka, J. Harl, A. Stroppa, A. Grüneis, M. Marsman, F. Mittendorfer, and G. Kresse, *Nat. Mat.*, 2010, **9**, 741.
[115] F. Göltl, A. Grüneis, T. Bučko, and J. Hafner, *J Chem Phys.* 2012*,* **137**, 114111.
[116] F. Karlický, P. Lazar, M. Dubecký, and M. Otyepka, *J. Chem. Theory Comput.* 2013, **9**, 3670.
[117] J. P. Perdew, K. Burke, and M. Ernzerhof, *Phys. Rev. Lett.* 1996, **77**, 3865.
[118] D. Bohm and D. Pines, *Phys. Rev*. 1951, **82**, 625.
[119] D. Pines and D. Bohm, *Phys. Rev*. 1952, **85**, 338.
[120] D. Bohm and D. Pines, *Phys. Rev*. 1953, **92**, 609.
[121] J. Harl, L. Schimka, and G. Kresse, *Phys. Rev. B* 2010, **81**, 115126.
[122] A. Ren, P. Rinke, C. Joas, and M. Scheffler, *J. Mater. Sci.* 2012, **47**, 7447.
[123] H. Eshuis, J. E. Bates, and F. Furche, *Theor. Chem. Acc.* 2012, **131**, 1084.
[124] F. Karlický and M. Otyepka, *J. Chem. Theory Comput.* 2011, **7**, 2876.
[125] J. Filip, F. Karlický, Z. Marusak, P. Lazar, M. Černík, M. Otyepka, and R. Zboril, *J. Phys. Chem. C* 2014, **118**, 13817.
[126] F. Karlický and F. Karlický, *Int. J. Quant. Chem.* 2014, **114**, 987.

[127] M. Eder and K. Terakura, *Phys. Rev. B* 2001, **64**, 15426.
[128] P. Lazar and M. Otyepka, *J. Phys. Chem. C* 2012, **116**, 25470.
[129] T. H. Dunning, *J. Chem. Phys*. 1989, **90**, 1007.
[130] N. B. Balabanov and K. A. Peterson, *J. Chem. Phys*. 2005, **123**, 064107.
[131] R. Seeger and J. A. Pople, *J. Chem. Phys*. 1977, **66**, 3045.
[132] R. Bauernschmitt and R. Ahlrichs, *J. Chem. Phys.* 1996, **104**, 9047.
[133] W. Zhang, D. G. Truhlar, and M. Tang, *J. Chem. Theory Comput*. 2013, **9**, 3965.
[134] J. A. Pople, M. Head-Gordon, and K. Raghavachari, *J. Chem. Phys*. 1987, **87**, 5968.
[135] M. Douglas and N. M. Kroll, *Ann. Phys.* 1974, **82**, 89.
[136] B. A. Hess, *Phys. Rev. A* 1985, **32**, 756.
[137] B. A. Hess, *Phys. Rev. A* 1986, **33**, 3742.
[138] G. Jansen and B. A. Hess, *Phys. Rev. A* 1989, **39**, 6016.
[139] J. M. L. Martin, *ACS Symp. Ser*. 1998, **677**, 212.
[140] D. G. Truhlar, *Chem. Phys. Lett*. 1998, **294**, 45.
[141] A. Karton and J. M. L. Martin, *Theor. Chem. Acc*. 2006, **115**, 330.
[142] A. Halkier, T. Helgaker, P. Jørgensen, W. Klopper, H. Koch, O. Jeppe, and A. K. Wilson, *Chem. Phys. Lett*. 1998, **286**, 243.
[143] M. J. Frisch, G. W. Trucks, H. B. Schlegel, G. B. Scuseria, M. A. Robb, R. J. Cheeseman, G. Scalmani, V. Barone, B. Mennucci, and G. A. Petersson, et al. Gaussian 09, 2009.
[144] H.-J. Werner, P. J. Knowles, G. Knizia, F. R. Manby, M. Schu¨tz, P. Celani, T. Korona, R. Lindh, A. Mitrushenkov, G. Rauhut, K. R. Shamasundar, T. B. Adler, R. D. Amos, A. Bernhardsson, A. Berning, D. L. Cooper, M. J. O. Deegan, A. J. Dobbyn, F. Eckert, E. Goll, C. Hampel, A. Hesselmann, G. Hetzer, T. Hre- nar, G. Jansen, C. Ko¨ppl, Y. Liu, A. W. Lloyd, R. A. Mata, A. J. May, S. J. McNicholas, W. Meyer, M. E. Mura, A. Nicklass, D. P. O'Neill, P. Palmieri, K. Pflu¨ger, R. Pitzer, M. Reiher, T. Shiozaki, H. Stoll, A. J. Stone, R. Tarroni, T. Thorsteinsson, M. Wang, and A. Wolf, *Molpro*, version 2010.1; University of Birmingham: Birmingham, 2010.
[145] G. Kresse and J. Hafner, *Phys. Rev. B* 1993, **47**, 558. G. Kresse and J. Hafner, *Phys. Rev. B* 1994, **49**, 14251.
[146] G. Kresse and J. Furthmuller, *Phys. Rev. B* 1996, **54**, 11169.
[147] P. E. Blohl, *Phys. Rev. B* 1994, **50**, 17953.
[148] G. Kresse and D. Joubert, *Phys. Rev. B* 1999, **59**, 1758.
[149] A. Ren, P. Rinke, and M. Scheffler, *Phys. Rev. B* 2009, **80**, 045402.
[150] M. Methfessel and A. T. Paxton *Phys. Rev. B* 1989, **40**, 3616.
[151] G. Henkelman, B. P. Uberuaga, and H. Jonsson, *J. Chem. Phys.* 2000, **113**, 9901.

[152] E. Bitzek, P. Koskinen, F. Gahler, M. Moseler, and P. Gumbsch, *Phys. Rev. Lett*. 2006**,** **97**, 107201.
[153] D. Sheppard, R. Terrell, and G. Henkelman, *J. Chem. Phys.* 2008, **128**, 134106.
[154] X. Xu, W. Zhang, M. Tang, and D. G. Truhlar, *J. Chem. Theory Comput.* 2015, **11**, 2306.
[155] Y. Zhao, H. T. Ng, R. Peverati, and D. G. Truhlar, *J. Chem. Theory Comput*. 2012, **8**, 2824.
[156] Y. Zhao and D. G. Truhlar, *J. Phys. Chem. A* 2005, **109**, 6624.
[157] G. E. Scuseria, T. M. Henderson, and D. C. Sorensen, *J. Chem. Phys.* 2008, **129**, 231101.
[158] J. Zheng, Y. Zhao, and D. G. Truhlar, *J. Chem. Theory Comput*. 2009, **5**, 808.
[159] B. J. Lynch, Y. Zhao, and D. G. Truhlar, *J. Phys. Chem. A* 2005, **109**, 1643.
[160] Y. Zhao, B. J. Lynch, and D. G. Truhlar, *Phys. Chem. Chem. Phys.* 2005, **7**, 43.
[161] J. E. Mondloch, W. Bury, D. Fairen-Jimenez, S. Kwon, E. J. DeMarco, M. H. Weston, A. A. Sarjeant, S. T. Nguyen, P. C. Stair, R. Q. Snurr, O. K. Farha, and T. J. Hupp, *J. Am. Chem. Soc.* 2013, **135**, 10294.
[162] N. Planas, J. E. Mondloch, S. Tussupbayev, J. Borycz, L. Gagliardi, J. T. Hupp, O. K. Farha, and C. J. Cramer, *J. Phys. Chem. Lett.* 2014, **5**, 3716.
[163] M. J. Frisch, G. W. Trucks, H. B. Schlegel, G. E. Scuseria, M. A. Robb, J. R. Cheeseman, G. Scalmani, V. Barone, B. Mennucci, G. A. Petersson, H. Nakatsuji, M. Caricato, X. Li, H. P. Hratchian, A. F. Izmaylov, J. Bloino, G. Zheng, J. L. Sonnenberg, M. Hada, M. Ehara, K. Toyota, R. Fukuda, J. Hasegawa, M. Ishida, T. Nakajima, Y. Honda, O. Kitao, H. Nakai, T. Vreven, J. A. Montgomery, Jr., J. E. Peralta, F. Ogliaro, M. Bearpark, J. J. Heyd, E. Brothers, K. N. Kudin, V. N. Staroverov, R. Kobayashi, J. Normand, K. Raghavachari, A. Rendell, J. C. Burant, S. S. Iyengar, J. Tomasi, M. Cossi, N. Rega, J. M. Millam, M. Klene, J. E. Knox, J. B. Cross, V. Bakken, C. Adamo, J. Jaramillo, R. Gomperts, R. E. Stratmann, O. Yazyev, A. J. Austin, R. Cammi, C. Pomelli, J. W. Ochterski, R. L. Martin, K. Morokuma, V. G. Zakrzewski, G. A. Voth, P. Salvador, J. J. Dannenberg, S. Dapprich, A. D. Daniels, Ö. Farkas, J. B. Foresman, J. V. Ortiz, J. Cioslowski, and D. J. Fox, Gaussian 09, revision C01; Gaussian, Inc., Wallingford CT, 2009.
[164] R. Dovesi, R. Orlando, A. Erba, C. M. Zicovich-Wilson, B. Civalleri, S. Casassa, L. Maschio, M. Ferrabone, M. De La Pierre, P. D'Arco, Y. Noel, M. Causa, M. Rerat, and B. Kirtman, *Int. J. Quant. Chem.* 2014, **114**, 1287.
[165] Y. Zhao and D. G. Truhlar, *J. Chem. Phys.* 2006, **125**, 194101.
[166] Y. Zhao and D. G. Truhlar, *Theor. Chem. Acc.* 2008, **120**, 215.
[167] H. Yu and D. G. Truhlar, *J. Chem. Theory Comput.* 2014, **10**, 2291.
[168] R. Ditchfield, W. J. Hehre, and J. A. Pople, *J. Chem. Phys.* 1971, **54**, 724.

[169] W. J. Hehre and J. A. Pople, *J. Chem. Phys.* 1972, **56**, 4233.
[170] J. S. Binkley and J. A. Pople, *J. Chem. Phys.* 1977, **66**, 879.
[171] W. J. Hehre, R. Ditchfield, and J. A. Pople, *J. Chem. Phys.* 1972, **56**, 2257.
[172] M. M. Francl, W. J. Pietro, W. J. Hehre, J. S. Binkley, M. S. Gordon, D. J. Defrees, J. A. Pople, *J. Chem. Phys.* 1982, **77**, 3654.
[173] D. Andrae, U. Haussermann, M. Dolg, H. Stoll, and H. Preuss, *Theor. Chem. Acc.* 1990, **77**, 123.
[174] J. M. L. Martin and A. Sundermann, *J. Chem. Phys.* 2001, **114**, 3408.
[175] M. Kaupp, P. V. Schleyer, H. Stoll, and H. Preuss, *J. Chem. Phys.* 1991, **94**, 1360.
[176] I. M. Alecu, J. Zheng, Y. Zhao, D. G. Truhlar, *J. Chem. Theory Comput.* 2010, **6**, 2872.
[177] H. S. Yu, L. J. Fiedler, I. M. Alecu, and D. G. Truhlar, *Comp. Phys. Commun.* 2016, *submitted*.
[178] P. Rittmeyer, U. Weitelmann, Hydrides. In *Ullmann's Encyclopedia of Industrial Chemistry*; Wiley - CVH Verlag GmbH & Co. KGaA, 2000; pp 103-132.
[179] J.A. Pople, Rev. *Mol. Phys.* 1999, **71**, 1267.
[180] H. H. Nielsen, *Encycl. Phys.* 1959, **37**, 173.
[181] I. M. Mills, In Molecular Spectroscopy: Modern Research; edited by K. N. Rao and C. W. Mathews; Academic: New York, 1972; pp. 115-140.
[182] Q. Zhang, P.N. Day, D.G. Truhlar, *J. Chem. Phys.* 1993, **98**, 4948.
[183] K.M. Kuhler, D.G. Truhlar, and A.D. Isaacson, *J. Chem. Phys.* 1996, **104**, 4664.
[184] A.D. Isaacson, *J. Chem. Phys.* 1998, **108**, 9978.
[185] V. Barone, *J. Chem. Phys.* 2005, **122**, 014108.
[186] J. Bloino, M. Biczyzko, and V. Barone, *J. Chem. Theory Comput.* 2012, **8**, 1015.
[187] R. J. Whitehead and N. C. Handy, *J. Mol. Spectrosc.* 1975, **55**, 356.
[188] S. Carter and N. C. Handy, *Phys. Rep.* 1986, **5**, 117.
[189] S. C. Tucker, T. C. Thompson, J. G. Lauderdale, and D. G. Truhlar, *Comput. Phys. Commun.* 1988, **51**, 233.
[190] B. T. Sutcliffe, S. Miller, and J. Tennyson, *Comput. Phys. Commun.* 1988, **51**, 73.
[191] D. H. Zhang and J. Z. H. Zhang, *J. Chem. Phys.* 1993, **99**, 6624.
[192] S. Carter, J. M. Bowman, and N. C. Handy, *Theor. Chem. Acc.* 1998, **100**, 191.
[193] M. Mladenovic and M. Lewerenz, *Chem. Phys. Lett.* 2000, **321**, 135.
[194] Y. Volobuev, W. C. Necoechea, and D. G. Truhlar, *Chem. Phys. Lett.* 2000, **330**, 471.
[195] D.P. Tew, N.C. Handy, and S. Carter, *Phys. Chem. Chem. Phys.* 2001, **3**, 1958.
[196] A. Chakraborty, D. G. Truhlar, J. M. Bowman, and S. Carter, *J. Chem. Phys.* 2004, **121**, 2071.
[197] S. L. Mielke, A. Chakraborty, and D. G. Truhlar, *J. Phys. Chem. A* 2013, **117**, 7327.
[198] R.D. Johnson III, K.K. Irikura, R.N. Kacker, and R. Kessel, *J. Chem. Theory Comput.* 2010, **6**, 2822.

[199] J.A. Pople, A.P. Scott, M.W. Wong, and L. Radom, Isr. *J. Chem.* 1993, **33**, 345.
[200] A.P. Scott and L. Radom, *J. Phys. Chem.* 1996, **100**, 16502.
[201] I.M. Alecu, J. Zheng, Y. Zhao, and D.G. Truhlar, *J. Chem. Theory Comput.* 2010, **6**, 2872.
[202] Y. Zhao and D.G. Truhlar, *Theor. Chem. Acc.* 2008, **120**, 215.
[203] P.L. Fast, J. Corchado, M.L. Sanchez, and D.G. Truhlar, *J. Phys. Chem. A* 1999, **103**, 3139.
[204] K.K. Irikura, *J. Phys. Chem. Ref. Data,* 2007, **36**, 389.
[205] R.S. Grev, C.L. Janssen, and H.F. Schaefer III, *J. Chem. Phys.* 1991, **95**, 5128.
[206] J.M.L. Martin, *J. Chem. Phys.* 1992, **97**, 5012.
[207] M.J. Frisch, G.W. Trucks, H.B. Schlegel, G.E. Scuseria, M.A. Robb, J.R. Cheeseman, J.A.J. Montgomery, T. Vreven, K.N. Kudin, J.C. Burant, J.M. Millam, S.S. Iyengar, J. Tomasi, V. Barone, B. Mennucci, M. Cossi, G. Scalmani, N. Rega, G.A. Petersson, H. Nakatsuji, M. Hada, M. Ehara, K. Toyota, R. Fukuda, J. Hasegawa, M. Ishida, T. Nakajima, Y. Honda, O. Kitao, H. Nakai, M. Klene, X. Li, J.E. Knox, H.P. Hratchian, J.B. Cross, V. Bakken, C. Adamo, J. Jaramillo, R. Gomperts, R.E. Stratmann, O. Yazyev, A.J. Austin, R. Cammi, C. Pomelli, J.W. Ochterski, P.Y. Ayala, K. Morokuma, G.A. Voth, P. Salvador, J.J. Dannenberg, V.G. Zakrzewski, S. Dapprich, A.D. Daniels, M.C. Strain, O. Farkas, D.K. Malick, A.D. Rabuck, K. Raghavachari, J.B. Foresman, J.V. Ortiz, Q. Cui, A.G. Baboul, S. Clifford, J. Cioslowski, B.B. Stefanov, G. Liu, A. Liashenko, P. Piskorz, I. Komaromi, R.L. Martin, D.J. Fox, T. Keith, A.-L.M. A, C.Y. Peng, A. Nanayakkara, M. Challacombe, P.M.W. Gill, B. Johnson, W. Chen, M.W. Wong, C. Gonzalez, and J.A. Pople, Gaussian 03, revision E.01; Gaussian, Inc., (Wallingford, CT, 2004).
[208] M.J. Frisch, G.W. Trucks, H.B. Schlegel, G.E. Scuseria, M.A. Robb, J.R. Cheeseman, G. Scalmani, V. Barone, B. Mennucci, G.A. Petersson, H. Nakatsuji, M. Caricato, X. Li, H.P. Hratchian, A.F. Izmaylov, J. Bloino, G. Zheng, J.L. Sonnenberg, M. Hada, M. Ehara, K. Toyota, R. Fukuda, J. Hasegawa, M. Ishida, T. Nakajima, Y. Honda, O. Kitao, H. Nakai, T. Vreven, J.A.J. Montgomery, J.E. Peralta, F. Ogliaro, M. Bearpark, J.J. Heyd, E. Brothers, K.N. Kudin, V.N. Staroverov, R. Kobayashi, J. Normand, K. Raghavachari, A. Rendell, J.C. Burant, S.S. Iyengar, J. Tomasi, M. Cossi, N. Rega, J.M. Millam, M. Klene, J.E. Knox, J.B. Cross, V. Bakken, C. Adamo, J. Jaramillo, R. Gomperts, R.E. Stratmann, O. Yazyev, A.J. Austin, R. Cammi, C. Pomelli, J.W. Ochterski, R.L. Martin, K. Morokuma, V.G. Zakrzewski, G.A. Voth, P. Salvador, J.J. Dannenberg, S. Dapprich, A.D. Daniels, O. Farkas, J.B. Foresman, J.V. Ortiz, J. Cioslowski, and D.J. Fox, Gaussian 09, revision A.02; Gaussian, Inc., (Wallingford, CT, 2009).
[209] A. D. Becke, *Phys. Rev. A* 1998, **38**, 3098.
[210] C. Lee, W. Yang, and R. G. Parr, *Phys. Rev. B* 1988, **37**, 785.

[211] R. Krishnan, J. S. Binkley, R. Seeger, and J. A. Pople, *J. Chem. Phys.* 1980, **72**, 650.
[212] A. D. McLean and G. S. Chandler, *J. Chem. Phys.* 1980, **72**, 5639.
[213] J. Zheng, T. Yu, E. Papajak, I, M. Alecu, S. L. Mielke, and D. G. Truhlar, *Phys. Chem. Chem. Phys.* 2011, **13**, 10885.
[214] J. Zheng, S. L Mielke, K. L Clarkson, and D. G. Truhlar, *Comput. Phys. Commun.* 2012, **183**, 1803.
[215] J. Zheng and D. G. Truhlar, *J. Chem. Theory Comput.* 2013, **9**, 1356.
[216] J. Zheng, R. Meana-Pañeda, and D. G. Truhlar, *Comput. Phys. Commun.* 2013, **184**, 2032.
[217] J. Zheng, R. Meana-Pañeda, and D. G. Truhlar, *J. Amer. Chem. Soc.* 2014, **136**, 5150.

Table 6.1 Bond Dissociation Energy, Charge on Ca in CaO and Excitation Energy of Ca^+(s). Sorted in Order of Increasing Magnitude of excitation energy.

	BDE	q(Ca)	EE Ca^+(s)
MN12-L	96.2	0.99	10.5
ωB97	102.5	1.17	16.3
M06-L	114.4	0.98	16.4
MN12-SX	98	1.06	17.2
τ-HTCHhyb	113.4	1.01	18.8
M11-L	91.9	0.95	19.3
N12-SX	109.5	1.04	20.5
OreLYP	116.8	0.9	20.8
M11	110.4	1.15	21
OLYP	118.9	0.91	21.3
revTPSS	115.3	0.94	21.5
BPW91	123.5	0.92	21.9
TPSSh	110.5	0.99	21.9
revTPSSVP86	116.8	0.94	22.5
mPWPW	124.9	0.92	22.8
N12	117.3	0.91	22.8
O3LYP	110.8	0.96	22.8
BP86	124.6	0.92	23.1
PW91	126.3	0.92	23.7
ωB97X-D	103.3	1.11	23.8
B97-1	106.4	1.02	23.9
PBEsol	132.8	0.92	24.1
PBE	124.3	0.92	24.3
MOHLYP	111.8	0.89	24.5
OHLYP	101.4	0.89	24.5
SOGGA	132.4	0.92	24.6
M06	102	1.04	25
B97-3	100.8	1.04	25.4
SOGGA11-X	92.6	1.1	25.7
BLYP	118.6	0.9	25.9

GVWN5	146.2	0.93	26.3
PBE0	103	1.04	26.4
HSE	102.8	1.03	26.7
M05-2X	93.6	1.14	26.9
M08-HX	94.7	1.12	27.1
B3LYP*	110	0.98	27.2
MPWLYP1M	115.4	0.92	27.3
M05	101	1.04	27.4
B3LYP	104.5	1.01	27.5
PW6B95	102.8	1.04	27.7
OptX	83.4	0.86	27.9
SOGGA11	123	0.92	28.1
CAM-B3LYP	102.3	1.09	28.2
MPW1B95	101.5	1.05	28.2
B1LYP	97.2	1.02	28.7
ωB97X	101.4	1.15	28.8
MPWB1K	91.6	1.11	29.4
M08-SO	90.1	1.12	31.4
B88X	-13	1.48	32.2
M06-2X	89.4	1.12	32.7
PBEX	85.3	0.85	34.6
HFLYP	48.3	1.29	35.7
HF	12	1.29	43.4

Table 6.2 Comparison of Chemical Properties of CaO Calculated by six Functionals

Property	MOHLYP	BLYP	B3LYP	M05	MPWB1K	M06-2X	Exp.
Dipole Moment (Debye)	7.8	7.9	8.8	9.1	9.7	9.8	8.7
Charge distribution of 8σ orbital	18.2% Ca 81.8% O	18.0% Ca 82.0% O	16.0% Ca 84.0% O	15.7% Ca 84.3% O	14.0% Ca 86.0% O	14.1% Ca 85.9% O	
Charge distribution of $3\pi_x$ and $3\pi_y$ orbitals	9.3% Ca 90.7% O	9.3% Ca 90.7% O	8.6% Ca 91.4% O	8.5% Ca 91.5% O	8.3% Ca 91.7% O	8.0% Ca 92.0% O	
BDE (kcal/mol)	111.8	118.6	104.5	101.0	91.6	89.4	95.8
IP (kcal/mol)	136.9	139.6	141.6	141.7	136.1	144.2	141.0
EA (kcal/mol)	35.4	42.1	38.8	31.6	26.3	32.5	33.9
EE (kcal/mol)	24.5	25.9	27.5	27.4	29.4	32.7	39.1
IE (kcal/mol)	237.8	242.0	234.9	238.5	230.8	233.9	242.0

Table 6.3 Average Mean Unsigned Errors (AUE) over 25 Energetic Data (8IP, 3EA, 6IE, and 8BDE) from Eight SR Molecules, 20 Energetic Data (3IP, 2EA, 3EE, 5IE and 7BDE) from Seven MR Molecules, and 43 Energetic Data (8IP, 4EA, 3EE, 13IE, 15BDE) from All 15 Molecules, Arranged by Type of Functional and Sorted in Order of Increasing Magnitude of the Overall Error (kcal/mol) for Each Type.

		AUE		
Type	Method	SR	MR	All
LSDA	GVWN5	10.96	17.17	13.88
GGA	OreLYP	3.61	5.72	4.63
	OLYP	3.60	6.78	5.03
	MOHLYP	4.56	6.64	5.54
	PBE	4.47	7.20	5.60
	BLYP	4.71	7.18	5.70
	BB95	4.96	7.83	6.15
	SOGGA	4.60	9.10	6.54
	SOGGA11	7.49	8.96	8.09
	OHLYP	8.53	13.45	10.58
	HFLYP	11.44	17.38	14.04
NGA	GAM	2.65	6.82	4.59
	N12	5.52	8.21	6.50
meta-GGA	revTPSS	2.56	5.85	4.05
	TPSS	2.75	5.68	4.08
	M06-L	5.92	10.87	8.19
	M11-L	7.34	10.93	9.08
meta-NGA	MN12-L	5.45	11.19	7.96
global hybrid GGA	B97-1	2.64	6.47	4.37
	O3LYP	3.30	6.81	4.93
	B97-3	2.71	7.57	4.94
	B3LYP*	3.95	6.86	5.21
	MPWLYP1M	4.80	6.26	5.37
	B1LYP	3.92	7.10	5.38
	B3LYP	3.85	7.30	5.40
	revB3LYP	3.64	7.28	5.42
	B1B95	3.24	8.39	5.49
	PBE0	4.10	7.17	5.49
	SOGGA11-X	3.77	7.79	5.68

	MPW1K	5.19	11.20	7.87
global hybrid meta-GGA	PW6B95	2.85	5.39	4.14
	M08-HX	2.46	6.02	4.18
	M05-2X	2.73	6.10	4.34
	τ-HCTHhyb	2.98	6.12	4.42
	M05	3.16	6.10	4.50
	M06-2X	3.80	6.54	5.08
	M06	3.36	7.36	5.14
	M08-SO	2.77	7.82	5.15
	MPW1B95	3.15	7.86	5.20
	TPSSh	5.37	7.03	6.20
	BB1K	4.27	9.89	6.68
	MPWB1K	4.25	11.12	7.25
	revTPSSh	9.15	9.44	9.49
range-separated hybrid GGA	HSE06	3.60	6.81	5.03
	CAM-B3LYP	3.62	7.49	5.37
	ωB97	4.14	7.45	5.55
	ωB97X	4.13	8.92	6.18
range-separated hybrid NGA	N12-SX	2.86	7.26	4.70
range-separated hybrid meta-	M11	3.46	7.45	5.33
range-separated hybrid meta-	MN12-SX	5.78	8.67	7.10
DFT-D	PW6B95-	2.86	5.21	4.05
	PW6B95-D3	2.87	5.28	4.08
	ωB97X-D	2.76	7.82	5.09

Table 6.4 Mean Unsigned Errors and Mean Signed Errors of 54 Methods Over 13 Geometric Data from 12 Main-group Molecules Sorted in the order of Increasing Magnitude of MUE(Å)

Name	MUE	MSE
B3LYP*	0.011	0.004
revTPSSh	0.011	0.004
revB3LYP	0.011	0.001
TPSSh	0.012	0.003
B3LYP	0.012	0.003
τ-HCTHhyb	0.012	0.008
B97-1	0.012	0.003
B1LYP	0.012	0.002
MN12-L	0.012	0.002
HSE	0.012	-0.004
M06-L	0.013	-0.002
B1B95	0.013	-0.004
revTPSS	0.013	0.010
TPSS	0.013	0.002
MN12-SX	0.013	0.000
PBE	0.013	-0.005
M05-2X	0.013	-0.002
M08-SO	0.013	0.004
M08-HX	0.013	0.002
SOGGA11	0.013	-0.004
PW6B95-D3(BJ)	0.013	-0.004
PW6B95-D3(0)	0.013	-0.004
GAM	0.014	0.008
MPW1B95	0.014	-0.006
B97-3	0.014	0.001
PBE0	0.014	0.011
M06-2X	0.014	-0.004
M05	0.014	-0.002
N12-SX	0.015	-0.007
MPWLYP1M	0.015	0.014
SOGGA11-X	0.015	0.001

O3LYP	0.015	0.008
M06	0.015	-0.005
CAM-B3LYP	0.016	-0.007
BB95	0.016	0.015
ωB97X-D	0.017	0.000
BB1K	0.018	-0.012
ωB97X	0.018	0.000
M11	0.019	0.003
N12	0.019	-0.012
BLYP	0.019	0.019
MPWB1K	0.019	-0.013
MPW1K	0.019	-0.014
ωB97	0.020	0.001
OreLYP	0.020	0.017
OLYP	0.021	0.018
PW6B95	0.022	0.007
Hartree-Fock	0.022	-0.007
M11-L	0.023	-0.017
GVWN5	0.024	-0.013
MOHLYP	0.034	0.034
OHLYP	0.036	0.036
HFLYP	0.038	-0.035
SOGGA	0.211	0.196

Table 6.5 Mean Unsigned Errors and Mean Signed Errors of Dipole Moment of All 15 Molecules Sorted in Order of Increasing Magnitude of the Error (Debye)

Method	MUE	MSE
MPWLYP1M	0.43	-0.13
PBE	0.49	-0.28
O3LYP	0.50	0.20
SOGGA	0.51	-0.26
MOHLYP	0.52	0.35
PW6B95-D3(0)	0.54	0.35
PW6B95-D3(BJ)	0.54	0.04
PW6B95	0.55	0.38
B1LYP	0.57	0.32
B3LYP	0.58	0.36
revTPSS	0.58	0.20
TPSS	0.60	0.21
TPSSh	0.60	0.35
M06-L	0.64	0.41
HSE	0.64	0.38
N12	0.66	0.09
BLYP	0.66	-0.03
τ-HCTHhyb	0.67	0.46
B3LYP*	0.67	0.33
GAM	0.68	0.35
revTPSSh	0.69	0.45
PBE0	0.71	0.56
OreLYP	0.72	-0.05
GVWN5	0.72	0.15
B97-1	0.72	0.56
MPWB1K	0.75	0.37
MN12-SX	0.75	0.62
B97-3	0.76	0.66
OHLYP	0.76	0.24
OLYP	0.77	0.00
M06	0.79	0.62
M08-SO	0.82	0.74

M08-HX	0.82	0.71
M11-L	0.82	0.55
M06-2X	0.83	0.68
M05	0.84	0.64
N12-SX	0.85	0.72
revB3LYP	0.85	0.64
B1B95	0.86	0.72
MN12-L	0.87	0.71
CAM-B3LYP	0.88	0.65
BB1K	0.88	0.59
SOGGA11-X	0.89	0.80
MPW1B95	0.93	0.77
M05-2X	0.95	0.88
ωb97X	0.96	0.83
ωB97X-D	0.98	0.86
BB95	1.00	0.31
MPW1K	1.07	0.57
SOGGA11	1.08	0.23
M11	1.08	0.84
ωB97	1.12	1.05
HFLYP	1.29	0.76
Hartree–Fock	1.63	0.47

Table 6.6 Reaction energies, enthalpies, and free energies for reactions 1-13 in kcal/mol

Reaction	*ΔE*	*ΔH*	*ΔG*
1	-67.7	-68.4	-81.3
2	29.6	28.7	17.8
3	-124.2	-124.6	-133.2
4	57.3	55.6	45.9
5	84.5	83.2	73.7
6	628.8	627.5	618.8
7	-217.3	-217.4	-229.8
8	-94.3	-94.8	-106.8
9	-41.5	-41.6	-53.9
10	191.9	184.4	184.6
11	-8.0	9.2	-20.8
12	-93.1	-93.7	-105.7
13	-99.3	-99.6	-111.4

Table 6.7 Hirshfeld Charges and CM5 Charges of T_d structures of IrO_4^+ and PtO_4^{2+}

	IrO_4^+		PtO_4^{2+}	
Center	CM5	Hirshfeld	CM5	Hirshfeld
Pt or Ir	1.63	1.01	1.85	1.28
O	-0.16	0.00	0.04	0.18

Table 6.8 Hirshfeld, CM5, and density dipole moments (in Debye) of the polar structures of PtO_4^{2+} and IrO_4^+

Dipole Moment	CM5	Hirshfeld	density
IrO_4^+ (C_{2v})	2.16	1.95	2.00
PtO_4^{2+} (C_{2v})	1.55	1.56	1.98
IrO_4^+ (C_s)	0.38	0.65	0.71
PtO_4^{2+} (C_s)	8.19	7.82	7.57

Table 6.9 Mean Errors (kcal per mole of water molecules) for Electrostatically Embedded Many-Body Approximations

Method	EE-3B	EE-PA
Mean Unsigned Error in 28 Relative Binding Energies (average: 0.651; standard deviation: 0.395)		
CCSD(T)-F12b/cc-pVDZ-F12	0.009	0.038
CCSD-F12b/cc-pVDZ-F12	0.031	0.054
Mean Signed Error in 8 Absolute Binding Energies[a] (average: −5.02; standard deviation: 0.54)		
CCSD(T)-F12b/cc-pVDZ-F12	−0.015	−0.070
CCSD-F12b/cc-pVDZ-F12	0.47	0.39

[a] The MUE in the absolute binding energy is for all cases the absolute value of the mean signed error. The absolute binding energy is negative, and a negative (positive) signed error corresponds to overbinding (underbinding)

Table 6.10 Relative computer times[a] for a calculation on $(H_2O)_{26}$

Method	EE-3B	EE-PA	3B	PA[a]
CCSD(T)-F12b/cc-pVDZ-F12	1500	15		
CCSD-F12b/cc-pVDZ	440	6		
M11/maug-cc-pVTZ	50	4	50	4
M11/MG3S	50	5	50	5
M06-2X/MG3S	15	1	50	1

[a] Rounded to nearest integer if less than ten or to the nearest round number otherwise.

Table 6.11 Mean Errors (kcal per mole of water molecules) for Many-Body and Electrostatically Embedded Many-Body Approximations

Method	EE-3B	EE-PA	3B	PA
Mean Unsigned Error in 28 Relative Binding Energies (average: 0.651; standard deviation: 0.395)				
M11/maug-cc-pVTZ	0.064	0.032	0.058	0.27
M11/MG3S	0.063	0.029	0.056	0.24
M06-2X/MG3S	0.046	0.061	0.050	0.23
Mean Signed Error in 8 Absolute Binding Energies[a] (average: -5.02; standard deviation: 0.54)				
M11/maug-cc-pVTZ	0.39	0.55	0.34	0.89
M11/MG3S	−0.092	0.042	-0.12	0.30 (0.31)
M06-2X/MG3S	−0.37	−0.73	−0.36	−0.48

[a] The MUE in the absolute binding energy is given in parenthesis when it differs from the MSE. The absolute binding energy is negative, and a negative (positive) signed error corresponds to overbinding (underbinding). For the EE calculations, for each method we calculated a new set of embedding charges with the method under consideration but the differences are small (values are given in the Supporting Information).

Table 6.12 The mechanism of the water splitting reaction on Fe(0)

Step	Description	Reaction
R1	Formation of first vdW complex	$Fe + H_2O \rightarrow Fe\ldots OH_2$
R2	Hydrogen migration reaction	$Fe\ldots OH_2 \rightarrow HFeOH$
R3	Formation of second vdW complex	$HFeOH + H_2O \rightarrow HFeOH\ldots H_2O$
R4	Dehydrogenation	$HFeOH\ldots H_2O \rightarrow HOFeOH\ldots H_2$
R5	Dissociation of third vdW complex	$HOFeOH\ldots H_2 \rightarrow HOFeOH + H_2$
overall (R_O)	Water splitting on Fe(0)	$Fe + 2H_2O \rightarrow HOFeOH + H_2$

Table 6.13. Density functionals tested in the current work

Type	Exchange	Correlation	Standard name
generalized gradient approx. (GGA)	local	local	BLYP
			MOHLYP
			MPWLYP1W
			PBE
			PBEsol
			PBE1W
			PBELYP1W
			SOGGA
			SOGGA11
nonseparable gradient approx. (NGA)	local	local	N12
meta-GGA	local	local	M06-L
			revTPSS
			TPSSLYP1W
			T-HCTH
range separated meta-GGA	local	local	M11-L
meta-NGA	local	local	MN12-L
global-hybrid GGA	nonlocal	local	B3LYP
			B97-1
			B97-2
			B97-3
			MPW1K
			PBE0
			SOGGA11-X
global-hybrid meta-GGA	nonlocal	local	M05
			M05-2X
			M06
			M06-2X
			M06-HF
			M08-HX
			M08-SO
			PW6B95
			PWB6K
range-separated-hybrid GGA	nonlocal	local	ωB97X

range-separated-hybrid meta-GGA	nonlocal	local	M11
screened-exchange hybrid GGA	nonlocal	local	HSE06
screened-exchange hybrid NGA	nonlocal	local	N12-SX
screened-exchange hybrid meta-NGA	nonlocal	local	MN12-SX
meta-GGA +MM[a]	nonlocal	local	M06-L-D3
global-hybrid meta-GGA +MM[a]	nonlocal	local	PW6B95-D3(BJ)
range-separated hybrid GGA +MM[a]	nonlocal	local	ωB97X-D
Exact exchange + nonlocal	nonlocal	nonlocal	EXX-RPA@PBE

[a] +MM denotes the addition of a molecular mechanics damped dispersion term.

Table 6.14 Relative energies (in units of kcal/mol) of various species at CCSD(T)-3*s*3*p*-DKH level of theory for Fe(0)–H_2O system based on the B97-1/cc-pVTZ geometries

Basis set	Fe+2H_2O	Fe–OH_2+H_2O	TS1+H_2O	HFeOH +H_2O	HFeOH– H_2O	TS2	Fe$(OH)_2$–H_2	Fe$(OH)_2$ +H_2	MUD
TZ[a]	0.00	-3.72	27.46	-26.68	-43.34	-24.19	-47.52	-45.33	1.57
aTZ[b]	0.00	-2.57	27.41	-27.69	-43.14	-24.27	-49.14	-46.83	0.90
aQZ[c]	0.00	-2.78	27.01	-28.11	-43.78	-25.19	-49.81	-47.23	0.38
CBS(TZ, QZ)[d]	0.00	-2.90	26.90	-28.40	-44.20	-25.70	-50.20	-47.30	0.12
CBS(aTZ, aQZ)-1[e]	0.00	-2.93	26.64	-28.54	-44.43	-26.13	-50.49	-47.67	0.14
CBS(aTZ, aQZ)-2[f]	0.00	-2.90	26.61	-28.64	-44.55	-26.31	-50.63	-47.77	0.24
CBS(aTZ, aQZ)-3[g]	0.00	-2.84	26.77	-28.44	-44.26	-25.88	-50.32	-47.57	0.00
Standard deviation	0.00	0.04	0.13	0.11	0.16	0.27	0.19	0.20	
Standard deviation	0.00	0.05	0.09	0.10	0.15	0.22	0.16	0.10	

[a] cc-pwCVTZ-DK for Fe, cc-pVTZ for O, cc-pVTZ for H; [b] cc-pwCVTZ-DK for Fe, aug-cc-pVTZ for O, cc-pVTZ for H; [c] cc-pwCVQZ-DK for Fe, aug-cc-pVQZ for O, cc-pVQZ for H; [d] CBS limits extrapolated from TZ and QZ data points, as reported in ref 116; [e] CBS limits extrapolated from ATZ and AQZ data points using eq. **Error! Reference source not found.** with α=3.4, β=2.4; [f] CBS limits extrapolated from ATZ and AQZ data points using eqn **Error! Reference source not found.** with α = 4.93, β = 2.13; [g] CBS limits extrapolated from ATZ and AQZ data points using eqs. **Error! Reference source not found.**, **Error! Reference source not found.**, and **Error! Reference source not found.**.

Table 6.15. The calculated errors (kcal/mol) of CCSD(T)-3s3p-DKH/CBS calculations for the bond dissociation energies of FeH and FeCl as compared to experimental data

	Errors						D*e*
	aTZ[a]	aQZ[b]	CBS[c]	aTZ′[d]	aQZ′[e]	CBS′[f]	(Exp.)[g,h]
FeH[h,i]	2.1	4.6	6.3	2.1	4.6	6.3	36.9
FeCl[h,j]	-1.0	1.6	3.3	-1.2	1.3	2.9	78.5
MUE[k]	1.6	3.1	4.8	1.6	2.9	4.6	

[a] aTZ basis set: cc-pwCVTZ-DK for Fe, aug-cc-pVTZ for Cl, cc-pVTZ for H

[b] aQZ basis set: cc-pwCVQZ-DK for Fe, aug-cc-pVQZ for Cl, cc-pVQZ for H

[c] CBS(aTZ, aQZ)-3: CBS limits extrapolated from aTZ and aQZ data points by using eqs 1, 2, and 3

[d] aTZ′ basis set: cc-pwCVTZ-DK for Fe, aug-cc-pVTZ-DK for Cl, cc-pVTZ-DK for H

[e] aQZ′ basis set: cc-pwCVQZ-DK for Fe, aug-cc-pVQZ-DK for Cl, cc-pVQZ-DK for H

[f] CBS′(aTZ′, aQZ′)-3: CBS limits extrapolated from aTZ and aQZ data points by using eqs 1, 2, and 3

[g] Experimental

[h] Experimental data and spin-orbit energies of molecules and atoms are from tables compiled by X. Xu, W. Zhang, M. Tang, and D. G. Truhlar, unpublished

[i] The bond lengths of FeH ($^4\Delta$) used in the calculations is 1.630 Å

[j] The bond length of FeCl ($^6\Delta$) used in the calculations is 2.179 Å

[k] MUE is the mean unsigned error of bond energies of the two molecules compared to experimental data.

Table 6.16 Classical (zero-point-energy exclusive) energies of reaction ΔE_{rxn} for reactions R1-R5 and the overall reaction R_O; forward and reverse classical barrier heights for reactions R2 and R4[a]. Mean unsigned deviations (MUDs) are computed with respect to CCSD(T)-3*s*3*p*-DK/CBS results. (Units: kcal/mol)

xc	R1	R2	R2	R2	R3	R4	R4	R4	R5	R_o	barrier heights		TK
GGA and NGA functionals													
MOHLYP	-6.06	19.8	43.38	-23.58	-8.72	11.6	21.77	-10.18	-2.61	-51.14	7.77	-7.77	5.65
PBELYP1W	-11.12	19.79	42.67	-22.89	-14.97	12.21	23.23	-11.02	1.49	-58.49	7.43	-7.43	5.87
BLYP	-10.24	18.75	42.45	-23.69	-13.94	11.7	22.58	-10.88	0.48	-58.28	8.04	-8.04	6.11
N12	-9.51	20.25	41.78	-21.53	-14.92	9.45	20.13	-10.68	0.93	-55.71	9.00	-9.00	6.22
MPWLYP1W	-11.39	19.06	42.38	-23.32	-15.16	11.77	21.55	-9.78	0.27	-59.38	8.22	-8.22	6.24
PBE1W	-11.58	17.81	41.76	-23.95	-15.21	11.01	20.7	-9.69	1.69	-58.73	9.09	-9.09	6.32
PW91[e]	-13.00	16.7	41.4	-24.7	-16.4	12.8	23.1	-10.3	3.8	-60.6	8.41	-8.41	6.36
PBE	-12.47	16.61	40.86	-24.25	-16.25	10.31	19.11	-8.81	2.22	-59.56	10.18	-10.18	6.74
SOGGA11	-8.93	18.6	41.16	-22.56	-11.13	7.46	16.43	-8.98	-1.3	-52.89	10.99	-10.99	7.01
PBEsol	-14.99	13.78	39.14	-25.36	-19.3	8.68	15.78	-7.1	3.62	-63.12	12.56	-12.56	8.36
SOGGA	-15.28	13.21	38.62	-25.41	-18.4	7.16	14.89	-7.72	3.74	-63.08	13.44	-13.44	8.71
Meta-GGA and meta-NGA functionals													
M11-L	-11.56	30.31	45.78	-15.47	-15.67	15.81	23.53	-7.71	1.01	-49.41	3.40	-3.05	3.78
M06-L	-11.39	23.7	50.24	-26.54	-19.05	16.53	21.72	-5.19	4.11	-58.06	3.86	-3.86	4.09
MN12-L	-14.10	31.33	44.16	-12.83	-16.96	18.38	23.39	-5.01	1.83	-47.05	3.46	-2.59	4.15
M06-L-D3	-11.38	23.33	49.88	-26.56	-19.08	16.52	21.72	-5.20	4.14	-58.07	4.04	-4.04	4.17
τHCTH	-10.17	18.83	45.36	-26.52	-15.89	10.71	19.72	-9.02	2.32	-59.29	8.25	-8.25	5.64
TPSSLYP1W	-11.24	18.48	46.41	-27.94	-14.95	12.22	26.95	-14.73	1.31	-67.54	7.15	-5.89	7.03

revTPSS	-12.00	15.03	46.83	-31.8	-15.95	11.79	25.09	-13.3	1.63	-71.43	7.55	-7.22	7.79

continued on next page

Table 6.16 Continued.

xc	R1	R2	R2	R2	R3	R4	R4	R4	R5	R_o	barrier heights		TK
Hybrid GGA and hybrid NGA functionals													
B97-3	-5.19	29.30	53.46	-24.16	-13.77	16.26	22.56	-6.30	1.54	-47.88	1.51	-1.51	1.36
ωB97X-D	-7.33	29.16	55.18	-26.01	-16.24	17.03	22.74	-5.71	2.92	-52.37	0.88	-0.88	1.42
MPW1K	-4.64	28.23	56.15	-27.92	-15.42	17.85	21.37	-3.52	1.96	-49.54	1.48	-1.01	1.57
SOGGA11-X	-1.85	33.50	55.76	-22.26	-16.69	18.58	22.10	-3.52	3.15	-41.17	1.75	0.58	2.15
B97-2	-6.15	26.98	52.25	-25.28	-14.37	14.32	21.20	-6.88	1.81	-50.88	3.22	-3.22	2.30
ωB97X	-7.63	29.99	58.14	-28.16	-18.46	17.82	23.22	-5.40	4.48	-55.16	1.27	0.39	2.51
B97-1[e]	-7.60	26.60	51.20	-24.60	-16.00	14.40	21.20	-6.80	2.90	-52.10	3.56	-3.56	2.56
B3LYP	-8.81	25.52	49.75	-24.23	-14.55	15.17	22.85	-7.68	1.32	-53.95	3.58	-3.58	3.24
PBE0	-9.12	23.68	50.10	-26.42	-15.80	14.75	20.01	-5.26	2.32	-54.28	4.77	-4.77	3.42
HSE06[e]	-10.30	24.70	49.60	-24.90	-16.20	15.20	20.00	-4.80	2.10	-54.10	4.53	-4.53	3.51
N12-SX	-10.92	25.79	51.08	-25.29	-16.40	13.18	20.73	-7.55	2.52	-57.64	4.21	-4.21	3.76

continued on next page

Table 6.16 Continued.

xc functional	R1 ΔE_{rxn}	R2 V_f	R2 V_r	R2 ΔE_{rxn}	R3 ΔE_{rxn}	R4 V_f	R4 V_r	R4 ΔE_{rx}	R5 ΔE_{rxn}	R_o ΔE_{rxn}	barrier MU	barrier MSD[c]	TK MUD[d]
Hybrid-meta GGA and hybrid meta-NGA functionals													
PWB6K	-4.12	31.63	57.45	-25.82	-17.11	18.75	22.85	-4.10	3.08	-48.07	1.56	0.77	1.18
M06-2X	-3.96	34.19	57.16	-22.97	-19.57	18.18	24.07	-5.89	4.89	-47.50	1.77	1.50	1.70
M05-2X	-1.33	34.87	60.41	-25.53	-18.86	17.22	23.32	-6.10	4.38	-47.45	3.18	2.05	1.91
M05	-4.55	31.60	52.26	-20.67	-17.98	16.71	22.76	-6.05	3.61	-45.63	2.07	-1.07	1.99
PW6B95	-7.95	26.66	51.47	-24.81	-16.04	15.95	22.71	-6.76	2.45	-53.12	2.71	-2.71	2.35
PW6B95-D3BJ	-8.48	26.79	51.45	-24.67	-16.62	15.93	22.65	-6.72	2.80	-53.69	2.70	-2.70	2.50
M08-HX	-4.73	33.50	61.21	-27.71	-19.03	19.22	22.24	-3.02	4.32	-50.17	3.23	2.14	2.74
M08-SO	-4.84	35.73	56.09	-20.35	-18.66	20.02	23.28	-3.26	4.07	-43.03	2.45	1.88	2.85
MN12-SX	-	32.81	55.08	-22.28	-17.05	17.08	25.10	-8.02	2.64	-56.49	1.32	0.61	2.98
M06	-6.28	31.91	50.79	-18.88	-19.63	17.97	22.89	-4.93	5.59	-44.12	2.17	-1.02	3.00
M11	-8.60	22.07	61.52	-39.45	-18.04	18.74	21.94	-3.20	3.32	-65.96	4.18	-0.84	6.04
M06-HF	-	36.32	61.78	-25.46	-19.92	18.56	24.40	-5.84	4.68	-72.61	3.38	3.36	6.81
Hartree-Fock exchange + nonlocal correlation													
EXX-RPA@PBE[e]	-	31.20	49.00	-17.80	-13.20	19.10	23.10	-4.00	-0.30	-45.40	2.47	-1.31	3.48
Benchmarks (not final)													
CCSD(T)/CBS(TZ,	-2.90	29.80	55.30	-25.50	-15.80	18.50	24.50	-6.00	2.90	-47.30	0.12	0.12	0.11
CCSD(T)/CBS(aTZ,	-2.93	29.57	55.18	-25.61	-15.88	18.29	24.36	-6.06	2.83	-47.67	0.06	-0.06	0.06
CCSD(T)/CBS(aTZ,	-2.90	29.51	55.25	-25.74	-15.91	18.24	24.32	-6.07	2.86	-47.77	0.09	-0.08	0.10
Final reference values													
CCSD(T)/CBS(aTZ,	-2.84	29.61	55.21	-25.59	-15.82	18.37	24.43	-6.06	2.75	-47.57	0.00	0.00	0.00

[a] Single-point energy calculations of various density functionals with cc-pVQZ basis are performed based on B97-1/cc-pVTZ geometries with ultrafine integral grids. [b] Mean unsigned deviations (MUDs) for the four barrier heights. [c] Mean signed deviations (MSDs) for the four barrier heights. [d] MUDs for full thermochemical kinetics (TK), i.e., both energies of reaction and forward and reverse barrier heights of all the reactions. [e] Computed from the data reported in ref 116.

Table 6.17 The hybrid functionals tested in the current work and their percentage of nonlocal Hartree-Fock exchange (%X).

Density functionals	%X	Density functionals	%X	functionals	%X
ωB97X	15.77–100[a]	PBE0	25	PWB6K	46
B3LYP	20	B97-3	26.93	M08-HX	52.23
B97-1	21	M06	27	M06-2X	54
B97-2	21	M05	28	M05-2X	56
ωB97X-D	22.2–100[a]	PW6B95	28	M08-SO	56.79
HSE06	25–0[b]	SOGGA11-X	35.42	EXX-RPA@PBE	100@0[c]
N12-SX	25–0[b]	MPW1K	42.8	M06-HF	100
MN12-SX	25–0[b]	M11	42.8–100[a]		

[a] The percentage of Hartree-Fock exchange increases from the first value listed for small interelectronic separation to 100% at large interelectronic separation.

[b] The percentage of Hartree-Fock exchange decreases from 25% at small interelectronic separation to 0 at large interelectronic separation.

[c] The percentage of Hartree-Fock exchange is 100% in the post-SCF calculation based on orbitals obtained with no Hartree-Fock exchange.

Table 6.18 Heats of reaction for Ca reacting with NU-1000[a]

Reactant	description	Model	product	Reaction
Benzoic acid	50% surface H	periodic	H_2+Ca^{2+}	-538
Benzoic acid	100% surface H	periodic	H_2+Ca^{2+}	-500
Benzoic acid	Gas phase	cluster	H_2+Ca^{2+}	-531
-OH_x	1 Ca in large pore	periodic	H_2+Ca^{2+}	-421
-OH_x	1 Ca in small pore	periodic	H_2+Ca^{2+}	-421
-OH_x	1 Ca in large pore	cluster	H_2+Ca^{2+}	-395
-OH_x	2 Ca in large pore sym: C_i	periodic	H_2+Ca^{2+}	-436
-OH_x	2 Ca in large pore sym: C_2	periodic	H_2+Ca^{2+}	-419
-OH_x	2 Ca in small pore sym: C_i	periodic	H_2+Ca^{2+}	-424
-OH_x	2 Ca in small pore sym: C_2	periodic	H_2+Ca^{2+}	-417
-OH_x	4 Ca, 1 Ca per face sym: C_i	periodic	H_2+Ca^{2+}	-459
-OH_x	4 Ca, 1 Ca per face sym: C_2	periodic	H_2+Ca^{2+}	-417
-OH_x	4 Ca in large pore sym: C_i	periodic	H_2+Ca^{2+}	-382
-OH_x	4 Ca in large pore sym: C_2	periodic	H_2+Ca^{2+}	-388
-OH_x	4 Ca in small pore sym: C_i	periodic	H_2+Ca^{2+}	-370
-OH_x	4 Ca in small pore sym: C_2	periodic	H_2+Ca^{2+}	-379
-OH_x	8 Ca in both pores	periodic	H_2+Ca^{2+}	-393
-OH_x	Hydride formation in large	periodic	Ca-H	-311
-OH_x	Hydride formation in large	cluster	Ca-H	-349
pyrene	2Ca inside the triangular pore	periodic	Ca_2^+···$pyrene^-$	-49
pyrene	2Ca outside the triangular	periodic	Ca_2^+···$pyrene^-$	-45
pyrene	2Ca on 1,3,6,8-tetrakis	cluster	Ca_2^+···$pyrene^-$	-62

[a] The thermocorrections obtained from the frequency calculation in cluster model was applied to the energy calculated in the periodic model to obtain the approximated reaction enthalpy. All results are in kJ per mole of Ca.

Table 6.19 The ZPE15 database: experimental ZPEs for the 15 molecules used in this work.

Molecule	ZPE (kcal/mol)
C_2H_2	16.490[a]
CH_4	27.710[a]
CO_2	7.3[a]
CO	3.0929144[a]
F_2	1.302[a]
H_2CO	16.1[a]
H_2O	13.26[a]
H_2	6.231[a]
HCN	10.000[a]
HF	5.864[a]
N_2O	6.770[b]
N_2	3.3618[a]
NH_3	21.200[c]
OH	5.2915[a]
Cl_2	0.7983[a]

[a] Irikura et al.[204]
[b] Grev et al.[205]
[c] Martin[206]

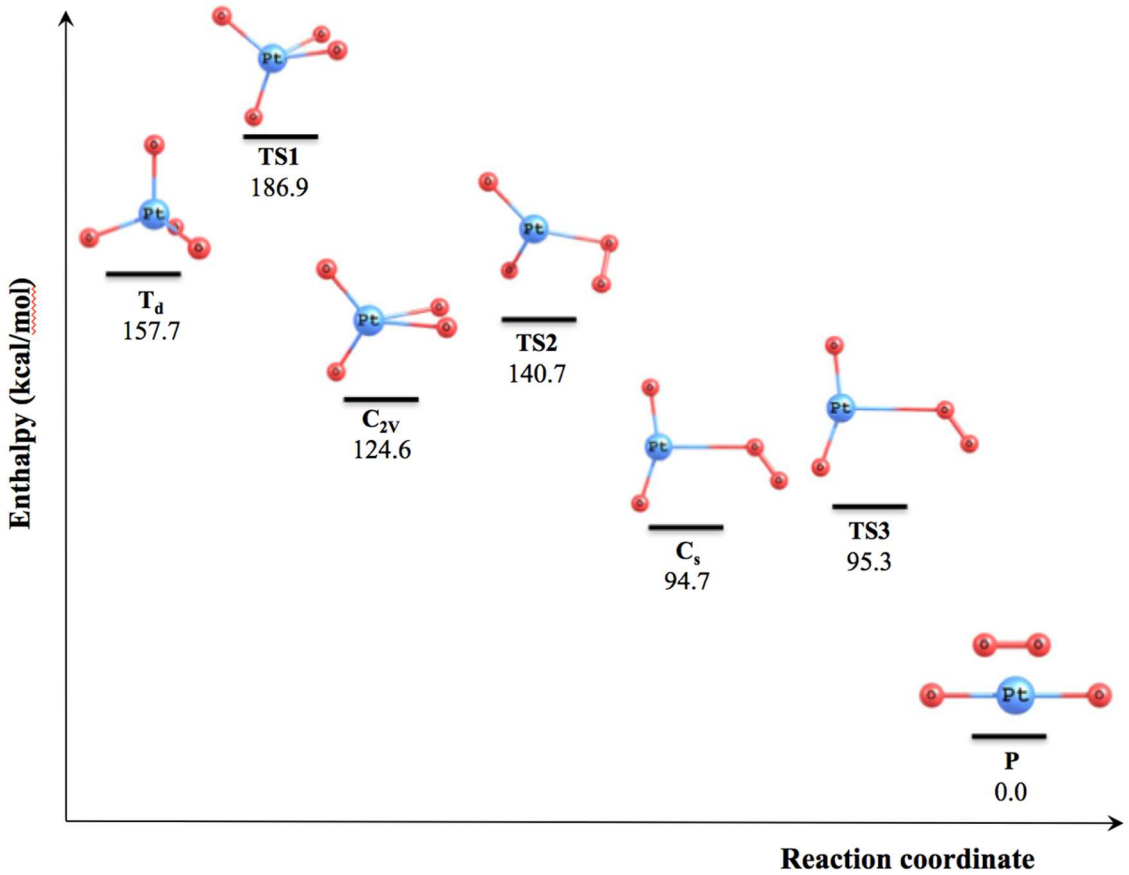

Figure 6.1 Enthalpy profile of reaction (3): $PtO_4^{2+} \rightarrow PtO_2^{+} + O_2^{+}$. The spin states for T_d, TS1, C_{2v}, TS2, C_s, and TS are all singlet. The spin states for O_2^{+} and PtO_2^{+} are doublet.

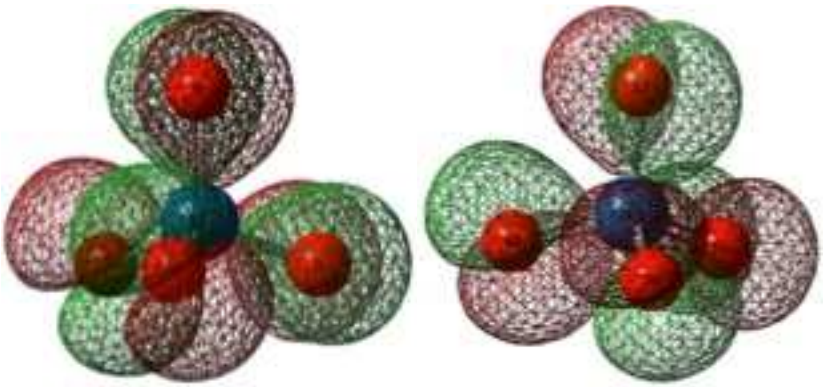

Figure 6.2 HOMO of IrO_4^+ (left) and PtO_4^{2+} (right).

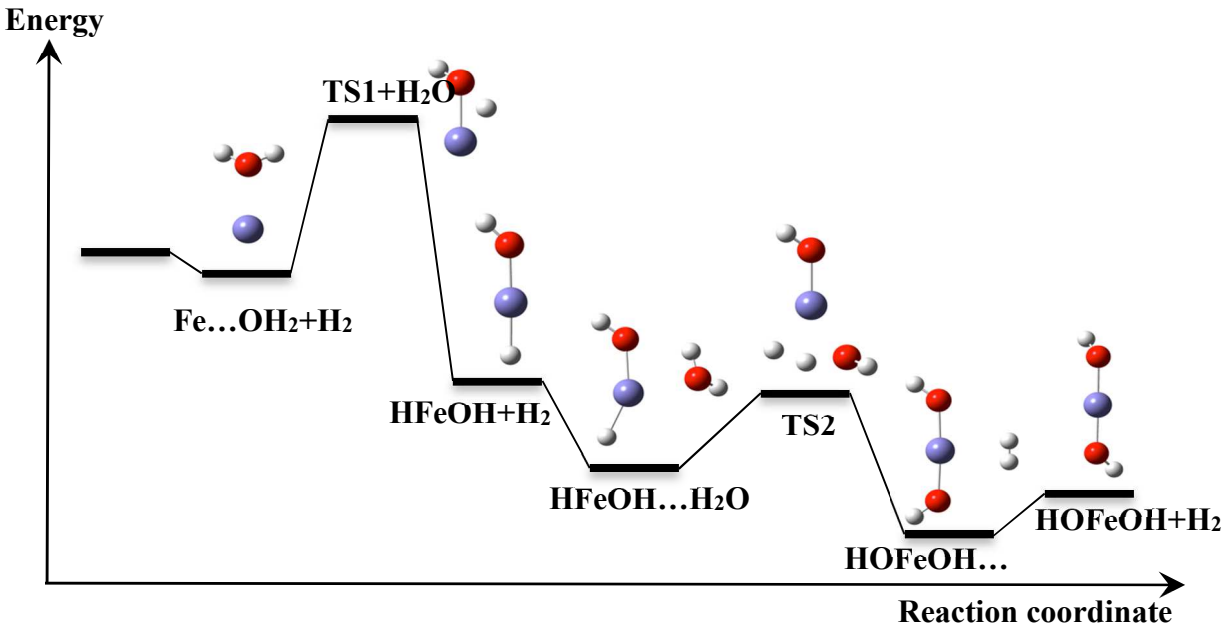

Figure 6.3 Schematic energy profile of the five-step water splitting reaction at atomic Fe(0).

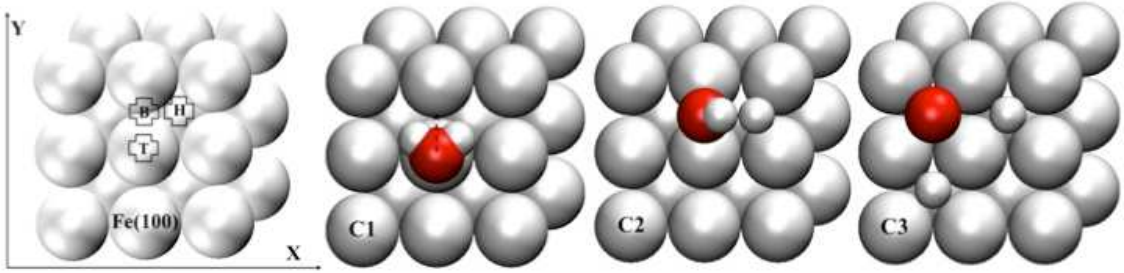

Figure 6.4 Illustration of the Fe+H2O → H-Fe-O-H reaction on (100) iron surface. The first snapshot illustrates the Fe(100) slab surface used in the calculation and provides definition of the three adsorption sites on the surface: 1) top (T); 2) bridge (B); and hollow (H). C1 is a graphical illustration of the initial configuration, corresponding to the locally stable site on the surface (T). The process of dissociation proceeds by water molecule moving towards the bridge site (B). At this site the molecule rotates in the (z-x) plane with concurrent elongation of one of the O-H bonds, such that it breaks. The free hydrogen atom moves to the hollow (H) site, while O-H moiety remains at the B location. In the final stage of dissociation (C3), the corresponding three atoms are distributed on the hollow sites.

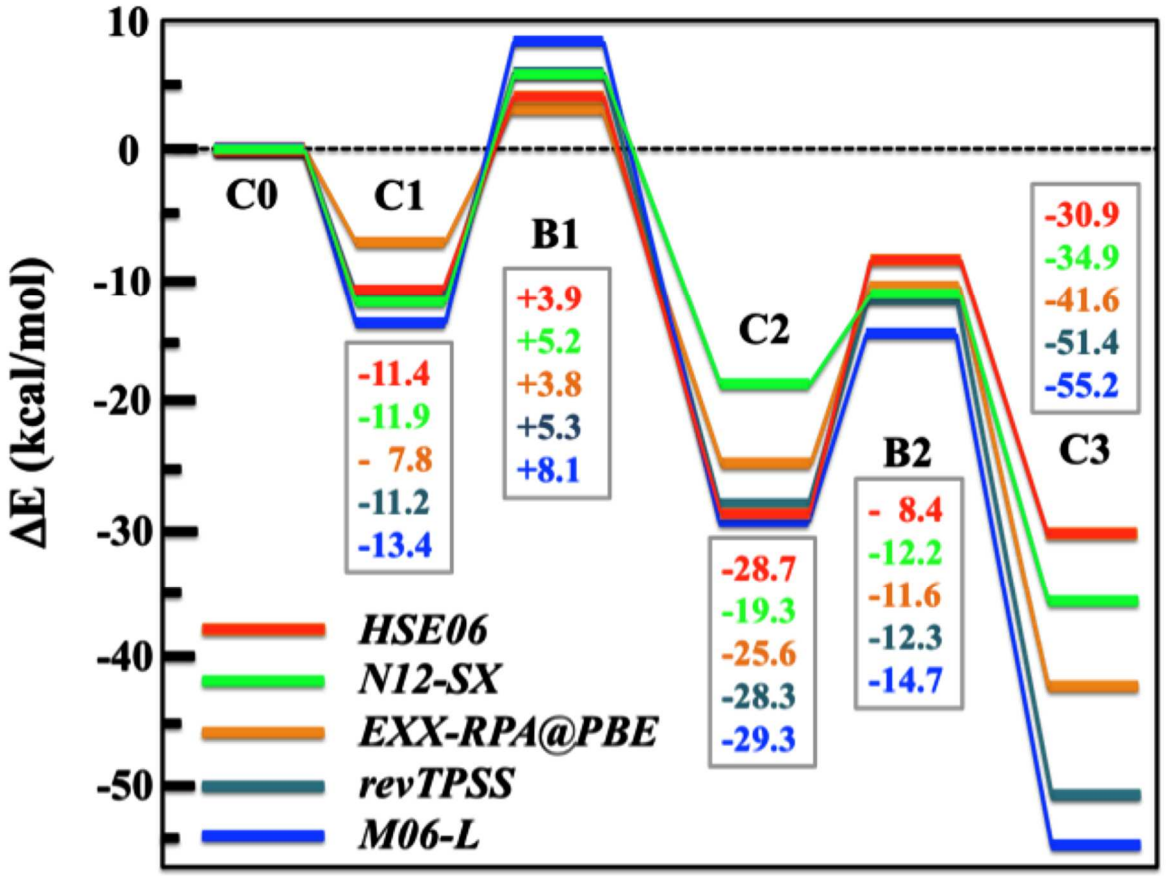

Figure 6.5 Relative energies for equilibrium structures C1, C2, and C3 (see Fig. 2) and transition structures B1 and B2 as calculated by five density functional methods at geometries optimized by PBE. All energies are in kcal/mol.

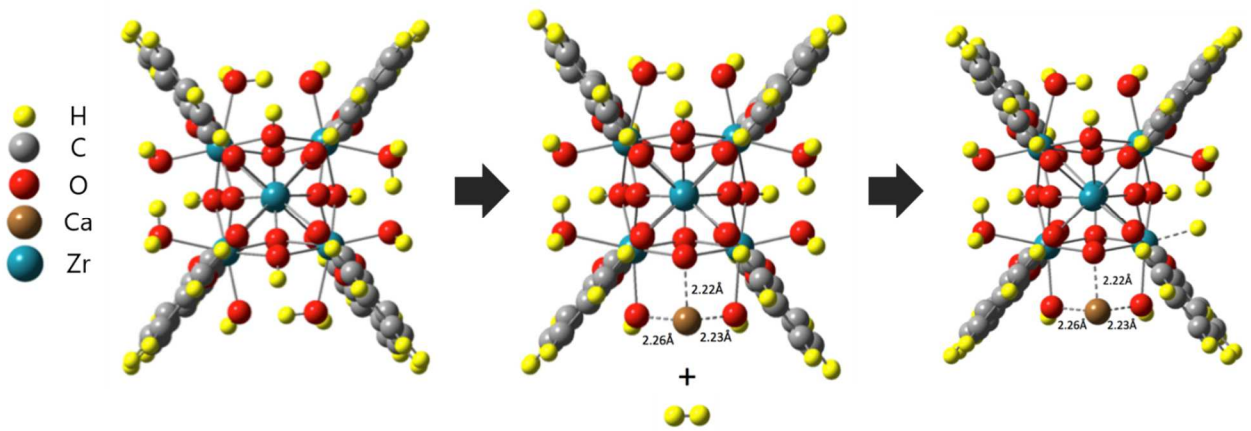

Figure 6.6 Predicted structures (optimized in the cluster calculation) of the initial Zr_6 oxide node with attached benzoates (to model linkers), the intermediate product $Zr_6C_{56}O_{32}H_{54}Ca$ formed during the reaction of Ca with a node-bound water-hydroxyl complex, which releases two H atoms, and the final product $Zr_6C_{56}O_{30}H_{54}Ca$ after losing two oxygen atoms. The lost H and O are expected to remain transiently bound to the solid in some way but quickly associate with another Ca to make solid $Ca(OH)_2$ nanoparticles (bound in some way to the MOF), as described in Reaction 1.

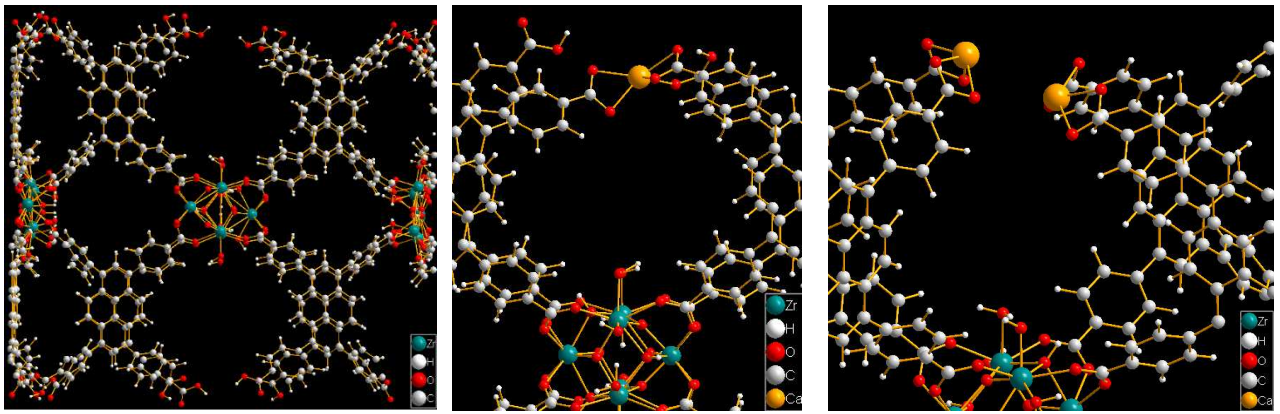

(A) (B) (C)

Figure 6.7 (A) The slab model of (001) surface of NU-1000 optimized in the periodic calculation with lattice constants constrained at bulk values. (B) 50% of surface benzoic acid reacting with Ca. (C) 100% of surface benzoic acid reacting with Ca

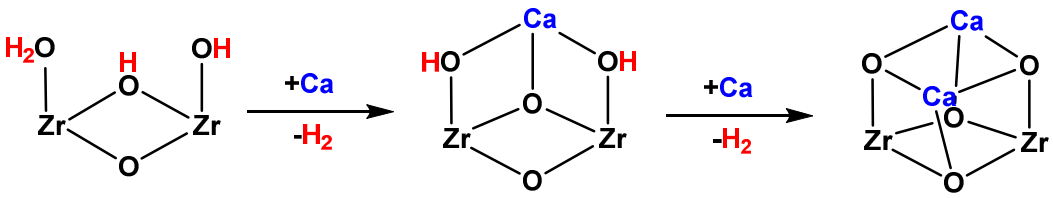

Figure 6.8 The most stable proton topology on the face of the Zr_6 node of NU-1000 and the proposed products of Ca reacting with protons. The figure only show one of four faces with $–OH_x$ of Zr_6 node.

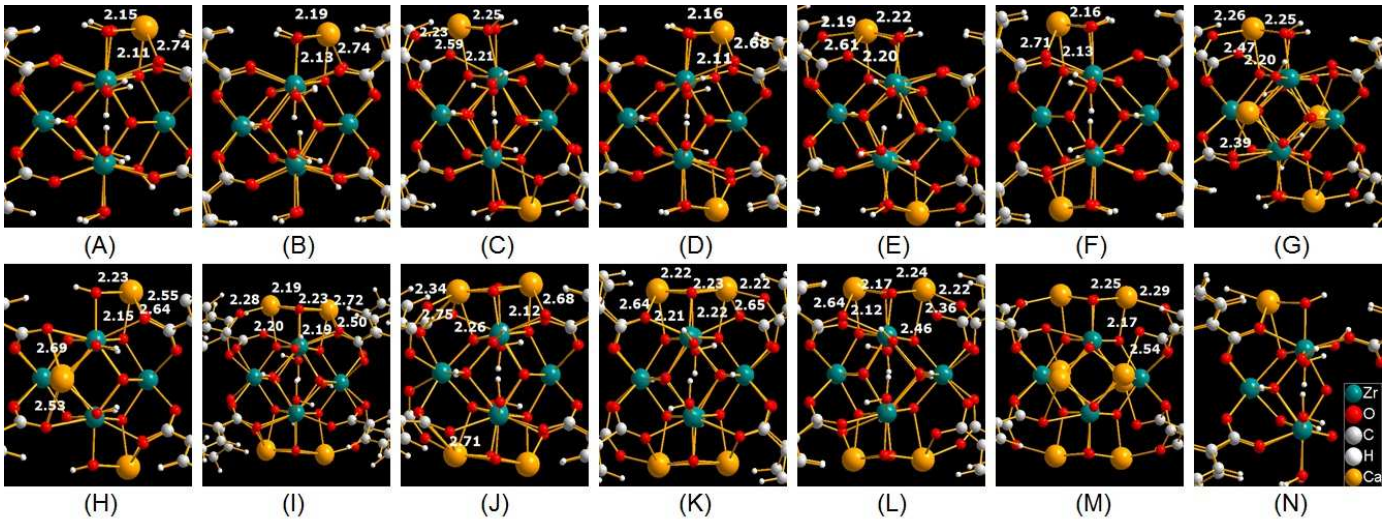

Figure 6.9 The product of Ca reacting with different number of protons on Zr_6 node optimized in the periodic calculation (as listed in Table 6.18). Some Ca-O distances were marked. (A) 1 Ca in the large pore. (B) 1 Ca in the small pore. (C) 2 Ca in the large pore with C_i symmetry. (D) 2 Ca in the large pore with C_2 symmetry. (E) 2 Ca in the small pore with C_i symmetry. (F) 2 Ca in the small pore with C_2 symmetry. (G) 4 Ca, 1 Ca per face with C_i symmetry. (H) 4 Ca, 1 Ca per face with C_2 symmetry. (I) 4 Ca in the large pore with C_i symmetry. (J) 4 Ca in the large pore with C_2 symmetry. (K) 4 Ca in the small pore with C_i symmetry. (L) 4 Ca in the small pore with C_2 symmetry. (M) 8 Ca in both pores (N) Hydride formation in large pore.

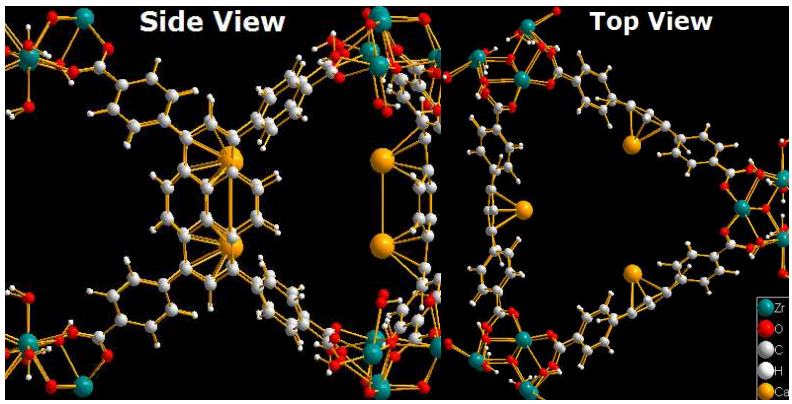

(A)

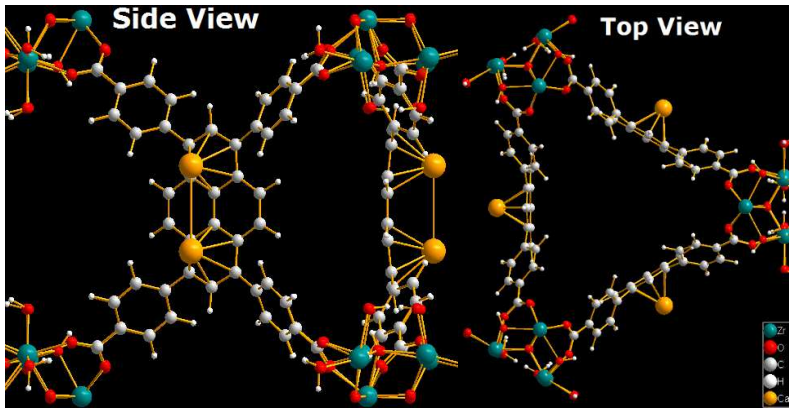

(B)

Figure 6.10 Two Ca deposited on pyrene optimized in the periodic calculation (as listed in Table 6.18): (A) inside the triangular pore; (B) outside the triangular pore.

Bibliography

A. Chakraborty, D. G. Truhlar, J. M. Bowman, and S. Carter, J. Chem. Phys. 2004, 121, 2071.
A. D. Becke and M. R. Roussel, Phys. Rev. A 1989, 39, 3761.
A. D. Becke, J. Chem, Phys. 1997, 107, 8554.
A. D. Becke, J. Chem. Phys. 1986, 84, 4524.
A. D. Becke, J. Chem. Phys. 1993, 98, 1372.
A. D. Becke, J. Chem. Phys. 1993, 98, 5648.
A. D. Becke, J. Chem. Phys. 1996, 104, 1040.
A. D. Becke, J. Chem. Phys. 1997, 107, 8554.
A. D. Becke, J. Chem. Phys. 1998, 109, 2092.
A. D. Becke, J. Chem. Phys. 2000, 112, 4020.
A. D. Becke, J. Chem. Phys., 1993, 98, 5648.
A. D. Becke, Phys. Rev. A. 1988, 38, 3098.
A. D. Boese and N. C. Handy, J. Chem. Phys., 2000, 114, 5497.
A. D. Boese, M. L. Martin, J. Chem. Phys. 2004, 121, 3405.
A. D. Boese, N. C. Handy, J. Chem. Phys., 2002, 116, 9559.
A. D. McLean and G. S. Chandler, J. Chem. Phys. 1980, 72, 5639.
A. Halkier, T. Helgaker, P. Jørgensen, W. Klopper, H. Koch, O. Jeppe, and A. K. Wilson, Chem. Phys. Lett. 1998, 286, 243.
A. J. Cohen, P. Mori-Sánchez, and W. Yang, Chem Rev. 2012, 112, 289.
A. J. Thakkar and S. P. McCarthy, J. Chem. Phys., 2009, 131, 134109.
A. K. Srivastava and N. Misra, Int. J. Quantum Chem. 2014, 114, 328.
A. Karton and J. M. L. Martin, J. Chem. Phys. 2010, 133, 144102.
A. Karton and J. M. L. Martin, Theor. Chem. Acc. 2006, 115, 330.
A. Karton, A. Tarnopolsky, J. F. Lamère, G. C. Schatz, J. M. L. Martin, J. Phys. Chem. A 2008, 112, 12868.
A. Karton, E. Rabinovich, J. M. L. Martin, and B. J. Ruscic, Chem. Phys. 2006, 125, 144108.
A. Karton, P. R. Taylor, and J. M. L. Martin, J. Chem. Phys. 2007, 127, 064104.
A. P. Rahalkar, B. K. Mishra, V. Ramanathan, and S. R. Gadre, Theor. Chem. Acc. 2011, 130, 491.
A. Posada-Borbón and A. Posada-Amarillas, Chem. Phys. Lett. 2015, 618, 66.
A. Ren, P. Rinke, and M. Scheffler, Phys. Rev. B 2009, 80, 045402.
A. Ren, P. Rinke, C. Joas, and M. Scheffler, J. Mater. Sci. 2012, 47, 7447.
A. Schäfer, C. Huber, and R. Ahlrichs, J. Chem. Phys. 1993, 100, 5829.
A. Taketoshi and M. Haruta, Chem Lett. 2014, 43, 380.
A. V. Marenich, S. V. Jerome, C. J. Cramer, and D. G. Truhlar, J. Chem. Theory

Comp. 2012, 8, 527.
A. W. Lange and G. A. Voth, J. Chem. Theory Comput. 2013, 9, 4018.
A.D. Isaacson, J. Chem. Phys. 1998, 108, 9978.
A.P. Scott and L. Radom, J. Phys. Chem. 1996, 100, 16502.
B. A. Hess, Phys. Rev. A 1985, 32, 756.
B. A. Hess, Phys. Rev. A 1986, 33, 3742.
B. Averkiev, Y. Zhao, and D. G. Truhlar, J. Mol. Cata. A: Chem. 2010, 324, 80.
B. G. Janesko, T. M. Henderson, and G. E. Scuseria, Phys. Chem. Chem. Phys. 2009, 11, 4443.
B. Hammer, L. Hansen and J. Norskov, Phys. Rev. B, 1999, 59, 7413.
B. J. Lynch and D. G. Truhlar, J. Phys. Chem. A 2003, 107, 3898.
B. J. Lynch, P. L. Fast, M. Harris, and D. G. Truhlar, J. Phys. Chem. A 2000, 104, 4811.
B. J. Lynch, Y. Zhao, and D. G. Truhlar, J. Phys. Chem. A 2003, 107, 1384.
B. J. Lynch, Y. Zhao, and D. G. Truhlar, J. Phys. Chem. A 2005, 109, 1643.
B. O. Roos, P. R. Taylor, and P. E. M. Siegbahn, Chem. Phys. 1980, 48, 157.
B. Soulé de Bas. H. E. Dorsett, and M. J. Ford, J. Phys. Chem. Solids 2003, 64, 495.
B. T. Sutcliffe, S. Miller, and J. Tennyson, Comput. Phys. Commun. 1988, 51, 73.
B.A. Hess, Phys. Rev. A 1986, 33, 3742.
C. Adamo and V. Barone, Chem. Phys. Lett. 1997, 274, 242.
C. Adamo and V. Barone, J. Chem. Phys. 1999, 110, 6158.
C. Adamo and V. Barone, J. Chem. Phys., 1997, 108, 664.
C. Adamo, V. Barone, J. Chem. Phys. 1999, 110, 6158.
C. E. Hoyer, L. G. Manni, D. G. Truhlar, and L. Gagliardi, J. Chem. Phys. 2014, 141, 204309.
C. K. Jørgensen, Naturwiss. 1976, 63, 292.
C. Lee, W. Yang, and R. P. Parr, Phys. Rev. B. 1988, 37, 785.
C. Møller and M. S. Plesset, Phys. Rev. 1934, 46, 618.
C. R. Jacob, M. Reiher, Int. J. Quantum Chem. 2012, 112, 3661.
C. W. Tsai, Y. C. Su, G. D. Li, and J. D. Chai, Phys. Chem. Chem. Phys. 2013, 15, 8352.
D. Andrae, U. Haussermann, M. Dolg, H. Stoll, and H. Preuss, Theor. Chem. Acc. 1990, 77, 123.
D. Bohm and D. Pines, Phys. Rev. 1951, 82, 625.
D. Bohm and D. Pines, Phys. Rev. 1953, 92, 609.
D. C. Comeau and R. J. Bartlett, Chem. Phys. Lett., 1993, 207, 414.
D. C. Langreth and J. P. Perdew, Phys. Rev. B 1977, 15, 2884.
D. C. Langreth and M. J. Mehl, Phys. Rev. B, 1983, 28, 1809.
D. C. Langreth, M. J. Mehl, Phys. Rev. B 1983, 28, 1809.
D. E. Woon and T. K. J. Dunning, J. Chem. Phys. 1995, 103, 4572.

D. Figgen, G. Rauhut, M. Dolg and H. Stoll, Chem. Phys., 2005 311, 227.
D. Figgen, K. A. Peterson, M. Dolg, and H. Stoll, J. Chem. Phys. 2009, 130, 164108.
D. G. Truhlar, Chem. Phys. Lett. 1998, 294, 45.
D. H. Zhang and J. Z. H. Zhang, J. Chem. Phys. 1993, 99, 6624.
D. Himmel, C. Knapp, M. Patzschke and S. Riedel, ChemPhysChem 2010, 11, 865.
D. J. Tozer and N. C. Handy, J. Phys. Chem. A, 1988, 102, 3162.
D. Pines and D. Bohm, Phys. Rev. 1952, 85, 338.
D. Sheppard, R. Terrell, and G. Henkelman, J. Chem. Phys. 2008, 128, 134106.
D. T. I. Nakazato, E. L. De Sá, and R. L. A. Haiduke, Int. J. Quant. Chem. 2010, 110, 1729.
D.E. Woon and T.H. Dunning Jr., J. Chem. Phys., 1993, 98, 1358.
D.P. Tew, N.C. Handy, and S. Carter, Phys. Chem. Chem. Phys. 2001, 3, 1958.
E. Bitzek, P. Koskinen, F. Gahler, M. Moseler, and P. Gumbsch, Phys. Rev. Lett. 2006, 97, 107201.
E. D. Bloch, L. J. Murray, W. L. Queen, S. Chavan, S. N. Maximoff, J. P. Bigi, R. Krishna, V. K. Peterson, F. Grandjean, G. J. Long, B. Smit, S. Bordiga, C. M. Brown and J. R. Long, J. Am. Chem. Soc., 2011, 133, 14814.
E. E. Dahlke and D. G. Truhlar, J. Chem. Theory Comput. 2007, 3, 1342.
E. E. Dahlke, H. R. Leverentz, and D. G. Truhlar, J. Chem. Theory Comput. 2008, 4, 33.
E. Fermi, Rend. Accad. Naz. Lincei, 1927, 6, 602.
E. I. Izgorodina, M. L. Coote, and L. Radom, J. Phys. Chem. A 2005, 109, 7558.
E. Papajak and D. G. Truhlar, J. Chem. Theory Comput., 2010, 6, 597.
E. Papajak and D. G. Truhlar, J. Chem. Theory Comput., 2011, 7, 10.
E. Papajak, H. R. Leverentz, J. Zheng and D. G. Truhlar, J. Chem. Theory Comput., 2009, 5, 1197.
E. Papajak, H. R. Leverentz, J. Zheng, and D. G. Truhlar, J. Chem. Theory Comput. 2009, 5, 1197. Errata and addendum: 2009, 5, 3330.
E. Teller, Rev. Mod. Phys. 1962, 34, 627.
E. Teller, Rev. Mod. Phys. 1962, 34, 627.
F. A. Hamprecht, A. J. Cohen, D. J. Tozer, and N. C. Handy, J. Chem. Phys. 1988, 109, 6264.
F. A. Hamprecht, A. J. Cohen, D. J. Tozer, N. C. Handy, J. Chem, Phys. 1988, 109, 6264.
F. Furche, Phys. Rev. B 2001, 64, 1951201.
F. Göltl, A. Grüneis, T. Bučko, and J. Hafner, J Chem Phys. 2012, 137, 114111.
F. Karlický and F. Karlický, Int. J. Quant. Chem. 2014, 114, 987.
F. Karlický and M. Otyepka, J. Chem. Theory Comput. 2011, 7, 2876.
F. Karlický, P. Lazar, M. Dubecký, and M. Otyepka, J. Chem. Theory Comput. 2013, 9, 3670.
F. L. Hirshfeld, Theor. Chem. Acc., 1977, 44, 129.

F. London, Trans. Faraday Soc. 1937, 33, 8.
F. London, Trans. Faraday Soc. 1937, 33, 8b-26.
F. Weigend and R. Ahlrichs, Phys. Chem. Chem. Phys., 2005, 7, 3297.
F. Weigend, M. Haser, H. Patzelt, and R. Ahlrichs, Chem. Phys. Lett. 1998, 294, 143.
G. E. Scuseria, T. M. Henderson, and D. C. Sorensen, J. Chem. Phys. 2008, 129, 231101.
G. Henkelman, B. P. Uberuaga, and H. Jonsson, J. Chem. Phys. 2000, 113, 9901.
G. Jansen and B. A. Hess, Phys. Rev. A 1989, 39, 6016.
G. Jansen and B. A. Hess, Phys. Rev. A 1989, 39, 6016.
G. Knizia, T. B. Adler, and H.-J. Werner, J. Chem. Phys. 2009, 130, 054104.
G. Kresse and D. Joubert, Phys. Rev. B 1999, 59, 1758.
G. Kresse and J. Furthmuller, Phys. Rev. B 1996, 54, 11169.
G. Kresse and J. Hafner, Phys. Rev. B 1993, 47, 558. G. Kresse and J. Hafner, Phys. Rev. B 1994, 49, 14251.
G. Purvis and R. J. Bartlett, J. Chem. Phys. 1982, 76, 1910.
G. Wang, M. Zhou, J. T. Goettel, G. J. Schrobilgen, J. Su, J. Li, T. Schlöder, and S. Riedel, Nature 2014, 514, 475.
H. Eshuis, J. E. Bates, and F. Furche, Theor. Chem. Acc. 2012, 131, 1084.
H. H. Nielsen, Encycl. Phys. 1959, 37, 173.
H. H. Nielsen, H. H. The vibration-rotation energies of molecules and their spectra in the infra-red. In Handbuch der Physik; Flügge, S., Ed.; Springer: Berlin, 1959; Vol. 37, pp. 173-313.
H. L. Schmider, A. D. Becke, J. Chem. Phys. 1998, 108, 9624.
H. S. Yu and D. G. Truhlar, J. Chem. Theory Comput. 2014, 10, 2291.
H. S. Yu, H. Xiao, D. G. Truhlar, MN15-L: A New Local Exchange-Correlation Functional for Kohn-Sham Density Functional Theory with Broad Accuracy for Atoms, Molecules, and Solids. J. Chem. Theory Comput. 2016, available online as Article ASAP. DOI: 10.1021/acs.jctc.5b01082
H. S. Yu, L. J. Fiedler, I. M. Alecu, and D. G. Truhlar, Comp. Phys. Commun. 2016, submitted.
H. S. Yu, W. Zhang, P. Verma, X. He, and D. G. Truhlar, Phys. Chem. Chem. Phys. 2015, 17, 12146.
H. S. Yu, X. He, and D. G. Truhlar, J. Chem. Theory Comput. 2016, 12, 1280.
H. S. Yu, X. He, S. Li, and D. G. Truhlar, Chem. Sci. 2016, DOI: 10.1039/c6sc00705h
H. Stoll and C. Pavlidou, Theor. Chim. Acta, 1978, 149, 143.
H. Stoll and E. Golka, Theor. Chim. Acta, 1980, 55, 29.
H. Stoll, Chem. Phys. Lett. 1992, 191, 548.
H. W. Qi, H. Leverentz, and D. G. Truhlar, J. Phys. Chem. A 2013, 117, 4486.
H. Yu and D. G. Truhlar, J. Chem. Theory Comput. 2014, 10, 2291.
H. Yu and D. G. Truhlar, J. Chem. Theory Comput. 2015, 11, 2968.

H.-J. Werner, P. J. Knowles, G. Knizia, F. R. Manby, M. Schu¨tz, P. Celani, T. Korona, R. Lindh, A. Mitrushenkov, G. Rauhut, K. R. Shamasundar, T. B. Adler, R. D. Amos, A. Bernhardsson, A. Berning, D. L. Cooper, M. J. O. Deegan, A. J. Dobbyn, F. Eckert, E. Goll, C. Hampel, A. Hesselmann, G. Hetzer, T. Hre- nar, G. Jansen, C. Ko¨ppl, Y. Liu, A. W. Lloyd, R. A. Mata, A. J. May, S. J. McNicholas, W. Meyer, M. E. Mura, A. Nicklass, D. P. O'Neill, P. Palmieri, K. Pflu¨ger, R. Pitzer, M. Reiher, T. Shiozaki, H. Stoll, A. J. Stone, R. Tarroni, T. Thorsteinsson, M. Wang, and A. Wolf, Molpro, version 2010.1; University of Birmingham: Birmingham, 2010.

HSSH. National Institute of standards and Technology (NIST). http://webbook.nist.gov/cgi/cbook.cgi?ID=C63344865&Units=SI (accessed on July 26, 2015).

http://cccbdb.nist.gov/expbondlengths1.asp, accessed on Oct. 29, 2014.

http://webbook.nist.gov/cgi/cbook.cgi?ID=C63344865&Units=SI, accessed on Jul. 26, 2015.

http://webbook.nist.gov/cgi/cbook.cgi?ID=C7446119&Units=SI, accessed on Jul. 26, 2015.

http://webbook.nist.gov/cgi/cbook.cgi?ID=C7664939&Units=SI&Mask=1#Thermo-Gas, accessed on Jul. 26, 2015.

I. C. Gerber and J. C. Ángyán, Chem. Phys. Lett. 2005, 415, 100.

I. M. Alecu, J. Zheng, Y. Zhao, D. G. Truhlar, J. Chem. Theory Comput. 2010, 6, 2872.

I. M. Mills, In Molecular Spectroscopy: Modern Research; edited by K. N. Rao and C. W. Mathews; Academic: New York, 1972; pp. 115-140.

I. Y. Zhang and X. Xu, Int. Rev. Phys. Chem. 2011, 30, 115.

I.M. Alecu, J. Zheng, Y. Zhao, and D.G. Truhlar, J. Chem. Theory Comput. 2010, 6, 2872.

J-D. Chai, M. Head-Gordon, Phys. Chem. Chem. Phys. 2008, 10, 6615.

J. A. Pople, J. S. Binkley, and R. Seeger, Int. J. Quantum Chem. Symp. 1976, 10, 1–19.

J. A. Pople, M. Head-Gordon, and K. Raghavachari, J. Chem. Phys. 1987, 87, 5968.

J. B. Foresman, M. Head-Gordon, J. A. Pople, and M. J. Frisch, J. Phys. Chem., 1992, 96, 135.

J. Bloino, M. Biczyzko, and V. Barone, J. Chem. Theory Comput. 2012, 8, 1015.

J. C. Slater, Phys. Rev. 1951, 81, 385.

J. D. Chai and M. Head-Gordon, Phys. Chem. Chem. Phys. 10, 6615 (2008) .

J. E. Mondloch, W. Bury, D. Fairen-Jimenez, S. Kwon, E. J. DeMarco, M. H. Weston, A. A. Sarjeant, S. T. Nguyen, P. C. Stair, R. Q. Snurr, O. K. Farha, and T. J. Hupp, J. Am. Chem. Soc. 2013, 135, 10294.

J. Filip, F. Karlický, Z. Marusak, P. Lazar, M. Černík, M. Otyepka, and R. Zboril, J. Phys. Chem. C 2014, 118, 13817.

J. Friedrich and J. Hänchen, J. Chem. Theory Comput. 2013, 9, 5381.

J. Friedrich, M. Hanrath, and M. Dolg, J. Chem. Phys. 2007, 126, 154110.

J. Harl, L. Schimka, and G. Kresse, Phys. Rev. B 2010, 81, 115126.
J. Harris and R. O. Jones, J. Phys. F 1974, 4, 1170.
J. Harris, Phys. Rev. A 1984, 29, 1648.
J. Heyd, G. E. Scuseria, and M. Ernzerhof, J. Chem. Phys., 2003, 118, 8207.
J. Heyd, G. E. Scuseria, M. Ernzerhof, J. Chem. Phys. 2003, 118, 8027.
J. Heyd, J. E. Peralta, G. E. Scuseria, and R. L. Martin, J. Chem. Phys. 2005, 123, 174101.
J. Irisawa and S. Iwata, Theor. Chim. Acta. 1992, 81, 223.
J. Koput and K. A. Peterson, J. Phys. Chem. A 2002, 106, 9595.
J. M. L. Martin and A. Sundermann, J. Chem. Phys. 2001, 114, 3408.
J. M. L. Martin, ACS Symp. Ser. 1998, 677, 212.
J. M. Tao, J. P. Perdew, V. N. Staroverov, and G. E. Scuseria, Phys. Rev. Lett. 2003, 91, 146401.
J. M. Tao, J. P. Perdew, V. N. Staroverov, G. E. Scuseria, Phys. Rev. Lett. 2003, 91, 146401.
J. Noga, S. Kedžuch, J. Šimunek, and S. Ten-no, J. Chem. Phys. 2008, 128, 174103.
J. P. Perdew and A. Zunger, Phys. Rev. B 1981, 23, 5048.
J. P. Perdew and Y. Wang, Phys. Rev. B 1986, 33, 8800.
J. P. Perdew and Y. Wang, Phys. Rev. B, 1992, 45, 13244.
J. P. Perdew and Y. Yang, Phys. Rev. B, 1986, 33, 8800.
J. P. Perdew, A. Ruzsinsky, G. I. Csonka, O. A. Vydrov, G. E. Scuseria, L. A. Constantin, X. Zhou and K. Burke, Phys. Re.v Lett., 2008, 100, 136406.
J. P. Perdew, A. Ruzsinszky, G. I. Csonka, L. A. Constantin and J. Sun, Phys. Rev. Lett., 2009, 103, 026403.
J. P. Perdew, A. Ruzsinszky, J. Tao, V. N. Staroverov, G. E. Scuseria, G. I. Csonka, J. Chem. Phys. 2005, 123, 062201.
J. P. Perdew, A. Zunger, Phys. Rev. B 1981, 23, 5048.
J. P. Perdew, in Electronic Structure of Solids ’91, edited by P. Ziesche and H. Eschrig (Akademie Verlag, Berlin, 1991), pp. 11–20.
J. P. Perdew, K. Burke, and M. Ernzerhof, Phys. Rev. Lett. 1996, 77, 3865..
J. P. Perdew, Phys. Rev. B, 1986, 33, 8822.
J. P. Perdew, Phys. Rev. Lett. 1985, 55, 1665.
J. P. Perdew, S. Kurth, A. Zupan, and P. Blaha, Phys. Rev. Lett. 1999, 82, 2544.
J. P. Perdew, S. Kurth, Lecture Notes Phys. 2003, 55, 1.
J. P. Perdew, Wang, Y. Phys. Rev. B 1992, 45, 13244.
J. P. Perdew, Y. Wang, Phys. Rev. B 1986, 33, 8800.
J. P. Ritchie and S. M. Bachrach, J. Comp. Chem. 1987, 8, 499.
J. Paier, M. Marsman, K. Hummer, G. Kresse, I. C. Gerbr, and J. G. Ángyán, J. Chem. Phys. 2006, 124, 154709.
J. Perdew and W. Yue, Phys. Rev. B 1986, 33, 8800.

J. Perdew, J. Chevary, S. Vosko, K. Jackson, M. Pederson, D. Singh and G. Fiolhais, Phys. Rev. B 1992, 46, 6671.
J. Řezáč, K. E. Riley, and P. Hobza, J. Chem. Theory Comput. 2011, 7, 2427.
J. Řezáč, K. E. Riley, P. Hobza, J. Chem. Theory Comput. 2011, 7, 2427.
J. S. Binkley and J. A. Pople, J. Chem. Phys. 1977, 66, 879.
J. Sun, R. Haunschild, B. Xiao, I. W. Bulik, G. E. Scuseria, J. P. Perdew, J. Chem. Phys. 2013, 138, 044113.
J. Toulouse, F. Colonna, and A. Savin, Phys. Rev. A 2004, 70, 062505.
J. Wellendorff, K. T. Lundgaard, A. Møgelhøj, V. Petzold, D. D. Landis, J. K. Nørskov, T. Bligaard, and K. W. Jacobsen, Phys. Rev, B 2012, 85, 235149.
J. Zhang, Y. Zhao, and D. G. Truhlar, J. Chem. Theory Comput. 2007, 3, 569.
J. Zheng and D. G. Truhlar, J. Chem. Theory Comput. 2013, 9, 1356.
J. Zheng, R. Meana-Pañeda, and D. G. Truhlar, Comput. Phys. Commun. 2013, 184, 2032.
J. Zheng, R. Meana-Pañeda, and D. G. Truhlar, J. Amer. Chem. Soc. 2014, 136, 5150.
J. Zheng, S. L Mielke, K. L Clarkson, and D. G. Truhlar, Comput. Phys. Commun. 2012, 183, 1803.
J. Zheng, T. Yu, E. Papajak, I, M. Alecu, S. L. Mielke, and D. G. Truhlar, Phys. Chem. Chem. Phys. 2011, 13, 10885.
J. Zheng, Y. Zhao, and D. G. Truhlar, J. Chem. Theory Comput. 2007, 3, 569.
J. Zheng, Y. Zhao, and D. G. Truhlar, J. Chem. Theory Comput. 2009, 5, 808.
J.-D. Chai and M. Head-Gordon, J. Chem. Phys. 2008, 128, 084106.
J.-D. Chai and M. Head-Gordon, Phys. Chem. Chem. Phys. 2008, 10, 6615.
J.-D. Chai, M. Head-Gordon, J. Chem. Phys. 2008, 128, 084106.
J.-W. Song, S. Tokura, T. Sato, M. A. Watson, and K. Hirao, J. Chem. Phys. 2007, 127, 154109.
J.A. Pople, A.P. Scott, M.W. Wong, and L. Radom, Isr. J. Chem. 1993, 33, 345.
J.A. Pople, Rev. Mol. Phys. 1999, 71, 1267.
J.M.L. Martin and A. Sundermann, J. Chem. Phys. 2001, 114, 3408.
J.M.L. Martin, J. Chem. Phys. 1992, 97, 5012.
K. A. Peterson and T. H. Dunning, J. Chem. Phys. 2002, 117, 10548.
K. A. Peterson, D. Figgen, M. Dolg, and H. Stoll, J. Chem. Phys. 2007, 126, 124101.
K. A. Peterson, D. Figgen, M. Dolg, and H. Stoll, J. Chem. Phys. 2009, 130, 163108.
K. Kudin and G. E. Scuseria, Phys. Rev. B, 2000, 61, 16440.
K. L. Schuchardt, B. T. Didier, T. Elsethagen, L. Sun, L., V. Gurumoorthi, J. Chase, J., J. Li and T. L. Windus, J. Chem. Inf. Model., 2007, 47, 1045.
K. Lee, W. C. Isley III, A. L. Dzubak, P. Verma, S. J. Stoneburner, L.-C. Lin, J. D. Howe, E. D. Bloch, D. A. Reed, M. R. Hudson, C. M. Brown, J. R. Long, J. B. Neaton, B. Smit, C. J. Cramer, D. G. Truhlar and L. Gagliardi, J. Am. Chem. Soc., 2014, 136, 698.
K. Peterson, T. Adler, and H.-J. Werner, J. Chem. Phys. 2008, 128, 084102.

K. Raghavachari, G. W. Trucks, J. A. Pople, and M. Head-Gordon, Chem. Phys. Lett. 1989, 157, 479.
K. Szalewicz, Wiley Interdis. Rev. Comp. Mol. Sci. 2012, 2, 254.
K. Szalewicz, Wiley Interdiscip. Rev.: Comput. Mol. Sci., 2012, 2, 254.
K. T. Tang and J. P. Toennies, J. Chem. Phys., 2003, 118, 4976.
K. Yang, R. Peverati, D. G. Truhlar, and R. Valero, J. Chem. Phys. 2011, 135, 044118.
K.A. Peterson and C. Puzzarini, Theor. Chem. Acc., 2005, 114, 283.
K.K. Irikura, J. Phys. Chem. Ref. Data, 2007, 36, 389.
K.M. Kuhler, D.G. Truhlar, and A.D. Isaacson, J. Chem. Phys. 1996, 104, 4664.
L. E. Chirlian and M. M. Francl, J. Comp. Chem. 1987, 8, 894.
L. Ferrighi, B. Hammer, and G. K. H. Madsen, J. Am. Chem. Soc. 2009, 131, 10605.
L. Goerigk, H. Kruse, S. Grimme, ChemPhysChem 2011, 12, 3421.
L. Goerigk, L., Grimme, S. Wiley Interdis. Rev. Comp. Mol. Sci. 2014, 4, 576.
L. Goerigk, S. Grimme, J. Chem. Theory Comput. 2011, 13, 6670.
L. Goerigk and S. Grimme, J. Chem. Theory Comput. 2010, 6, 107.
L. Goerigk and S. Grimme, J. Chem. Theory Comput. 2011, 7, 291.
L. H. Thomas, Math. Proc. Cambridge Philos. Soc., 1927, 23, 542.
L. Hu, H. Chen, J. Chem. Theory Comput. 2015, 11, 4601.
L. Schimka, J. Harl, A. Stroppa, A. Grüneis, M. Marsman, F. Mittendorfer, and G. Kresse, Nat. Mat., 2010, 9, 741.
L. Schimka, J. Harl, and G. Kresse, J. Chem. Phys. 2011, 134, 024116.
M. Caricato, G. W. Trucks, M. J. Frisch and K. B. Wiberg, J. Chem. Theory Comput., 2010, 6, 370.
M. Dion, H. Rydberg, E. Schröder, D. C. Langreth, and B. I. Lundqvist, Phys. Rev. Lett. 2004, 92, 246401.
M. Douglas and N.M. Kroll, Ann. Phys. 1974, 82, 89.
M. E. Casida and M. Huix-Rotllant, Annu. Rev. Phys. Chem., 2012, 63, 287.
M. E. Casida, in Recent Advances in Density Functional Methods, Part I, ed. D. P. Chong, World Scientific: Singapore1995, pp. 155-193.
M. Eder and K. Terakura, Phys. Rev. B 2001, 64, 15426.
M. Head-Gordon, R. J. Rico, M. Oumi, and T. J. Lee, Chem. Phys. Lett., 1994, 219, 21.
M. Head-Gordorn, J. A. Pople, and M. J. Frisch, Chem. Phys. Lett. 1988, 153, 503.
M. Isegawa, B. Wang, and D. G. Truhlar, J. Chem. Theory Comput. 2013, 9, 1381-1393.
M. Isegawa, R. Peverati and D. G. Truhlar, J. Chem. Phys., 2012, 137, 244104.
M. J. Frisch, et al., Gaussian 09, Revision C.1, Gaussian, Inc., 2009.
M. J. Frisch, et al., Gaussian 09, revision C01 (Gaussian, Inc., Wallingford CT, 2009).
M. J. Frisch, G. W. Trucks, H. B. Schlegel, G. E. Scuseria, M. A. Robb, J. R. Cheeseman, G. Scalmani, V. Barone, B. Mennucci, G. A. Petersson, H. Nakatsuji, M.

Caricato, X. Li, H. P. Hratchian, A. F. Izmaylov, J. Bloino, G. Zheng, J. L. Sonnenberg, M. Hada, M. Ehara, K. Toyota, R. Fukuda, J. Hasegawa, M. Ishida, T. Nakajima, Y. Honda, O. Kitao, H. Nakai, T. Vreven, J. A. Montgomery, Jr., J. E. Peralta, F. Ogliaro, M. Bearpark, J. J. Heyd, E. Brothers, K. N. Kudin, V. N. Staroverov, R. Kobayashi, J. Normand, K. Raghavachari, A. Rendell, J. C. Burant, S. S. Iyengar, J. Tomasi, M. Cossi, N. Rega, J. M. Millam, M. Klene, J. E. Knox, J. B. Cross, V. Bakken, C. Adamo, J. Jaramillo, R. Gomperts, R. E. Stratmann, O. Yazyev, A. J. Austin, R. Cammi, C. Pomelli, J. W. Ochterski, R. L. Martin, K. Morokuma, V. G. Zakrzewski, G. A. Voth, P. Salvador, J. J. Dannenberg, S. Dapprich, A. D. Daniels, Ö. Farkas, J. B. Foresman, J. V. Ortiz, J. Cioslowski, and D. J. Fox, Gaussian 09, revision C01; Gaussian, Inc., Wallingford CT, 2009.

M. J. Frisch, J. A. Pople, and J. S. Binkley, J. Chem. Phys. 1984, 80, 3265.

M. Kaupp, P. V. Schleyer, H. Stoll, and H. Preuss, J. Chem. Phys. 1991, 94, 1360.

M. Levy and J. P. Perdew, Int. J. Quantum Chem. 1994, 49, 539.

M. M. Francl, W. J. Pietro, W. J. Hehre, J. S. Binkley, M. S. Gordon, D. J. Defrees, J. A. Pople, J. Chem. Phys. 1982, 77, 3654.

M. M. Kreevoy and D. G. Truhlar, Tech. Chem. (N.Y.), 4th ed., 1986, 6/Pt. 1, 13.

M. Methfessel and A. T. Paxton Phys. Rev. B 1989, 40, 3616.

M. Mladenovic and M. Lewerenz, Chem. Phys. Lett. 2000, 321, 135.

M. O. Sinnokrot and C. D. Sherril, J. Phys. Chem. A 2003, 108, 10200.

M. Piccardo, E. Penocchio, C. Puzzarini, M. Biczysko, V. Barone, J. Phys. Chem. A 2015, 119, 2058.

M. Steinmetz, A. Hansen, S. Ehrlich, and T. Risthaus, Grimme, S. Top. Curr. Chem. 2015, 365, 1.

M. Valiev, E. J. Bylaska, N. Govind, K. Kowalski, T. P. Straatsma, H. J. J. van Dam, D. Wang, J. Nieplocha, E. Apra, T. L. Windus, and W. A. de Jong, Comput. Phys. Commun. 2010, 181, 1477.

M. Vasiliu, D. Feller, J. L. Gole, and D. A. Dixon, J. Phys. Chem. A 2010, 114, 9349.

M. Yoshimine, J. Phys. Soc. Jpn. 1968, 25, 1100.

M.J. Frisch, G.W. Trucks, H.B. Schlegel, G.E. Scuseria, M.A. Robb, J.R. Cheeseman, G. Scalmani, V. Barone, B. Mennucci, G.A. Petersson, H. Nakatsuji, M. Caricato, X. Li, H.P. Hratchian, A.F. Izmaylov, J. Bloino, G. Zheng, J.L. Sonnenberg, M. Hada, M. Ehara, K. Toyota, R. Fukuda, J. Hasegawa, M. Ishida, T. Nakajima, Y. Honda, O. Kitao, H. Nakai, T. Vreven, J.A.J. Montgomery, J.E. Peralta, F. Ogliaro, M. Bearpark, J.J. Heyd, E. Brothers, K.N. Kudin, V.N. Staroverov, R. Kobayashi, J. Normand, K. Raghavachari, A. Rendell, J.C. Burant, S.S. Iyengar, J. Tomasi, M. Cossi, N. Rega, J.M. Millam, M. Klene, J.E. Knox, J.B. Cross, V. Bakken, C. Adamo, J. Jaramillo, R. Gomperts, R.E. Stratmann, O. Yazyev, A.J. Austin, R. Cammi, C. Pomelli, J.W. Ochterski, R.L. Martin, K. Morokuma, V.G. Zakrzewski, G.A. Voth, P. Salvador, J.J. Dannenberg, S. Dapprich, A.D. Daniels, O. Farkas, J.B. Foresman, J.V. Ortiz, J. Cioslowski, and D.J. Fox, Gaussian 09, revision A.02; Gaussian, Inc., (Wallingford, CT, 2009).

M.J. Frisch, G.W. Trucks, H.B. Schlegel, G.E. Scuseria, M.A. Robb, J.R. Cheeseman, J.A.J. Montgomery, T. Vreven, K.N. Kudin, J.C. Burant, J.M. Millam, S.S. Iyengar, J. Tomasi, V. Barone, B. Mennucci, M. Cossi, G. Scalmani, N. Rega, G.A. Petersson, H. Nakatsuji, M. Hada, M. Ehara, K. Toyota, R. Fukuda, J. Hasegawa, M. Ishida, T. Nakajima, Y. Honda, O. Kitao, H. Nakai, M. Klene, X. Li, J.E. Knox, H.P. Hratchian, J.B. Cross, V. Bakken, C. Adamo, J. Jaramillo, R. Gomperts, R.E. Stratmann, O. Yazyev, A.J. Austin, R. Cammi, C. Pomelli, J.W. Ochterski, P.Y. Ayala, K. Morokuma, G.A. Voth, P. Salvador, J.J. Dannenberg, V.G. Zakrzewski, S. Dapprich, A.D. Daniels, M.C. Strain, O. Farkas, D.K. Malick, A.D. Rabuck, K. Raghavachari, J.B. Foresman, J.V. Ortiz, Q. Cui, A.G. Baboul, S. Clifford, J. Cioslowski, B.B. Stefanov, G. Liu, A. Liashenko, P. Piskorz, I. Komaromi, R.L. Martin, D.J. Fox, T. Keith, A.-L.M. A, C.Y. Peng, A. Nanayakkara, M. Challacombe, P.M.W. Gill, B. Johnson, W. Chen, M.W. Wong, C. Gonzalez, and J.A. Pople, Gaussian 03, revision E.01; Gaussian, Inc., (Wallingford, CT, 2004).

N. B. Balabanov and K. A. Peterson, J. Chem. Phys. 2005, 123, 064107.

N. C. Handy, J. A. Pople, M. Head-Gordon, K. Raghavachari and G. W. Trucks, Chem. Phys. Lett., 1989, 164, 185.

N. E. Schultz, Y. Zhao, and D. G. Truhlar, J. Phys. Chem. A 2005, 109, 11127.

N. E. Schultz, Y. Zhao, and D. G. Truhlar, J. Phys. Chem. A 2005, 109, 4388.

N. Handy and A. Cohen, Mol. Phys., 2001, 99, 403.

N. J. Mayhall and K. Raghavachari, J. Chem. Theory Comput. 2012, 9, 2669.

N. Mardiossian and M. Head-Gordon, J. Chem. Phys. 2015, 142, 074111.

N. Mardirossian and M. Head-Gordon, J. Chem. Theory Comput., 2013, 9, 4453.

N. Mardirossian and M. Head-Gordon, Phys. Chem. Chem. Phys. 2014, 16, 9904.

N. Planas, J. E. Mondloch, S. Tussupbayev, J. Borycz, L. Gagliardi, J. T. Hupp, O. K. Farha, and C. J. Cramer, J. Phys. Chem. Lett. 2014, 5, 3716.

N. Schuch, F. Verstraete, Nature Phys. 2009, 5, 732.

N. W. Ashcroft and N. D Mermin, Solid State Physics (Saunders College, Philadelphia, 1976), pp. 337-344

O. A. Vydrov and G. E. Scuseria, J. Chem. Phys. 2006, 125, 234109.

O. A. Vydrov and T. Van Voorhis, J. Chem. Phys. 2009, 130, 104105.

O. A. Vydrov and T. Van Voorhis, J. Chem. Phys. 2010, 133, 244103..

O. A. Vydrov, G. E. Scuseria, J. Chem. Phys. 2006, 125, 234109.

O. A. Vydrov, G. E. Scuseria, J. P. Perdew, J. Chem. Phys. 2007, 126, 154109.

O. A. Vydrov, J. Heyd, A. V. Krukau, G. E. Scuseria, J. Chem. Phys. 2006, 125, 074106.

O. Gunnarsson and B. I. Lundqvist, Phys. Rev. B 1976, 13, 4274.

O. Tishchenko, J. Zheng, and D. G. Truhlar, J. Chem. Theory. Comput. 2008, 4, 1208.

O. Tishchenko, J. Zheng, D. G. Truhlar, J. Chem. Theory Comput. 2008, 4, 1208.

O. Vydrov and T. V. Voorhis, J. Chem. Phys. 2010, 133, 244103.

P. A. M. Dirac, Math. Proc. Cambridge Philos. Soc., 1930, 26, 376.

P. E. Blohl, Phys. Rev. B 1994, 50, 17953.
P. Haas, F. Tran, and P. Blaha, Phys. Rev. B 2009, 79, 085104.
P. Hao, Y. Fang, J. Sun, G. I. Csonka, P. H. T. Philipsen, and J. P. Perdew, Phys. Rev. B 2012, 85, 014111.
P. Hohenberg, W. Kohn, Phys. Rev. 1964, 136, B864.
P. J. Hay and W. R. Wadt, J. Chem. Phys. 1985, 82, 284.
P. J. Hay and W. R. Wadt, J. Chem. Phys. 1985, 82, 299.
P. J. Hay and W. R. Wadt, J. Chem. Phys., 1985, 82, 270.
P. J. Stephens, F. J. Devlin, C. F. Chabalowski, and M. J. Frisch, J. Phys. Chem. 1994, 98, 11623.
P. L. Fast and D. G. Truhlar, J. Phys. Chem. A 2000, 104, 6111.
P. Lazar and M. Otyepka, J. Phys. Chem. C 2012, 116, 25470.
P. Maity, S. Yamazoe, and T. Tsukuda, ACS Catal. 2013, 3, 182.
P. Pyykkö and M. Atsumi, Chem. Eur. J. 2009, 15, 12770.
P. Pyykkö and M. Atsumi, Chem. Eur. J. 2009, 15, 186.
P. Pyykkö and W.-H., Xu, Angew. Chem. Int. Ed. 2015, 54, 1080.
P. Rinke, M. Winkelnkemper, A. Qteish, D. Bimberg, J. Neugebauer, and M. Scheffler, Phys. Rev. B 2008, 77, 075202.
P. Rittmeyer, U. Weitelmann, Hydrides. In Ullmann's Encyclopedia of Industrial Chemistry; Wiley - CVH Verlag GmbH & Co. KGaA, 2000; pp 103-132.
P. Verma, X. Xu and D. G. Truhlar, J. Phys. Chem. C, 2013, 117, 12648.
P. Wernet, D. Nordlund, U. Bergmann, M. Cavalleri, M. Odelius, H. Ogasawara, L. A. Naslund, T. K. Hirsch, L. Ojamae, and P. Glatzel, et al. Science 2004, 304, 995.
P.L. Fast, J. Corchado, M.L. Sanchez, and D.G. Truhlar, J. Phys. Chem. A 1999, 103, 3139.
Q. Zhang, P. N. Day, and D. G. Truhlar, J. Chem. Phys. 1993, 98, 4948.
R. Gáspár, Acta Phys. Hung., 1954, 3, 263. (b) R. Gáspár, Acta Phys. Hung., 1974, 35, 213.
R. A. Kendall, T. H. Dunning, and R. Harrison, J. Chem. Phys. 1991, 96, 6796.
R. Bauernschmitt and R. Ahlrichs, J. Chem. Phys. 1996, 104, 9047.
R. Ditchfield, W. J. Hehre, and J. A. Pople, J. Chem. Phys. 1971, 54, 724.
R. Dovesi, R. Orlando, A. Erba, C. M. Zicovich-Wilson, B. Civalleri, S. Casassa, L. Maschio, M. Ferrabone, M. De La Pierre, P. D'Arco, Y. Noel, M. Causa, M. Rerat, and B. Kirtman, Int. J. Quant. Chem. 2014, 114, 1287.
R. G. Parr and W. Yang, in Density Functional Theory of atoms and molecules, (Oxford University Press, Inc, 1989); R. M. Dreizler and E. K. U. Gross, in Density Functional Theory, (New York, Plenum Press, 1995).
R. Huenerbein, B. Schirmer, J. Moellmann, and S. Grimme, Phys. Chem. Chem. Phys. 2010, 12, 6940.
R. J. Whitehead and N. C. Handy, J. Mol. Spectrosc. 1975, 55, 356.
R. Krishnan, J. S. Binkley, R. Seeger, and J. A. Pople, J. Chem. Phys. 1980, 72, 650.

R. Li, R. Peverati, M. Isegawa, and D. G. Truhlar, J. Phys. Chem. A 2012, 117, 169.
R. M. Richard and J. M. Herbert, J. Chem. Phys. 2012, 137, 06411.
R. Matz and H. Lütz, Appl. Phys. 1979, 18, 123.
R. McWeeny, Methods of Molecular Quantum Mechanics, 2nd Edition; Academic Press: London, 1992; pp 435-438.
R. Peverati and D. G. Truhlar, J. Chem. Phys. 2011, 135, 191102.
R. Peverati and D. G. Truhlar, J. Chem. Phys. 2012, 136, 134704.
R. Peverati and D. G. Truhlar, J. Chem. Theory Comput., 2012, 8, 2310.
R. Peverati and D. G. Truhlar, J. Phys. Chem. Lett. 2011, 2, 2810.
R. Peverati and D. G. Truhlar, J. Phys. Chem. Lett., 2011, 3, 117.
R. Peverati and D. G. Truhlar, Phil. Trans. R. Soc. A, 2014, 372, 20120476.
R. Peverati and D. G. Truhlar, Phil. Trans. Roy. Soc. A 2013, dx.doi.org/10.1098/rsta.2012.0476 [also published online at http:// http://arxiv.org/abs/1212.0944 (accessed Dec. 29, 2013)].
R. Peverati and D. G. Truhlar, Phil. Trans. Roy. Soc. A 2014, 372, 20120476.
R. Peverati and D. G. Truhlar, Phys. Chem. Chem. Phys. 2012, 14, 13171.
R. Peverati and D. G. Truhlar, Phys. Chem. Chem. Phys. 2012, 14, 16187.
R. Peverati, D. G. Truhlar, J. Chem. Phys. 2011, 135, 191102.
R. Peverati, D. G. Truhlar, J. Phys. Chem. Lett. 2011, 2, 2810.
R. Peverati, D. G. Truhlar, Phys. Chem. Chem. Phys. 2012, 14, 13171.
R. Peverati, D. G. Truhlar, Phys. Chem. Chem. Phys. 2012, 14, 16187.
R. Peverati, Y. Zhao, and D. G. Truhlar, J. Phys. Chem. Lett. 2011, 2, 1991.
R. R. Reeber, J. Appl. Phys. 1970, 41, 5063.
R. Seeger and J. A. Pople, J. Chem. Phys. 1977, 66, 3045.
R.D. Johnson III, K.K. Irikura, R.N. Kacker, and R. Kessel, J. Chem. Theory Comput. 2010, 6, 2822.
R.S. Grev, C.L. Janssen, and H.F. Schaefer III, J. Chem. Phys. 1991, 95, 5128.
S. C. Tucker, T. C. Thompson, J. G. Lauderdale, and D. G. Truhlar, Comput. Phys. Commun. 1988, 51, 233.
S. Carter and N. C. Handy, Phys. Rep. 1986, 5, 117.
S. Carter, J. M. Bowman, and N. C. Handy, Theor. Chem. Acc. 1998, 100, 191.
S. Chakravorty, S. Gwaltney, E. R. Davidson, F. Parpia, and C. Fischer, Phys. Rev. A 1993, 47, 3649.
S. Grimme, J. Antony, S. Ehrlich, and H. Krieg, J. Chem. Phys. 2010, 132, 154104.
S. Grimme, J. Chem. Phys. 2006, 124, 034108.
S. Grimme, J. Comput. Chem. 2006, 27, 1787.
S. Grimme, S. Ehrlich, and L. Goerigk, J. Comput. Chem. 2011, 32, 1456.
S. H. Vosko, L. Wilk and M. Nusair, Can. J. Phys., 1980, 58, 1200.
S. Hua, W. Li, and S. Li, ChemPhysChem. 2013, 14, 108.
S. K. Ghosh and R. G. Parr, Phys. Rev. A 1986, 34, 785.

S. Kozuch, D. Gruzman, J. M. L. Martin, J. Phys. Chem. C 2010, 114, 20801.
S. L. Li and D. G. Truhlar, J. Chem. Phys., 2014, 141, 104106.
S. L. Li and D. G. Truhlar, J. Chem. Theory Comput., 2015, 11, 3123.
S. L. Mielke, A. Chakraborty, and D. G. Truhlar, J. Phys. Chem. A 2013, 117, 7327.
S. Lundqvist and N. H. March, in Theory of the Inhomogeneous Electron Gas, (Plenum, New York, 1983)
S. Luo and D. G. Truhlar, J. Chem. Theory Comput. 2012, 8, 4112.
S. Luo, B. Averkiev, K. R. Yang, X. Xu, and D. G. Truhlar, J. Chem. Theory Comput. 2014, 10, 102.
S. Luo, Y. Zhao, and D. G. Truhlar, Phys. Chem. Chem. Phys. 2011, 13, 13683.
S. R. Pruitt, M. A. Addicoat, M. A. Collins, and M. S. Gordon, Phys. Chem. Chem. Phys. 2012, 14, 7752.
S. Reidel and M. Kaupp, Coord. Chem. Rev. 2009, 253, 606.
S. Sima, Found. Chem. 2009, 11, 135.
S. Wen, K. Nanda, Y. Huang, and G. J. O. Beran, Phys. Chem. Chem. Phys. 2012, 14, 7562.
Sulfur Trioxide. National Institute of standards and Technology (NIST). http://webbook.nist.gov/cgi/cbook.cgi?ID= C7446119&Units=SI (accessed on July 26, 2015).
Sulfuric Acid. National Institute of standards and Technology (NIST). http://webbook.nist.gov/cgi/cbook.cgi?ID= C7664939&Units=SI&Mask=1#Thermo-Gas (accessed on July 26, 2015).
T. B. Adler, G. Knizia, and H.-J. Werner, J. Chem. Phys. 2007, 127, 221106.
T. E. Sorensen and W. B. England, Int. J. Quant. Chem. 2000, 76, 259.
T. H. Dunning Jr. and P. J. Hay, in Modern Theoretical Chemistry, ed. Schaefer III, Plenum, New York, 1977, vol.3, pp. 1-28.
T. H. Dunning, Jr., J. Chem. Phys. 1989, 90, 1007.
T. H. Dunning, Jr., K. A. Peterson, and A. K. Wilson, J. Chem. Phys. 2001, 114, 9244.
T. H. Jr. Dunning and P. J. Hay, in Modern Theoretical Chemistry, Ed. H. F. Schaefer III, Vol. 3, Plenum: New York, 1977, pp. 1-28.
T. H. Jr. Dunning, J. Chem. Phys., 1989, 90, 1007.
T. Helgaker, P. Jorgensen, and J. Olsen, Modern Electronic Structure Theory; Wiley: Chichester, 2000; p. 188.
T. J. Lee and P. R. Taylor, Int. J. Quantum Chem. Symp. 1989, 23, 199-207.
T. M. Henderson, A. F. Izmaylov, G. E. Scuseria, and A. Savin, J. Chem. Theory Comp. 2008, 4, 1254.
T. M. Henderson, A. F. Izmaylov, G. Scalmani and G. E. Scuseria, J. Chem. Phys., 2009, 131, 044108.
T. Nagata, D. G. Fedorov, and K. Kitaura, Chem. Phys. Lett. 2012, 544, 87.
T. Schwabe, Phys. Chem. Chem. Phys. 2014, 16, 14559.
T. V. Voorhis, G. E. Scuseria, J. Chem. Phys. 1998, 109, 400.

T. van Mourik and T. H. Dunning, Jr., Int. J. Quantum Chem., 2000, 76, 205.
T. W. Keal and D. J. Tozer, J. Chem. Phys. 2005, 123, 121103.
T. W. Keal, D. J. Tozer, J. Chem. Phys. 2005, 123, 121103.
T. Weymuth, E. P. A. Couzijn, P. Chen, and M. Reiher, J. Chem. Theory Comput. 2014, 10, 3092.
T. Yanai, D. Tew, and N. C. Handy, Chem. Phys. Lett. 2004, 393, 51.
T. Yanai, D. Tew, N. Hanyd, Chem. Phys. Lett. 2004, 393, 51.
T.H. Dunning Jr., J. Chem. Phys., 1989, 90, 1007.
U. von Barth, L. Hedin, J. Phys. C: Solid State Phys. 1972, 5, 1629.
V. Barone, J. Chem. Phys. 2005, 122, 014108.
V. Beutel, H. G. Krämer, G. L. Bhale, M. Kuhn, K. Weyers and W. Demtröder, J. Chem. Phys., 1993, 98, 2699.
V. N. Staroverov, G. E. Scuseria, J. Tao, and J. P. Perdew, J. Chem. Phys. 2003, 119, 12129.
V. N. Staroverov, G. E. Scuseria, J. Tao, and J. P. Perdew, Phys. Rev. B 2004, 69, 075102.
W. J. Balfour, J. Cao, C.V.V. Prasad, and C.X.W. Qian, J. Chem. Phys. 1995, 103, 4046.
W. J. Hehre and J. A. Pople, J. Chem. Phys. 1972, 56, 4233.
W. J. Hehre, L. Radom, P. V. R. Schleyer, and J. A. Pople, Ab initio molecular orbital theory (New York, NY: Wiley, 1986)
W. J. Hehre, R. Ditchfield, and J. A. Pople, J. Chem. Phys. 1972, 56, 2257.
W. Jorgensen, J. Chandrasekhar, J. D. Madura, R. W. Impey, and M. L. Klein, J. Chem. Phys. 1983, 79, 926.
W. Kohn and L. J. Sham, Phys. Rev. 1965, 140, A1133.
W. Kohn, A. D. Becke and R. G. Parr, J. Phys. Chem., 1996, 100, 12974.
W. Kohn, L. J. Sham, Phys. Rev. 1965, 140, A1133.
W. Kohn, Rev. Mod. Phys. 1999, 71, 1253.
W. Zhang, D. G. Truhlar, and M. Tang, J. Chem. Theory Comput. 2013, 9, 3965.
W. Zhang, D. G. Truhlar, and M. Tang, J. Chem. Theory Comput., 2014, 10, 2399.
W.-M. Hoe, A. J. Cohen, N. C. Handy, Chem. Phys. Lett. 2001, 341, 319.
X. Jia, X. Wang, J. Liu, J.Z.H. Zhang, Y. Mei, and X. He, J. Chem. Phys. 2013, 139, 214104.
X. Li, X. Xu, X. You, and D. G. Truhlar, J. Phys. Chem. A, 2016, Accepted.
X. Li, X. Xu, X. Yu, D. G. Truhlar, Benchmark Calculations for Bond Dissociation Enthalpies of Unsaturated Methyl Esters. 2016, J. Phys. Chem A, accepted.
X. Xu, W. Zhang, M. Tang, and D. G. Truhlar, J. Chem. Theory Comput. 2015, 11, 2306.
Y. Andersson, D. C. Langreth, and B. I. Lundqvist, Phys. Rev. Lett. 1996, 76, 102.
Y. Guo, J. Robertson, and S. J. Clark, J. Phys.: Condens. Matter 2015, 27,025501.
Y. Sun, H. Chen, J. Chem. Theory Comput. 2013, 9, 4735.

Y. Sun, H. Chen, J. Chem. Theory Comput. 2014, 10, 579.
Y. Tawada, T. Tsuneda, S. Yanagisawa, T. Yanai, K. Hirao, J. Chem. Phys. 2004, 120, 8425.
Y. Volobuev, W. C. Necoechea, and D. G. Truhlar, Chem. Phys. Lett. 2000, 330, 471.
Y. Wang, C. P. Sosa, A. Cembran, D. G. Truhlar, and J. Gao, J. Phys. Chem. B 2012, 116, 6781.
Y. Zhang and W. Yang, Phys. Rev. Lett., 1997, 80, 890.
Y. Zhao and D. G. Truhlar, J. Chem. Phys. 2006, 125, 194101.
Y. Zhao and D. G. Truhlar, J. Chem. Phys. 2008, 128, 184109.
Y. Zhao and D. G. Truhlar, J. Chem. Phys. 2009, 130, 074103.
Y. Zhao and D. G. Truhlar, J. Chem. Theory Comput. 2005, 1, 415.
Y. Zhao and D. G. Truhlar, J. Chem. Theory Comput. 2008, 4, 1849.
Y. Zhao and D. G. Truhlar, J. Phys. Chem. A 2005, 109, 5656.
Y. Zhao and D. G. Truhlar, J. Phys. Chem. A 2005, 109, 6624.
Y. Zhao and D. G. Truhlar, J. Phys. Chem. A 2006, 110, 10478.
Y. Zhao and D. G. Truhlar, J. Phys. Chem. A, 2004, 108, 6908.
Y. Zhao and D. G. Truhlar, J. Phys. Chem. A, 2005, 109, 5656.
Y. Zhao and D. G. Truhlar, J. Phys. Chem. A, 2006, 110, 13126.
Y. Zhao and D. G. Truhlar, Org. Lett. 2006, 8, 5753.
Y. Zhao and D.G. Truhlar, Theor. Chem. Acc. 2008, 120, 215.
Y. Zhao, and D. G. Truhlar, J. Chem. Phys. 2006, 125, 194101.
Y. Zhao, B. J. Lynch, and D. G. Truhlar, J. Phys. Chem. A 2004, 108, 2715.
Y. Zhao, B. J. Lynch, and D. G. Truhlar, J. Phys. Chem. A 2004, 108, 4786.
Y. Zhao, B. J. Lynch, and D. G. Truhlar, Phys. Chem. Chem. Phys. 2005, 7, 43.
Y. Zhao, B. J. Lynch, D. G. Truhlar, J. Phys. Chem. A 2004, 108, 2715.
Y. Zhao, B. J. Lynch, D. G. Truhlar, J. Phys. Chem. A 2004, 108, 4786.
Y. Zhao, D. G. Truhlar, J. Chem. Phys. 2006, 125, 194101.
Y. Zhao, D. G. Truhlar, J. Chem. Theory Comput. 2008, 4, 1849.
Y. Zhao, D. G. Truhlar, J. Phys. Chem. A 2005, 109, 5656.
Y. Zhao, D. G. Truhlar, Theor. Chem. Acc. 2008, 120, 215.
Y. Zhao, H. T. Ng, R. Peverati, and D. G. Truhlar, J. Chem. Theory Comput. 2012, 8, 2824.
Y. Zhao, J. Pu, B. J. Lynch, and D. G. Truhlar, Phys. Chem. Chem. Phys. 2004, 6, 673.
Y. Zhao, N. E. Schultz, and D. G. Truhlar, J. Chem. Phys., 2005, 123, 161103.
Y. Zhao, N. E. Schultz, and D. G. Truhlar, J. Chem. Theory Comput. 2005, 2, 364.
Y. Zhao, N. E. Schultz, and D. G. Truhlar, J. Chem. Theory Comput., 2006, 2, 364.
Y. Zhao, N. González-García, and D. G. Truhlar, J. Phys. Chem. A, 2005, 109, 2012.
Y. Zhao, N.E. Schultz, and D. G. Truhlar, J. Chem. Phys. 2005, 123, 161103.
Y. Zhao, O. Tishchenko, J. R. Gour, W. Li, J. J. Lutz, P. Piecuch, and D. G. Truhlar, J. Phys. Chem. A 2009, 113, 5786.

Y. Zhao, O. Tishchenko, J. R. Gour, W. Li, J. J. Lutz, P. Piecuch, D. G. Truhlar, J. Phys. Chem. A 2009, 113, 5786.
Y. Zhao, R. Peverati, K. R. Yang, S. Luo, H. Yu, X. He, and D. G. Truhlar, MN-GFM, version 6.5: Minnesota Gaussian Functional Module; University of Minnesota: Minneapolis, MN, 2015.
Y. Zhao, R. Peverati, K. Yang, S. Luo and D. G. Truhlar, MN-GFM, version 6.4: Minnesota Gaussian Functional Module; University of Minnesota: Minneapolis, MN, 2012.
Y. Zhao, R. Peverati, K. Yang, S. Luo, H. S. Yu, and D. G. Truhlar, MN-GFM, version 6.6: Minnesota Gaussian Functional Module; University of Minnesota: Minneapolis, MN, 2015.
Z. Yan, J. P. Perdew, and S. Kurth, Phys. Rev. B 2000, 61, 16430.
A. Dhakshinamoorthy and H. Garcia, Chem. Soc. Rev. 2012, 41, 5262.
A. Uzun, V. Ortalan, N. D. Browning, and B. C. Gates, Chem. Comm. 2009, 31, 4657.
C. Aydin, J. Lu, N. D. Browning, and B. C. Gates, Angew. Chem. Int. Ed. 2012, 51, 5929.
D. Yardimci, P. Serna, and B. C. Gates, ACS Catalysis 2012, 2, 2100.
G. E. Johnson, R. Mitrić, V. Bonačić-Koutecký, A. Castleman, Jr. W. Chem. Phys. Lett. 2009, 475, 1.
K. An and G. A. Somorjai, ChemCatChem 2012, 4, 1512.
K. Shimizu, K. Ohshima, and A. Satsuma, Chem. Eur. J.. 2009, 15, 9977.
Lopez-Acevedo, O.; Kacprzak, K. A.; Akola, J.; Häkkinen, H. Nat. Chem. 2010, 2, 329.
M. Flytzani-Stephanopoulos and B. C. Gates, Annu. Rev. Chem. Biomol. Eng. 2012, 3, 545.
P. Hohenberg and W. Kohn, Phys. Rev. 1964, 136, B864.
V. Dal Santo, M. Guidotti, R. Psaro, L. Marchese, F. Carniato, and C. Bisio, Proc. R. Soc. A 2012, 468, 1904.
W. Kohn and L. J. Sham, Phys. Rev. 1965, 140, A1133.
Y. Lu and W. Chen, Chem. Soc. Rev. 2012, 41, 3594.